Aqueous dispersions of conducting polymers for opto-electronic applications

Anna Hofmann

université de BORDEAUX

Thèse

présentée à

L'UNIVERSITÉ BORDEAUX

Ecole Doctorale des Sciences Chimiques

par

Anna Hofmann

pour obtenir le grade de

DOCTEUR

Spécialité: Polymères

Aqueous Dispersions of Conducting Polymers for Opto-Electronic Applications

---

Soutenue le 9 Décembre 2016

Devant la commission d'examen formée de:

Prof. Natalie Stingelin-Stutzmann, Georgia Institute of Technology, USA	*Rapporteur*
Prof. Xavier Crispin, Universitet Linköping, Suède	*Rapporteur*
Prof. Georges Malliaras, MINES Saint-Etienne, France	*Examinateur*
Prof. Hamid Kellay, Université Bordeaux, France	*Examinateur*
Dr. Ilias Iliopoulos, Arkema France	*Examinateur*
Prof. Georges Hadziioannou, Université Bordeaux, France	*Directeur de Thèse*
Dr. Eric Cloutet, Université Bordeaux, France	*Directeur de Thèse*

Acknowledgments

This thesis contains the work of three years of research, which would not have been possible without the contribution, guidance , help and support of different people to whom I would like to express my acknowledgments and gratitude.

First I would like to thank **Prof. Georges Hadziioannou** for the opportunity to do my PhD research in his lab, for his strong believe in this project and his support. I also would like to thank **Dr. Eric Cloutet** for his advise, his tireless efforts to correct my presentations and manuscripts, his encouragement and the possibility to let me develop own ideas and projects, which made me enjoy research.
Furthermore I would like to acknowledge **ARKEMA France** for the funding of my research project and **Dr. Ilias Iliopoulos** for his pertinent remarks and support.

During this PhD research project I had the opportunity to collaborate with different research groups, which was an enriching personal experience and essential for the success of this PhD project. Therefor my sincere thanks goes to **Prof. Hamid Kellay** and **Dr. Antoine Déblais** at the LOMA (Université Bordeaux) for their help regarding rheology and DLS analysis, their patience and their enthusiasm for scientific discussions. Furthermore I would like to thank **Prof. Georges Malliaras** and his team (especially **Dr. Sahika Inal**) from the Centre Microélectronique de Provence (EMSE) in Gardanne for welcoming me in their lab and for showing me how to fabricate and measure OECT devices. A sincere thanks goes to **Dr. Olaf Hild and Falk Schuetze** from the Fraunhofer Institute of Organic Electronics in Dresden, for the fabrication and measurement of the OLED devices. In addition, I am grateful for the help of **Christine Labrugère** (PLACAMAT Bordeaux) regarding XPS analysis, **Sabrina Lacomme** (Bordeaux Imaging Centre), **Prof. Alexander Kuhn** (ISM Bordeaux) and **Prof. Laurence Vigneau** and **Prof. Lionel Hirsch** (IMS Bordeaux).

My sincere thanks also goes to my colleagues, who helped and inspired me, especially to **Dr. Gilles Pecastaings** for his help with AFM imaging, to **Gérard Dimier** for his help with thermal analysis, to **Najim Ounajma** and **Wiljan Smaal** for the good collaboration, precision, reliability and friendship, to **Dr. Eleni Pavlopoulou**, who made me discover new scattering techniques and the wonders of Greece,and **Dr. Christophe Schatz** for his advise regarding polyelectrolytes. This work would not have been possible without **Dr. Muhammad Mumtaz and Dr. Dimitrios Katsigiannopoulos**, who synthesized the divers polyelectrolytes. Furthermore I would like to thank all my other colleagues, in the first place Ségolène, Yianni and Jon, for the scientific and non scientific discussions, the fun we had and their moral support.
I also would like to thank Mama und Papa and my family and my friends here in Bordeaux (Nono, Julien, Aurore, Corey, Frank...) and abroad (Sabrina, Ju, Codi, Anne, Alessandro...) for being at my side and for supporting me, without you I would have given up a hundred times.

Anna

Contents

Abstract/Résumé

Aqueous Dispersions of Conducting Polymers for Opto-Electronic Applications

In this work different aqueous dispersions of conducting poly(3,4-ethylenedioxythiophene) :polyelectrolyte (PEDOT:polyelectrolyte) complexes, made from anionic polysaccharides and from synthetic bis(sulfonylimide) substituted polystyrenes, have been synthesized and characterized regarding their doping, morphology, rheological behavior and opto-electronic properties. A systematic study revealed, that high molar mass polyelectrolytes with strongly acidic groups and a rigid backbone structure were favorable for a high doping and an efficient dispersion of PEDOT and allowed the development of highly conducting PEDOT:polyelectrolyte complexes. The use of the polyelectrolyte poly(4-styrene trifluoromethane(bissulfonylimide)) (PSTFSI) as complexing agent for PEDOT resulted in stable dispersions with gel character, which allowed easy processing by spin coating and doctor blading. The obtained PEDOT:PSTFSI films were highly transparent, displayed a conductivity of up to 330S.cm^{-1} and were successfully integrated as electrodes in OLED, OPV and OECT devices.

Key words: transparent electrode, conducting polymer, PEDOT, organic electronics

Dispersions Aqueuses de Polymères Conducteurs pour les Applications Opto-Electroniques

Dans ce travail, différentes solutions aqueuses de PEDOT:polyelectrolyte ont été synthétisées à partir de polymères anioniques de types polysaccharides et polystyrènes substitués par des groupements bis(sulfonylimide). Leurs morphologies, dopages, comportements rhéologiques ainsi que leurs propriétés opto-électroniques ont notamment été caractérisés. Une étude systématique a révélé que les polyélectrolytes de masse molaire élevée portant un groupement fortement acide et ayant un squelette rigide permettent d'obtenir un dopage élevé, une dispersion efficace du PEDOT et donc des complexes PEDOT :polyelectrolyte plus conducteurs. L'utilisation du polyelectrolyte PSTFSI en tant qu'agent de complexation pour le PEDOT donne une dispersion stable montrant les caractéristiques d'un gel, ce qui facilite la fabrication de films minces par 'spin coating' ou doctor blade. Les films de PEDOT :PSTFSI ainsi obtenus montrent une transparence élevée et une conductivité de 330S.cm^{-1}. Ces propriétés ont permis de les intégrer avec succès comme matériaux d'électrodes dans des dispositifs OLED, OPV et OECT.

Mots clés: électrode transparente, polymère conducteur, PEDOT, électronique organique

Laboratoire de Chimie des Polymères Organiques (LCPO), UMR 5629 Allée Geoffroy Saint Hilaire, Batiment 8, 33615 Pessac Cedex

List of Abbreviations

AA	Acrylic Acid
AFM	Atomic Force Microscopy
Alq_3	Tris(8-hydroxyquinolinato)aluminium
CMC	Carboxymethyl Cellulose
CNT	Carbon Nanotube
CVD	Chemical Vapor Deposition
DEG	Diethylene Glycol
DLS	Dynamic Light Scattering
DMF	Dimethylformamide
DMSO	Dimethylsulfoxide
DS	Dextran Sulfate
DSC	Differential Scanning Calorimetry
EG	Ethylene Glycol
FF	Fill Factor
FoM	Figure of Merit
GIWAXS	Grazing Incidence Wide Angle X-ray Scattering
HLA	Hyaluronic Acid
ITO	Indium Tin Oxide
LiTFSI	Lithium bistrifluoromethanesulfonimide
MEH-PPV	Poly(2-methoxy-5-(2-ethylhexyloxy)-1,4-phenylenevinylene)
MWCNT	Multi Walled Carbon Nanotube
NP	Nano-Particle
NPD	N,N′-Di(1-naphthyl)-N,N′-diphenyl-(1,1′-biphenyl)-4,4′-diamine
NW	Nano-Wire
OECT	Organic Electrochemical Transistor
OLED	Organic Light Emitting Diode
OPV	Organic Photovoltaic
P3HT	Poly(3-hexylthiophene-2,5-diyl)
PANI	Polyaniline

PCBM	(6,6)-Phenyl C61 butyric acid methyl ester
PCE	Power Conversion Efficiency
PDMS	Poly(dimethylsiloxane)
Pec	Pectin
PEDOT	Poly(3,4-ethylenedioxythiophene)
PMaTFSI	Poly(methacrylate trifluoromethyl(bissulfonylimide))
PPy	Polypyrrole
PPP	Poly(p-phenylene)
PSMSI	Poly(4-styrene methyl(bissulfonylimide))
PSPSI	Poly(4-styrene phenyl(bissulfonylimide))
PSS	Poly(4-styrenesulfonate)
PSTFSI	Poly(4-styrene trifluoromethyl(bissulfonylimide))
PT	Polythiophene
pTSA	para-Toluenesulfonic Acid
SWCNT	Single Walled Carbon Nanotube
Tos	Toluene sulfonate
UV/Vis	Ultra Violet/Visible
VRH	Variable Range Hopping
XPS	X-ray Photoelectron Spectroscopy

List of Symbols and Physical Constants

a	(cm^{-1})	Absorption Coefficient
A	-	Absorbance
e	(C)	Elementary Charge = $1.6021766208 \cdot 10^{-19}$
$\overrightarrow{E}$	($V.m^{-1}$)	Electric Field
ϵ_0	($F.m^{-1}$)	Vacuum Permittivity = $8.8541878 \cdot 10^{-12}$
η	($lm.W^{-1}$)	Power Efficiency
G', G''	(Pa)	Storage Modulus, Loss Modulus
g_m	(S)	Transconductance
γ	($cd.A^{-1}$)	Current Efficiency
I_D	(A)	Drain Current
I_{SC}	(A)	Short Circuit Current
$\overrightarrow{j}$	($A.m^{-2}$)	Current Density
k_B	($eV.K^{-1}$)	Boltzmann Constant = $8.6173324 \cdot 10^{-5}$
L	($cd.cm^{-2}$)	Luminance
λ	(m)	Wavelength
M_W	($Da=g.mol^{-1}$)	Molar Mass
ω	($rad.s^{-1}$)	Angular Frequency
P	($J.s^{-1}$)	Power
π	-	3.14159
r	(m)	Radius
R_q	(m)	Roughness (root mean squared)
R_S	($Ohm.sq^{-1}$)	Sheet Resistance
σ	($S.m^{-1}$)	Conductivity
T	(%)	Transmittance
$\boldsymbol{T}$	(K)/(°C)	Temperature
T_g	(K)/(°C)	Glass Transition Temperature
$tan\delta$	-	Loss Factor
V_D	(V)	Drain Voltage
V_G	(V)	Gate Voltage
V_{OC}	(V)	Open Circuit Voltage

General Introduction

Nowadays electronic devices are omnipresent in our daily life and have improved the standard of living in so many fields, such as communication, entertainment, health and security, that our modern society can not be imagined without electronics. However, their production and use bring about an important consumption of resources and energy. As the stock of fossil fuels and certain raw materials decreases and the environmental pollution reaches an alarming level, the development of technologies, which allow a sustainable production of energy, and of highly energy efficient devices, become more and more important. In addition, emerging technologies create a demand for innovative materials for applications, which are not accessible with classical electronic devices.

Therefore conducting polymers have attracted a great deal of attention as a new class of materials since their discovery by MacDiarmid, Shirakawa and Heeger in 1977. Conducting polymers combine the electronic conductivity of inorganic materials with the flexibility, chemical stability, low density and solution processability of polymers, which allows the fabrication of flexible, light weight devices. Especially the development of aqueous dispersions of conducting polymers, such as PEDOT:PSS, made it possible to print flexible, transparent and bio-compatible thin films for a wide range of application in energy [1, 2, 3, 4, 5, 6, 7], such as solar cells, in entertainment [8, 9, 10, 11, 12], such as OLEDs lighting and displays, and in the biomedical field [13, 14, 15]. These organic devices show very promising performances and some of them, such as OLED applications, have already been commercialized. However, there is still a need for new polymeric conducting materials, which allow the development of a new generation of organic electronic devices with improved stability and higher efficiencies.

A crucial component of all opto-electronic devices is the transparent electrode, which allows the in/out coupling of light from the device. The criteria for the evaluation of transparent electrodes and fundamental principles for their characterization are presented in **chapter 1**. Furthermore, this chapter contains an overview of different inorganic and organic materials, which can be used as transparent electrodes, together with a brief discussion of their respective advantages and drawbacks for the application in organic electronic devices.

Due to its good opto-electronic performance, but also due to a lack of alternatives, the current polymeric material of choice for most organic-electronic applications is PEDOT:PSS (Poly (3,4-ethylenedioxythiophene): Polystyrene sulfonate). However, considering the diversity of the potential applications, it is desirable to design alternative PEDOT:polyelectrolyte systems, which match better the specific needs of the different applications.

In **chapter 2** we present a new approach to stabilize PEDOT in aqueous dispersions by replacing the polystyrenesulfonic acid by the anionic polymer poly(4-styrenetrifluoromehtyl (bissulfonylimide)) (PSTFSI), which is known for its application as polyelectrolyte in Lithium batteries. It was shown, the PEDOT:PSTFSI complex displays very promising opto-electronic properties. In order to improve the understanding of the complex system, the polyelectrolyte PSTFSIK and its behavior in aqueous solution as well as the complex formation upon synthesis of PEDOT in the presence of PSTFSI was studied. A particular attention was paid to the acid base behavior of PSTFSI and the pH of the synthesis medium, which were found to greatly influence the opto-electronic properties of the final PEDOT:PSTFSI complex. The comprehensive study of the impact of different synthesis parameters, such as the synthesis temperature and time, as well as the choice of oxidants, on the opto-electronic properties of PEDOT:PSTFSI allowed the definition of an optimized synthesis protocol.

For the fabrication of thin PEDOT:PSTFSI films the PEDOT:PSTFSI dispersion can be processed by various coating techniques, such as by spray and spin coating, as well as by doctor blading. In **chapter 3** it was shown, that the opto-electronic properties of the resulting films were barely affected by the ink concentration or coating conditions. Furthermore, different approaches for the formulation of PEDOT:PSTFSI with high boiling point solvents and salts are presented, which allowed the decisive enhancement of the conductivity of several orders of magnitude. In addition, we developed a method to fabricate conducting PEDOT:PSTFSI films with extremely high transparency by simple formulation of PEDOT:PSTFSI with the PSTFSIK polyelectrolyte, which are of potential interest for the fabrication of composite electrodes.

For the application and a potential scale up of PEDOT:PSTFSI, a good colloidal stability of the dispersion and an excellent chemical stability of the dry films are crucial. Using UV/Vis, Raman and XPS spectroscopy techniques, as well as rheological characterization the long term stability of the PEDOT:PSTFSI inks was confirmed and the stability of the opto-electronic properties of PEDOT:PSTFSI under ambient conditions, as well as at elevated temperatures up to 190°C was demonstrated in **chapter 4**.

Owing to their good opto-electronic performance, thin PEDOT:PSTFSI films were successfully integrated as transparent electrodes in organic light emitting diodes, which outperformed reference devices with PEDOT:PSS electrodes, as well as in organic solar cells, which showed promising results. In addition, it was demonstrated in **chapter 5**, that PEDOT:PSTFSI can be used as mixed ion-hole conductor in organic electrochemical transistors.

To further enlarge the palette of conducting aqueous PEDOT dispersions, several PEDOT:polyelectrolyte systems based on polysaccharide and polysulfonylimide type polyelectrolytes were studied in **chapter 6**. The obtained PEDOT:polyelectrolyte systems were characterized regarding the doping and the morphology of the polymer complexes in dispersion, as well as regarding the opto-electronic properties and the morphology of the dry PEDOT:polyelectrolyte films. Furthermore, the influence of polyelectrolyte backbone and of the anionic groups on the properties of the resulting PEDOT:polyelectrolyte complex was investigated. It was shown, that the use of polysaccharide type electrolytes, such as dextran sulfate, is a promising way to develop low cost and highly bio-compatible conducting PEDOT complexes, whereas PEDOT:PSTFSI films displayed the highest transparencies.

Introduction Générale

De nos jours, les appareils électroniques sont omniprésents et ils permettent de faciliter notre vie quotidienne dans de nombreux domaines, tel que la communication, les loisirs, la santé et la sécurité. Néanmoins, la fabrication et l'usage de ces dispositifs a pour conséquence une consommation plus ou moins importante d'énergie et de ressources primaires. Si on considère que les réserves de pétrole ainsi que de certaines matières premières risquent de s'épuiser et le fait que la pollution atteint un niveau dangereux dans certaines régions, le développement de technologies durables et d'appareils à basse consommation d'énergie devient prépondérant. De plus, certaines technologies émergeantes qui ne sont pas accessibles avec des dispositifs électroniques classiques, créent une demande de matériaux innovants comme des éléments flexibles grandes surfaces optoélectroniques.

Dans ce contexte et depuis leur découverte par MacDiarmid, Shirakawa et Heeger en 1977, les polymères conducteurs sont au centre de l'attention pour le développement d'une nouvelle classe de matériaux pour l'optoélectronique. Les polymères conducteurs combinent la conductivité électronique des matériaux inorganiques avec la fléxibilité, la stabilité chimique ainsi que la faible densité des polymères permettant la fabrication de dispositifs bas coût, flexibles et légers. Entre autres, le développement de dispersions aqueuses de polymères conducteurs tel que le poly(3,4 éthylènedioxythiophène):poly(styrène sulfonate) (PEDOT:PSS) rend possible l'impression de films minces flexibles, transparents et biocompatibles ayant un grand nombre d'applications dans les dispositifs pour l'énergie [1, 2, 3, 4, 5, 6, 7], tels que le photovoltaïque, les écrans d'affichage [8, 9, 10, 11, 12] et le domaine médical [13, 14, 15]. Ces dispositifs organiques montrent des performances très prometteuses et certains d'entre eux, tels que les OLEDs (diodes électroluminescentes organiques), ont déjà été commercialisés. Néanmoins, le développement d'une nouvelle génération de dispositifs électroniques organiques plus stables et plus efficaces nécessite de nouveaux matériaux.

Parmi les composants indispensables pour la fabrication de dispositifs opto-électroniques l'électrode transparente qui permet notamment l'émission ou l'absorption de la lumière sera traitée dans le ***chapitre 1****. Ce dernier fait ainsi un état de l'art des électrodes transparentes organiques et inorganiques afin de les évaluer selon leurs avantages et inconvénients en fonction des technologies et applications envisagées.*

Parmi les matériaux de choix pour ces technologies, le PEDOT:PSS qui se trouve sous forme d'une dispersion aqueuse permet la fabrication de films transparents conducteurs via des techniques d'impression adaptées aux grandes surfaces 'plastiques'. Cependant, pour certaines applications et en fonction des conditions le PEDOT:PSS n'est pas la panacée. Ainsi, au cours du ***chapitre 2****, je présenterai une alternative consistant principalement à remplacer le PSS par le polymère anionique poly(4-styrenetrifluoromethyl (bissulfonylimide)) (PSTFSI) autrement connu comme polyelectrolyte dans des accumulateurs lithium. De bonnes caractéristiques optoélectroniques ont été obtenues pour des films minces à base de dispersions aqueuses de PEDOT:PSTFSI en faisant ainsi un candidat de choix pour des applications électrode transparente dans des dispositifs électroniques. Afin de mieux comprendre ce système complexe de PEDOT:PSTFSI, les caractéristiques du polyélectrolyte PSTFSI en solution et la formation du complexe PEDOT:PSTFSI ont été étudiées. Une attention particulière a été accordée au comportement acido-basique du PSTFSI et au pH du milieu de synthèse, qui influencent de manière importante les propriétés opto-électroniques du PEDOT:PSTFSI. Enfin, l'impact de différents paramètres de synthèse, tels que la température, la durée de la synthèse et les oxydants, sur les propriétés opto-électroniques ont été examinés.*

es dispersions aqueuses de PEDOT:PSTFSI ont permis la fabrication de films conducteurs et transparents via des techniques d'enduction différentes, comme le 'spin coating', le 'spray coating' ou le 'doctor blading'. Dans le ***chapitre 3*** *l'effet de la technique d'enduction sur les propriétés opto-électroniques des films PEDOT:PSTFSI a été étudié. De plus, il a été montré que les propriétés opto-électroniques des films PEDOT:PSTFSI peuvent être modifiées par formulation des encres, à partir desquelles ils sont élaborés.*

Nous avons notamment trouvé que la conductivité peut être améliorée de plusieurs ordres de grandeur grâce à la formulation de l'encre avec certains solvants ou sels, tandis que la transmittance et l'épaisseur des films ont par exemple pu être augmentées par la formulation avec du PSTFSI utilisé comme additif.

Dans l'objectif d'une valorisation potentielle de telles encres polymères aqueuses de PEDOT:PSTFSI, nous avons consacré le chapitre 4 à l'étude leurs stabilités colloïdale et chimique. Pour ce faire, nous avons utilisé de nombreuses techniques de caractérisation de spectroscopie UV/Vis, Raman et XPS, ainsi que des analyses rhéologiques. Par exemple, il a été montré que les films de PEDOT:PSTFSI étaient stables sous atmosphère ambiante et à température élevée jusqu'à 190°C.

Dans le ***chapitre 5****, consacré à l'intégration de ces matériaux dans des dispositifs opto-électroniques, nous avons montré que les films de PEDOT:PSTFSI pouvaient jouer le rôle d'électrodes transparentes dans des cellules solaires organiques ou des diodes électroluminescentes organiques montrant des performances égales ou supérieures à celles des dispositifs de référence disposant d'une électrode en PEDOT:PSS ou en ITO dans le cas des dispositifs flexibles. Enfin, les électrodes de PEDOT:PSTFSI ont montré de bons résultats dans des transistors électrochimiques organiques lorsqu'ils étaient utilisés comme conducteurs ambivalents de trous et d'ions.*

Dans l'objectif de moduler les caractéristiques opto-électroniques des films à base de dispersions aqueuses de PEDOT:polyélectrolyte nous avons étudié toute une série de polyélectrolytes de types polysaccharides et polystyrenes substitués par des groupements bissulfonylimides. L'influence du groupement anionique ainsi que l'influence de la structures/rigidité des polyélectrolytes sur les complexes PEDOT:polyélectrolyte et donc sur les caractéristiques finales de leurs films minces ont été étudiées dans le ***chapitre 6****. Il ressort notamment que le complexe de type PEDOT:Poly(4-styrene bissulfonylimide) donne les meilleurs résultats en terme de compromis transmittance/conductivité électronique mais aussi que les complexes bio-sourcés à base de sulfate de dextrane sont très prometteurs pour le développement des dispersions PEDOT:polyelectrolyte biocompatibles et à bas coût.*

Bibliography

[1] A. J. Heeger, "Semiconducting and Metallic Polymers: The Fourth Generation of Polymeric Materials (Nobel Lecture)," *Angewandte Chemie International Edition*, vol. 40, no. 14, pp. 2591–2611, 2001.

[2] H. Do, M. Reinhard, H. Vogeler, A. Puetz, M. F. Klein, W. Schabel, A. Colsmann, and U. Lemmer, "Polymeric anodes from poly(3,4-ethylenedioxythiophene):poly(styrenesulfonate) for 3.5% efficient organic solar cells," *Thin Solid Films*, vol. 517, pp. 5900–5902, Aug. 2009.

[3] F. C. Krebs, "All solution roll-to-roll processed polymer solar cells free from indium-tin-oxide and vacuum coating steps," *Organic Electronics*, vol. 10, pp. 761–768, Aug. 2009.

[4] E. Ahlswede, W. Mühleisen, M. W. bin Moh Wahi, J. Hanisch, and M. Powalla, "Highly efficient organic solar cells with printable low-cost transparent contacts," *Applied Physics Letters*, vol. 92, pp. 143307–143307–3, Apr. 2008.

[5] C. Brabec, N. Sariciftci, and J. Hummelen, "Plastic solar cells," *Advanced Funtional Materials*, vol. 11, no. 1, pp. 15–26, 2001.

[6] S. K. Hau, H.-L. Yip, J. Zou, and A. K.-Y. Jen, "Indium tin oxide-free semi-transparent inverted polymer solar cells using conducting polymer as both bottom and top electrodes," *Organic Electronics*, vol. 10, pp. 1401–1407, Nov. 2009.

[7] Y. Xia, K. Sun, and J. Ouyang, "Solution-Processed Metallic Conducting Polymer Films as Transparent Electrode of Optoelectronic Devices," *Advanced Materials*, vol. 24, pp. 2436–2440, May 2012.

[8] Y. Kim, J. Lee, S. Hofmann, M. Gather, L. Müller-Meskamp, and K. Leo, "Achieving high efficiency and improved stability in ITO-free transparent organic light-emitting diodes with conductive polymer electrodes," *Advanced Functional Materials*, vol. 23, no. 30, pp. 3763–3769, 2013.

[9] L. Groenendaal, F. Jonas, D. Freitag, H. Pielartzik, and J. R. Reynolds, "Poly(3,4-ethylenedioxythiophene) and Its Derivatives: Past, Present, and Future," *Advanced Materials*, vol. 12, pp. 481–494, Apr. 2000.

[10] A. K. Havare, M. Can, S. Demic, M. Kus, and S. Icli, "The performance of OLEDs based on sorbitol doped PEDOT:PSS," *Synthetic Metals*, vol. 161, pp. 2734–2738, Jan. 2012.

[11] A. Argun, A. Cirpan, and J. Reynolds, "The First Truly All-Polymer Electrochromic Devices," *Advanced Materials*, vol. 15, pp. 1338–1341, Aug. 2003.

[12] J. Kawahara, P. A. Ersman, I. Engquist, and M. Berggren, "Improving the color switch contrast in PEDOT:PSS-based electrochromic displays," *Organic Electronics*, vol. 13, pp. 469–474, Mar. 2012.

[13] D. Khodagholy, J. Rivnay, M. Sessolo, M. Gurfinkel, P. Leleux, L. H. Jimison, E. Stavrinidou, T. Herve, S. Sanaur, R. M. Owens, and G. G. Malliaras, "High transconductance organic electrochemical transistors," *Nature Communications*, vol. 4, July 2013.

[14] S. Inal, J. Rivnay, A. I. Hofmann, I. Uguz, M. Mumtaz, D. Katsigiannopoulos, C. Brochon, E. Cloutet, G. Hadziioannou, and G. G. Malliaras, "Organic electrochemical transistors based on PEDOT with different anionic polyelectrolyte dopants," *Journal of Polymer Science Part B: Polymer Physics*, vol. 54, pp. 147–151, Oct. 2015.

[15] D. Khodagholy, T. Doublet, P. Quilichini, M. Gurfinkel, P. Leleux, A. Ghestem, E. Ismailova, T. Hervé, S. Sanaur, C. Bernard, and G. G. Malliaras, "In vivo recordings of brain activity using organic transistors," *Nature Communications*, vol. 4, p. 1575, Mar. 2013.

1 Fundamentals of Transparent Electrodes

Fundamental principles for the characterization of transparent electrodes are introduced. The properties of different inorganic and organic transparent electrode materials are discussed, as well as their respective advantages and drawbacks for the application in devices.

Ce chapitre fait un état de l'art d'électrodes transparentes organiques et/ou inorganiques qui sont passées en revue et évaluées par rapport à leurs avantages et inconvénients selon les technologies envisagées.

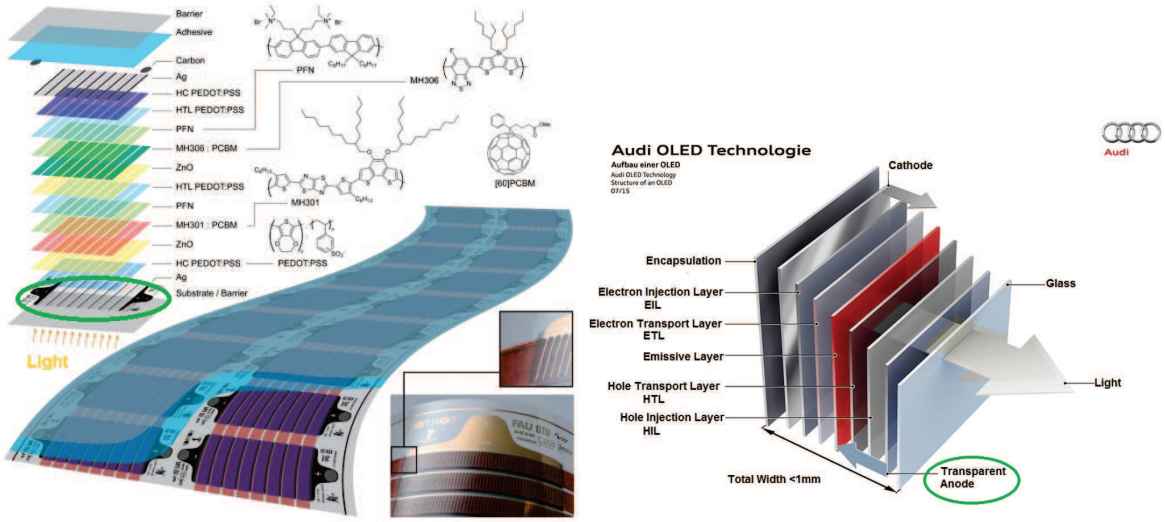

Fig. 1.1: Schematic structure of a roll-to-roll fabricated organic solar cell [1] and of an OLED, presented by Audi

1.1 Requirements and Characterization

As illustrated in figure 1.1, modern opto-electronic devices such as organic photovoltaics (OPVs) or organic light emitting diodes (OLEDs) are sandwich structures, comprising several layers, which allow the optimization of the device performance. Many different device architectures have been reported, but independently of the exact device structure, a common crucial component in all opto-electronic devices is an electrode, which is transparent in the visible regime and allows the in- or out-coupling of light.

Crucial characteristics of transparent electrodes are a low sheet resistance R_S and a high transmittance T in the visible regime, which is commonly measured at 550nm. As displayed in figure 1.2a, the graphical plot of the transmittance T as a function of the sheet resistance R_S for different film thicknesses allows the comparison of different transparent electrode materials. Materials with the "best" opto-electronic performance can be found in the top left of the graph, as indicated by the green box. For thin conducting films the sheet resistance R_S and the transmittance T can be related via [2]

$$T(\lambda) = (1 + \frac{188.5\sigma_{opt(\lambda)}}{R_S\sigma_{DC}})^{-2} \tag{1.1}$$

with $\sigma_{opt(\lambda)}$) being the optical conductivity at wavelength λ and σ_{DC} being the direct current (DC) conductivity. The DC conductivity is frequency independent and relates the current density $\overrightarrow{j}$ with the applied static electrical field $\overrightarrow{E}(\omega = 0)$ via the Ohm's law

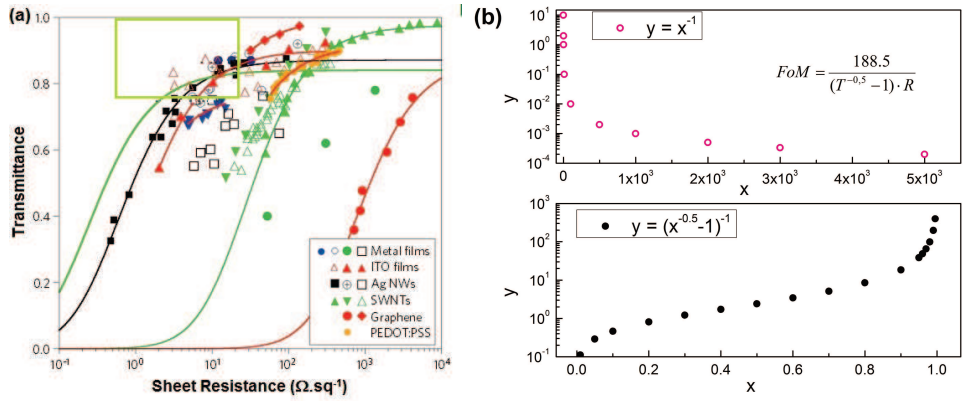

Fig. 1.2: a) Transmittance versus sheet resistance for transparent conducting films made of different materials [2] and b) plot of the dependencies of the FoM on the trasmittance T and on the sheet resistance R_S

$$\vec{j} = \sigma_{DC}\vec{E}. \tag{1.2}$$

The optical conductivity is the frequency dependent conductivity $\sigma(\omega)$ under the influence of an external alternating electromagnetic field $\vec{E}(\omega \neq 0)$, with ω in the optical frequency range. Using the Lambert-Beer's law $\sigma(\omega)$ can be related to the film transmission.

In order to facilitate the comparison of the opto-electronic properties of different materials with different film thicknesses the σ_{DC}/σ_{opt} ratio can be used as figure of merit (FoM) for transparent conducting films. Via transformation of equation 1.1 we obtain

$$FoM = \frac{\sigma_{DC}}{\sigma_{opt}} = \frac{188.5}{(\frac{1}{\sqrt{T}} - 1)R_S} \tag{1.3}$$

which shows that the FoM is maximized for high transmittance at low sheet resistance. The solid lines in figure 1.2a represent the calculated $R_S - T$ values for a constant FoM. However, it has to be taken into account, that the relation (1.1) was established for free standing films [2], whereas in experimental practice most transparent film are measured on glass or plastic substrates. Furthermore, the FoM diverges per definition for very high transmittance values >95% and extremely low sheet resistance values, as it is illustrated in figure 1.2, which shows plots of the dependencies of the FoM on R_S (pink curve) and on T (black curve).

Two other thickness independent measures, which are commonly used to characterize transparent electrodes are the conductivity σ and the absorption coefficient a, which can be calculated using

$$\sigma = \frac{1}{R_S d} \tag{1.4}$$

$$a = \frac{A}{d} = \frac{-log_{10}(T)}{d} \tag{1.5}$$

with R_S being the sheet resistance, T the transmittance, d the film thickness and A the absorbance.

Generally speaking, the device performance will be improved for a transparent electrode with maximum conductivity at minimum absorption. In order to be considered for industrial application, a transparent electrode material should show a sheet resistance of less than $100\Omega.sq^{-1}$ at more than 90% transmittance, which corresponds to a FoM of higher than 34 [3]. However, the specific requirements on the electrode performance depend strongly on the target application [4, 5]. For the fabrication of OLEDs, for instance, the decisive criterion is a high conductivity [4], whereas the integration in OPV devices necessitates a very high transparency [5].

Besides good opto-electronic properties, another crucial criterion for the integration in devices is the work function of the electrode material, which should be close to the HOMO level of the active layer material, in order to ensure efficient hole extraction (OPV) or injection (OLED), as exemplary illustrated in figure 1.3.

Further criteria are a smooth electrode surface, to avoid short circuits and high leakage currents, good chemical stability for long device lifetimes, easy and cost efficient processing as well as flexibility, for the application in flexible devices. The current inorganic bench mark material for transparent electrodes is the inorganic oxide indium tin oxide (ITO), which shows excellent opto-electronic properties and a suitable work function, but is costly in production, toxic and brittle. Therefore, alternative materials to ITO are needed to enable the large scale and low cost production of flexible organic electronic devices. An overview of different electrode materials and a brief discussion of their characteristics and respective advantages for the application in devices is given in the following chapter.

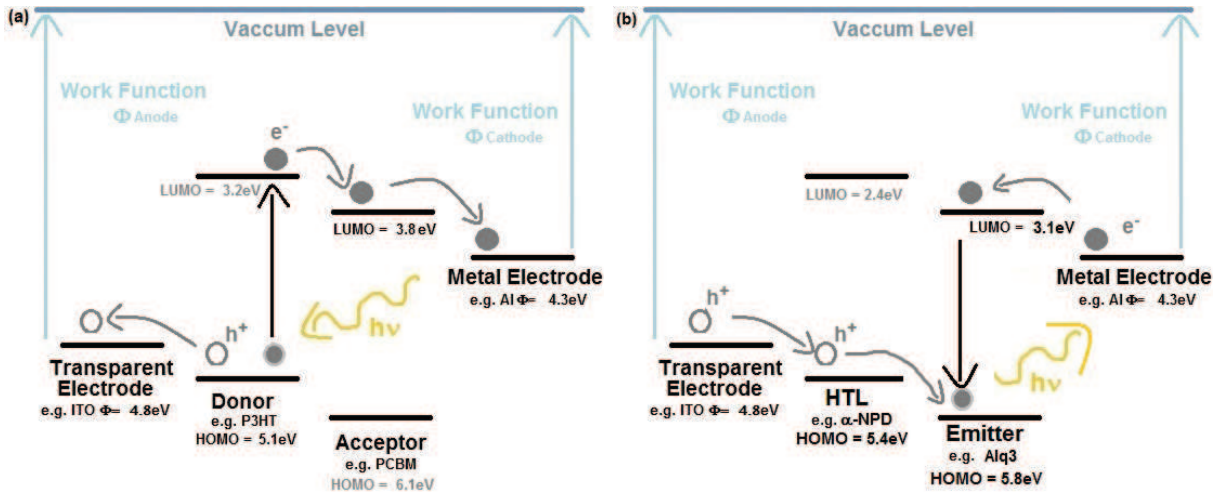

Fig. 1.3: Schematic diagram of the energy levels in an a)OPV device in case of a bulk hetero junction with a P3HT:PCBM active layer and an ITO transparent anode and an Al cathode (adapted from [6]) and b)OLED device with an α-NPD hole transport layer (HTL) and an Alq_3 emitting layer and an ITO transparent anode and an Al cathode (adapetd from [7])

1.2 Materials

1.2.1 Inorganic Transparent Conducting Films

Oxides

As already mentioned, ITO is the benchmark material for transparent electrodes. It is obtained by doping of indium oxide In_2O_3 with tin (Sn), which substitutes In cations in the In_2O_3 cubic bixbyite lattice (see figure 1.4). Upon reaction of tin with oxygen, the tin impurities can be found in different oxidation states, such as SnO and SnO_2, and electrons are released to the conduction band of ITO. This increases the charge carrier density in the conduction band and leads to an enhancement of the conductivity. Therefore Sn can be regarded as a n-type donor. ITO shows very high electric conductivity in the range of 10^4 S.cm^{-1} and a high charge carrier concentration in the range of 10^{21} cm^{-3} [8]. Due to a band gap bigger than 3.75eV its transmittance is very high in the visible range (>80% for 370nm< λ <1000nm) [8], which, together with its high conductivity, results in a FoM of up to 500. The work function of ITO is measured to be 4.8eV, which is a suitable value for the use as transparent electrode in organic photovoltaics [9]. In addition to these outstanding electrical and optical properties, the production of thin ITO films with controlled thickness and doping can be realized by different methods like sputtering,

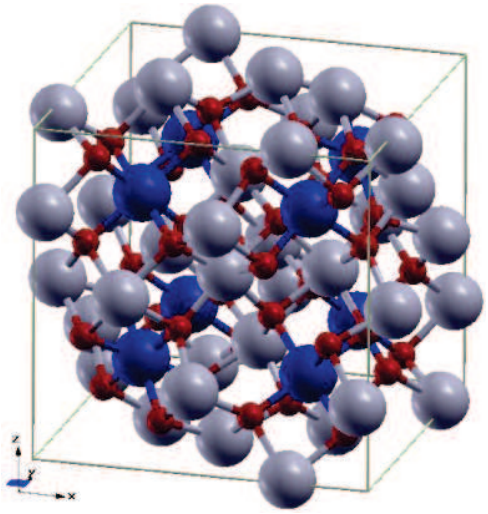

Figure 1.4: Cubic conventional cell of In_2O_3, with the blue, gray and red spheres representing the In^1, In^2 and O atoms [19], in which In sites are partially replaced by Sn ions in the case of ITO

thermal evaporation, ion beam assisted deposition or sol-gel processes [10]. This is why ITO is mainly chosen as material for transparent electrodes.

However, the use of ITO as transparent electrode involves several drawbacks. Limited availability of Indium [11] and complex processing render the production of ITO electrodes expensive [12]. Only recently one pot methods for the synthesis of ITO nano-crystal inks were reported, trying to render the fabrication of ITO films more simple [10]. Furthermore, ITO is environmentally hazardous and due to its ceramic nature ITO is not suitable for the application in flexible devices. Other problems of ITO electrodes in organic electronic devices are the diffusion of oxygen and indium into the active layer, which leads to the oxidation and degradation of the active layer material and shortens the lifetime of the devices [13, 14, 15, 16, 17], as well as its high surface roughness, which can be directly related to high leakage currents [18]. For this reasons, alternative materials, which can replace ITO as transparent electrodes, are of special interest for the development of flexible devices with long lifetimes.

One approach to replace ITO is the use of other metal oxides, which contain less Indium or no Indium at all, with the objective to reduce the toxicity of the material. Like ITO most of these metal oxides are n-type semiconductors.

Among the best studied oxides for replacing ITO are Titanium based oxides, especially TiO_2 in the anatase phase. Films made of TiO_2 doped with Fluorine (F), Niobium (Nb), Tantalum (Ta) or Tungsten (W) show resistivities in the range of 10^{-5} to 10^{-3} Ωcm at transparencies of about 95%. However, these films have to be produced by epitaxial growth, which makes them too expensive for broad base application [20, 21, 22, 23]. Also multi-component oxides based on Zn-In-Sn-O have been investigated [24]. Systems

such as ZnO-In_2O_3, In_2O_3-SnO_2 and $Zn_2In_2O_5 - In_4Sn_3O_{12}$ displayed film resistivities in the range of 10^{-4} Ωcm and flexible, amorphous Zn-In-Sn-O films showed a sheet resistance lower 20 $\Omega.sq^{-1}$ at 80% transmittance (FoM≈80) [24]. However, by varying the In content it was shown that the conductivity of Zn-In-Sn-O systems increase with increasing In_2O_3 content, leading to the conclusion that ITO shows the highest conductivity [25].

Transparent electrodes based on non-toxic ZnO display good opto-electronic properties and ZnO, which is heavily doped with Ga or Al, can even outperform ITO [11]. The thin transparent ZnO films can be fabricated by various methods, ranging from vapor deposition to sol-gel processes [26, 27]. However, the work function of untreated ZnO is about 4.3eV, which creates injection barriers to most materials in organic electronic devices. Therefore the ZnO work function has to be modified by surface treatments for the application of ZnO electrodes in devices [27]. In addition, ZnO is very sensitive to heat and humidity, which induce rapid degradation of the opto-electronic properties [11, 28, 25].

Furthermore, also metal-metal oxide composite structures have been investigated. For electrodes based on metal oxide-silver sandwich structures a sheet resistance as low as $3\Omega.sq^{-1}$ at 90% transmittance were reported (FoM≈1100) [29, 30, 31, 32] and solution processed transparent films made of Al doped ZnO and silver nanowires showed a sheet resistance of $11\Omega.sq^{-1}$ for a transparency higher than 93% (FoM≈460) [33, 34].

In summary, metal oxide thin films display extremely high conductivities and transparencies, which makes them attractive as transparent electrode material. However, they are not suitable for flexible applications, owing to their brittle nature. In addition, complex processing renders the production of these electrodes expensive. The non-toxic and solution processable ZnO, shows a too high work function and undergoes rapid degradation.

Metal grids and nanowires

Metals are known for their high conductivity, which results from the free electron character of the valence electrons. Furthermore, bulk metals are famous for their coloured and shiny appearance, which indicates that metals absorb in the visible range and are therefore not transparent. Therefore only ultra thin metal films with a thickness

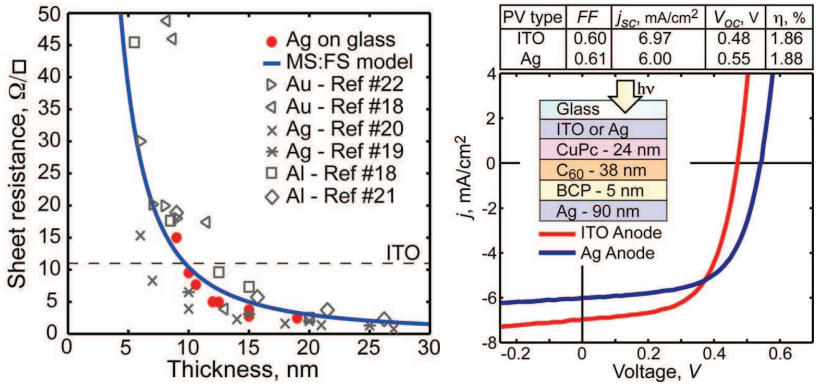

Fig. 1.5: Sheet resistance versus film thickness for thin Ag, Al and Au films compared to the sheet resistance of ITO (left) and IV characteristics of OPV devices under 106mW.cm^{-1} illumination with 9nm Ag and 150nm ITO anodes [39]

below 10nm become transparent. However, with decreasing thickness the resistivity of metal films increases due to electron scattering at the surface and grain boundaries [35]. Therefore a compromise between sufficient transparency and conductivity must be found in order to fabricate transparent metal electrodes.

Gold (Au), Chromium (Cr), Nickel (Ni) and Platinum (Pt) films with the thickness of some nanometers expose both a high conductivity and a high transparency and can compete with ITO films [36, 37, 38]. O'Connor *et al.* [39] reported, that a photovoltaic cell with a 9nm silver (Ag) electrode displayed even a slightly higher efficiency than the ITO reference cell (see figure 1.5). Schubert *et al.* [40] reported, that thin films evaporated from a Ca:Ag blend displayed a sheet resistance of 27Ω.sq^{-1} at 93% transmittance (FoM≈190). OPV devices based on these Ca:Ag electrode showed a higher efficiency than the ITO reference device, but underwent rapid degradation. Despite the good performance in devices, the application of ultra-thin metal films as electrodes faces problems due the fragility, costly production and the relatively high surface roughness of the thin metallic films.

A simple and cheap way to produce transparent conducting electrodes from metals is the fabrication of metal nanosize grids by nanoimprint lithography (see figure 1.6). By varying the thickness and the pattern size of the grid the conductivity and transmittance of the electrode can be tuned. However, for pattern dimensions in the range of the wavelength of visible light, interference effects have be considered, which can affect the

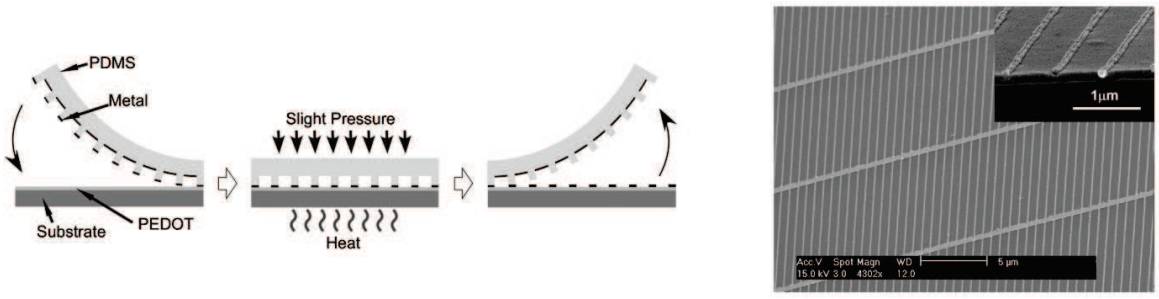

Fig. 1.6: Scheme of the fabrication of nano patterned Cu by nano imprinting using a PDMS stamp and SEM image of the Cu electrode on a PEDOT:PSS coated glass substrate [43]

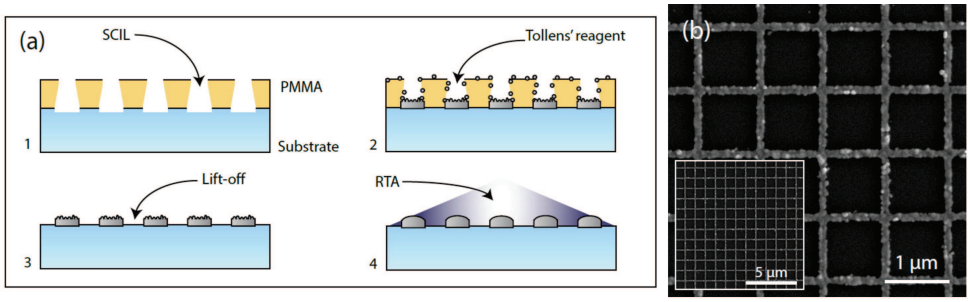

Fig. 1.7: a)Scheme for the fabrication of solution grown Ag nano structures and b)SEM image of the solution grown Ag network before rapid thermal annealing (RTA)[45]

transmittance of the electrode [41]. By optimization of the pattern dimensions, values of 70% or 84% transmittance in the visible range with a resistance of $4.79\Omega.\text{sq}^{-1}$ or $24\Omega.\text{sq}^{-1}$, respectively, can be obtained [42, 43, 44], which corresponds to a FoM of approximately 150. Upon integration in photovoltaic cells, the metal grid based devices exhibited the same performance as ITO reference cells [42, 43, 44].

More recently Sciacca *et al.* [45] reported the fabrication of patterned Ag electrodes, realized by a combination of soft imprint lithography and solution processing (see figure 1.7), which showed a higher conductivity than thermally evaporated networks. A top down method for the fabrication of micro structured metal electrodes consists in the patterning of thin metal films using three beam direct laser interference patterning [46]. With this technique Al electrodes with $25\Omega.\text{sq}^{-1}$ to $50\Omega.\text{sq}^{-1}$ at 81% transmittance were be obtained [47] (see figure 1.8).

Due to the good opto-electronic performance and cost efficient processing methods, the main problem for the application of patterned metal electrodes is their extremely high surface roughness.

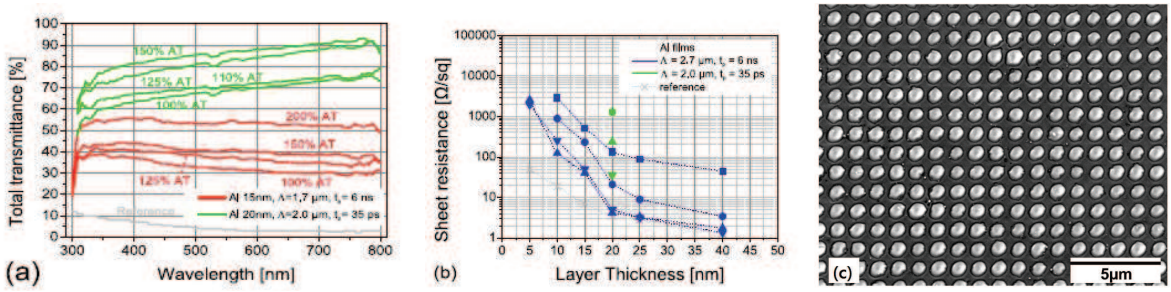

Fig. 1.8: a)Transmittance in the optical range, b)sheet resistance as a function of the film thickness and c)SEM image of a laser patterned Al film with a spatial pattern period of Λ*=1.7µm [47]*

Another approach to transparent, metallic electrodes is the fabrication of thin films from metal nanowires [5]. The metal nanowires used for this purpose show high aspect ratios with typical diameters smaller than 100nm and several micrometers in length. Most of the them are made of silver or copper, as these nanowires can be easily synthesized in solution via the reduction of silver nitrate or of copper ion complexes, respectively [48, 49, 50, 51, 52, 53, 54]. The obtained dispersion can then be directly coated on a substrate by roll-to-roll techniques, resulting in flexible films with promising electrical and optical properties, such as a sheet resistance of about $10\Omega.sq^{-1}$ - $13\Omega.sq^{-1}$ at 85% to 90% transmittance , corresponding to a FoM of 190 to 280 [55, 56, 57]. OPV devices based on such Ag nanowire electrodes showed very similar performance to the ITO reference devices [56]. Owing to their metallic character, the metal wires display high conductivities, so that the main resistivity of the nanowire films is caused by the resistivity of the inter-wire junctions [58]. Therefore, several approaches were developed to increase the film conductance by improving the wire to wire junction contact. The most common method is the thermal annealing of the films [56]. Mechanical pressing of the metal nanowire films results in a decrease in the sheet resistance [58], but is detrimental to the transparency of the films. Hu *et al.* reported that the junction resistance in Ag nanowire films was drastically decreased from $> 10G\Omega$ to 450Ω upon deposition of a thin gold layer on the wire network (see figure 1.9).

Furthermore, it was shown that the resistivity of Ag nanowire films can be decreased by immersion in graphene oxide dispersion, which supposedly decreased the contact resistance between the single Ag wires [59] (see figure 1.10). A similar approach was presented by Stapleton *et al.* [60], who found, that solution processed films of

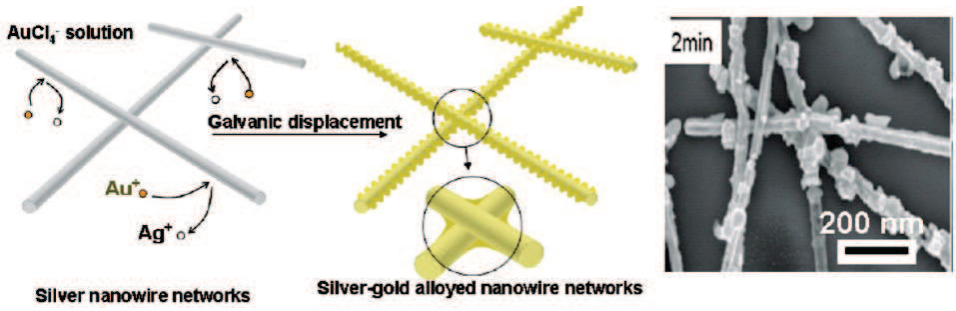

Fig. 1.9: Scheme for the galvanostatic deposition of Au on a Ag nanowire network and TEM images of the obtained AgNW-Au film

inter-woven Ag nanofibres and carbon nanotubes displayed a sheet resistance between $4\Omega.\text{sq}^{-1}$ to $24\Omega.\text{sq}^{-1}$ at 82% transparency. In these films the carbon nanotubes were found to wrap around the silver wires (see figure 1.10), which created conductive interconnections and increased, in addition, the mechanical stability of the film.

Another technique for the production of metal nanowires is electrospinning, which allows to produce nanowires of different metals with extremely high aspect ratios. By using a template network of soluble polymer fibers, on which Cu is evaporated, transparent Cu films with a sheet resistance of $9\Omega.\text{sq}^{-1}$ at 90% transmittance (FoM=387) were obtained [61]. Photovoltaic cells with copper nano network electrodes of $50\Omega.\text{sq}^{-1}$ at 90% transmittance (FoM=70), produced via annealing of electro-spun polymer/Cu-precursor fibers, reach efficiencies of 3%, which is comparable to cells with ITO electrode [62]. Furthermore, Hsu *et al.* [63] reported that, by combining Ag nanowire networks with meso scale Cu wires of 1 to 50μm, the sheet resistance of Ag nanowire films was drastically decreased down to $0.36\Omega.\text{sq}^{-1}$, while a high transmittance of 92% was maintained.

In analogy to the patterned metal electrodes, the main drawback for the application of these highly conducting and transparent metal nanowire films is their high surface roughness, which hinders good contact of the film to the active layer.

Therefore several approaches have been studied, how the surface can be flattened and the film adhesion can be increased. By coating of the nano wires with ZnO [64] or ITO nano-particles [65], the conductivity as well as the mechanical and thermal stability of the films can be enhanced (AgNW-ITO composite electrode: $30\Omega.\text{sq}^{-1}$ at 87% transmittance, FoM=87). Another common approach is the embedding of the rough nano-wire networks in polymers, which will be discussed in section 1.2.3.

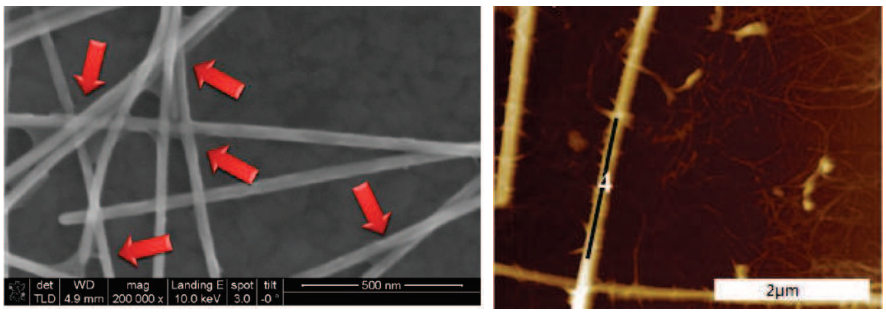

Fig. 1.10: SEM image of the Ag nanowire - graphene oxide film [59] (left) and AFM image of the Ag nanowire - carbon nanotube composite film [60]

1.2.2 Organic Alternatives

Graphene and Carbon Nanotubes

Graphene is a monolayer of graphite in which sp^2 hybridized carbon atoms form a 2D honeycomb structure. This bonding situation leads to 2D delocalized electrons which enable scattering free in plane charge carrier transport [12], resulting in an extremely high charge carrier mobility of about $2 \cdot 10^5$ cm^2.Vs [66]. Therefore the theoretical sheet resistance of a single graphene sheet is about $30\Omega.sq^{-1}$ [66], which renders graphene interesting for transparent electrode applications. However, the experimentally measured sheet resistance of graphene is commonly some hundreds of Ohms per layer, which is related to defects and grain boundaries in the single sheets. In graphene films composed of several sheets, the main resistivity arises from the sheet to sheet contacts [12]. The fabrication of graphene using the famous and simple scotch peel method is not suitable for the production of graphene on large scales. Therefore, the graphene sheets used for the fabrication of conducting electrodes are either synthesized by chemical vapor deposition (CVD) or from organic precursor molecules, which show large hexagonal carbon structures.

CVD grown graphene shows a sheet resistance of $230\Omega.sq^{-1}$ or higher, a maximum transmittance of 91% and is highly transparent in the infra-red regime [66]. The specific electrical and optical properties, however, depend on the synthesis conditions during the CVD process. It was found, that, for instance, the thickness of the graphene films increased with increasing process temperature. Choe *et al.* [67] reported, that graphene

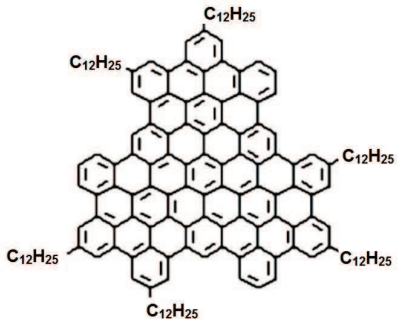

Fig. 1.11: Chemical structure of hexadodecyl-substituted superphenalene [72]

films grown at 1000°C displayed a sheet resistance of 600Ω.sq^{-1} at a transmittance of 87% (FoM=4), whereas films grown at 800°C were thinner and showed a sheet resistance of 1700Ω.sq^{-1} at 91% transmittance (FoM=2). The sheet resistance of CVD graphene sheets can be further reduced by chemical doping with $AuCl_3$, HNO_3 or $SOCl_2$ [68, 69, 70]. Kim *et al.* [70] observed a drop in the sheet resistance of graphene of 77% upon doping with $AuCl_3$ to 150Ω.sq^{-1} at 87% transmittance (FoM=17). This trend was confirmed by Park *et al.* [69] who found, that the doping of graphene electrodes with $AuCl_3$ resulted in a significant increase in the power conversion efficiency of OPV devices. More recently, Chen *et al.* [71] presented carbon enclosed CVD as novel method for the synthesis of graphene, by which graphene sheets with a sheet resistance of 5Ω.sq^{-1} at 93% transmittance (FoM=1020) were obtained.

Transparent graphene films can also be obtained from large organic precursor molecules, as reported by Wang *et al.* [72]. By thermal annealing of hexadodecyl-substituted superphenalene (see figure 1.11) at 1100°C on a quartz substrate under argon atmosphere, graphene films of 4nm and 30nm thickness were obtained, which displayed a conductivity of 206S.cm^{-1} (R_S(4nm)=12000Ω.sq^{-1}, R_S(30nm)=1600Ω.sq^{-1}) and a transmittance of 90% and 55% (at 500nm), respectively, which corresponds to a FoM of smaller than 1. Furthermore, it was shown that the conductivity of the obtained graphene was strongly affected by the nature of the substrate, so that the same process on SiO_2/Si resulted in graphene with a conductivity of 2000S.cm^{-1}.

Solution processing of graphene has been proven to be difficult, owing to its very stable π-bond system, which leads to strong inter-plane interactions and renders

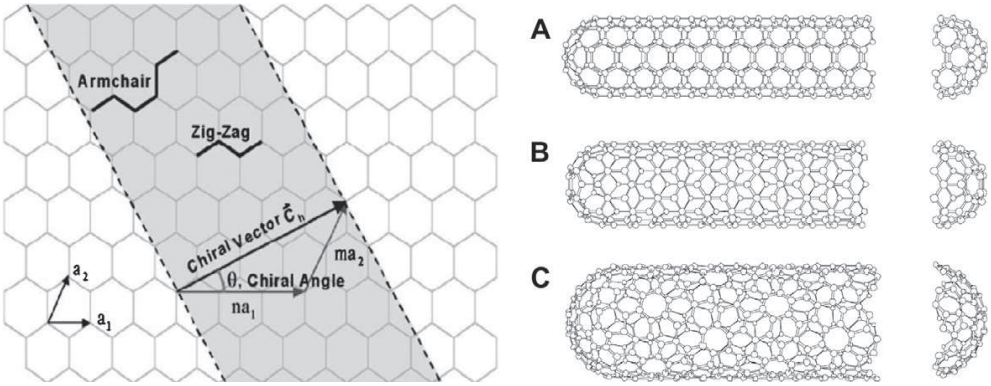

Fig. 1.12: Scheme of a carbon nanotubes with different chiralities [78]

graphene indispersible. One possibility to exfoliate and disperse graphene in a solvent is by functionalization, such as oxidation. However, graphene oxide shows a high resistivity, as the large structure of delocalized electrons is destroyed. Therefore, oxidized graphene films have to be reduced again before being used as electrodes. Films produced from functionalized graphene can show high transparencies, but due to incomplete reduction also the post treated films display very high resistivities of $800\Omega.sq^{-1}$ - $5k\Omega.sq^{-1}$ or more [73, 74, 75]. Thus, OPV devices with electrodes fabricated by solution processing of graphene oxide displayed poorer performance than ITO reference devices [74, 75].

Independently of the synthesis method and properties of the graphene, most devices with transparent graphene electrodes can hardly compete with ITO reference devices. This is not only related to the opto-electronic performance of the graphene sheets, but also to the properties of the electrode - active layer interface [76, 77, 69]. On the one hand, the graphene layers are rough and very hydrophobic, which leads to inhomogeneities with the adjacent hole injecting layer, such as PEDOT:PSS. On the other hand, graphene has a very low work function with respect to the active layer materials, which leads to poor charge collection and a high electrode resistance. Thus, the surface of graphene electrodes has to be modified, for instance by the deposition of MoO_3 layers [76, 77], in order to increase the device performance.

Another form of sp^2 hybridized carbon similar to graphene, are carbon nanotubes (CNTs). CNTs are artificial allotropes of carbon and consist of graphene sheets, which are rolled up to cylinders with an approximate diameter of one nanometer and whose ends are partly closed by fullerene like structures (see figure 1.12). With an extremely high aspect ratio up to 1000, CNTs are thought of as one dimensional material.

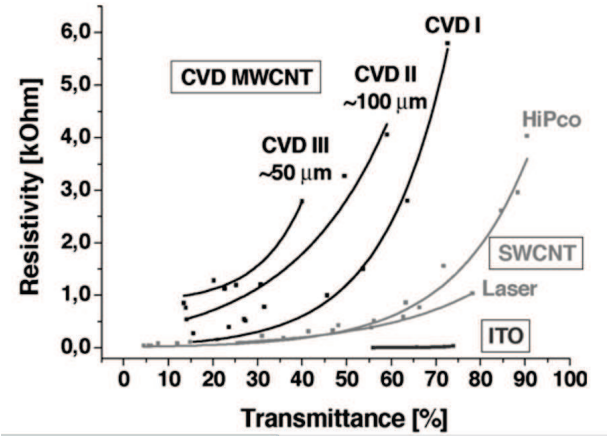

Fig. 1.13: Resistivity vs. transmittance of different spray coated MWCNT and SWCNT films and ITO [80]

However, CNTs are heterogeneous materials, which show differences in structure and opto-electronic properties (see figure 1.13) [78, 79, 80]. One of the main structural difference for CNTs is the number of sp^2 carbon sheets, which form the single tube. There are CNTs, which consist of only one rolled up graphene layer, called single walled carbon nanotubes (SWCNTs), and CNTs with several graphene layers, which interact via van der Waals forces, called multi walled carbon nanotubes (MWCNTs). Furthermore, the hexagonal network of the sp^2 carbon sheets can be arranged in different ways around the tube axis, which is described by the so called tube chirality [78, 79] (see figure 1.12).

Depending on their chirality CNTs display either semiconducting or metallic behavior. Metallic CNTs show similar band structures as metals and very high conductivities up to 10^5 S.cm^{-1}. However, metallic CNTs show, in analogy to bulk metals, high absorbance in the optical range, whereas semiconducting tubes are transparent. Furthermore, the optical transitions vary with the tube diameter, as the tube diameter is inversely proportional to the band gap of CNTs [81]. As in most production processes there is no specific chirality, which is preferentially formed, customary CNT samples contain semiconducting and metallic CNTs in the ratio 2:1. However, only the use of CNTs, which are monodisperse in electronic type and diameter, allows the fabrication of films with uniform electrical and optical properties, which are essential for the successful application in opto-electronic devices. Consequently, much effort is made to efficiently separate CNTs regarding to their electrical properties and

their diameter [82, 83, 78, 81, 84, 85].

Another challenge working with CNTs is their limited dispersability, caused by strong van der Waals forces between the tubes, which renders the fabrication of homogeneous thin films difficult. Attempts to disperse CNTs by sonication showed, that upon sonication the nanotubes tend to break into shorter pieces, which lowers the conductivity of the obtained films [86]. Another approach is to disperse CNTs by non-covalent functionalization of the CNT surface with surfactants, such as sodium dodecylsulfonate, or polymers, such as poly(3-hexylthiophene) (P3HT) or sodium carboxymethyl cellulose (CMC) [87, 86]. However, after film deposition these molecules are often difficult to remove.

Despite the difficult processing, CNTs are of interest for the fabrication of transparent electrodes, owing to their extremely high conductivity and a suitable work function in the range of 4.8eV to 5.1eV [88, 89].

The fabrication of transparent electrodes from double walled CNTs (DWCNTs) via solution processing was reported by Jeon *et al.* [90]. By optimization of the key factors of the system, such as the DWCNT length, their dispersion and the concentration of the dispersant CMC, films with a sheet resistance of $350\Omega.\text{sq}^{-1}$ at 94% transmittance (FoM=17) and a surface roughness R_q of 8 to 10nm were obtained. Electrodes made from SWCNTs via solution processing with CMC and doped by post-treatment with nitric acid, displayed a sheet resistance of $50\Omega.\text{sq}^{-1}$ and $150\Omega.\text{sq}^{-1}$ at 77% and 85% average transmittance (400nm - 1800nm) and a FoM of 27 and 15, respectively. The percolation threshold in these films was calculated to be extremely low with $0.011\mu\text{g.cm}^{-2}$. OPV devices based on a $60\Omega.\text{sq}^{-1}$ SWCNT transparent electrode and a P3HT:PCBM active layer displayed an efficiency of 3.1% [86].

Kaskela *et al.* [91] reported the fabrication of transparent SWCNT films by aerosol chemical vapor deposition, in which SWCNT are formed upon the thermal decomposition of ferrocene vapor in carbon monoxide atmosphere. After chemical doping with HNO_3 the transparent electrodes showed a sheet resistance of $110\Omega.\text{sq}^{-1}$ at 90% transmittance (FoM=32). Similar transparent electrodes fabricated by aerosol chemical vapor deposition were successfully integrated in OPVs and perovskite solar cells [90, 92]. However, the OPV devices showed only low efficiencies of 1.9% [90].

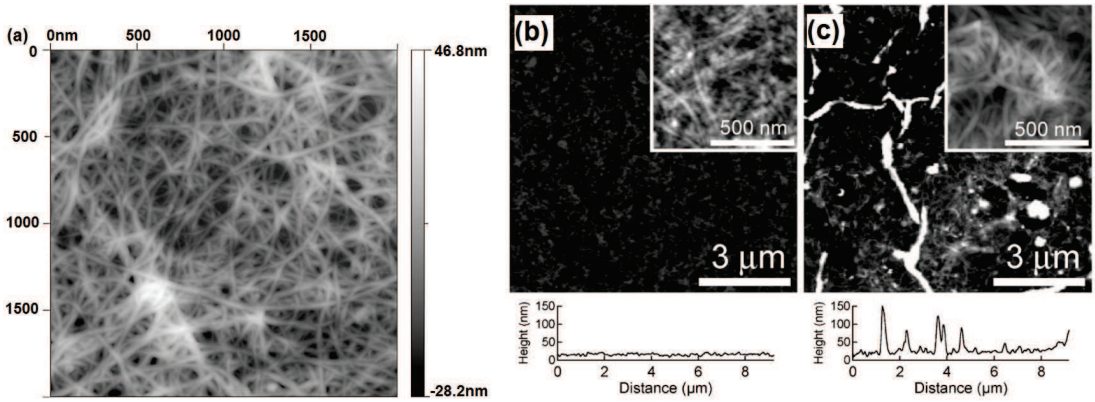

Fig. 1.14: AFM images of a SWCNT film prepared by a)spray coating from SDS dispersion [89], b)ultrasonic spray coating from CMC dispersion and treatment with HNO_3 [86] and c) vacuum filtration and membrane transfer from CMC dispersion and treatment with HNO_3 [86]

The low efficiency of devices with pure CNT electrodes can be explained by the high surface roughness and porosity of CNT electrodes (see figure 1.14), which causes bad contact between the electrode and the active layer, as well as diffusion of the active layer components such as P3HT:PCBM into the CNT film [89, 12]. A common approach to address this problem is the embedding of CNTs films in conducting polymers, which will be discussed in detail in section 1.2.3.

Furthermore, also carbon nanotube - graphene hybrid electrodes have been studied. Tung *et al.* [93], for instance, fabricated transparent hybrid films from CNTs and chemically converted graphene by solution processing, which showed a resistance of $240\Omega.sq^{-1}$ at 86% transmittance (FoM=10). Films made from SWCNT and CVD deposited graphene displayed a similar sheet resistance of $300\,\Omega.sq^{-1}$, but a much higher transmittance of 96%, resulting in a FoM of 30 [94]. Similar hybrid films made of MWCNT and CVD graphene were studied by Kholmanov *et al.* [95], who showed that the opto-electronic properties of the hybrid electrodes depended strongly on the process protocol, such as on the order in which the graphene and CNT layers are deposited. The integration of a SWCNT - graphene oxide hybrid system in an OPV device with P3HT/PCBM active layer was reported by Tu *et al.* [96]. This OPV device, comprising a SWCNT electrode and separate hole transporting interfacial layer of graphene oxide, showed power conversion efficiency of 3.1%.

To summarize it can be stated, that, despite the extremely high conductivity of CNTs and graphene, the opto-electronic properties of thin graphene and CNT films can not

compete with those of metal or metal oxide based transparent electrodes, which can be attributed to structural defects and high junction resistances. In addition, the solution processing of graphene and CNT was proven to be difficult, owing to the poor dispersability of the chemically inert carbon structure. Furthermore, the obtained graphene and CNT films show a high surface roughness, which is detrimental for the integration in devices.

Conducting polymers

Polymers are traditionally known as good insulating materials. Therefore, (semi)conducting polymers have attracted a great deal of attention as new class of materials and have been extensively studied since their discovery in the 1970s. The conductivity in conducting polymers is based on a conjugated π-electron system, which enables charge transport via delocalized electrons along the polymer backbone. Therefore the electronic properties depend strongly on the chemical structure of the polymer backbone. Even if the first polymer, in which conductivity was observed, is the linear polacethylene, most conducting polymers are aromatic, such as polyaniline (PANI), Polypyrrole (PPy), poly (para-phenylene) (PPP) and polythiophene (PT) and their substituted derivatives.

The electronic structure of these π-conjugated polymers can be described by a band structure, in which the energetically lower π band is completely filled, whereas the energetically higher energy band π^* is empty. Therefore most conducting polymers are actually semiconductors. Via doping of the polymer, for instance by oxidation, electronic states are generated in the band gap. At low oxidation (doping) levels radical cations, so called polarons, are formed on the polymer chain and represent localized states in the band diagram. Upon further oxidation spin-less di-cations, called bipolarons, are formed, which form, with increasing doping, bipolaronic bands in the energy gap (see figure 1.15). This doping process does not only render the polymer conducting, but also affects its optical properties, which become dominated by sub-band gap transitions. For the doping of a semiconducting polymer several processes can be used, including photochemical, interfacial or electrochemical reactions. The big

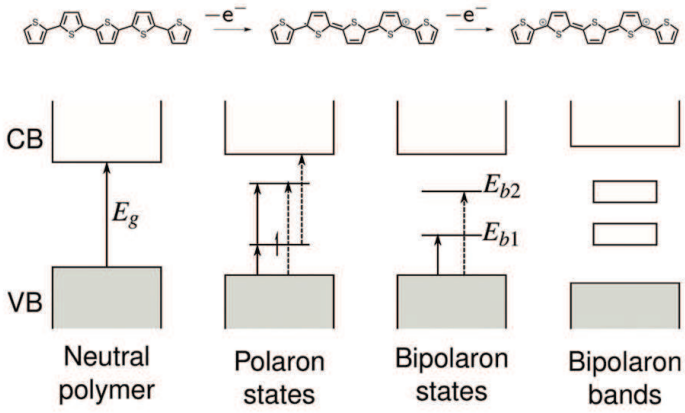

Fig. 1.15: Chemical structure of neutral, simple and double oxidized oligothiophene and schematic of the corresponding band diagram

advantages of conducting polymers compared to all other classes of conducting materials are their chemical and mechanical stability, their flexibility, bio-compatibility, and the possibility to process them on a large scale at ambient temperatures.

One of the most studied conducting polymers is PANI, which exist in several oxidation and protonation states (see figure 1.16), of which the most stable and conducting form is the emeraldine salt [97]. The conducting PANI is soluble in common organic solvents and absorbs in the range of 300nm to 500nm, which gives it a greenish color. Thin PANI films can be obtained by either chemical oxidation of aniline in acidic aqueous medium or by electro-polymerization and typically show a conductivity in the range of 5S.cm^{-1} to 20S.cm^{-1} [97, 98, 99, 100]. Especially in the early stages of the research on conducting polymers several attempts were made to fabricate PANI transparent electrodes [13, 101, 102, 103]. Heeger and coworkers [101] fabricated thin PANI films with 100Ω.sq^{-1} at 70% transmittance at 475nm to 675nm. A simple flexible OLED devices (PANI/MEH-PPV/Ca) with similar PANI electrodes showed a quantum efficiency of 1% and a turn on voltage of 1.8V [102]. The performance of the devices was limited by the low transmittance of electrodes, which leads to a drastic loss on the device efficiency [103]. In addition, the work function of PANI was reported to be 4.4eV [101], which is very low compared to commonly used active layer materials and results therefore in a high energy barrier and a high series resistance in the devices.

A more promising alternative to PANI for transparent electrodes is the substituted thiophene poly(3,4-ethylenedioxythiophene)(PEDOT) (see figure 1.17), which is highly

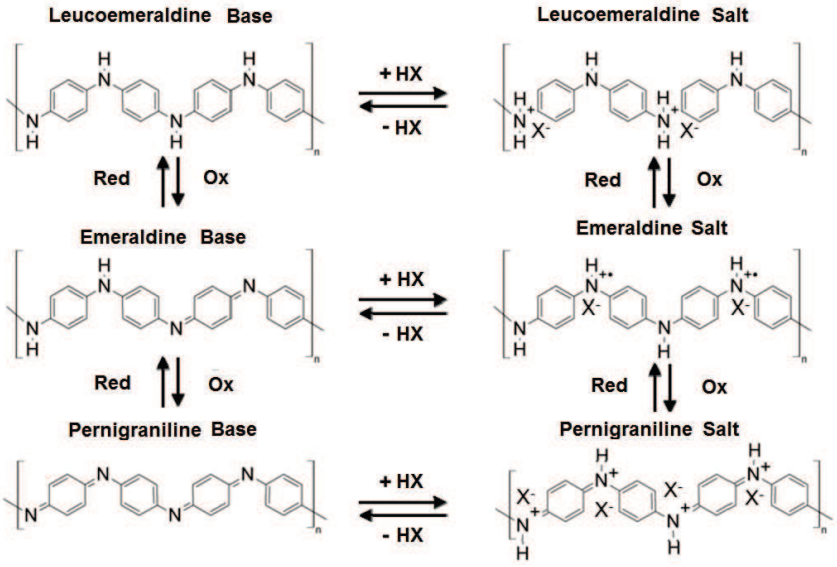

Fig. 1.16: Different oxidation and protonation states of polyaniline (PANI)

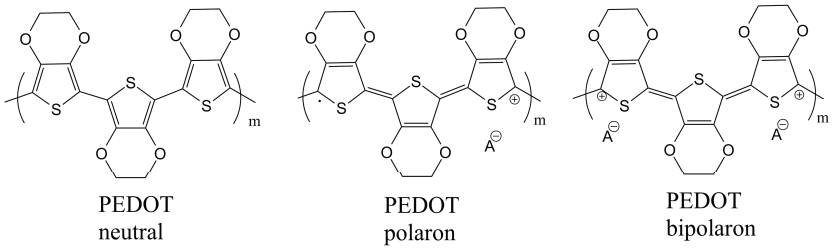

Fig. 1.17: Different oxidation states of poly(3,4-ethylenedioxythiophene) (PEDOT)

conducting and sky blue in the doped state. Doping of PEDOT is obtained by partial oxidation of the thiophene units and it has been shown that the optimized doping is reached for about 33% to 36% charged repeating units [104, 105, 97, 106, 107]. To counter balance the positive charges on PEDOT, anionic counter ions are integrated in the PEDOT structure. Depending on the nature and size of these counter ions, the structure and doping of the obtained PEDOT system can be affected [108].

The work function of PEDOT materials is reported to be between 4.8eV and 5.2eV [9, 109, 110, 111], which is close to the work function of ITO (4.8eV) and allows the use of PEDOT films as anode in organic electronic devices. A drawback for the application is, that PEDOT is not soluble in any known solvent. Therefore three main methods have been developed which allow the fabrication of conducting PEDOT films.

One possibility is the electro-polymerization of PEDOT films onto a conducting substrate. This process allows a good control of the oxidation level and the incorporation of different small or polymeric counter ions and results in transparent

films with a conductivity from 50S.cm^{-1} to 700S.cm^{-1} [112, 113, 114, 115, 116, 117, 108]. However, electro-polymerization is not possible on insulating substrates such as poly(ethylene terephtalate) (PET) and is not compatible with large scale printing production of organic electronic devices.

An alternative process is the oxidative polymerization of EDOT, which has been described in innumerable protocols, using different oxidants, counter ions, catalysts, temperatures and synthesis times [118, 119, 120, 121, 122, 123, 124, 125, 126, 106, 105]. One possibility is the in-situ oxidative polymerization of EDOT in liquid phase, for which the PEDOT film is directly polymerized from a solution containing the EDOT monomer and the oxidizing agents, such as $FeCl_3$, onto the substrate. By using a solution of EDOT and $FeCl_3$ in acetonitrile, Hohnholz *et al.* [127] obtained PEDOT:Cl films with a sheet resistance of 945Ω.sq^{-1}. However, it was shown that the conductivity can be significantly increased by choosing Fe(III)p-toluenesulfonate ($Fe(Tos)_3$) as oxidant, a low molecular weight alcohol, such as butanol, as solvent and by the addition of a weak base, such as imidazole or pyridine, which slows down the reaction kinetics [128, 126, 129, 130, 131]. From a solution of EDOT, $Fe(Tos)_3$ and imidazole in methanol Ha *et al.* [126] fabricated thin PEDOT:Tos films with a sheet resistance of 150Ω.sq^{-1} at a transmittance higher than 80% (FoM=11) and a conductivity of 900S.cm^{-1}. More recently Bubnova *et al.* reported an even higher conductivity of semi-crystalline PEDOT:Tos films of 1500S.cm^{-1} [130].

The same reaction, which is used for the liquid in-situ polymerization of EDOT, can also be performed in the vapor phase. For this process a substrate coated with a mixture of the oxidant, *e.g.* $Fe(Tos)_3$, and a base, such as pyridine, is exposed to EDOT vapors under ambient conditions or in vacuum [132], which results in the slow formation of a PEDOT:anion film on the substrate. In this way PEDOT:Tos films with extremely high conductivities of up to 3400S.cm^{-1} can be obtained, which show opto-electronic properties (R_S=45Ω.sq^{-1} at T>80%, FoM=35) that would allow the replacement of ITO films [133]. The integration of less conducting vapor polymerized PEDOT:Tos films, for instance with R_S=215Ω.sq^{-1} at T>84%, in OPV devices resulted in comparable device performance as the benchmark devices [134, 135]. An analogous route was presented by Gleason and co-workers [105], who obtained 100nm thick PEDOT films with a conductivity of 105S.cm^{-1} at 84% transmittance by exposing a substrate coated with

EDOT monomer to oxidants and pyridine vapors. However, the synthesis of PEDOT from vapor phase is time consuming and not straight forward to set up.

For the sake of simple processing, aqueous PEDOT dispersions have been developed, which make it possible to fabricate PEDOT thin films by various coating techniques, such as spin coating, roll-to-roll coating or printing. In order to stabilize the insoluble PEDOT in aqueous medium, the EDOT is polymerized in the presence of an anionic polyelectrolyte, which acts in the same time as counter ion, template and stabilizer for the doped PEDOT. The polyanion commonly used for this purpose is poly(styrenesulfonic)acid (PSS), which is the polymeric homolog of p-toluene sulfonic acid and which is transparent in the visible range. The resulting PEDOT:PSS dispersion shows excellent film-forming properties, flexibility, good thermal stability and a high transparency in the visible range. Upon drying of the PEDOT:PSS films PEDOT rich domains are formed, which are embedded in a PSS rich phase [136]. This insulating PSS phase represents an energy barrier for the charge transport in the film, so that PEDOT:PSS shows a much lower conductivity than PEDOT:Tos of only about 0.1S.cm^{-1} to 10S.cm^{-1} [122, 137, 138]. As this conductivity is far too low for an efficient application of PEDOT:PSS as transparent electrode in opto-electronic devices, a huge effort has been made to improve the conductivity of PEDOT:PSS by formulation and post-treatments.

It is well established that the conductivity of PEDOT:PSS can be enhanced for more than three orders of magnitude via formulation or post-treatment with high boiling point solvents, such as ethylene glycol (EG), diethylene glycol (DEG), dimethylsulfoxide (DMSO), N,N-dimethylformamide (DMF) or sorbitol [139, 140, 141, 142, 143, 144, 137, 130, 145, 111, 146, 139, 147]. PEDOT:PSS films, fabricated with different co-solvents showing conductivities of 300S.cm^{-1} to 600S.cm^{-1} (e.g. 80Ω.sq^{-1} at 74% transmittance, FoM=15), were successfully integrated as transparent electrode in flexible OPV devices [148, 149, 150]. The devices showed an efficiency of about 3%, which was comparable to the efficiency of the ITO reference devices [148, 149, 150] and the efficiency of was stable over 300 bending cycles [148]. Ouyang *et al.* [139] reported the integration of EG treated PEDOT:PSS electrodes (σ=160S.cm^{-1}) in OLEDs, which displayed an power efficiency of 1.5% and similar characteristics as the ITO reference device.

The underlying mechanism, which leads to the increase in conductivity, has been widely discussed, but is yet not fully understood. However, it was shown that the oxidation state of PEDOT was not affected and that the change in conductivity is related to morphological changes on the nanometric and micrometric scale. On the one hand, the presence of a high boiling point solvent induces a phase segregation of the PEDOT rich and the PSS rich phase, which leads to the growth of the PEDOT rich domains [146, 151], better percolation [146, 145, 143, 130, 137, 108] and the reduction of the PSS rich surface layer [137, 152, 143, 147]. In addition, the co-solvents can act as plasticizer, which incites the re-arrangement and better packing of the PEDOT chains [153, 111, 141, 152, 154, 155, 156].

Furthermore, it was reported that the treatment of PEDOT:PSS with certain salts, zwitterions and ionic liquids can induce a similar increase in the film conductivity [157, 158, 159, 160, 161, 162, 163]. This was explained by the charge screening effect of the ions, which weakens the PEDOT - PSS interactions and allow a re-arrangement of the polymer chains [158, 159, 160]. By using a treatment with methylammonium iodide in DMF Ouyang and co-workers [162] obtained PEDOT:PSS films with a conductivity of up to 2200S.cm^{-1}. The integration of such films into OPV devices revealed, that similar characteristics and performance can be obtained with highly conducting PEDOT:PSS electrodes as for ITO electrodes. Very similar results were presented by Badre *et al.* [163], who obtained PEDOT:PSS films with a sheet resistance of 31Ω.sq^{-1} at T>96% (σ=2084S.cm^{-1}, FoM=295), upon formulation of PEDOT:PSS with the ionic liquid 1-ethyl-3-methylimidazolium tetracyanoborate. However, potential residual ions which remain in the films will move through the film under the application of an electric field, which could influence the device performance.

Another approach to enhance the conductivity of PEDOT:PSS is the post coating treatment of PEDOT:PSS films with strong acids [157, 164, 165, 166]. Upon repeated rinsing with sulfuric acid PEDOT:PSS films with conductivities of higher than 3000S.cm^{-1} were obtained, which displayed metallic conduction behavior at room temperature [157]. OPV devices fabricated with H_2SO_4 treated PEDOT:PSS electrodes of 109nm thickness with R_S=39Ω.sq^{-1} and T>80%, displayed comparable characteristics and efficiencies as ITO reference devices[157]. However, the treatment with strong acids is not adapted to large scale processing, owing to the corrosivity of the

acids, which can damage other material involved in the process and raises safety issues during processing.

In conclusion, transparent conducting films based on PEDOT show very good opto-electronic properties with conductivities of up to 3000S.cm^{-1} and very high transparency, which are comparable to the characteristics of metal based transparent electrodes. In addition, the aqueous dispersion PEDOT:PSS allows the solution processing of conducting, thin, smooth and flexible films, which display comparable performance in devices as ITO reference electrodes. However, the use of PEDOT:PSS in devices was shown to accelerate device degradation, due to its hygroscopic and corrosive nature [167, 168, 169].

1.2.3 Composite Materials

A promising approach for high performance transparent electrodes are composite materials of carbon nanotubes or metal nano-structures and conducting polymers, as they combine the high conductivity of the nano-structures and the high transparency, flexibility and smooth surface of polymer films.
The fabrication process of metal nanowire - polymer composites commonly includes several steps. One possible fabrication method is the deposition of the metal nanowire film in the first step and the subsequent over-coating of the metal network with the transparent polymer [170, 171, 172]. Another possibility is the separate preparation of the two films, which are then laminated onto each other [173, 174, 175, 176]. As metal nanowire films show a very high conductivity, any transparent and flexible polymer can be used in the composite film in order to assure the mechanical stability of the electrode. Therefore several combinations of silver nanowire films with different polymers, such as polyimides [170], polymethacrylate [171], polyvinylacetate (PVA) [172] and polyurethane urea (PUU) - polydimethylsiloxane (PDMS) [32] have been studied. With these systems, typical sheet resistances of 8Ω.sq^{-1} to 10Ω.sq^{-1} at 80% transmittance (FoM 160 to 200) have been achieved [171, 176, 170]. By varying the density of the nanowire network it is possible to play on the transparency and conductivity of the films [176] (see figure 1.18). In order to reduce the cost of the integrated nanowires, the use of the more abundant

Cu is of interest. Promising results for the replacement of Ag by Cu nanowires were presented by Song *et al.* [174], who reported PDMS - Cu nanowire based composite electrodes with a sheet resistances of $62\Omega.sq^{-1}$ and 80% transmittance (FoM=26), which were integrated in highly flexible and stretchable OLED devices ($35lm.W^{-1}$, $57Cd.a^{-1}$, $10mA.m^{-2}$). For all metal nanowire composites, in which insulating polymers are used as matrix material, it is crucial, that the metal structure is exposed to the surface of the electrode, in order to ensure good electric contact with the active layer in devices. This can either be assured by choosing an appropriate fabrication process or by the post-treatment of the film by plasma etching, which removes polymer on the film surface [170]. Therefore, the use of insulating polymers as support for metal nanowires films enhances the mechanical stability of the films, but does not drastically decrease the surface roughness. However, by using a conducting polymer, such as PEDOT:PSS, as matrix material, the metal nano-structure can be fully embedded in a smooth film. In addition, PEDOT:PSS can provide electrical contact at the nanowires junctions, which allows to omit the thermal annealing step that is commonly used to improve the electrical contact between the single Ag wires [177]. McGehee and co-workers presented PEDOT:PSS - Ag nanowire composite elcetrodes, which were obtained by lamination of a Ag network on PEDOT:PSS films with different thicknesses [173] (see figure 1.19). These electrodes showed a very good opto-electronic performance with R_S=12 $\Omega.sq^{-1}$ at 86% transmittance (FoM=200) and good flexibility. By over-coating of a Ag nanowire network with PEDOT:PSS, composite electrodes with R_S=$14\Omega.sq^{-1}$ - 25 $\Omega.sq^{-1}$ and T> 80% were obtained [177, 178], which were successfully integrated in an A4-size touch screen panel [177] and OPV devices with an efficiency of 3.1% (ITO reference: 3.5%) [178]. Similar results were obtained for hydrothermally synthesized Cu nanowires embedded in PEDOT:PSS, which displayed a sheet resistance of $46\Omega.sq^{-1}$ at 93% transmittance, FoM=111 [179]. Apart from nanowire networks also metal nano-grids were successfully combined with PEDOT:PSS films. Kang *et al.* [180], for instance, fabricated a transparent composite electrode with R_S=$22\Omega.sq^{-1}$ at 78% transmittance (FoM=65) by roll-to-roll processing of a nano-imprinted Cu mesh on a PEDOT:PSS film, which showed comparable performance to ITO electrodes in OPV devices.

It has to be taken into account, that transparent metal nanowire electrodes are almost always coated with PEDOT:PSS upon integration into devices, as PEDOT:PSS

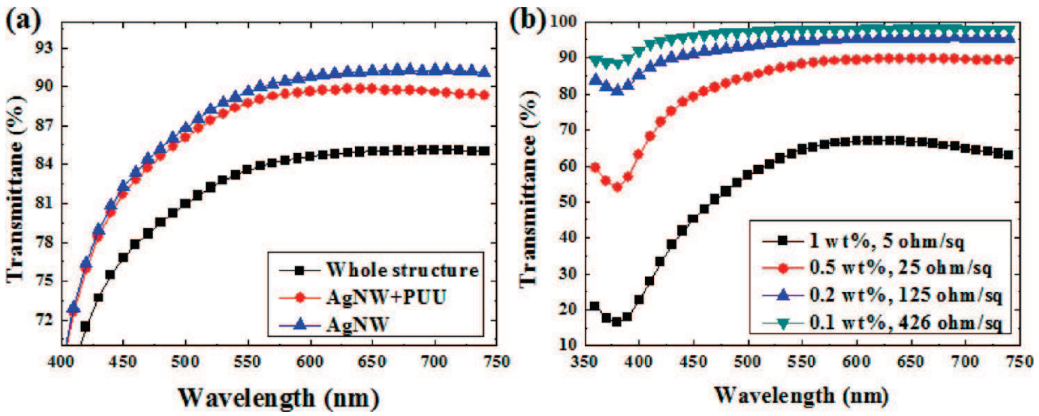

Fig. 1.18: Transmittance of the AgNW/PUU/PDMS film: (a) comparison of transmittance for AgNW/PUU/PDMS, AgNW/PUU, and AgNW layers ($R_S = 30\Omega.sq^{-1}$) and (b) effect of nanowire density on transmittance of AgNW layer [176])

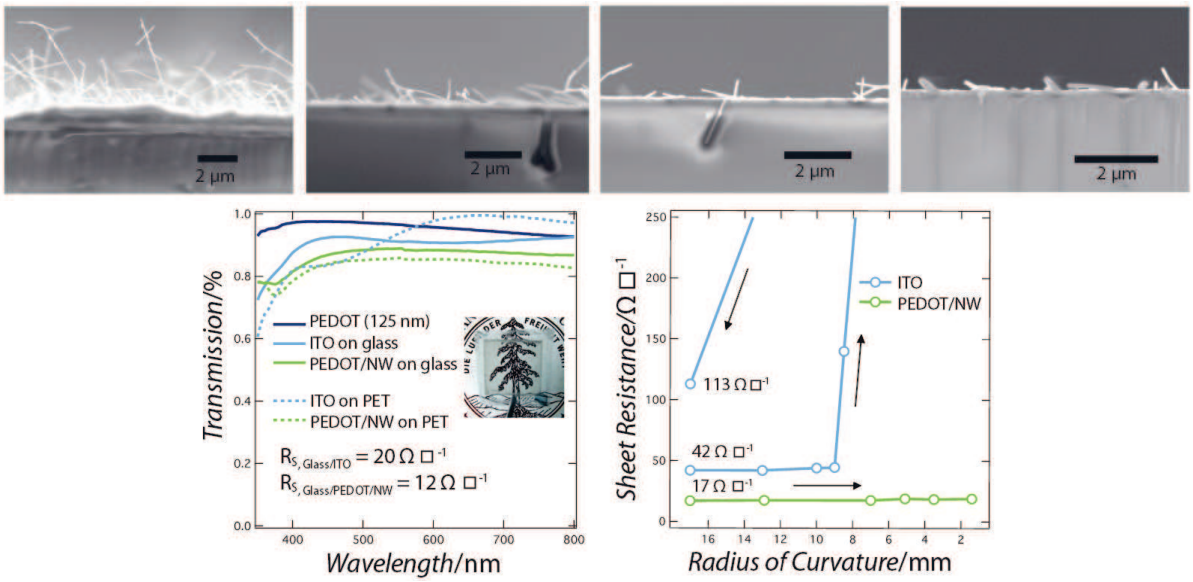

Fig. 1.19: SEM images of a Ag nanowire network laminated on PEDOT:PSS films of different thickness (top), transmission in the visible spectrum of ITO, PEDOT:PSS and Ag nanowire-PEDOT:PSS films and sheet resistance of an ITO and a Ag nanowire-PEDOT:PSS film as a function of bending radius[173]

is used as standard hole transport layer. In addition, it smoothens the surface of the metal film, which reduces the leakage current [172]. Therefore almost all electrodes presented in literature as metal nanowire electrodes can be actually seen as metal - conducting polymer composite systems [57].

Another extensively studied composite material are carbon nanotube (CNT) - conducting polymer composites. In these systems the CNTs represent the highly conducting component, whereas the polymer accounts for the processability, transparency and flexibility of the material. The main resistance of the macroscopic CNT films is caused by the junctions between the CNTs, which represent an energy barrier to the charge transport. Therefore the electronic properties of such CNT - polymer composites are strongly dependent on the concentration of the CNTs in the polymer matrix, which can be explained by the percolation theory [78]. At low CNT concentrations there are no continuous highly conducting paths through the film and the conductivity is dominated by the electrical properties of the polymer matrix. At a critical CNT concentration, called the percolation threshold, a continuous network of the highly conducting CNTs is formed and therefore the electrical conductivity of the composite jumps up. For higher CNT concentrations the conductivity saturates, as multiple conducting paths have already been formed. By using nano-structures with high aspect ratios the percolation threshold can be lowered, which is beneficial for the fabrication of highly transparent films.

A straight forward approach to the fabrication of CNT-polymer composite films is the mixing of the two components in dispersion, which allows the film fabrication in one coating step. By using this approach flexible SWCNT-PEDOT:PSS electrodes with typical sheet resistances of $80\Omega.\text{sq}^{-1}$ to $130\Omega.\text{sq}^{-1}$ at 75% transmittance (FoM=15) were obtained [3, 181, 182]. De *et al.* [3] reported that the opto-electronic performance was maximized for a SWCNT content of 60%, at which the composite film even outperformed the pure SWCNT in terms of the FoM (see figure 1.20). SWCNT-PEDOT:PSS electrodes fabricated by layer-by-layer coating of SWCNT and pristine PEDOT:PSS displayed a very similar performance [89, 183], which was strongly dependent on the quality of the SWCNT dispersion [183]. Despite their higher sheet resistance, the SWCNT-PEDOT:PSS composite electrodes outperformed the SWCNT

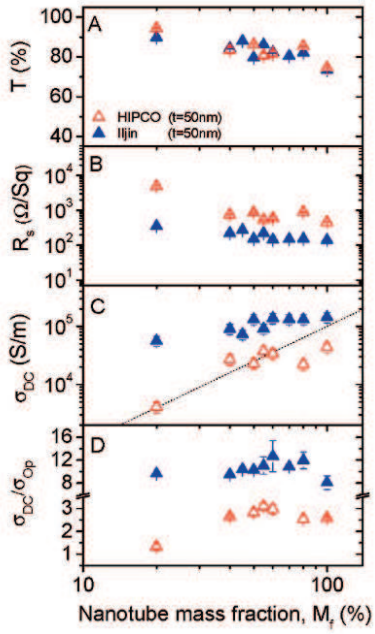

Figure 1.20: Opto-electronic properties of SWCNT-PEDOT:PSS composite films as a function of the SWCNT mass fraction [3]

electrodes in OPV devices, showing a power conversion efficiency of 1.5% and 0.5%, respectively [89], which was explained by a smoother electrode-active layer interface. Flexible OLEDs comprising SWCNT-PEDOT:PSS electrode showed a higher luminance than the ITO reference device for low driving voltages $< 15V$, which can be related to the higher work function of PEDOT:PSS compared to ITO. At higher driving voltage the composite device displayed lower luminance than the ITO device, owing to the higher sheet resistance of the SWCNT-PEDOT:PSS electrode [182].

Jo *et al.* reported that the sheet resistance of a SWCNT film was significantly decreased from $1250\Omega.sq^{-1}$ to $280\Omega.sq^{-1}$ upon vapor deposition of PEDOT:Tos on the SWCNT network. The beneficial effect of PEDOT:Tos on the film conductivity was explained by the formation of conducting PEDOT:Tos bridges between the SWCNTs. Via these bridges, the charge transfer from CNT to PEDOT to CNT allowed effective percolation, leading to a reduction of the sheet resistance [184] (see figure 1.21).

More recently Cho *et al.* presented a more complex composite system, composed of MWCNT, gold and PEDOT:PSS, which showed a far better opto-electronic performance than the approaches presented above, with a sheet resistance of $51\Omega.sq^{-1}$ at 86% transmittance, resulting in a FoM of 47. For the fabrication of these electrodes, gold nano-particles (AuNP) were synthesized on MWCNT using a polyol process. The AuNP covered MWCNT were subsequently dispersed in PEDOT:PSS containing 5%DMSO. After the film deposition by spin coating the films were treated with plasma

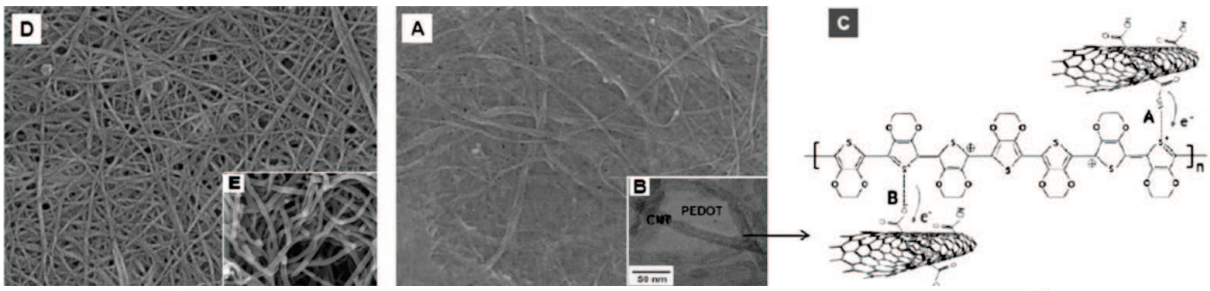

Sample	Conductivity; σ (S/cm)	Sheet resistance at 85% transmittance; R_s (Ω/sq.)
SWCNT(1) only	800	1250
SWCNT(2) only	285	3500
SWCNT(1):PEDOT(1:0.8) hybrid	2900	350
SWCNT(2):PEDOT(1:0.8) hybrid	1200	700

Fig. 1.21: a)SEM image, b)TEM image and c)schematic structure of a SWCNT-PEDOT:Tos composite film and d) SEM image, e) TEM image of pure SWCNT film and comparison of the opto-electronic properties of both systems (bottom) [184]

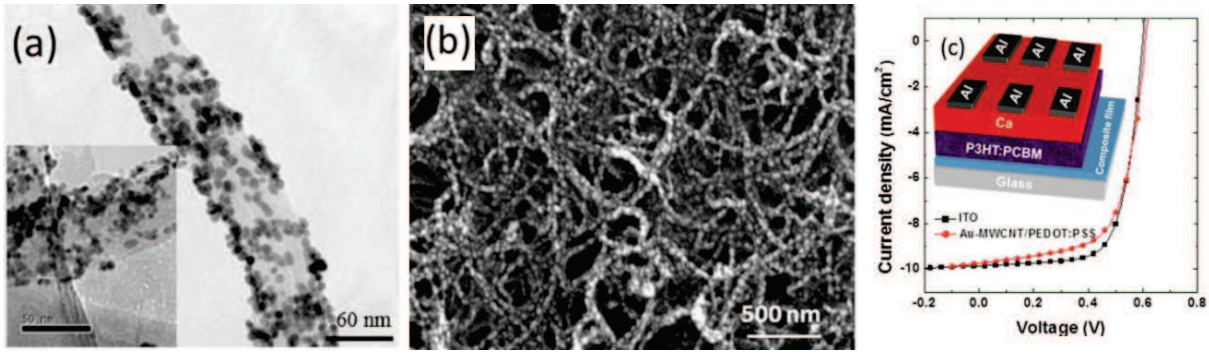

Fig. 1.22: a)TEM image of AuNP covered MWCNT, b)SEM image of a AuNP - MWCNT film after plasma treatment and c) IV characteristics and schematic structure of OPV devices with MWCNT-Au-PEDOT:PSS or ITO electrode [185]

irradiation leading to the fusion of the AuNP, which formed conducting bridges between the MWCNTs (see figure 1.22).

Apart from PEDOT:PSS, other conducting polymers have been investigated as matrix material for CNT composite electrodes. Both, Polyaniline (PANI) and polypyrrole (PPy), for instance, are cheap, flexible and show a high conductivity and are therefore interesting candidates for the fabrication of CNT-polymer composite electrodes. Ferrer- Anglada *et al.* [186] fabricated transparent CNT-PANI and CNT-PPy electrodes by electro-polymerization of PANI or PPy on CNT films. Upon the deposition of the conducting polymer layer on the CNT network, the conductivity of the films increased from 3-20S.cm^{-1} to up to 60S.cm^{-1} for film transmittance between 75% and 90%. Taking into account that the conductivity of the pure polymers is much

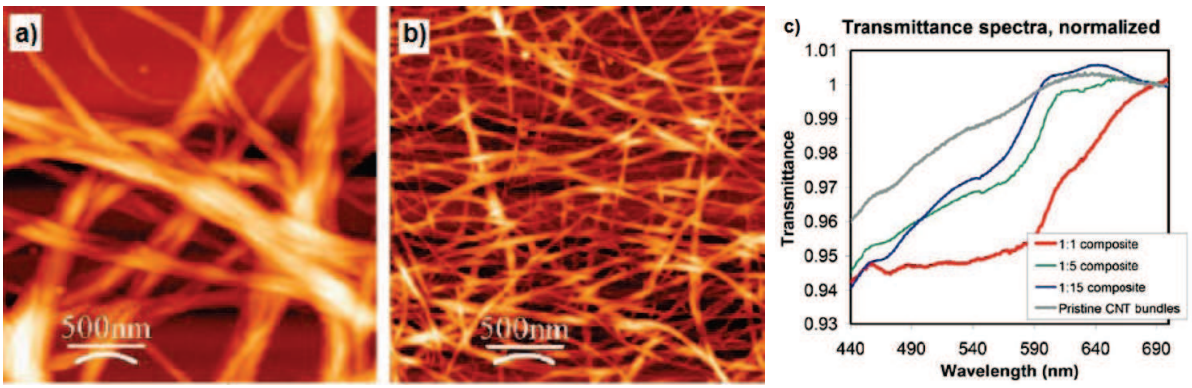

Fig. 1.23: AFM images of a)a pristine CNT film, b) a CNT-P3HT film with P3HT:CNT=15:1 and c)the transmittance of CNT-P3HT films in the visible range [187]

poorer than the conductivity of the pure nanotubes, the increasing conductivity of the composite was attributed to a decreasing contact resistance between the nanotubes.
The conjugated polymer poly(3-hexylthiophene-2,5-diyl)(P3HT), well known as active layer component in organic solar cells, was found to disperse CNTs in chlorinated solvents. This allows the solution processing of thin, transparent conducting CNT-P3HT composite films, as it was shown by Hellstrom *et al* [187] (see figure 1.23). After a post treatment with $SOCl_2$, which dopes the CNTs and removes excess polymer, the composite films displayed a sheet resistance of $170\Omega.sq^{-1}$ at 81% transmittance (FoM=10) and of 80 $\Omega.sq^{-1}$ at 72% transmittance (FoM=13) for P3HT to CNT ratios of 15:1 and 5:1, respectively.

1.2.4 Summary and Conclusion

The above presented materials show promising characteristics for the application as transparent conducting electrode in organic devices. Nevertheless, a breakthrough material has not been found yet. Metal oxides display excellent opto-electronic properties, but their brittleness makes them unsuitable for the integration in flexible devices. Furthermore, the need for low cost solutions and simple processing with high quality is another limiting factor for the broad base application of metal oxides. Metallic nano-structures, such as metal grids or metal nano-wires, allow the fabrication of thin and flexible films with an extremely low sheet resistance and good transparency. However, their high surface roughness and mechanical fragility renders the application difficult. Similar problems are encountered for carbon nanotube and graphene films. In addition, their opto-electronic are poorer, despite the extremely high conductivity of the

single carbon nano-structures, caused high junction resistances between the nano-structures. The big advantage of conducting polymer electrodes, mainly based on PEDOT, are their solution processability, extremely high flexibility and smooth surface roughness. For a long time their application was limited due to their insufficient opto-electronic properties. Recent developments, however, allow the fabrication of transparent polymer electrodes which can compete with CNT and metal nanowire electrodes in terms of the figure of merit. By combining metallic nano-structures with conducting polymers in hybrid films, the outstanding conductivity of the metal structure and the high transparency and mechanical stability of polymer result in thin films with excellent opto-electronic performance.

Inspired by the promising results for the conducting polymer PEDOT:PSS and by the simplicity of its processing, this work focuses on the development of aqueous conducting PEDOT:polyelectrolyte dispersions. A fundamental study of different the obtained PEDOT:polyelectrolyte dispersions and films allowed to gain a deeper understanding of these complex systems and to develop a pomising alternative material to PEDOT:PSS.

Bibliography

[1] T. R. Andersen, H. F. Dam, M. Hösel, M. Helgesen, J. E. Carlé, T. T. Larsen-Olsen, S. A. Gevorgyan, J. W. Andreasen, J. Adams, N. Li, F. Machui, G. D. Spyropoulos, T. Ameri, N. Lemaître, M. Legros, A. Scheel, D. Gaiser, K. Kreul, S. Berny, O. R. Lozman, S. Nordman, M. Välimäki, M. Vilkman, R. R. Søndergaard, M. Jørgensen, C. J. Brabec, and F. C. Krebs, "Scalable, ambient atmosphere roll-to-roll manufacture of encapsulated large area, flexible organic tandem solar cell modules," *Energy & Environmental Science*, vol. 7, p. 2925, June 2014.

[2] K. Ellmer, "Past achievements and future challenges in the development of optically transparent electrodes," *Nature Photonics*, vol. 6, pp. 809–817, Dec. 2012.

[3] S. De, P. E. Lyons, S. Sorel, E. M. Doherty, P. J. King, W. J. Blau, P. N. Nirmalraj, J. J. Boland, V. Scardaci, J. Joimel, and J. N. Coleman, "Transparent, Flexible, and Highly Conductive Thin Films Based on Polymer−Nanotube Composites," *ACS Nano*, vol. 3, no. 3, pp. 714–720, 2009.

[4] R. G. Gordon, "Criteria for choosing transparent conductors," *MRS bulletin*, vol. 25, no. 08, pp. 52–57, 2000.

[5] D. Langley, G. Giusti, C. Mayousse, C. Celle, D. Bellet, and J.-P. Simonato, "Flexible transparent conductive materials based on silver nanowire networks: a review," *Nanotechnology*, vol. 24, p. 452001, Nov. 2013.

[6] J. Y. Kim, K. Lee, N. E. Coates, D. Moses, T.-Q. Nguyen, M. Dante, and A. J. Heeger, "Efficient Tandem Polymer Solar Cells Fabricated by All-Solution Processing," *Science*, vol. 317, pp. 222–225, July 2007.

[7] M. Weis, T. Otsuka, D. Taguchi, T. Manaka, and M. Iwamoto, "Charge injection and accumulation in organic light-emitting diode with PEDOT:PSS anode," *Journal of Applied Physics*, vol. 117, p. 155503, Apr. 2015.

[8] C. Granqvist and A. Hultåker, "Transparent and conducting ITO films: new developments and applications," *Thin Solid Films*, vol. 411, pp. 1–5, May 2002.

[9] A. Solanki, "Effect of PEDOT:PSS Layer and ITO Ozonization in Arylenevinylene-<i>co</i>-Pyrrolenevinylene (AVPV) Based Solar Cell Devices," *Materials Sciences and Applications*, vol. 02, no. 12, pp. 1702–1707, 2011.

[10] J. Song, S. A. Kulinich, J. Li, Y. Liu, and H. Zeng, "A General One-Pot Strategy for the Synthesis of High-Performance Transparent-Conducting-Oxide Nanocrystal Inks for All-Solution-Processed Devices," *Angewandte Chemie*, vol. 127, pp. 472–476, Jan. 2015.

[11] H. Liu, V. Avrutin, N. Izyumskaya, . Özgür, and H. Morkoç, "Transparent conducting oxides for electrode applications in light emitting and absorbing devices," *Superlattices and Microstructures*, vol. 48, pp. 458–484, Nov. 2010.

[12] A. Kumar and C. Zhou, "The Race To Replace Tin-Doped Indium Oxide: Which Material Will Win?," *ACS Nano*, vol. 4, no. 1, pp. 11–14, 2010.

[13] S. A. Carter, M. Angelopoulos, S. Karg, P. J. Brock, and J. C. Scott, "Polymeric anodes for improved polymer light-emitting diode performance," *Applied Physics Letters*, vol. 70, pp. 2067–2069, Apr. 1997.

[14] F. Garten, A. Hilberer, F. Cacialli, E. Esselink, Y. van Dam, B. Schlatmann, R. H. Friend, T. M. Klapwijk, and G. Hadziioannou, "Efficient blue LEDs from a partially conjugated Si-containing PPV copolymer in a double-layer configuration," *Advanced Materials*, vol. 9, pp. 127–131, Feb. 1997.

[15] M. P. de Jong, D. P. L. Simons, M. A. Reijme, L. J. van IJzendoorn, A. W. Denier van der Gon, M. J. A. de Voigt, H. H. Brongersma, and R. W. Gymer, "Indium diffusion in model polymer light-emitting diodes," *Synthetic Metals*, vol. 110, pp. 1–6, Mar. 2000.

[16] S. T. Lee, Z. Q. Gao, and L. S. Hung, "Metal diffusion from electrodes in organic light-emitting diodes," *Applied Physics Letters*, vol. 75, pp. 1404–1406, Sept. 1999.

[17] D. E. Gallardo, C. Bertoni, S. Dunn, N. Gaponik, and A. Eychmüller, "Cathodic and Anodic Material Diffusion in Polymer/Semiconductor-Nanocrystal Composite Devices," *Advanced Materials*, vol. 19, pp. 3364–3367, Oct. 2007.

[18] Y.-H. Tak, K.-B. Kim, H.-G. Park, K.-H. Lee, and J.-R. Lee, "Criteria for ITO (indium–tin-oxide) thin film as the bottom electrode of an organic light emitting diode," *Thin Solid Films*, vol. 411, pp. 12–16, May 2002.

[19] Z. R. Xiao, X. F. Fan, L. X. Guan, C. H. A. Huan, J. L. Kuo, and L. Wang, "First-principles study of the magnetization of oxygen-depleted In 2 O 3 (001) surfaces," *Journal of Physics: Condensed Matter*, vol. 21, no. 27, p. 272202, 2009.

[20] Y. Furubayashi, T. Hitosugi, Y. Yamamoto, K. Inaba, G. Kinoda, Y. Hirose, T. Shimada, and T. Hasegawa, "A transparent metal: Nb-doped anatase TiO2," *Applied Physics Letters*, vol. 86, pp. 252101–252101–3, June 2005.

[21] D.-m. Chen, G. Xu, L. Miao, S. Nakao, and P. Jin, "Sputter deposition and computational study of M-TiO2 (M=Nb, Ta) transparent conducting oxide films," *Surface and Coatings Technology*, vol. 206, pp. 1020–1023, Nov. 2011.

[22] U. Takeuchi, A. Chikamatsu, T. Hitosugi, H. Kumigashira, M. Oshima, Y. Hirose, T. Shimada, and T. Hasegawa, "Transport properties and electronic states of anatase Ti1−xWxO2 epitaxial thin films," *Journal of Applied Physics*, vol. 107, pp. 023705–023705–4, Jan. 2010.

[23] S. Mohri, Y. Hirose, S. Nakao, N. Yamada, T. Shimada, and T. Hasegawa, "Transparent conductivity of fluorine-doped anatase TiO2 epitaxial thin films," *Journal of Applied Physics*, vol. 111, pp. 093528–093528–5, May 2012.

[24] N. Zhou, D. B. Buchholz, G. Zhu, X. Yu, H. Lin, A. Facchetti, T. J. Marks, and R. P. H. Chang, "Ultraflexible Polymer Solar Cells Using Amorphous Zinc−Indium−Tin Oxide Transparent Electrodes," *Advanced Materials*, vol. 26, pp. 1098–1104, Feb. 2014.

[25] T. Minami, "Substitution of transparent conducting oxide thin films for indium tin oxide transparent electrode applications," *Thin Solid Films*, vol. 516, pp. 1314–1321, Feb. 2008.

[26] H. Nanto, T. Minami, S. Shooji, and S. Takata, "Electrical and optical properties of zinc oxide thin films prepared by rf magnetron sputtering for transparent electrode applications," *Journal of Applied Physics*, vol. 55, pp. 1029–1034, Feb. 1984.

[27] I. Lange, S. Reiter, J. Kniepert, F. Piersimoni, M. Pätzel, J. Hildebrandt, T. Brenner, S. Hecht, and D. Neher, "Zinc oxide modified with benzylphosphonic acids as transparent electrodes in regular and inverted organic solar cell structures," *Applied Physics Letters*, vol. 106, p. 113302, Mar. 2015.

[28] T. Minami, "Present status of transparent conducting oxide thin-film development for Indium-Tin-Oxide (ITO) substitutes," *Thin Solid Films*, vol. 516, pp. 5822–5828, July 2008.

[29] C.-H. Lee, R. Pandey, B.-Y. Wang, W.-K. Choi, D.-K. Choi, and Y.-J. Oh, "Nano-sized indium-free MTO/Ag/MTO transparent conducting electrode prepared by RF sputtering at room temperature for organic photovoltaic cells," *Solar Energy Materials and Solar Cells*, vol. 132, pp. 80–85, Jan. 2015.

[30] D. R. Sahu, S.-Y. Lin, and J.-L. Huang, "ZnO/Ag/ZnO multilayer films for the application of a very low resistance transparent electrode," *Applied Surface Science*, vol. 252, pp. 7509–7514, Aug. 2006.

[31] C. Guillén and J. Herrero, "ITO/metal/ITO multilayer structures based on Ag and Cu metal films for high-performance transparent electrodes," *Solar Energy Materials and Solar Cells*, vol. 92, pp. 938–941, Aug. 2008.

[32] A. Kim, Y. Won, K. Woo, C.-H. Kim, and J. Moon, "Highly Transparent Low Resistance ZnO/Ag Nanowire/ZnO Composite Electrode for Thin Film Solar Cells," *ACS Nano*, vol. 7, pp. 1081–1091, Feb. 2013.

[33] A. Kim, Y. Won, K. Woo, S. Jeong, and J. Moon, "All-Solution-Processed Indium-Free Transparent Composite Electrodes based on Ag Nanowire and Metal Oxide for Thin-Film Solar Cells," *Advanced Functional Materials*, vol. 24, pp. 2462–2471, May 2014.

[34] K. Zilberberg, F. Gasse, R. Pagui, A. Polywka, A. Behrendt, S. Trost, R. Heiderhoff, P. Görrn, and T. Riedl, "Highly Robust Indium-Free Transparent Conductive Electrodes Based on Composites of Silver Nanowires and Conductive Metal Oxides," *Advanced Functional Materials*, vol. 24, pp. 1671–1678, Mar. 2014.

[35] L. Hu, H. Wu, and Y. Cui, "Metal nanogrids, nanowires, and nanofibers for transparent electrodes," *MRS Bulletin*, vol. 36, pp. 760–765, Oct. 2011.

[36] D. S. Ghosh, L. Martinez, S. Giurgola, P. Vergani, and V. Pruneri, "Widely transparent electrodes based on ultrathin metals," *Optics Letters*, vol. 34, p. 325, Jan. 2009.

[37] R. A. Hatton, M. R. Willis, M. A. Chesters, and D. Briggs, "A robust ultrathin, transparent gold electrode tailored for hole injection into organic light-emitting diodes," *Journal of Materials Chemistry*, vol. 13, pp. 722–726, Mar. 2003.

[38] S. Conoci, S. Petralia, P. Samorì, F. M. Raymo, S. Di Bella, and S. Sortino, "Optically Transparent, Ultrathin Pt Films as Versatile Metal Substrates for Molecular Optoelectronics," *Advanced Functional Materials*, vol. 16, pp. 1425–1432, July 2006.

[39] B. O'Connor, C. Haughn, K.-H. An, K. P. Pipe, and M. Shtein, "Transparent and conductive electrodes based on unpatterned, thin metal films," *Applied Physics Letters*, vol. 93, pp. 223304–223304–3, Dec. 2008.

[40] S. Schubert, L. Müller-Meskamp, and K. Leo, "Unusually High Optical Transmission in Ca:Ag Blend Films: High-Performance Top Electrodes for Efficient Organic Solar Cells," *Advanced Functional Materials*, vol. 24, pp. 6668–6676, Nov. 2014.

[41] P. B. Catrysse and S. Fan, "Nanopatterned Metallic Films for Use As Transparent Conductive Electrodes in Optoelectronic Devices," *Nano Letters*, vol. 10, pp. 2944–2949, Aug. 2010.

[42] M.-G. Kang and L. J. Guo, "Nanoimprinted Semitransparent Metal Electrodes and Their Application in Organic Light-Emitting Diodes," *Advanced Materials*, vol. 19, no. 10, pp. 1391–1396, 2007.

[43] M.-G. Kang, M.-S. Kim, J. Kim, and L. J. Guo, "Organic Solar Cells Using Nanoimprinted Transparent Metal Electrodes," *Advanced Materials*, vol. 20, pp. 4408–4413, Dec. 2008.

[44] J. Zou, H.-L. Yip, S. K. Hau, and A. K.-Y. Jen, "Metal grid/conducting polymer hybrid transparent electrode for inverted polymer solar cells," *Applied Physics Letters*, vol. 96, p. 203301, May 2010.

[45] B. Sciacca, J. van de Groep, A. Polman, and E. C. Garnett, "Solution-Grown Silver Nanowire Ordered Arrays as Transparent Electrodes," *Advanced Materials*, vol. 28, pp. 905–909, Feb. 2016.

[46] L. Müller-Meskamp, S. Schubert, T. Roch, S. Eckhardt, A.-F. Lasagni, and K. Leo, "Transparent Conductive Metal Thin-Film Electrodes Structured by Direct Laser Interference Patterning," *Advanced Engineering Materials*, vol. 17, pp. 1215–1219, Aug. 2015.

[47] S. Eckhardt, M. Siebold, and A. F. Lasagni, "Laser microstructured metal thin films as promising alternative for indium based transparent electrodes," *Optics Express*, vol. 24, p. A553, Mar. 2016.

[48] J. Jiu, T. Araki, J. Wang, M. Nogi, T. Sugahara, S. Nagao, H. Koga, K. Suganuma, E. Nakazawa, M. Hara, H. Uchida, and K. Shinozaki, "Facile synthesis of very-long silver nanowires for transparent electrodes," *Journal of Materials Chemistry A*, vol. 2, no. 18, p. 6326, 2014.

[49] F. Cui, Y. Yu, L. Dou, J. Sun, Q. Yang, C. Schildknecht, K. Schierle-Arndt, and P. Yang, "Synthesis of Ultrathin Copper Nanowires Using Tris(trimethylsilyl)silane for High-Performance and Low-Haze Transparent Conductors," *Nano Letters*, vol. 15, pp. 7610–7615, Nov. 2015.

[50] M. Mohl, P. Pusztai, A. Kukovecz, Z. Konya, J. Kukkola, K. Kordas, R. Vajtai, and P. M. Ajayan, "Low-Temperature Large-Scale Synthesis and Electrical Testing of Ultralong Copper Nanowires," *Langmuir*, vol. 26, pp. 16496–16502, Nov. 2010.

[51] W. Wang, G. Li, and Z. Zhang, "A facile templateless, surfactantless hydrothermal route to ultralong copper submicron wires," *Journal of Crystal Growth*, vol. 299, pp. 158–164, Feb. 2007.

[52] A. R. Rathmell and B. J. Wiley, "The Synthesis and Coating of Long, Thin Copper Nanowires to Make Flexible, Transparent Conducting Films on Plastic Substrates," *Advanced Materials*, vol. 23, pp. 4798–4803, Nov. 2011.

[53] F. Meng and S. Jin, "The Solution Growth of Copper Nanowires and Nanotubes is Driven by Screw Dislocations," *Nano Letters*, vol. 12, pp. 234–239, Jan. 2012.

[54] D. Zhang, R. Wang, M. Wen, D. Weng, X. Cui, J. Sun, H. Li, and Y. Lu, "Synthesis of Ultralong Copper Nanowires for High-Performance Transparent Electrodes," *Journal of the American Chemical Society*, vol. 134, pp. 14283–14286, Sept. 2012.

[55] S. De, T. M. Higgins, P. E. Lyons, E. M. Doherty, P. N. Nirmalraj, W. J. Blau, J. J. Boland, and J. N. Coleman, "Silver Nanowire Networks as Flexible, Transparent, Conducting Films: Extremely High DC to Optical Conductivity Ratios," *ACS Nano*, vol. 3, pp. 1767–1774, July 2009.

[56] J.-Y. Lee, S. T. Connor, Y. Cui, and P. Peumans, "Solution-Processed Metal Nanowire Mesh Transparent Electrodes," *Nano Letters*, vol. 8, pp. 689–692, Feb. 2008.

[57] J. Krantz, M. Richter, S. Spallek, E. Spiecker, and C. J. Brabec, "Solution-Processed Metallic Nanowire Electrodes as Indium Tin Oxide Replacement for Thin-Film Solar Cells," *Advanced Functional Materials*, vol. 21, pp. 4784–4787, Dec. 2011.

[58] L. Hu, H. S. Kim, J.-Y. Lee, P. Peumans, and Y. Cui, "Scalable Coating and Properties of Transparent, Flexible, Silver Nanowire Electrodes," *ACS Nano*, vol. 4, pp. 2955–2963, May 2010.

[59] J. Liang, L. Li, K. Tong, Z. Ren, W. Hu, X. Niu, Y. Chen, and Q. Pei, "Silver Nanowire Percolation Network Soldered with Graphene Oxide at Room Temperature and Its Application for Fully Stretchable Polymer Light-Emitting Diodes," *ACS Nano*, vol. 8, pp. 1590–1600, Feb. 2014.

[60] A. J. Stapleton, R. A. Afre, A. V. Ellis, J. G. Shapter, G. G. Andersson, J. S. Quinton, and D. A. Lewis, "Highly conductive interwoven carbon nanotube and silver nanowire transparent electrodes," *Science and Technology of Advanced Materials*, vol. 14, p. 035004, Mar. 2013.

[61] P.-C. Hsu, D. Kong, S. Wang, H. Wang, A. J. Welch, H. Wu, and Y. Cui, "Electrolessly Deposited Electrospun Metal Nanowire Transparent Electrodes," *Journal of the American Chemical Society*, vol. 136, pp. 10593–10596, July 2014.

[62] H. Wu, L. Hu, M. W. Rowell, D. Kong, J. J. Cha, J. R. McDonough, J. Zhu, Y. Yang, M. D. McGehee, and Y. Cui, "Electrospun Metal Nanofiber Webs as High-Performance Transparent Electrode," *Nano Letters*, vol. 10, pp. 4242–4248, Oct. 2010.

[63] P.-C. Hsu, S. Wang, H. Wu, V. K. Narasimhan, D. Kong, H. Ryoung Lee, and Y. Cui, "Performance enhancement of metal nanowire transparent conducting electrodes by mesoscale metal wires," *Nature Communications*, vol. 4, Sept. 2013.

[64] F. S. F. Morgenstern, D. Kabra, S. Massip, T. J. K. Brenner, P. E. Lyons, J. N. Coleman, and R. H. Friend, "Ag-nanowire films coated with ZnO nanoparticles as a transparent electrode for solar cells," *Applied Physics Letters*, vol. 99, pp. 183307–183307–3, Nov. 2011.

[65] C.-C. Chen, L. Dou, R. Zhu, C.-H. Chung, T.-B. Song, Y. B. Zheng, S. Hawks, G. Li, P. S. Weiss, and Y. Yang, "Visibly Transparent Polymer Solar Cells Produced by Solution Processing," *ACS Nano*, vol. 6, pp. 7185–7190, Aug. 2012.

[66] A. Iwan and A. Chuchmała, "Perspectives of applied graphene: Polymer solar cells," *Progress in Polymer Science*, vol. 37, pp. 1805–1828, Dec. 2012.

[67] M. Choe, B. H. Lee, G. Jo, J. Park, W. Park, S. Lee, W.-K. Hong, M.-J. Seong, Y. H. Kahng, K. Lee, and T. Lee, "Efficient bulk-heterojunction photovoltaic cells with transparent multi-layer graphene electrodes," *Organic Electronics*, vol. 11, pp. 1864–1869, Nov. 2010.

[68] Y. Sun, W. Zhang, H. Chi, Y. Liu, C. L. Hou, and D. Fang, "Recent development of graphene materials applied in polymer solar cell," *Renewable and Sustainable Energy Reviews*, vol. 43, pp. 973–980, Mar. 2015.

[69] H. Park, J. A. Rowehl, K. K. Kim, V. Bulovic, and J. Kong, "Doped graphene electrodes for organic solar cells," *Nanotechnology*, vol. 21, p. 505204, Dec. 2010.

[70] K. K. Kim, A. Reina, Y. Shi, H. Park, L.-J. Li, Y. H. Lee, and J. Kong, "Enhancing the conductivity of transparent graphene films via doping," *Nanotechnology*, vol. 21, no. 28, p. 285205, 2010.

[71] Y.-Z. Chen, H. Medina, H.-W. Tsai, Y.-C. Wang, Y.-T. Yen, A. Manikandan, and Y.-L. Chueh, "Low Temperature Growth of Graphene on Glass by Carbon-Enclosed Chemical Vapor Deposition Process and Its Application as Transparent Electrode," *Chemistry of Materials*, vol. 27, pp. 1646–1655, Mar. 2015.

[72] X. Wang, L. Zhi, N. Tsao, e. Tomović, J. Li, and K. Müllen, "Transparent Carbon Films as Electrodes in Organic Solar Cells," *Angewandte Chemie*, vol. 120, no. 16, pp. 3032–3034, 2008.

[73] J. Wu, H. A. Becerril, Z. Bao, Z. Liu, Y. Chen, and P. Peumans, "Organic solar cells with solution-processed graphene transparent electrodes," *Applied Physics Letters*, vol. 92, pp. 263302–263302–3, July 2008.

[74] E. Kymakis, E. Stratakis, M. M. Stylianakis, E. Koudoumas, and C. Fotakis, "Spin coated graphene films as the transparent electrode in organic photovoltaic devices," *Thin Solid Films*, vol. 520, pp. 1238–1241, Dec. 2011.

[75] J. Wu, M. Agrawal, H. A. Becerril, Z. Bao, Z. Liu, Y. Chen, and P. Peumans, "Organic Light-Emitting Diodes on Solution-Processed Graphene Transparent Electrodes," *ACS Nano*, vol. 4, pp. 43–48, Jan. 2010.

[76] P. Paletti, R. Pawar, G. Ulisse, F. Brunetti, G. Iannaccone, and G. Fiori, "Can graphene outperform indium tin oxide as transparent electrode in organic solar cells?," *2D Materials*, vol. 2, p. 045006, Nov. 2015.

[77] Y. Wang, S. W. Tong, X. F. Xu, B. Özyilmaz, and K. P. Loh, "Interface Engineering of Layer-by-Layer Stacked Graphene Anodes for High-Performance Organic Solar Cells," *Advanced Materials*, vol. 23, pp. 1514–1518, Apr. 2011.

[78] P.-C. Ma, N. A. Siddiqui, G. Marom, and J.-K. Kim, "Dispersion and functionalization of carbon nanotubes for polymer-based nanocomposites: A review," *Composites Part A: Applied Science and Manufacturing*, vol. 41, pp. 1345–1367, Oct. 2010.

[79] M. F. L. D. Volder, S. H. Tawfick, R. H. Baughman, and A. J. Hart, "Carbon Nanotubes: Present and Future Commercial Applications," *Science*, vol. 339, pp. 535–539, Feb. 2013.

[80] M. Kaempgen, G. S. Duesberg, and S. Roth, "Transparent carbon nanotube coatings," *Applied Surface Science*, vol. 252, pp. 425–429, Oct. 2005.

[81] M. C. Hersam, "Progress towards monodisperse single-walled carbon nanotubes," *Nature Nanotechnology*, vol. 3, pp. 387–394, May 2008.

[82] R. Krupke, F. Hennrich, H. v. Löhneysen, and M. M. Kappes, "Separation of Metallic from Semiconducting Single-Walled Carbon Nanotubes," *Science*, vol. 301, pp. 344–347, July 2003.

[83] M. Zheng, A. Jagota, E. D. Semke, B. A. Diner, R. S. Mclean, S. R. Lustig, R. E. Richardson, and N. G. Tassi, "DNA-assisted dispersion and separation of carbon nanotubes," *Nature Materials*, vol. 2, pp. 338–342, May 2003.

[84] R. Voggu, K. V. Rao, S. J. George, and C. N. R. Rao, "A Simple Method of Separating Metallic and Semiconducting Single-Walled Carbon Nanotubes Based on Molecular Charge Transfer," *Journal of the American Chemical Society*, vol. 132, pp. 5560–5561, Apr. 2010.

[85] M. Arnold, A. Green, J. Hulvat, S. Stupp, and M. Hersam, "Sorting carbon nanotubes by electronic structure using density differentiation.," *Nature nanotechnology*, vol. 1, no. 1, pp. 60–65, 2006.

[86] R. C. Tenent, T. M. Barnes, J. D. Bergeson, A. J. Ferguson, B. To, L. M. Gedvilas, M. J. Heben, and J. L. Blackburn, "Ultrasmooth, Large-Area, High-Uniformity, Conductive Transparent Single-Walled-Carbon-Nanotube Films for Photovoltaics Produced by Ultrasonic Spraying," *Advanced Materials*, vol. 21, no. 31, pp. 3210–3216, 2009.

[87] M. Giulianini, E. R. Waclawik, J. M. Bell, M. De Crescenzi, P. Castrucci, M. Scarselli, and N. Motta, "Regioregular poly(3-hexylthiophene) helical self-organization on carbon nanotubes," *Applied Physics Letters*, vol. 95, pp. 013304–013304–3, July 2009.

[88] K.-i. Okazaki, "Absolute potential of the Fermi level of isolated single-walled carbon nanotubes," *Physical Review B*, vol. 68, no. 3, 2003.

[89] J. van de Lagemaat, T. M. Barnes, G. Rumbles, S. E. Shaheen, T. J. Coutts, C. Weeks, I. Levitsky, J. Peltola, and P. Glatkowski, "Organic solar cells with carbon nanotubes replacing In[sub 2]O[sub 3]:Sn as the transparent electrode," *Applied Physics Letters*, vol. 88, no. 23, p. 233503, 2006.

[90] I. Jeon, K. Cui, T. Chiba, A. Anisimov, A. G. Nasibulin, E. I. Kauppinen, S. Maruyama, and Y. Matsuo, "Direct and Dry Deposited Single-Walled Carbon Nanotube Films Doped with MoOx as Electron-Blocking Transparent Electrodes for Flexible Organic Solar Cells," *Journal of the American Chemical Society*, vol. 137, pp. 7982–7985, July 2015.

[91] A. Kaskela, A. G. Nasibulin, M. Y. Timmermans, B. Aitchison, A. Papadimitratos, Y. Tian, Z. Zhu, H. Jiang, D. P. Brown, A. Zakhidov, and E. I. Kauppinen, "Aerosol-Synthesized SWCNT Networks with Tunable Conductivity and Transparency by a Dry Transfer Technique," *Nano Letters*, vol. 10, pp. 4349–4355, Nov. 2010.

[92] Z. Li, S. A. Kulkarni, P. P. Boix, E. Shi, A. Cao, K. Fu, S. K. Batabyal, J. Zhang, Q. Xiong, L. H. Wong, N. Mathews, and S. G. Mhaisalkar, "Laminated Carbon Nanotube Networks for Metal Electrode-Free Efficient Perovskite Solar Cells," *ACS Nano*, vol. 8, pp. 6797–6804, July 2014.

[93] V. C. Tung, L.-M. Chen, M. J. Allen, J. K. Wassei, K. Nelson, R. B. Kaner, and Y. Yang, "Low-Temperature Solution Processing of Graphene−Carbon Nanotube Hybrid Materials for High-Performance Transparent Conductors," *Nano Letters*, vol. 9, pp. 1949–1955, May 2009.

[94] S. H. Kim, W. Song, M. W. Jung, M.-A. Kang, K. Kim, S.-J. Chang, S. S. Lee, J. Lim, J. Hwang, S. Myung, and K.-S. An, "Carbon Nanotube and Graphene Hybrid Thin Film for Transparent Electrodes and Field Effect Transistors," *Advanced Materials*, vol. 26, pp. 4247–4252, July 2014.

[95] I. N. Kholmanov, C. W. Magnuson, R. Piner, J.-Y. Kim, A. E. Aliev, C. Tan, T. Y. Kim, A. A. Zakhidov, G. Sberveglieri, R. H. Baughman, and R. S. Ruoff, "Optical, Electrical, and Electromechanical Properties of Hybrid Graphene/Carbon Nanotube Films," *Advanced Materials*, vol. 27, pp. 3053–3059, May 2015.

[96] K.-H. Tu, S.-S. Li, W.-C. Li, D.-Y. Wang, J.-R. Yang, and C.-W. Chen, "Solution processable nanocarbon platform for polymer solar cells," *Energy & Environmental Science*, vol. 4, no. 9, p. 3521, 2011.

[97] P.-C. Wang, L.-H. Liu, D. Alemu Mengistie, K.-H. Li, B.-J. Wen, T.-S. Liu, and C.-W. Chu, "Transparent electrodes based on conducting polymers for display applications," *Displays*, vol. 34, pp. 301–314, Oct. 2013.

[98] W. W. Focke, G. E. Wnek, and Y. Wei, "Influence of oxidation state, pH, and counterion on the conductivity of polyaniline," *The Journal of Physical Chemistry*, vol. 91, pp. 5813–5818, Oct. 1987.

[99] D. L. Cowan, V. Priest, T. R. Marrero, and D. W. Slaughter, "Electrical conductivity in polyaniline," *Journal of Physics and Chemistry of Solids*, vol. 51, pp. 307–312, Jan. 1990.

[100] J. Stejskal, I. Sapurina, J. Prokeš, and J. Zemek, "In-situ polymerized polyaniline films," *Synthetic Metals*, vol. 105, pp. 195–202, Sept. 1999.

[101] Y. Cao, G. M. Treacy, P. Smith, and A. J. Heeger, "Solution cast films of polyaniline: Optical quality transparent electrodes," *Applied Physics Letters*, vol. 60, pp. 2711–2713, June 1992.

[102] G. Gustafsson, G. M. Treacy, Y. Cao, F. Klavetter, N. Colaneri, and A. J. Heeger, "The "plastic" led: A flexible light-emitting device using a polyaniline transparent electrode," *Synthetic Metals*, vol. 57, no. 1, pp. 4123–4127, 1993.

[103] Y. Yang and A. J. Heeger, "Polyaniline as a transparent electrode for polymer light emitting diodes: Lower operating voltage and higher efficiency," *Applied Physics Letters*, vol. 64, pp. 1245–1247, Mar. 1994.

[104] O. Bubnova, Z. U. Khan, A. Malti, S. Braun, M. Fahlman, M. Berggren, and X. Crispin, "Optimization of the thermoelectric figure of merit in the conducting polymer poly(3,4-ethylenedioxythiophene)," *Nature Materials*, vol. 10, pp. 429–433, June 2011.

[105] J. P. Lock, S. G. Im, and K. K. Gleason, "Oxidative Chemical Vapor Deposition of Electrically Conducting Poly(3,4-ethylenedioxythiophene) Films," *Macromolecules*, vol. 39, pp. 5326–5329, Aug. 2006.

[106] T. A. Skotheim, *Handbook of Conducting Polymers, Second Edition,*. CRC Press, Nov. 1997.

[107] A. Elschner, S. Kirchmeyer, W. Lovenich, U. Merker, and K. Reuter, *PEDOT: Principles and Applications of an Intrinsically Conductive Polymer*. CRC Press, Nov. 2010.

[108] G. Zotti, S. Zecchin, G. Schiavon, F. Louwet, L. Groenendaal, X. Crispin, W. Osikowicz, W. Salaneck, and M. Fahlman, "Electrochemical and XPS Studies toward the Role of Monomeric and Polymeric Sulfonate Counterions in the Synthesis, Composition, and Properties of Poly(3,4-ethylenedioxythiophene)," *Macromolecules*, vol. 36, pp. 3337–3344, May 2003.

[109] L. Lindell, A. Burquel, F. L. E. Jakobsson, V. Lemaur, M. Berggren, R. Lazzaroni, J. Cornil, W. R. Salaneck, and X. Crispin, "Transparent, Plastic, Low-Work-Function Poly(3,4-ethylenedioxythiophene) Electrodes," *Chemistry of Materials*, vol. 18, pp. 4246–4252, Sept. 2006.

[110] F. Jakobsson, X. Crispin, L. Lindell, A. Kanciurzewska, M. Fahlman, W. Salaneck, and M. Berggren, "Towards all-plastic flexible light emitting diodes," *Chemical Physics Letters*, vol. 433, pp. 110–114, Dec. 2006.

[111] A. Nardes, M. Kemerink, M. de Kok, E. Vinken, K. Maturova, and R. Janssen, "Conductivity, work function, and environmental stability of PEDOT:PSS thin films treated with sorbitol," *Organic Electronics*, vol. 9, pp. 727–734, Oct. 2008.

[112] L. Groenendaal, G. Zotti, P.-H. Aubert, S. Waybright, and J. Reynolds, "Electrochemistry of Poly(3,4-alkylenedioxythiophene) Derivatives," *Advanced Materials*, vol. 15, pp. 855–879, June 2003.

[113] J. Xia, N. Masaki, K. Jiang, and S. Yanagida, "The influence of doping ions on poly(3,4-ethylenedioxythiophene) as a counter electrode of a dye-sensitized solar cell," *Journal of Materials Chemistry*, vol. 17, no. 27, p. 2845, 2007.

[114] E. Poverenov, M. Li, A. Bitler, and M. Bendikov, "Major Effect of Electropolymerization Solvent on Morphology and Electrochromic Properties of PEDOT Films," *Chemistry of Materials*, vol. 22, pp. 4019–4025, July 2010.

[115] J. Yan, C. Sun, F. Tan, X. Hu, P. Chen, S. Qu, S. Zhou, and J. Xu, "Electropolymerized poly(3,4-ethylenedioxythiophene):poly(styrene sulfonate) (PEDOT:PSS) film on ITO glass and its application in photovoltaic device," *Solar Energy Materials and Solar Cells*, vol. 94, pp. 390–394, Feb. 2010.

[116] S. Ahmad, J.-H. Yum, Z. Xianxi, M. Grätzel, H.-J. Butt, and M. K. Nazeeruddin, "Dye-sensitized solar cells based on poly (3,4-ethylenedioxythiophene) counter electrode derived from ionic liquids," *Journal of Materials Chemistry*, vol. 20, no. 9, p. 1654, 2010.

[117] C. Louet, S. Cantin, J.-P. Dudon, P.-H. Aubert, F. Vidal, and C. Chevrot, "A comprehensive study of infrared reflectivity of poly(3,4-ethylenedioxythiophene) model layers with different morphologies and conductivities," *Solar Energy Materials and Solar Cells*, vol. 143, pp. 141–151, Dec. 2015.

[118] R. Corradi and S. P. Armes, "Chemical synthesis of poly (3, 4-ethylenedioxythiophene)," *Synthetic metals*, vol. 84, no. 1, pp. 453–454, 1997.

[119] F. Louwet, L. Groenendaal, J. Dhaen, J. Manca, J. Van Luppen, E. Verdonck, and L. Leenders, "PEDOT/PSS: synthesis, characterization, properties and applications," *Synthetic Metals*, vol. 135-136, pp. 115–117, Apr. 2003.

[120] N. Paradee and A. Sirivat, "Synthesis of poly(3,4-ethylenedioxythiophene) nanoparticles via chemical oxidation polymerization: Synthesis of PEDOT nanoparticles," *Polymer International*, pp. n/a–n/a, May 2013.

[121] J. Wang, G. Cai, X. Zhu, and X. Zhou, "Oxidative chemical polymerization of 3, 4-ethylenedioxythiophene and its applications in antistatic coatings," *Journal of Applied Polymer Science*, vol. 124, pp. 109–115, Apr. 2012.

[122] L. Groenendaal, F. Jonas, D. Freitag, H. Pielartzik, and J. R. Reynolds, "Poly(3,4-ethylenedioxythiophene) and Its Derivatives: Past, Present, and Future," *Advanced Materials*, vol. 12, pp. 481–494, Apr. 2000.

[123] C.-H. Wu, T.-M. Don, and W.-Y. Chiu, "Characterization and conversion determination of stable PEDOT latex nanoparticles synthesized by emulsion polymerization," *Polymer*, vol. 52, pp. 1375–1384, Mar. 2011.

[124] C. Jiang, G. Chen, and X. Wang, "High-conversion synthesis of poly(3,4-ethylenedioxythiophene) by chemical oxidative polymerization," *Synthetic Metals*, vol. 162, pp. 1968–1971, Dec. 2012.

[125] M. R. Nabid, S. Asadi, M. Shamsianpour, R. Sedghi, S. Osati, and N. Safari, "Oxidative polymerization of 3,4-ethylenedioxythiophene using transition-metal tetrasulfonated phthalocyanine," *Reactive and Functional Polymers*, vol. 70, pp. 75–80, Jan. 2010.

[126] Y.-H. Ha, N. Nikolov, S. Pollack, J. Mastrangelo, B. Martin, and R. Shashidhar, "Towards a Transparent, Highly Conductive Poly(3,4-ethylenedioxythiophene)," *Advanced Functional Materials*, vol. 14, pp. 615–622, June 2004.

[127] D. Hohnholz, A. G. MacDiarmid, D. M. Sarno, and J. Wayne E. Jones, "Uniform thin films of poly-3,4-ethylenedioxythiophene (PEDOT) prepared by in-situ deposition," *Chemical Communications*, pp. 2444–2445, Nov. 2001.

[128] D. M. de Leeuw, P. A. Kraakman, P. F. G. Bongaerts, C. M. J. Mutsaers, and D. B. M. Klaassen, "Electroplating of conductive polymers for the metallization of insulators," *Synthetic Metals*, vol. 66, pp. 263–273, Oct. 1994.

[129] J. H. Chen, C.-A. Dai, and W.-Y. Chiu, "Synthesis of highly conductive EDOT copolymer films via oxidative chemicalin situ polymerization," *Journal of Polymer Science Part A: Polymer Chemistry*, vol. 46, pp. 1662–1673, Mar. 2008.

[130] O. Bubnova, Z. U. Khan, H. Wang, S. Braun, D. R. Evans, M. Fabretto, P. Hojati-Talemi, D. Dagnelund, J.-B. Arlin, Y. H. Geerts, S. Desbief, D. W. Breiby, J. W. Andreasen, R. Lazzaroni, W. M. Chen, I. Zozoulenko, M. Fahlman, P. J. Murphy, M. Berggren, and X. Crispin, "Semi-metallic polymers," *Nature Materials*, vol. 13, pp. 190–194, Dec. 2013.

[131] J. S. Choi, J.-H. Yim, D.-W. Kim, J.-K. Jeon, Y. S. Ko, and Y. Kim, "Effects of various imidazole-based weak bases and surfactant on the conductivity and transparency of poly(3,4-ethylenedioxythiophene) films," *Synthetic Metals*, vol. 159, pp. 2506–2511, Dec. 2009.

[132] B. Winther-Jensen and K. West, "Vapor-Phase Polymerization of 3,4-Ethylenedioxythiophene: A Route to Highly Conducting Polymer Surface Layers," *Macromolecules*, vol. 37, pp. 4538–4543, June 2004.

[133] M. V. Fabretto, D. R. Evans, M. Mueller, K. Zuber, P. Hojati-Talemi, R. D. Short, G. G. Wallace, and P. J. Murphy, "Polymeric Material with Metal-Like Conductivity for Next Generation Organic Electronic Devices," *Chemistry of Materials*, vol. 24, pp. 3998–4003, Oct. 2012.

[134] S. Admassie, O. Inganäs, W. Mammo, E. Perzon, and M. R. Andersson, "Electrochemical and optical studies of the band gaps of alternating polyfluorene copolymers," *Synthetic Metals*, vol. 156, pp. 614–623, Apr. 2006.

[135] B. Winther-Jensen and F. C. Krebs, "High-conductivity large-area semi-transparent electrodes for polymer photovoltaics by silk screen printing and vapour-phase deposition," *Solar Energy Materials and Solar Cells*, vol. 90, pp. 123–132, Jan. 2006.

[136] A. Nardes, M. Kemerink, R. Janssen, J. Bastiaansen, N. Kiggen, B. Langeveld, A. van Breemen, and M. de Kok, "Microscopic Understanding of the Anisotropic Conductivity of PEDOT:PSS Thin Films," *Advanced Materials*, vol. 19, pp. 1196–1200, May 2007.

[137] S. Jönsson, J. Birgerson, X. Crispin, G. Greczynski, W. Osikowicz, A. Denier van der Gon, W. Salaneck, and M. Fahlman, "The effects of solvents on the morphology and sheet resistance in poly(3,4-ethylenedioxythiophene)–polystyrenesulfonic acid (PEDOT–PSS) films," *Synthetic Metals*, vol. 139, pp. 1–10, Aug. 2003.

[138] H. Shi, C. Liu, Q. Jiang, and J. Xu, "Effective Approaches to Improve the Electrical Conductivity of PEDOT:PSS: A Review," *Advanced Electronic Materials*, vol. 1, p. 1500017, Apr. 2015.

[139] J. Ouyang, C.-W. Chu, F.-C. Chen, Q. Xu, and Y. Yang, "High-Conductivity Poly(3,4-ethylenedioxythiophene):Poly(styrene sulfonate) Film and Its Application in Polymer Optoelectronic Devices," *Advanced Functional Materials*, vol. 15, pp. 203–208, Feb. 2005.

[140] J. Y. Kim, J. H. Jung, D. E. Lee, and J. Joo, "Enhancement of electrical conductivity of poly(3,4-ethylenedioxythiophene)/poly(4-styrenesulfonate) by a change of solvents," *Synthetic Metals*, vol. 126, pp. 311–316, Feb. 2002.

[141] J. Ouyang, Q. Xu, C.-W. Chu, Y. Yang, G. Li, and J. Shinar, "On the mechanism of conductivity enhancement in poly(3,4-ethylenedioxythiophene):poly(styrene sulfonate) film through solvent treatment," *Polymer*, vol. 45, pp. 8443–8450, Nov. 2004.

[142] Y. Xia and J. Ouyang, "PEDOT:PSS films with significantly enhanced conductivities induced by preferential solvation with cosolvents and their application in polymer photovoltaic cells," *Journal of Materials Chemistry*, vol. 21, no. 13, p. 4927, 2011.

[143] X. Crispin, F. L. E. Jakobsson, A. Crispin, P. C. M. Grim, P. Andersson, A. Volodin, C. van Haesendonck, M. Van der Auweraer, W. R. Salaneck, and M. Berggren, "The Origin of the High Conductivity of Poly(3,4-ethylenedioxythiophene)−Poly(styrenesulfonate) (PEDOT−PSS) Plastic Electrodes," *Chemistry of Materials*, vol. 18, pp. 4354–4360, Sept. 2006.

[144] X. Crispin, S. Marciniak, W. Osikowicz, G. Zotti, A. W. D. van der Gon, F. Louwet, M. Fahlman, L. Groenendaal, F. De Schryver, and W. R. Salaneck, "Conductivity, morphology, interfacial chemistry, and stability of poly(3,4-ethylene dioxythiophene)–poly(styrene sulfonate): A photoelectron spectroscopy study," *Journal of Polymer Science Part B: Polymer Physics*, vol. 41, pp. 2561–2583, Nov. 2003.

[145] A. M. Nardes, R. A. J. Janssen, and M. Kemerink, "A Morphological Model for the Solvent-Enhanced Conductivity of PEDOT:PSS Thin Films," *Advanced Functional Materials*, vol. 18, pp. 865–871, Mar. 2008.

[146] I. Cruz-Cruz, M. Reyes-Reyes, M. A. Aguilar-Frutis, A. G. Rodriguez, and R. López-Sandoval, "Study of the effect of DMSO concentration on the thickness of the PSS insulating barrier in PEDOT:PSS thin films," *Synthetic Metals*, vol. 160, pp. 1501–1506, July 2010.

[147] Y. H. Kim, C. Sachse, M. L. Machala, C. May, L. Müller-Meskamp, and K. Leo, "Highly Conductive PEDOT:PSS Electrode with Optimized Solvent and Thermal Post-Treatment for ITO-Free Organic Solar Cells," *Advanced Functional Materials*, vol. 21, pp. 1076–1081, Mar. 2011.

[148] S.-I. Na, S.-S. Kim, J. Jo, and D.-Y. Kim, "Efficient and Flexible ITO-Free Organic Solar Cells Using Highly Conductive Polymer Anodes," *Advanced Materials*, vol. 20, no. 21, pp. 4061–4067, 2008.

[149] H. Do, M. Reinhard, H. Vogeler, A. Puetz, M. F. Klein, W. Schabel, A. Colsmann, and U. Lemmer, "Polymeric anodes from poly(3,4-ethylenedioxythiophene):poly(styrenesulfonate) for 3.5% efficient organic solar cells," *Thin Solid Films*, vol. 517, pp. 5900–5902, Aug. 2009.

[150] E. Ahlswede, W. Mühleisen, M. W. bin Moh Wahi, J. Hanisch, and M. Powalla, "Highly efficient organic solar cells with printable low-cost transparent contacts," *Applied Physics Letters*, vol. 92, pp. 143307–143307–3, Apr. 2008.

[151] S. Timpanaro, M. Kemerink, F. J. Touwslager, M. M. De Kok, and S. Schrader, "Morphology and conductivity of PEDOT/PSS films studied by scanning–tunneling microscopy," *Chemical Physics Letters*, vol. 394, pp. 339–343, Aug. 2004.

[152] L. Ouyang, C. Musumeci, M. J. Jafari, T. Ederth, and O. Inganäs, "Imaging the Phase Separation Between PEDOT and Polyelectrolytes During Processing of Highly Conductive PEDOT:PSS Films," *ACS Applied Materials & Interfaces*, p. 150825124148009, Aug. 2015.

[153] N. Kim, B. H. Lee, D. Choi, G. Kim, H. Kim, J.-R. Kim, J. Lee, Y. H. Kahng, and K. Lee, "Role of Interchain Coupling in the Metallic State of Conducting Polymers," *Physical Review Letters*, vol. 109, Sept. 2012.

[154] L. A. A. Pettersson, S. Ghosh, and O. Inganäs, "Optical anisotropy in thin films of poly(3,4-ethylenedioxythiophene)–poly(4-styrenesulfonate)," *Organic Electronics*, vol. 3, pp. 143–148, Dec. 2002.

[155] J. Zhou, D. H. Anjum, G. Lubineau, E. Q. Li, and S. T. Thoroddsen, "Unraveling the Order and Disorder in Poly(3,4-ethylenedioxythiophene)/Poly(styrenesulfonate) Nanofilms," *Macromolecules*, vol. 48, pp. 5688–5696, Aug. 2015.

[156] Q. Wei, M. Mukaida, Y. Naitoh, and T. Ishida, "Morphological Change and Mobility Enhancement in PEDOT:PSS by Adding Co-solvents," *Advanced Materials*, vol. 25, no. 20, pp. 2831–2836, 2013.

[157] J. Ouyang, ""Secondary doping" methods to significantly enhance the conductivity of PEDOT:PSS for its application as transparent electrode of optoelectronic devices," *Displays*, vol. 34, pp. 423–436, Dec. 2013.

[158] Y. Xia and J. Ouyang, "Salt-Induced Charge Screening and Significant Conductivity Enhancement of Conducting Poly(3,4-ethylenedioxythiophene):Poly(styrenesulfonate)," *Macromolecules*, vol. 42, pp. 4141–4147, June 2009.

[159] Y. Xia and J. Ouyang, "Anion effect on salt-induced conductivity enhancement of poly(3,4-ethylenedioxythiophene):poly(styrenesulfonate) films," *Organic Electronics*, vol. 11, pp. 1129–1135, June 2010.

[160] R. J. Murphy, K. M. Weigandt, D. Uhrig, A. Alsayed, C. Badre, L. Hough, and M. Muthukumar, "Scattering Studies on Poly(3,4-ethylenedioxythiophene)–Polystyrenesulfonate in the Presence of Ionic Liquids," *Macromolecules*, vol. 48, pp. 8989–8997, Dec. 2015.

[161] M. Reyes-Reyes, I. Cruz-Cruz, and R. López-Sandoval, "Enhancement of the Electrical Conductivity in PEDOT:PSS Films by the Addition of Dimethyl Sulfate," *The Journal of Physical Chemistry C*, vol. 114, pp. 20220–20224, Dec. 2010.

[162] Z. Yu, Y. Xia, D. Du, and J. Ouyang, "PEDOT:PSS Films with Metallic Conductivity through a Treatment with Common Organic Solutions of Organic Salts and Their Application as a Transparent Electrode of Polymer Solar Cells," *ACS Applied Materials & Interfaces*, vol. 8, pp. 11629–11638, May 2016.

[163] C. Badre, L. Marquant, A. M. Alsayed, and L. A. Hough, "Highly Conductive Poly(3,4-ethylenedioxythiophene):Poly (styrenesulfonate) Films Using 1-Ethyl-3-methylimidazolium Tetracyanoborate Ionic Liquid," *Advanced Functional Materials*, vol. 22, no. 13, pp. 2723–2727, 2012.

[164] R. M. Howden, E. D. McVay, and K. K. Gleason, "oCVD poly(3,4-ethylenedioxythiophene) conductivity and lifetime enhancement via acid rinse dopant exchange," *J. Mater. Chem. A*, vol. 1, no. 4, pp. 1334–1340, 2013.

[165] Y. Xia and J. Ouyang, "Significant Conductivity Enhancement of Conductive Poly(3,4-ethylenedioxythiophene): Poly(styrenesulfonate) Films through a Treatment with Organic Carboxylic Acids and Inorganic Acids," *ACS Applied Materials & Interfaces*, vol. 2, pp. 474–483, Feb. 2010.

[166] S. Mukherjee, R. Singh, S. Gopinathan, S. Murugan, S. Gawali, B. Saha, J. Biswas, S. Lodha, and A. Kumar, "Solution-Processed Poly(3,4-ethylenedioxythiophene) Thin Films as Transparent Conductors: Effect of p-Toluenesulfonic Acid in Dimethyl Sulfoxide," *ACS Applied Materials & Interfaces*, vol. 6, pp. 17792–17803, Oct. 2014.

[167] M. Jørgensen, K. Norrman, and F. C. Krebs, "Stability/degradation of polymer solar cells," *Solar Energy Materials and Solar Cells*, vol. 92, pp. 686–714, July 2008.

[168] W. Greenbank, L. Hirsch, G. Wantz, and S. Chambon, "Interfacial thermal degradation in inverted organic solar cells," *Applied Physics Letters*, vol. 107, p. 263301, Dec. 2015.

[169] R. Rösch, D. M. Tanenbaum, M. Jørgensen, M. Seeland, M. Bärenklau, M. Hermenau, E. Voroshazi, M. T. Lloyd, Y. Galagan, B. Zimmermann, U. Würfel, M. Hösel, H. F. Dam, S. A. Gevorgyan, S. Kudret, W. Maes, L. Lutsen, D. Vanderzande, R. Andriessen, G. Teran-Escobar, M. Lira-Cantu, A. Rivaton, G. Y. Uzunoğlu, D. Germack, B. Andreasen, M. V. Madsen, K. Norrman, H. Hoppe, and F. C. Krebs, "Investigation of the degradation mechanisms of a variety of organic photovoltaic devices by combination of imaging techniques—the ISOS-3 inter-laboratory collaboration," *Energy & Environmental Science*, vol. 5, pp. 6521–6540, Mar. 2012.

[170] K.-H. Ok, J. Kim, S.-R. Park, Y. Kim, C.-J. Lee, S.-J. Hong, M.-G. Kwak, N. Kim, C. J. Han, and J.-W. Kim, "Ultra-thin and smooth transparent electrode for flexible and leakage-free organic light-emitting diodes," *Scientific Reports*, vol. 5, p. 9464, Mar. 2015.

[171] Z. Yu, L. Li, Q. Zhang, W. Hu, and Q. Pei, "Silver Nanowire - Polymer Composite Electrodes for Efficient Polymer Solar Cells," *Advanced Materials*, vol. 23, pp. 4453–4457, Sept. 2011.

[172] X.-Y. Zeng, Q.-K. Zhang, R.-M. Yu, and C.-Z. Lu, "A New Transparent Conductor: Silver Nanowire Film Buried at the Surface of a Transparent Polymer," *Advanced Materials*, vol. 22, pp. 4484–4488, Oct. 2010.

[173] W. Gaynor, G. F. Burkhard, M. D. McGehee, and P. Peumans, "Smooth Nanowire/Polymer Composite Transparent Electrodes," *Advanced Materials*, vol. 23, no. 26, pp. 2905–2910, 2011.

[174] J. Song, J. Li, J. Xu, and H. Zeng, "Superstable Transparent Conductive Cu@Cu $_4$ Ni Nanowire Elastomer Composites against Oxidation, Bending, Stretching, and Twisting for Flexible and Stretchable Optoelectronics," *Nano Letters*, vol. 14, pp. 6298–6305, Nov. 2014.

[175] B. Deng, P.-C. Hsu, G. Chen, B. N. Chandrashekar, L. Liao, Z. Ayitimuda, J. Wu, Y. Guo, L. Lin, Y. Zhou, M. Aisijiang, Q. Xie, Y. Cui, Z. Liu, and H. Peng, "Roll-to-Roll Encapsulation of Metal Nanowires between Graphene and Plastic Substrate for High-Performance Flexible Transparent Electrodes," *Nano Letters*, vol. 15, pp. 4206–4213, June 2015.

[176] D.-H. Kim, K.-C. Yu, Y. Kim, and J.-W. Kim, "Highly Stretchable and Mechanically Stable Transparent Electrode Based on Composite of Silver Nanowires and Polyurethane–Urea," *ACS Applied Materials & Interfaces*, vol. 7, pp. 15214–15222, July 2015.

[177] J. Lee, P. Lee, H. B. Lee, S. Hong, I. Lee, J. Yeo, S. S. Lee, T.-S. Kim, D. Lee, and S. H. Ko, "Room-Temperature Nanosoldering of a Very Long Metal Nanowire Network by Conducting-Polymer-Assisted Joining for a Flexible Touch-Panel Application," *Advanced Functional Materials*, vol. 23, pp. 4171–4176, Sept. 2013.

[178] J.-H. Lee, H.-S. Shin, Y.-J. Noh, S.-I. Na, and H.-K. Kim, "Brush painting of transparent PEDOT/Ag nanowire/PEDOT multilayer electrodes for flexible organic solar cells," *Solar Energy Materials and Solar Cells*, vol. 114, pp. 15–23, July 2013.

[179] C. Mayousse, C. Celle, A. Carella, and J.-P. Simonato, "Synthesis and purification of long copper nanowires. Application to high performance flexible transparent electrodes with and without PEDOT:PSS," *Nano Research*, vol. 7, pp. 315–324, Mar. 2014.

[180] M.-G. Kang, H. Joon Park, S. Hyun Ahn, and L. Jay Guo, "Transparent Cu nanowire mesh electrode on flexible substrates fabricated by transfer printing and its application in organic solar cells," *Solar Energy Materials and Solar Cells*, vol. 94, pp. 1179–1184, June 2010.

[181] L. Valentini, M. Cardinali, D. Bagnis, and J. M. Kenny, "Solution casting of transparent and conductive carbon nanotubes/poly(3,4-ethylenedioxythiophene)–poly(styrenesulfonate) films under a magnetic field," *Carbon*, vol. 46, pp. 1513–1517, Sept. 2008.

[182] G.-F. Wang, X.-M. Tao, and R.-X. Wang, "Flexible organic light-emitting diodes with a polymeric nanocomposite anode," *Nanotechnology*, vol. 19, p. 145201, Apr. 2008.

[183] H. T. Ham, Y. S. Choi, M. G. Chee, M. H. Cha, and I. J. Chung, "PEDOT-PSS/singlewall carbon nanotubes composites," *Polymer Engineering & Science*, vol. 48, no. 1, pp. 1–10, 2008.

[184] S.-H. Jo, Y.-K. Lee, J.-W. Yang, W.-G. Jung, and J.-Y. Kim, "Carbon nanotube-based flexible transparent electrode films hybridized with self-assembling PEDOT," *Synthetic Metals*, vol. 162, pp. 1279–1284, Aug. 2012.

[185] E.-C. Cho, C.-P. Li, J.-H. Huang, K.-C. Lee, and J.-H. Huang, "Three-Dimensional Conductive Nanocomposites Based on Multiwalled Carbon Nanotube Networks and PEDOT:PSS as a Flexible Transparent Electrode for Optoelectronics," *ACS Applied Materials & Interfaces*, vol. 7, pp. 11668–11676, June 2015.

[186] N. Ferrer-Anglada, V. Gomis, Z. El-Hachemi, U. D. Weglikovska, M. Kaempgen, and S. Roth, "Carbon nanotube based composites for electronic applications: CNT–conducting polymers, CNT–Cu," *physica status solidi (a)*, vol. 203, no. 6, pp. 1082–1087, 2006.

[187] S. L. Hellstrom, H. W. Lee, and Z. Bao, "Polymer-Assisted Direct Deposition of Uniform Carbon Nanotube Bundle Networks for High Performance Transparent Electrodes," *ACS Nano*, vol. 3, no. 6, pp. 1423–1430, 2009.

2 Comprehensive Study of poly (3,4-ethylenedioxythiophene):poly(4-styrenetrifluoromethyl(bissulfonylimide) (PEDOT:PSTFSI)

In this chapter it was shown, that the polymer complex PEDOT:PSTFSI displays good opto-electronic properties and that is therefore a promising candidate for the application as transparent electrode in organic electronic devices. In order to improve the understanding of the complex system, the polyelectrolyte PSTFSIK and its behavior in aqueous solution as well as the complex formation upon synthesis of PEDOT in the presence of PSTFSI was studied. A particular attention was paid to the acid base behavior of PSTFSI and the pH of the synthesis medium, which were found to greatly influence the opto-electronic properties of the final PEDOT:PSTFSI complex. Furthermore, the impact of different synthesis parameters, such as the synthesis temperature and time, as well as the choice of oxidants, on the opto-electronic properties of PEDOT:PSTFSI were investigated.

De bonnes caractéristiques optoélectroniques ont été obtenues pour des films minces à base de dispersions aqueuses de PEDOT:PSTFSI en faisant ainsi un candidat de choix pour des applications électrode transparente dans des dispositifs électroniques. Afin de mieux comprendre ce système complexe de PEDOT:PSTFSI, les caractéristiques du polyélectrolyte PSTFSI en solution et la formation du complexe PEDOT:PSTFSI ont été étudiées. Une attention particulière a été accordée au comportement acido-basique du PSTFSI et au pH du milieu de synthèse, qui influencent de manière prépondérante les propriétés opto-électroniques du PEDOT:PSTFSI. Enfin, l'impact de différents paramètres de synthèse, tels que la température, la durée de la synthèse et les oxydants, sur les propriétés opto-électroniques ont été examinés.

2.1 Introduction

The decisive advantages of conducting polymers are, that they combine electronic conductivity of inorganic materials with the flexibility, chemical stability, low density and solution processability of polymers, which allows the fabrication of flexible, light weight devices. For transparent and flexible electrode applications the current bench mark material is the conducting polymer complex poly(3,4-ethylenedioxythiophene): poly(4-styrene sulfonate) (PEDOT:PSS), which is commercially available in the form of an aqueous dispersion. It is composed of the positively charged, conducting, but insoluble PEDOT, and of the insulating and water soluble polyanion PSS, which acts as counter ion for PEDOT and allows the dispersion of PEDOT in aqueous medium. Owing to its good opto-electronic properties, but also due to a lack of alternatives, PEDOT:PSS is used for various applications, such as OPVs, OLEDs, anti-static coatings, electrochromic devices or bio-medical sensors. Given the huge variety of potential applications it is desirable to design aqueous PEDOT:polyelectrolyte systems which meet better the specific requirements of each application.

In this work we present a new approach to stabilize PEDOT in aqueous dispersions by replacing the polystyrenesulfonic acid by the anionic polymer poly(4-styrenetrifluoromehtyl(bissulfonylimide)) (PSTFSI), which is known for its application as polyelectrolyte in Lithium batteries. It was shown, that the PEDOT:PSTFSI complex displays very promising opto-electronic properties, with a conductivity comparable to the one of synthesized PEDOT:PSS and a much higher transparency. The comprehensive study of the EPDOT:PSTFSI system and of different parameters such as composition, monomer dispersion, pH and temperature on the physical chemical properties of PEDOT:PSTFSI, allowed to gain a deeper understanding of the complex system. The acquired knowledge helped us to improve opto-electronic properties of PEDOT:PSTFSI and can also be of use for the development of new PEDOT:polyelectrolyte systems.

2.2 The Polyelectrolyte Poly (4-styrenetrifluoromethyl (bissulfonylimide)) Potassium Salt (PSTFSIK)

Poly(4-styrenetrifluoromehtyl(bissulfonylimide)) potassium salt (PSTFSIK) is an anionic polyelectrolyte, which consists of a styrenic backbone, to which a trifluoromethyl bissulfonyl imide group is attached and a potassium cation as counter ion (see figure 2.1). Due to the structural similarity of the functional group to bis(trifluoromethane) sulfonylimide lithium salt (see figure 2.1), which is known as super acid, it can be expected to be stable in the anionic form. The PSTFSI lithium salt (PSTFSILi) is well known for its application as solid electrolyte in lithium batteries and therefore PSTFSILi has been well characterized in literature regarding its ion conducting properties in solid state [1, 2, 3]. However, in the function as counter ion and template for conducting PEDOT, PSTFSIK is used in aqueous solution. Therefore its solubility, its conformation in aqueous solution and the distribution of negative charges along the polymer chain are crucial for the interaction with PEDOT and the properties of the final PEDOT:PSTFSI complex. The following study of PSTFSIK in aqueous medium was performed to give a fundamental insight in the intrinsic properties of the polyelectrolyte, before passing to the more complex system PEDOT:PSTFSI.

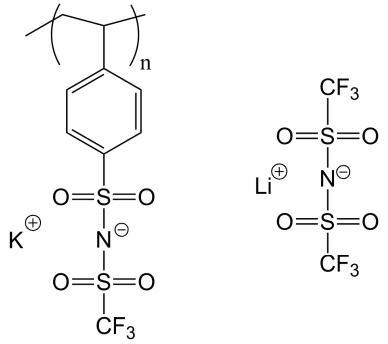

Fig. 2.1: Chemical structures of PSTFSI$^-$ K$^+$ and LiTFSI

The PSTFSIK polymer used in this work was synthesized by reversible addition-fragmentation chain-transfer (RAFT) polymerization. A detailed description of the synthesis protocol can be found in the experimental part page 203.

Upon the use of PSTFSI as template for PEDOT in aqueous dispersion, PSTFSI is subjected to a highly acidic environment, which is generated during the EDOT polymerization. This is why the behavior of PSTFSI under highly acidic conditions is of special interest for this work, as it could influence the complex formation with PEDOT

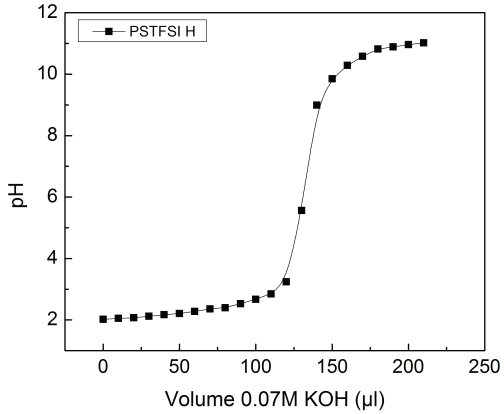

Fig. 2.2: Titration curve of PSTFSIH

and affect the properties of the resulting PEDOT:PSTFSI.

Despite the structural similarity of the STFSI unit to the super acid triflic acid, an acid base reaction of PSTFSIK was observed in acidic conditions. The resulting protonated PSTFSIH showed a pH of 2.0 in solution (c_{STFSI}= 0.025 mol.l^{-1}) and the pK_a of 2.3 was determined by titration (see figure 2.2). The potentially basic nature of PSTFSIK can be explained by the acidity reducing effect of negative charges on neighboring repeating units, which has been described for other polyanionic sytems [4, 5].

In order to investigate the charge distribution on PSTFSIK and PSTFSIH in more detail, XPS measurements were performed (see figure 2.3). The N1s spectrum of the PSTFSIK salt showed one main peak at 398.6eV, which can be attributed to a negatively charged nitrogen atom in PSTFSI. For PSTFSIH the highest peak was located at 400.2eV, which corresponds to a neutral, protonated nitrogen and signifies, that PSTFSIH is partially protonated and partially in the potassium salt form. The contributions at around 402eV correspond to very electron poor or positively charged nitrogen species [6]. This was confirmed by a XPS N1s reference spectrum of a polyvinylimidazolium:PSTFSI complex, which was formed by mixing of the two polyelectrolytes in aqueous solution (see figure 2.3). In the spectrum of PSTFSIH this peak could be explained by potential residues of triethylammonium which is used during the PSTFSIK synthesis. However, elemental analysis did not confirm the presence of a nitrogen containing impurity (see table 2.1).

The existence of a positively charged nitrogen in PSTFSI seemed unlikely owing to its acidic nature and was also excluded by DFT simulations. Durrieu *et al.* [7] observed

	C(wt%)	H(wt%)	N(wt%)	S(wt%)	F(wt%)	K(wt%)
STFSIK $_{theo}$	30.5	2.0	4.0	18.1	16.1	11.0
STFSIK $_{exp}$	30.8	2.0	3.9	18.0	14.9	10.9
PSTFSIK $_{exp}$	29.8	2.1	3.8	16.8	14.2	9.7

Tab. 2.1: Theoretical and experimental composition determined by elemental analysis of the STFSIK unit and the PSTFSIK polymer

a similar peak at high binding energies in the N1s spectrum of secondary amines due to hydrogen bonding of the amine functionalities with neighboring groups. In analogy to these findings we propose a model (see figure 2.4), in which the hydrogen atoms of protonated STFSIH units interact via hydrogen bonding with neighbouring STFSI groups, which leads to the appearance of an additional peak in the N1s spectrum.
Furthermore, the comparison of the spectra in figure 2.3 showed, that the interaction of $PSTFSI^-$ with different counter ions (K^+, $PEDOT^+$, polyvinylimidazolium) did not lead to a clear shift in the XPS N1s peak at around 398.6eV.

The comparison of the XPS O1s spectra of PSTFSIK and PSTFSIH in figure 2.4 shows that the peak of PSTFSIH is broadened towards higher binding energies, which is another indicator for hydrogen bonding to the oxygen atoms.
DFT simulations of STFSI trimers confirmed the presence of hydrogen bonds between protonated nitrogen and neighbouring oxygen atoms, which leads to a stabilization of the protons in the PSTFSI structure (see schematics in figure 2.4 and figure 2.5). The energy gain owing to hydrogen bonding in the PSTFSI structure can explain the relatively low acidity of PSTFSI compared to TFSI.

The partial protonation of PSTFSIH was further supported by the comparison of experimental and simulated infra-red (IR) spectra of PSTFSIK/H. Both simulated and experimental IR spectra clearly showed the signature peaks of the N-H bond at 750cm^{-1} to 900cm^{-1} (S-N-S assymetric mode) and at 1400cm^{-1} (bulk chain movement), which qualitatively confirmed the presence of N-H bonds.

Interestingly, ion exchange reactions of different batches of PSTFSIK in 0.05M to 1M hydrochloric acid all resulted in PSTFSIH with 31% to 41% remaining $PSTFSI^-$ units, which indicates that an equilibrium state was reached.

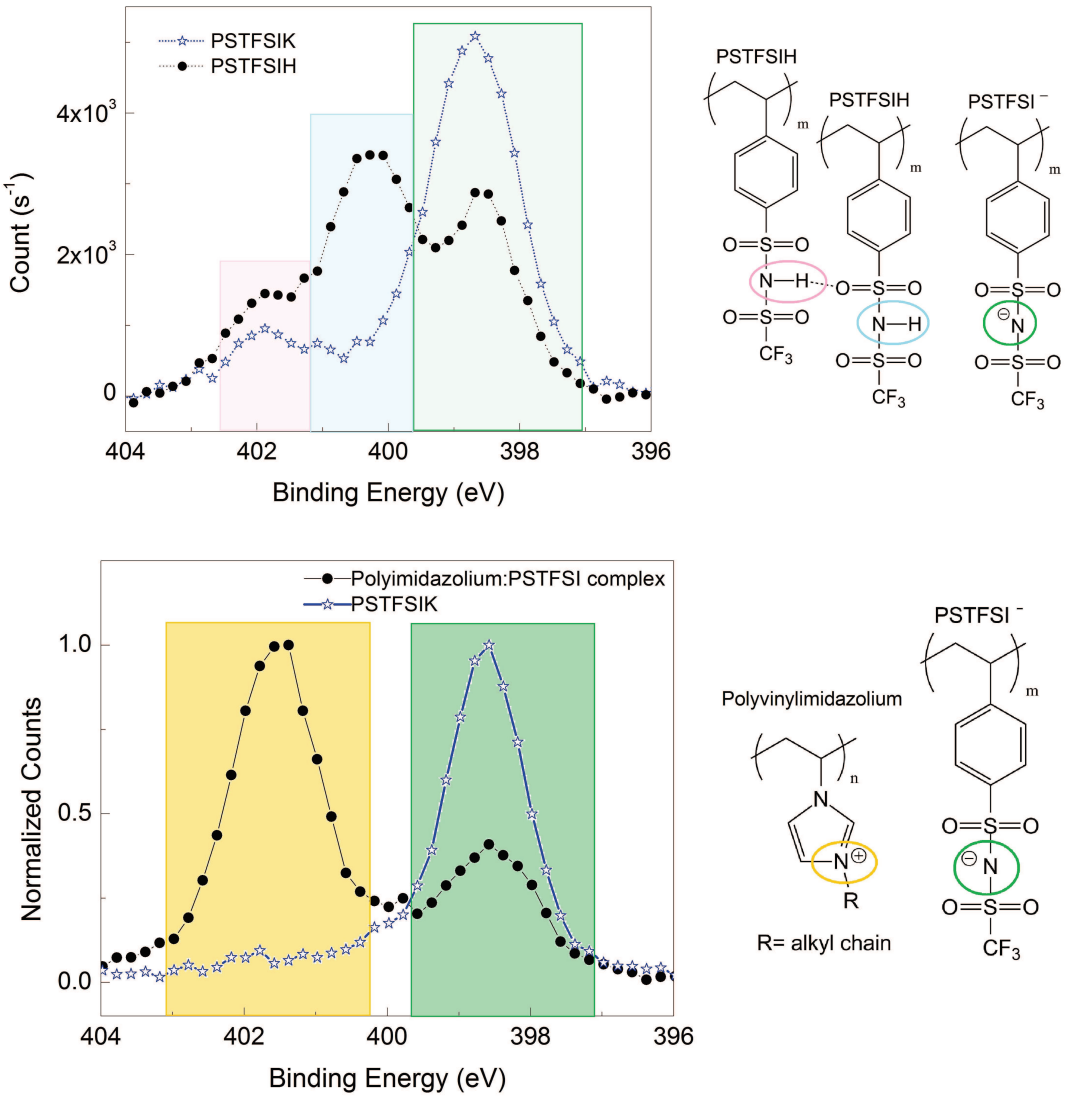

Fig. 2.3: XPS N1s spectra and chemical structures of PSTFSIK, PSTFSIH and a polyvinylimidazolium:PSTFSI complex

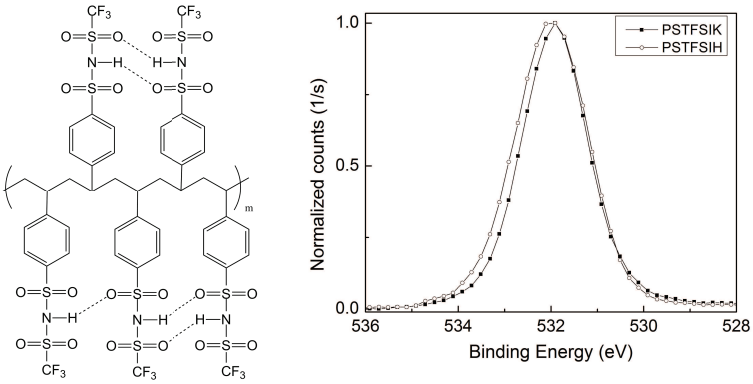

Fig. 2.4: Structure of PSTFSIH with possible hydrogen bonds between the protonated STFSI units and XPS O1s spectrum of PSTFSIK and PSTFSIH

In order to gain more information on the dissociation behavior of PSTFSIK and PSTFSIH in aqueous solution, the ionic conductivity of the solutions was measured as a function of the PSTFSI concentration. Strong electrolytes, which are completely dissociated in solution, obey the Kohlrausch's law which is

$$\Lambda = \Lambda_0 - KC_S^{0.5} \tag{2.1}$$

with Λ being the molar conductivity, Λ_0 the limiting molar conductivity, K being the Kohlrausch coefficient and C_S being the solute concentration [8]. Therefore, the plot of the molar conductivity versus the square root of the molar electrolyte concentration is linear for strong electrolytes.

As it can be seen from figure 2.6, the molar ionic conductivity of the aqueous PSTFSIK solution does not obey the Kohlrausch law, but shows the typical behavior of a weak electrolyte, for which the molar conductivity increases exponentially for very dilute solutions. This is related to an increasing dissociation at low electrolyte concentrations.

The limiting molar conductivity Λ_0 can be calculated by

$$\Lambda_0 = \sum \nu_i \lambda_i \tag{2.2}$$

with ν_i being the moles of ions i created from 1 mole dissolved electrolyte and λ_i being the limiting molar conductivity of ion i.

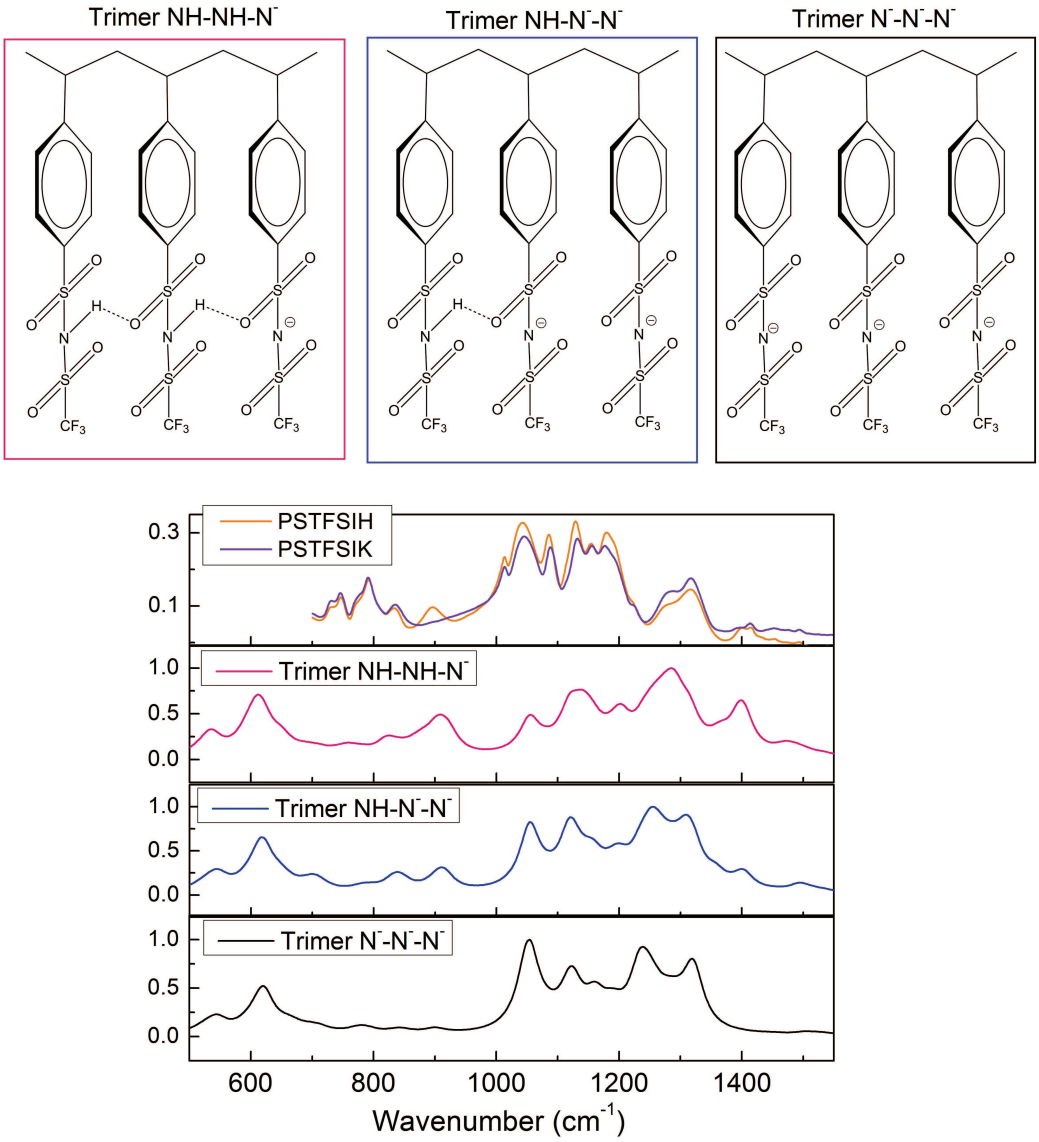

Fig. 2.5: Experimental IR spectra of PSTFSIK and PSTFSIH and simulated IR spectra and schematic structure of STFSI trimers, with 0, 1 and 2 protonated STFSI units

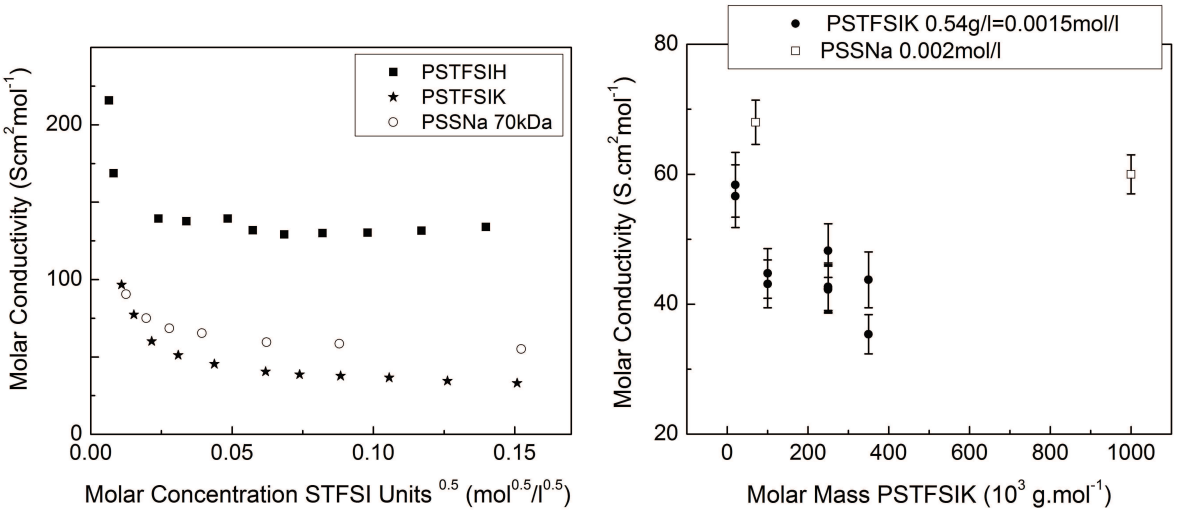

Fig. 2.6: Ionic conductivity of PSTFSIK, PSTFSIH 350kDa and PSSNa 70kDa aqueous solutions as a function of the concentration of anionic functional units and molar ionic conductivity of PSTFSIK solutions as a function of the molar mass of PSTFSIK for constant molar concentration of STFSIK units

As expected, PSTFSIH shows a higher ion conductivity due to the higher limiting molar conductivity of H^+ ($\lambda_i(H^+)$= 350S.cm^{2}mol^{-1}, $\lambda_i(K^+)$= 74S.cm^{2}mol^{-1}) in aqueous solution. Using the values obtained by fitting of the XPS N1s spectra (PSTFSIK 94% N^-K^+, 6% N-H; PSTFSIH 36% N^-K^+, 64% N-H) the Λ_0 (PSTFSIK) and Λ_0 (PSTFSIH) have been estimated by

$$\Lambda_0(PSTFSIK) = 0.94 \times 74 S.cm^2 mol^{-1} + 0.06 \times 350 S.cm^2 mol^{-1} = 91 S.cm^2 mol^{-1} \quad (2.3)$$

$$\Lambda_0(PSTFSIH) = 0.36 \times 74 S.cm^2 mol^{-1} + 0.64 \times 350 S.cm^2 mol^{-1} = 251 S.cm^2 mol^{-1} \quad (2.4)$$

assuming that the contribution of $PSTFSI^-$ to the ionic conductivity is low and can be therefore neglected.

Using the method proposed by Hanibah *et al.* [8] for the determination of the limiting molar conductivity from experimental data, we found Λ_0 (PSTFSIK)= 51S.cm^{2}mol^{-1} and Λ_0(PSTFSIH)= 141S.cm^{2}mol^{-1} (plots and fitting see figure A.2 in appendix, page 216). Interestingly, both experimentally determined values of Λ_0 are equivalent to 56% of the theoretical value. Such deviations originate from the differences in dissociation behavior between monomeric electrolytes and polyelectrolytes. In case of monomeric polyelectrolytes the functional units can be regarded independently. In contrast, the dissociation behavior of polyelectrolytes is strongly influenced by the state of the

neighbouring groups and screening effects [4, 9, 5].

For monomeric electrolyte solutions the degree of dissociation α can be estimated using $\alpha = \frac{\Lambda}{\Lambda_{0experimental}}$. In the case of PSTFSIK this leads to an estimate dissociation of around 65% and 94% for PSTFSIK and PSTFSIH at 0.026mol.l^{-1} (concentration used for PEDOT:PSTFSI synthesis), respectively. The higher solubility of the acid PSTFSIH might be related to an enhanced interaction with the solvent due to the formation of hydrogen bonding.

For the sake of comparison the same measurements were performed in aqueous PSSNa solutions, which revealed that PSSNa shows a less strong deviation from the Kohlrausch's law. The measured molar conductivity is approximately 55S.cm^{2}mol^{-1}. In case of complete dissociation of the PSSNa salt and taking into account the experimental error bar, this is in coherence with the value for the limiting molar conductivity of Na^+ cations of 50S.cm^{2}mol^{-1}.

From figure 2.6 it can be seen that the ionic conductivity of PSTFSIK solutions decreases for higher molar masses. This can be explained by a lower solubility of polymers with high molar mass, as well as by a further decrease in mobility of long polymer chains in solution. The same trend was observed for PSSNa solutions (see figure 2.6).

The limited solubility of PSTFSIK with molar masses higher than 200kDa were confirmed by optical inspection of the solution, in which tiny fibrils were discernible by eye. Imaging of these solutions by liquid AFM confirmed the presence of needle like structures in the solutions (see figure 2.7). The regular shape indicates, that these micrometer sized objects were not randomly formed agglomerates, but self assembled structures.

DLS measurements on the PSTFSI solutions confirmed the presence of objects of some nanometers and of objects of some hundreds of nanometers. Table 2.2 shows the hydrodynamic radii of PSTFSIK and of PSTFSIH with M_W ≈350kDa in aqueous solution (correlation function and fitting see figure 2.8). The decreasing particle size for PSTFSIH can be either a sign for a better solubility of PSTFSIH or for the collapse of the PSTFSI chains in acidic solution.

However, taking into account the polydispersity of the scatterers in PSTFSI solutions, the accuracy of DLS measurements is limited, as the Stokes Einstein model,

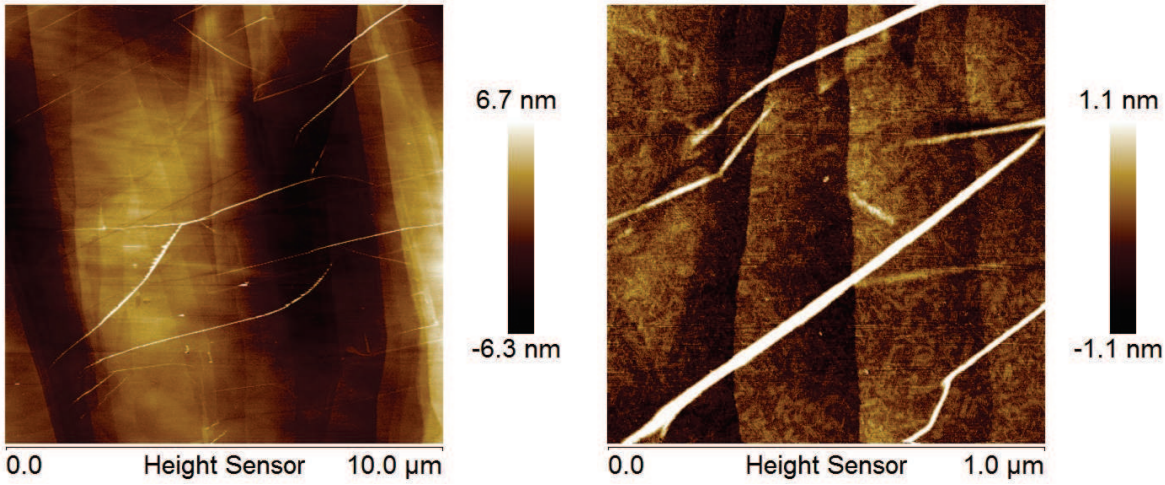

Fig. 2.7: Liquid AFM images of PSTFSIK 350kDa in aqueous solution at two different magnifications

Polyelectrolyte	Radius 1 (nm)	Radius 2 (nm)
PSTFSIK	7± 10	306± 100
PSTFSIH	0.7± 0.4	150± 40

Tab. 2.2: Object size determined by DLS for PSTFSIK and PSTFSIH ≈350kDa in aqueous solution

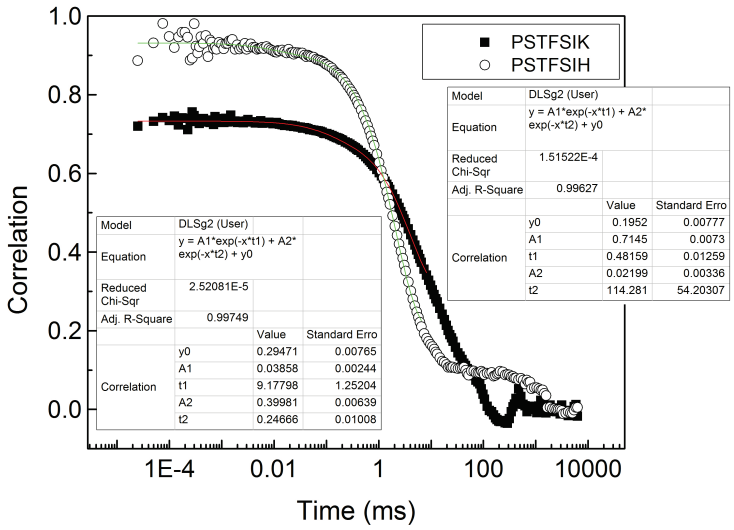

Fig. 2.8: DLS correlation funtion of aqueous PSTFSIK and PSTFSIH solutions, M_W ≈350kDa

polyelectrolyte	medium	Radius 1 (nm)	Radius 2 (nm)
PSTFSI 20kDa	DI	6± 1	93± 19
	0.1M HCl	5± 1	84±16
	0.05M KOH	11±2	63±12
PSTFSI 350kDa	DI	9± 0.5	450± 200
	0.1M HCl	6± 1	100±30
	0.05M KOH	6±2	250±60

Tab. 2.3: Object size determined by DLS for PSTFSI 20kDa and 350kDa in DI water, 0.1M HCl and 0.05M KOH

which is used for analysis, was developed for monodisperse solutions of spherical particles.

As the ionic strength and acidity of the solution change during the EDOT polymerization, the conformational changes of PSTFSIK upon the addition of bases and acids was investigated. From table 2.3 it can be seen that the measured radius of PSTFSIK shrank due to the presence of ions in the solution. This is a typical behavior for polyelectrolytes in solution and commonly explained by a collapse of the polyelectrolyte chains due to shielding effects [10, 11]. Therefore it can be expected, that the decrease of the pH during the EDOT polymerization influences the conformation of the PSTFSIK template polymer.

In conclusion, we can state, that the ionic strength and the pH of the solutions affects strongly the properties of the PSTFSI polyelectrolyte. As reported for other polyelectrolytes, the PSTFSIK chains collapse in solutions with high ionic strength. In highly acidic conditions the PSTFSIK salt reacts as a base and is transformed into a partially protonated form, bearing 30% to 40% residual, negatively charged functional groups. It was shown that the protonated form of PSTFSI is stabilized by hydrogen bonding between the STFSIH functional groups, which explains the rather high pK_a of 2.3 and the smaller hydrodynamic radius of PSTFSIH. As the ionic strength of the PSTFSI synthesis medium changes during the EDOT polymerization, the effect on the charge distribution on PSTFSI and on its conformation has to be taken into account.

2.3 Study of the PEDOT:PSTFSI Complex Formation

The common method to synthesize aqueous PEDOT:polyelectrolyte dispersions, such as PEDOT:PSS, is the oxidative polymerization of EDOT in aqueous polyelectrolyte solution at 20°C to 60°C, using $FeCl_3$, $Fe(Tos)_3$, different persulfate salts or a

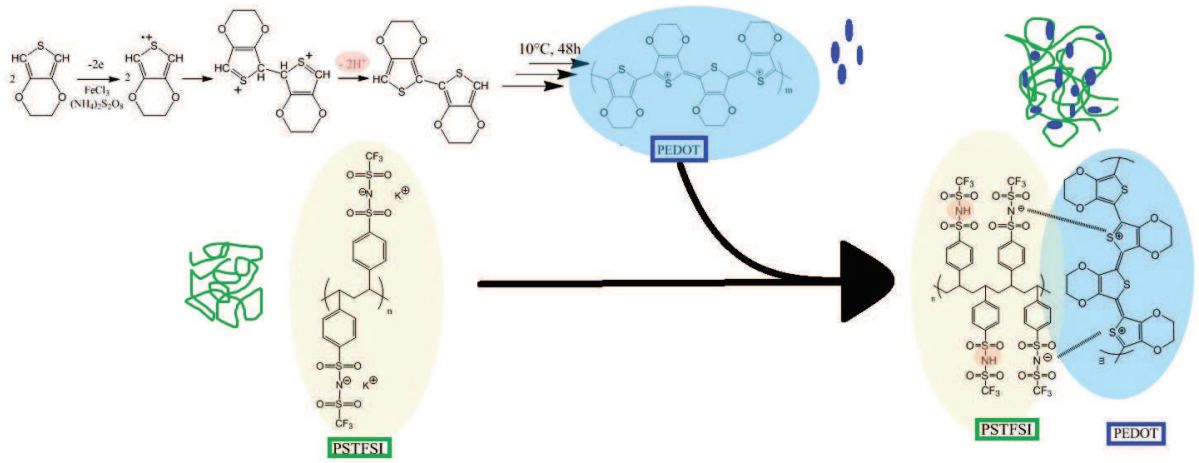

Fig. 2.9: Schematic of the oxidative dispersion polymerization of EDOT in aqueous PSTFSIK solution

combination of them as oxidants [12, 13, 14]. During the polymerization reaction the EDOT monomer is polymerized to neutral PEDOT, which is then further oxidized into the positively charged, so called "doped" conducting form of PEDOT [15, 16]. In order to stabilize the positive charges, the doped PEDOT forms a complex with negatively charged counter ions. This is where the solubilized anionic polyelectrolyte comes into play. It acts as counter ion and template for the positively charged PEDOT oligomers/polymers and allows the formation of stable, water dispersable PEDOT:polyelectrolyte complexes (see scheme in figure 2.9) [17, 18, 15]. As the EDOT polymerization, the doping of PEDOT and the complex formation with PSTFSI occur in the same time, the polymerization conditions strongly affect the doping and the morphology and consequently the conductivity of the obtained PEDOT:polyelectrolyte complex. Therefore, the influence of different synthesis parameters, such as the temperature, the ratio of the reactants and the dispersion of EDOT on the properties of PEDOT:PSTFSI was investigated. The objective of this fundamental study was to gain a better insight in the complexing mechanism of PEDOT:PSTFSI and to define an optimized synthesis protocol.

The above presented model of the PEDOT:polyelectrolyte complex was confirmed for PEDOT:PSTFSI by liquid AFM imaging (see figure 2.10), which displayed a three dimensional network of coiled chains with thick nodal points, which can be interpreted as PEDOT rich domains in a network of PSTFSI chains. A more detailed discussion of the

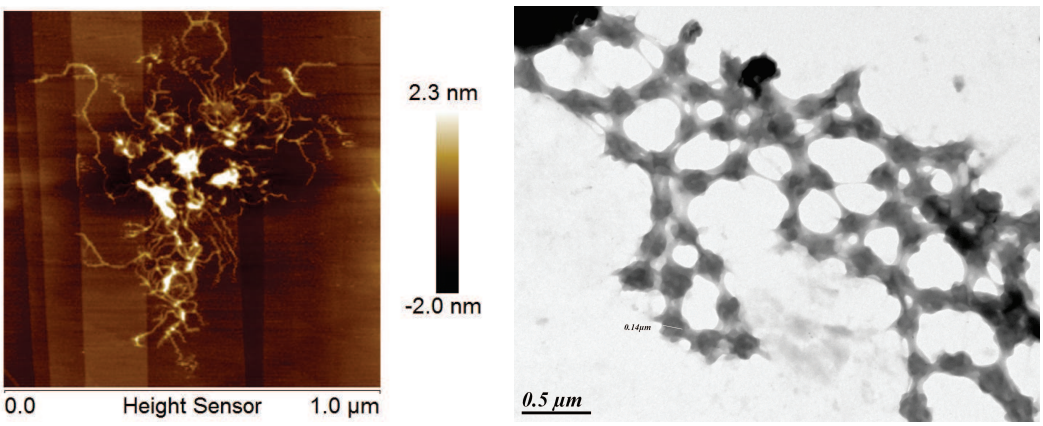

Fig. 2.10: PEDOT:PSTFSI imaged in dispersion by liquid AFM and as dry monolayer by TEM

structure of the PEDOT:PSTFSI complex in dispersion and a comparison to PEDOT:PSS is given in chapter 6, page 179.

The strength of the interactions between PEDOT and PSTFSI in the PEDOT:PSTFSI complex were qualitatively tested using capillary electrophoresis. Figure 2.11 displays the obtained chromatograms, which were recorded at different detection wavelengths, in order to selectively detect either PSTFSI (230nm) or PEDOT (550nm). It can be seen, that the main PSTFSI and PEDOT contributions were detected at the same time, which proves that the complex was not separated in the electric field of the capillary and which is a sign of strong interactions between PEDOT and PSTFSI. The second peak, which was detected at 230nm at higher retention times, can be attributed to an excess of negatively charged PSTFSI. This is coherent to the results presented by Diah *et al.* [19, 20], who found that excess PSS can be separated from the PEDOT:PSS complex by electrophoresis.

The presence of excess polyelectrolyte in the dispersion suggests, that the concentration of conducting PEDOT in the complex could be increased, with the objective to obtain higher conductivities. In order to optimize the ink composition, PEDOT:PSTFSI with different ratios of EDOT to PSTFSI were synthesized and characterized regarding their complex morphology, opto-electronic properties, doping and rheology.

Figure 2.12 shows the absorption coefficient, conductivity and FoM as a function of the ratio of EDOT to STFSI unit. A schematic illustration of PEDOT:PSTFSI complexes with different EDOT to STFSI ratios is given in figure 2.13.

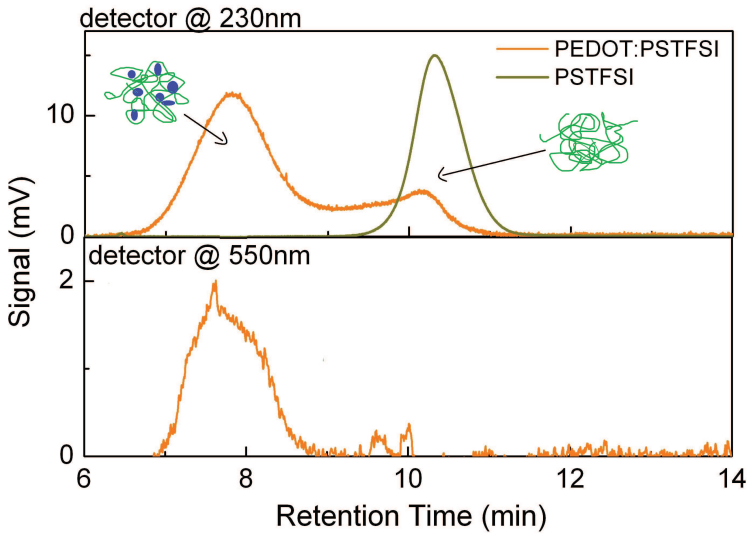

Fig. 2.11: Chromatogram of PEDOT:PSTFSI for the detection wavelengths 230nm (top) and 550nm

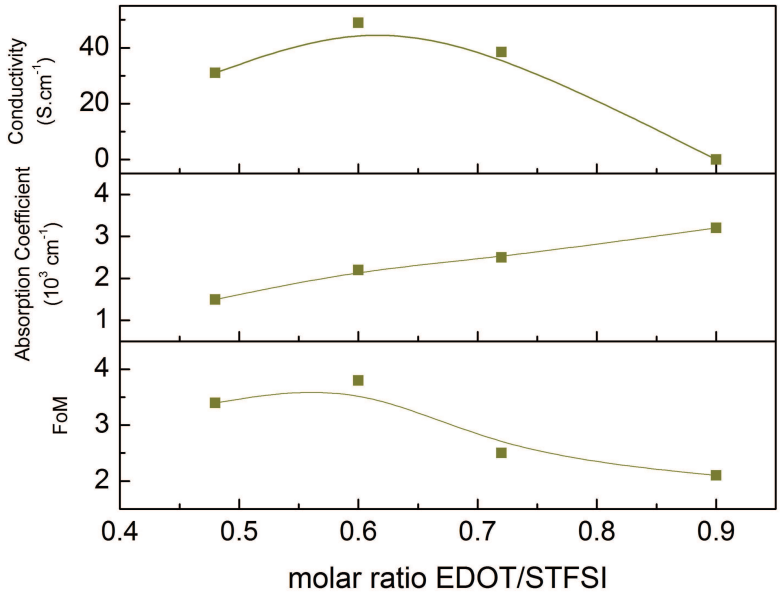

Fig. 2.12: Conductivity, absorption coefficient and FoM of PEDOT:PSTFSI with different molar EDOT to STFSI ratios, synthesis at 10°C 55rpm under N_2, M_W(PSTFSIK)≈250kDa

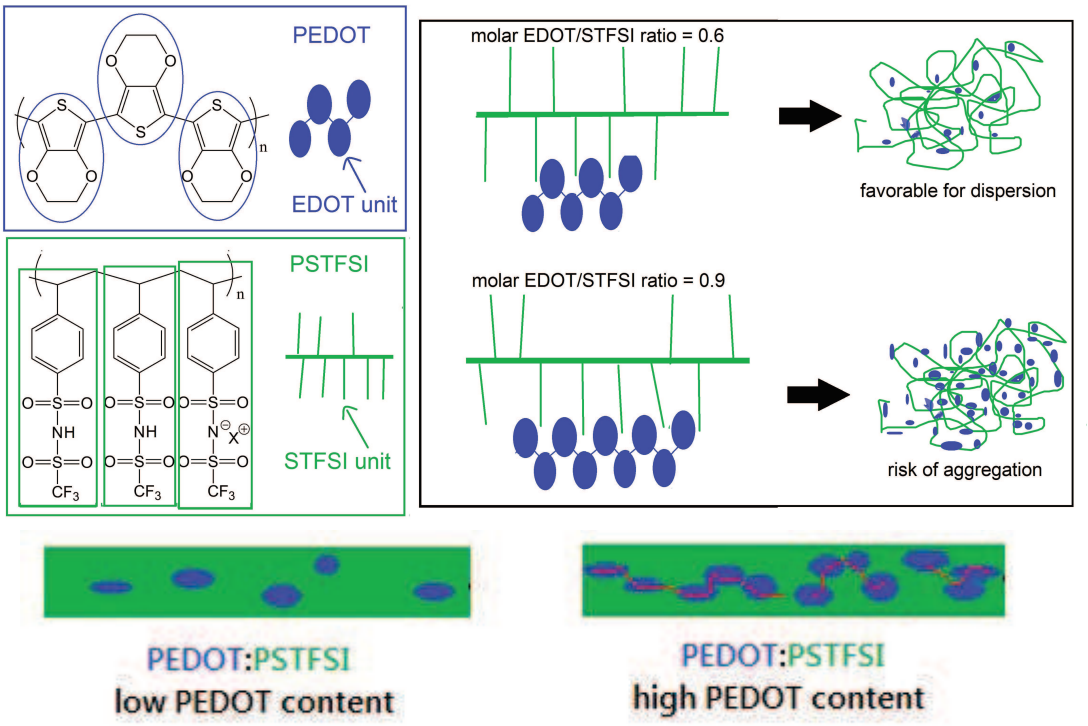

Fig. 2.13: Schematic illustration of the molar EDOT to STFSI ratio and of the percolation of PEDOT rich domains in PEDOT:PSTFSI films for different EDOT to STFSI ratios

The absorption coefficient, measured at 550nm, increased almost linearly with an increasing ratio of EDOT unit to STFSI repeating unit. This indicates that the conversion of EDOT was not significantly affected by changes in the composition of the reactants. Therefore we can state, that an increasing EDOT to STFSI ratio in the synthesis brings about a higher PEDOT concentration in the final PEDOT:PSTFSI complex.

Regarding the evolution of the conductivity, two regimes can be distinguished. Up to a certain concentration of EDOT a gain in conductivity was observed, whereas for a further increase of the EDOT concentration the conductivity declined.

The FoM was found to be maximized at a EDOT/STFSI ratio of 0.6, at which the complex shows the highest conductivity and a relatively low absorption.

To elucidate the underlying mechanism of the complex formation, which leads to such differences in conductivity as a function of composition, the doping as well as the morphology of the different PEDOT:PSTFSI complexes were studied.

To characterize the doping of the PEDOT:PSTFSI complexes, UV/Vis spectroscopy was performed. The comparison of the obtained absorption spectra (see figure 2.14)

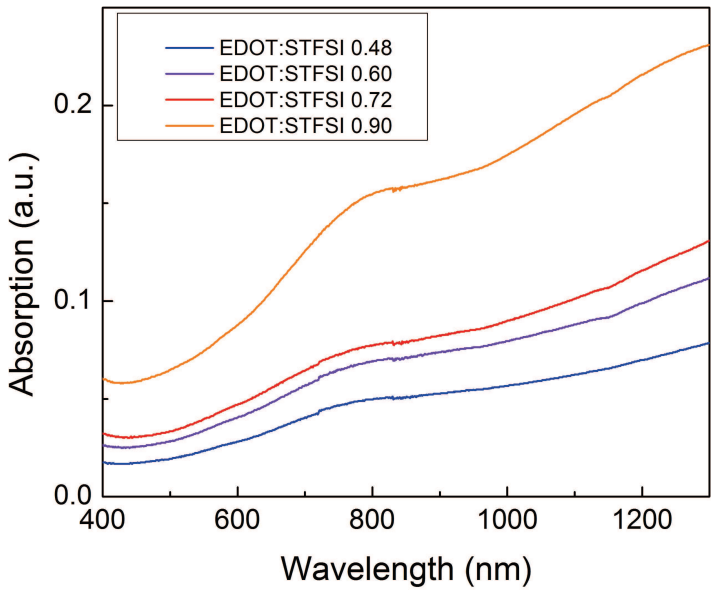

Fig. 2.14: UV/Vis absoprtion spectra of PEDOT:PSTFSI as a function of the molar EDOT to STFSI ratio, synthesis at 10°C 55rpm under N_2, M_W(PSTFSIK)≈250kDa

revealed, that the shape of the absorption spectra was unaffected for low EDOT concentrations, whereas for EDOT to STFSI ratios higher than 0.9, the absorption spectra were strongly flattened in the bipolaronic absorption regime (λ >1100nm). This indicates, that the doping level was constant for low EDOT concentrations and that the initial gain in conductivity with increasing EDOT concentrations can be attributed to a better percolation of the PEDOT rich domains, as illustrated in figure 2.13. For a further increase of the EDOT concentration the doping level decreased, which explains the drop of the conductivity.

However, the difference in doping could not be observed by Raman spectroscopy (see figure A.3, appendix page 217), which indicates, that Raman spectroscopy is less sensitive to changes in the doping level of PEDOT:polyelectrolyte complexes than UV/Vis spectroscopy.

In order to get an insight in the charge distribution on PSTFSI in PEDOT:PSTFSI, PEDOT:PSTFSI with different EDOT to STFSI ratios were studied by XPS (see figure 2.15). In the XPS S2p spectrum two main peak areas can be distinguished. The doublet at lower binding energies (163eV to 166eV) can be attributed to the sulfur atom in PEDOT, whereas the broad peak at higher binding energies originates from the overlap of several

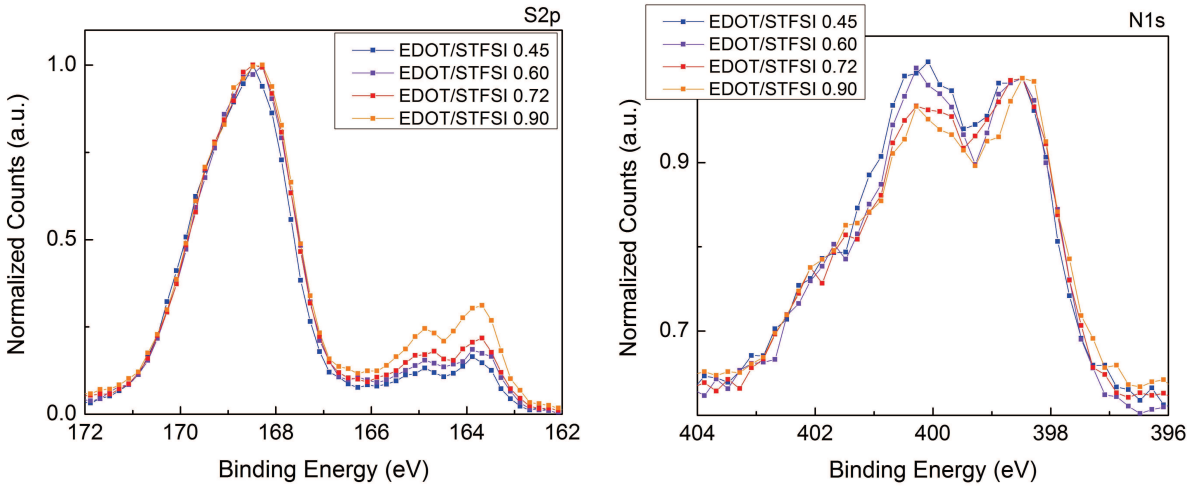

Fig. 2.15: XPS S2p (left) and N1s (right) spectra of PEDOT:STFSI with different EDOT to STFSI ratios, measured on film

$(\frac{EDOT}{STFSI})_{theo}$	$(\frac{EDOT}{STFSI})_{expS2p}$	$(\frac{STFSI^-}{STFSI})_{expN1s}$
0.48	0.30	0.36
0.60	0.33	0.36
0.72	0.38	0.40
0.90	0.52	0.40

Tab. 2.4: Theoretical and experimental composition (determined from XPS S2p spectra) and percentage of negatively charged STFSI units in PSTFSI (determined from XPS N1s spectra) of PEDOT:PSTFSI with varying EDOT to STFSI ratios

doublets of the sulfur atoms in the sulfonate environment of PSTFSI [21, 22, 23, 24, 25, 26, 27, 28]. By peak fitting and integration of these peaks the increasing PEDOT content in the complex with increasing EDOT to STFSI ratio was confirmed. However, the experimental EDOT to STFSI ratios obtained from integration of the XPS peaks were much lower than the theoretical EDOT to STFSI ratios (see table 2.4). This can be explained by the segregation of excess polyelectrolyte to the film surface, which has been described for PEDOT:PSS [29, 18].

A comparison of the N1s spectra of PSTFSIH and PEDOT:PSTFSI revealed, that for low PEDOT concentrations the PSTFSI in the PEDOT:PSTFSI complex is found in the same charge configuration as the pure PSTFSI polyelectrolyte in its acid form,

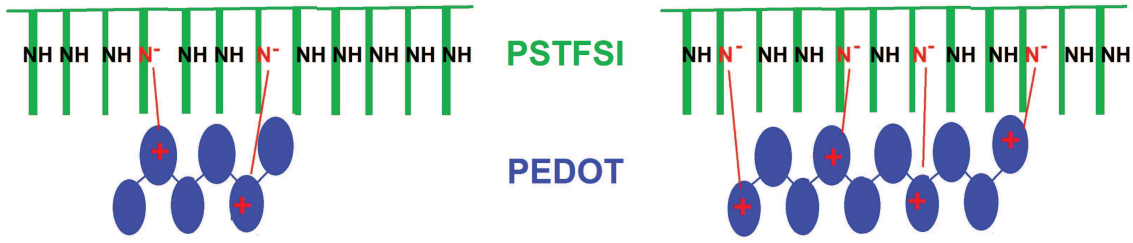

Fig. 2.16: Schematic illustration of the influence of the PEDOT concentration in PEDOT:PSTFSI on the charge distribution on the polymeric PSTFSI counter ion

bearing 36% to 40% negatively charged STFSI units. As it was shown in section 2.2, a mixed charged state with about 35% of negative STFSI units is energetically favorable for the system, due to the minimization of electrostatic repulsion and the formation of hydrogen bonding between the functional units. Therefore PSTFSI undergoes an acid base reaction under the acidic conditions of the EDOT polymerization and the partially charged form of PSTFSI is formed.

From figure 2.15 it can be seen, that for higher PEDOT concentrations the percentage of protonated STFSI-H units (peak at 400.2eV) decreased with respect to the negatively charged functionality (peak at 398.5eV). This is a sign for the decrease of excess PSTFSI (namely STFSI-H) and a higher percentage of negatively charged PSTFSI units interacting with PEDOT ($STFSI^-$-$PEDOT^+$) (see schematic in figure 2.16). However, the change in the charge distribution of PSTFSI was much less pronounced than the change in the composition of the PEDOT:PSTFSI complex. This suggests that the number of negatively charged STFSI units per EDOT unit decreased for higher PEDOT concentrations.

In order to exclude, that this observation was based on a surface effect, provoked by the segregation of excess PSTFSI to the film surface, XPS measurements were performed on PEDOT:PSTFSI powder. The analysis of different probing spots on the same PEDOT:PSTFSI sample confirmed the heterogeneity of the PEDOT:PSTFSI system (see figure 2.17 and scheme in figure 2.18). Therefore, the measured composition of PEDOT:PSTFSI differed strongly from measuring point to measuring point and the average composition over three probing spots did not reflect the overall composition.

However, by correlating the S2p and N1s spectra of different probing spots, it was confirmed, that at the given pH the excess PSTFSI adopts a charge configuration with about 37% negatively charged STFSI units (see figure 2.17 and figure 2.18, "point1").

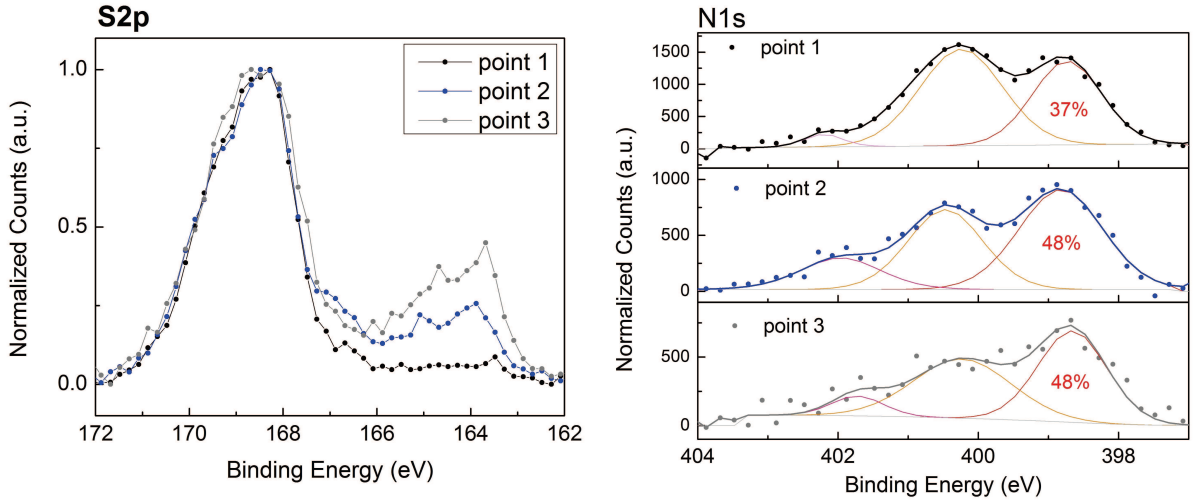

Fig. 2.17: XPS S2p and N1s spectra of PEDOT:STFSI, synthesized with EDOT to STFSI ratio 0.9 at 625rpm, measured on powder

Although the percentage of negative charges on PSTFSI increased with higher PEDOT concentrations (see figure 2.17 and figure 2.18, "point2" and "point3"), peak fitting of the N1s spectra revealed, that from a certain PEDOT concentration on the percentage of the negatively charged STFSI units stayed constant at 48% to 49%. This observation suggests, that the presence of doped PEDOT promotes, the stabilization of negative charges on PSTFSI. This is in perfect coherence with the results presented by Stoll and co-workers [30, 31, 32], who reported, that the percentage of the charged polyelectrolyte units increases upon the presence of oppositely charged macro-ions or nano-particles.
We can conclude, that in the PEDOT:PSTFSI complex PSTFSI bears negatively charged functional groups, which act as counter ion for the doped PEDOT, while the excess PSTFSI is protonated. With increasing PEDOT concentration the percentage of negatively charged STFSI groups increased until a maximum of negative charges was reached for about 50% $STFSI^-$ and 50% STFSIH units.
Therefore it can be assumed, that the degree of ionization of PSTFSI at the given pH and counter ion concentration is an inherent characteristic of the PEDOT:PSTFSI system.

Using the percentage of negatively charged groups on PSTFSI and the theoretical EDOT to STFSI ratio, the approximate number of negatively charged STFSI units (denoted by $STFSI^-$) per EDOT repeat unit can be estimated by

Fig. 2.18: Schematic illustration of the difference for XPS measurements on film and on powder

$$\frac{STFSI^-}{EDOT} \approx \frac{(STFSI^-/STFSI)_{N1s}}{(EDOT/STFSIX)_{theo}} \tag{2.5}$$

which results in $\frac{0.37}{0.9} = 0.41 < \frac{STFSI^-}{EDOT} < \frac{0.48}{0.9} = 0.53$ for an EDOT to STFSI ratio of 0.9 and $\frac{0.37}{1.1} = 0.34 < \frac{STFSI^-}{EDOT} < \frac{0.48}{1.1} = 0.44$ for an EDOT to STFSI ratio of 1.1, under the assumption that 37% to 48% of the STFSI units are negatively charged (as obtained from XPS fitting, see figure 2.17). Assuming that for an optimized doping of PEDOT about 35% of the EDOT units are positively charged [28, 33, 34], the $STFSI^-$ to EDOT ratio should be at least 0.35 in order to assure sufficient charge compensation. This approximation shows, that for high PEDOT concentrations in PEDOT:PSTFSI (EDOT to STFSI ratios >0.9) the estimated $STFSI^-$ to EDOT ratio approaches the critical theoretical value of 0.35. This indicates, that at these high PEDOT concentrations the density of negative charges on PSTFSI is not sufficient for an efficient charge compensation of the PEDOT.

Furthermore, it has been reported for colloidal systems of polyelectrolytes and surfactants, that the amount of polyelectrolyte, which is necessary for the formation of stable colloidal polyelectrolyte-surfactant complexes, is higher than the amount of polyelectrolyte, which leads to the charge compensation of the surfactant micelles [31].

In analogy to these findings the decrease in doping of PEDOT:PSTFSI for EDOT/STFSI >0.9 could be explained by the insufficient abundance of negative charges on PSTFSI, caused by the protonation of PSTFSI in the highly acidic synthesis conditions of PEDOT:PSTFSI with a pH<pK_a(PSTFSI).

Therefore we can conclude, that the inherent properties of the PSTFSI polyelectrolyte, such as its pK_a, can affect the doping and the complexation of the PEDOT in PEDOT:PSTFSI.

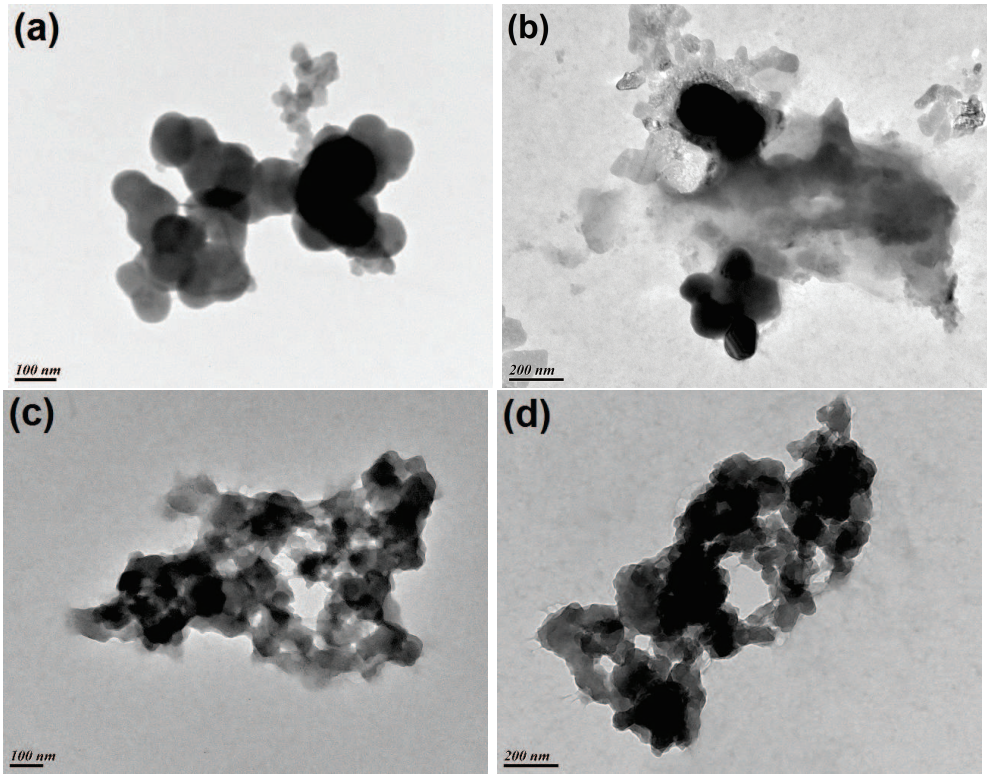

Fig. 2.19: TEM images of PEDOT:PSTFSI with molar EDOT/STFSI ratio of a)0.48, b)0.60, c)0.72 and d)0.90

In order to investigate, if the morphology of the PEDOT:PSTFSI complex was affected by the changing EDOT to PSTFSI ratios, the dispersions where characterized by microscopy, electrophoresis and rheology experiments.
TEM images of PEDOT:PSTFSI with an EDOT to STFSI ratio of 0.48 showed aggregates of round particles with an approximate diameter of 70nm to 100nm (see figure 2.19). For higher EDOT concentrations, the agglomerate size increased and for EDOT/STFSI>0.72 no distinct particles could be observed. This is a sign for the saturation of the PSTFSI template with PEDOT, which resulted in heterogeneous agglomerates of PEDOT:PSTFSI.

As already mentioned, capillary electrophoresis allows to separate the PEDOT:PSTFSI complex from the excess PSTFSI in the dispersion. The analysis of PEDOT:PSTFSI dispersions with different compositions (see figure 2.20) confirmed, that the amount of excess PSTFSI was reduced with increasing PEDOT content. By peak integration it was found, that the relative peak area of the peak corresponding to the PEDOT:PSTFSI complex (indicated as P1 in figure 2.20) correlated with the EDOT to STFSI ratio (see table 2.5). However, this correlation did not hold for EDOT to

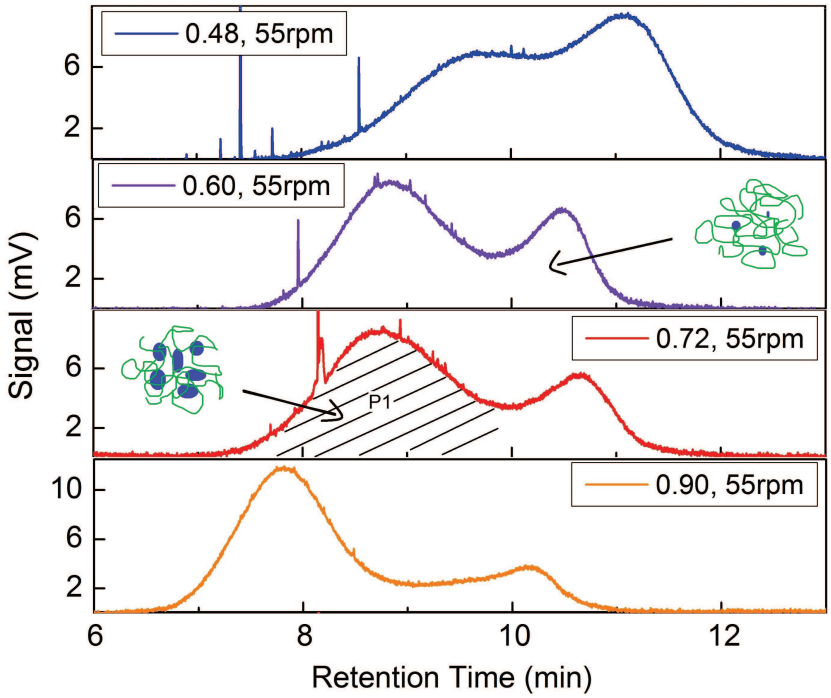

Fig. 2.20: Electro chromatogram of PEDOT:PSTFSI dispersions with molar EDOT to STFSI ratios of 0.48, 0.6, 0.72 and 0.9; detection wavelength 230nm

Molar Ratio $\frac{EDOT}{STFSI}$	$\frac{PeakAreaP1}{TotalPeakArea}$
0.48	0.48
0.60	0.65
0.72	0.72
0.90	0.77

Tab. 2.5: Molar EDOT to STFSI ratio and percentage of the peak area corresponding to the PEDOT:PSTFSI complex

STFSI ratios of 0.90, for which the detected amount of PEDOT:PSTFSI was lower than the one expected. This supports, that for EDOT to STFSI ratios of 0.9 or higher the PSTFSI complexing agent becomes saturated with PEDOT. However, even at high EDOT concentrations a certain amount of excess PSTFSI was found in the dispersion, indicating, that a perfectly efficient complexation between PEDOT and PSTFSI was not reached.

The rheological characterization of the PEDOT:PSTFSI dispersions gave a further insight in the structure of the PEDOT:PSTFSI complexes. The PEDOT:PSTFSI dispersions displayed the typical behavior of shear thinning viscoelastic fluids, in which

a higher loss modulus G" than storage modulus G' and the absence of a plateau of G' at low frequencies signifies weak colloidal forces and a low degree of internal structure (see figure 2.21). However, the presence of a low yield stress of 0.02Pa (see figure A.4, appendix page 218), which corresponds to the critical stress to make the dispersion flow, confirmed a certain degree of internal structure. With increasing EDOT concentration the absolute value of the moduli and of the viscosity increased slightly (see figure 2.21 and figure A.4, appendix page 218) and at an EDOT to STFSI ratio of 0.9 a change in the rheological properties was observed. At this concentration the dispersion showed a more elastic behavior at low strain (<5%) (see figure 2.21), indicating higher colloidal forces and a higher degree of internal structure at rest. However, this structure was easily disrupted for shear strains >1.5% and frequencies >40rad.s^{-1} and the absence of a yield stress affirmed the low structural strength (see figure A.4, appendix page 218).

The increase of the viscosity and of the degree of internal structure with increasing PEDOT concentration up to an EDOT to STFSI ratio of approximately 0.72 can be explained by the assumption, that the doped PEDOT interacts with several PSTFSI stabilizer chains and forms PEDOT rich domains, which represent nodal points in a three dimensional PEDOT:PSTFSI network. Therefore, a higher concentration of PEDOT corresponds to a higher degree of crosslinking in the network, resulting in higher viscosity and a higher degree of solid-like behavior. At a critical PEDOT concentration the soluble PSTFSI stabilizer becomes saturated with insoluble PEDOT, which explains the development of rheological instabilities and the eventual precipitation of the complexes from the dispersions.
This is in coherence with the decrease in doping of PEDOT observed in the PEDOT:PSTFSI complexes with EDOT to STFSI ratios of 0.9 or higher. Therefore, the colloidal stability and the doping of the PEDOT:PSTFSI system depend in equal measure on the complex composition and are determined by the inherent stabilization capacity of PSTFSI.

For the sake of comparison, a corresponding study was performed on synthesized PEDOT:PSS. As is can be seen from figure 2.22 the absorption coefficient of PEDOT:PSS increased proportionally to the EDOT concentration, in analogy to the

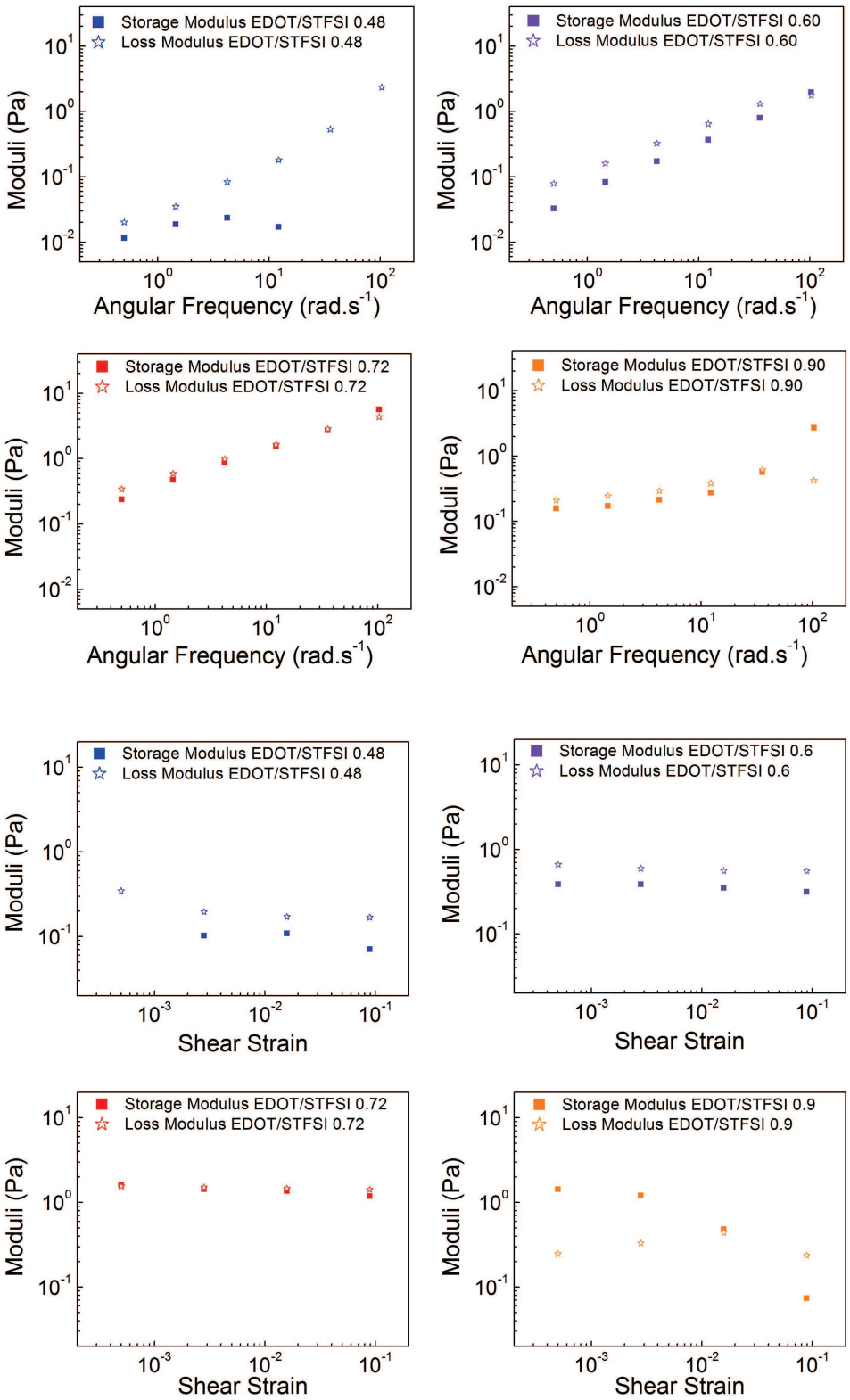

Fig. 2.21: Storage and Loss Moduli of PEDOT:PSTFSI with EDOT to STFSI ratios of 0.48, 0.6, 0.72 and 0.9 as a function of shear frequency at 2% strain and as a function of strain at 10rad.s^{-1}

behavior observed for PEDOT:PSTFSI. However, the absolute value of the absorption coefficient of PEDOT:PSS was considerably higher than the one of PEDOT:PSTFSI at the same ratio of EDOT to polyelectrolyte unit and the same synthesis conditions. An increase in the absorption coefficient could either be explained by a higher conversion of EDOT, or by a different scattering of the film, as light scattering effects were not taken into account for the measurement of T and the calculation of the absorption coefficient a.

Regarding the evolution of the conductivity with the complex composition, PEDOT:PSS shows a comparable behavior as PEDOT:PSTFSI. For low EDOT concentrations the conductivity increased with the EDOT content, which can be attributed to a better percolation of the conducting PEDOT rich domains in the PEDOT:polyelectrolyte films with increasing PEDOT concentration. For molar ratios of EDOT to PSS units >1 a decrease in the conductivity was observed, which is in analogy to the behavior of the PEDOT:PSTFSI system. The highest FoM was reached for a molar EDOT/SS ratio of about 0.5 to 0.6, which corresponds to a weight ratio of PSS/PEDOT between 2.3 and 2.6. This ratio is in perfect agreement with the EDOT/SS ratios, which are reported for highly conducting PEDOT:PSS in literature [35, 25, 36, 37, 38, 39, 40].

In conclusion, it was shown, that the ratio of PEDOT to PSTFSI does significantly influence the opto-electronic properties of the resulting PEDOT:PSTFSI complex. On one hand, the PEDOT concentration has to be high enough to allow the formation of a percolated conducting network in the PEDOT:PSTFSI film. On the other hand, at a too high PEDOT concentration a saturation of PSTFSI with PEDOT is reached. This leads to a decrease of the colloidal stability of the dispersion, a decrease of the doping level of PEDOT and a drop of the conductivity. The stabilization capacity of the PSTFSI polyelectrolyte was found to be influenced by its acid-base behavior and the charge distribution on the STFSI units in the acidic medium during the EDOT polymerization. The highest FoM for PEDOT:PSTFSI was found for a EDOT to STFSI ratio of 0.6. The comparison to PEDOT:PSS revealed, that the evolution of the opto-electronic properties as a function of the PEDOT concentration is very similar in both systems.

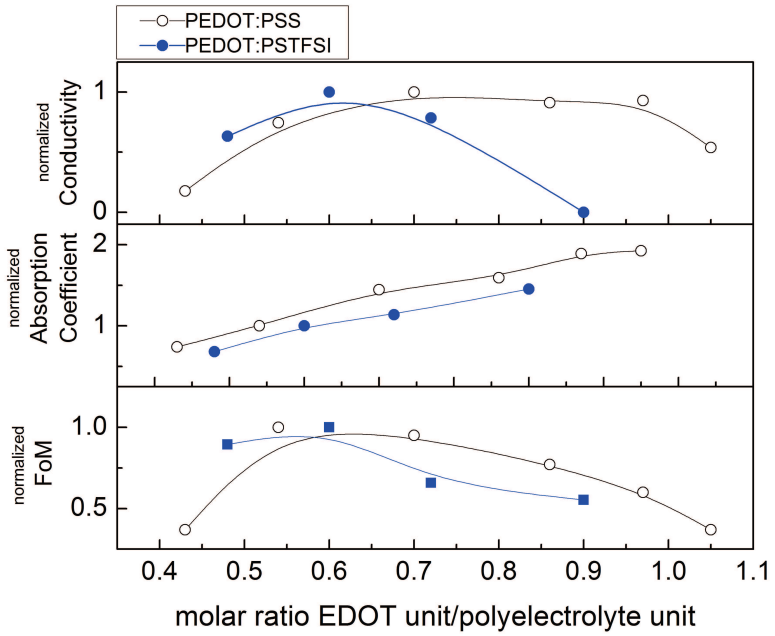

Fig. 2.22: Conductivity, absorption coefficient and FOM of PEDOT:PSS ($M_W(PSS)$ ≈200kDa) and PEDOT:PSTFSI ($M_W(PSTFSIK)$ ≈300kDa) as a function of the molar ratio EDOT/polyelectrolyte repeating unit, synthesized at 10°C and magnetic stirring at 625rpm

2.4 The Role of the pH During the PEDOT:PSTFSI Synthesis

It has been reported in literature, that the reaction kinetics of the oxidative polymerization of EDOT and the opto-electronic properties of the resulting PEDOT complexes are susceptible to changes in the pH. For the in situ polymerization of PEDOT, for example, bases such as pyridine or imidazole are widely used to slow down the reaction kinetics, which leads to a drastic enhancement of the film conductivity [41, 42, 43]. In contrast, the presence of acids in the synthesis medium was reported to accelerate the polymerization kinetics of PEDOT and to favor the formation of EDOT dimers and trimers [15]. As these observations concern the synthesis of PEDOT in non aqueous medium, our objective was to investigate whether the pH of the aqueous PSTFSI synthesis medium influences the reaction kinetics of the EDOT polymerization and opto-electronic properties of the resulting PEDOT:PSTFSI.

2.4.1 Synthesis of PEDOT:PSTFSI in Basic Conditions

In order to investigate if the beneficial effect of organic bases on the conductivity of in-situ PEDOT:Tos can be transferred to the aqueous dispersion polymerization of EDOT, PEDOT:PSTFSI was synthesized in the presence of imidazole. Table 2.6 displays the opto-electronic properties of PEDOT:PSTFSI, synthesized with different concentrations of imidazole in the aqueous synthesis medium. It can be seen that the conductivity was suppressed due to the presence of the base. Upon the addition of imidazole in a molar ratio of imidazole/Fe^{3+} higher than 13 the polymerization was completely inhibited.

The corresponding UV/Vis spectra (see figure 2.23) show that the presence of imidazole resulted in a decrease of the bipolaronic absorption in PEDOT:PSTFSI, which can be interpreted as a lower degree of doping. A closer look on the spectrum of PEDOT:PSTFSI synthesized with a high imidazole concentration reveals the presence of two atypical kinks, at 950nm and at 1120nm, for which no explanation was found.

It is known that under basic conditions iron hydroxide complexes, *e.g.* $FeOH_3$ or $[Fe(OH)_2(H_2O)_4]^+$, are formed, which are insoluble and form a brownish precipitate in the solution. Therefore, the addition of a base to the synthesis medium leads to the precipitation of Fe^{3+} complexes, which rendered the synthesis medium slightly yellowish-brown. This precipitation simply corresponds to a decreasing concentration of the oxidizing specie and results in lower doping of PEDOT or, in the extreme case, in the quenching of the reaction. An inhibited reaction could be re-initiated upon the addition of excess $FeCl_3$ or upon the neutralization of the solution with acid. This reversible inhibition of the polymerization was also observed upon the addition of other inorganic bases, such as NaOH, or ion exchange resins with proton accepting functionalities, which confirms that this effect is caused by the strong presence of hydroxide ions and was not specifically linked to the molecule imidazole.

Therefore we can conclude that the presence of a base shows a detrimental effect on the doping and conductivity of dispersion polymerized PEDOT:PSTFSI.

Molar Ratio Imidazole/EDOT	Molar Ratio Imidazole/$FeCl_3$	Conductivity[a,b] ($S.cm^{-1}$)	Absorption Coefficient[a] (10^3 cm^{-1})	FoM[a]
0	0	55±5	1.7±0.4	5±0.5
1	3.6	1±0.5	2.1±0.4	0.7 ±0.2
2	7.1	0	2.7±0.5	0
4	14.2	-	-	-

[a] average on 8 measurements or more [b] determined by 4-point measurements

Tab. 2.6: Opto-electronic performance of PEDOT:PSTFSI synthesized with different concentrations of Imidazole, at 10°C, M_W(PSTFSIK)≈20kDa, stirring 100rpm

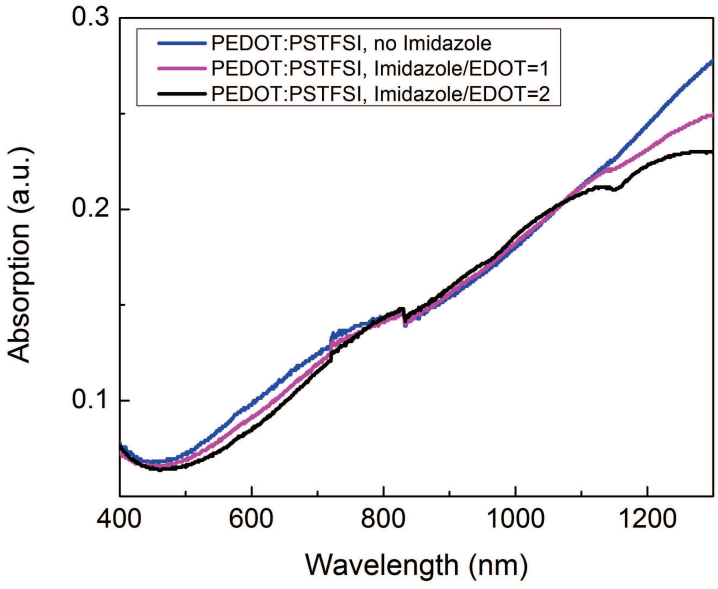

Fig. 2.23: UV/Vis spectra of PEDOT:PSTFSI films, synthesized with different concentrations of Imidazole at 10°C, PSTFSIK 20kDa, stirring 100rpm

2.4.2 Synthesis of PEDOT:PSTFSI in Acidified Solution

Unlike the decelerating effect of bases on the PEDOT reaction kinetics, the presence of acids was reported to accelerate the EDOT polymerization and to stabilize PEDOT in the dimeric and trimeric form [15]. To investigate if this applies to the synthesis of PEDOT:PSTFSI, EDOT was polymerized in acidified PSTFSI solutions and the reaction kinetics were studied by monitoring of the UV/Vis absorption.

From figure 2.24 it can be seen, that the conductivity of PEDOT:PSTFSI synthesized in acidified solution (in 0.01M HCl: PEDOT:PSTFSI$_{HCl0.01M}$ and in 0.1mM HCl: PEDOT:PSTFSI$_{HCl0.1mM}$, respectively) was about 50% lower than the one of the reference sample, independently of the acid concentration. In contrast, the absorption coefficient of PEDOT:PSTFSI$_{HCl0.1mM}$ was equal to the absorption coefficient of PEDOT:PSTFSI$_{reference}$, whereas the synthesis in 0.01M HCl PSTFSI solution gave rise to a 1.5 fold increase in the absorption coefficient. Resulting from the loss in conductivity and the rise of the absorption, the FoM decreased drastically as a function of the acid concentration (FoM$\sim \sigma$ and FoM$\sim \frac{1}{a}$).

In order to study the influence of the pH on the reaction kinetics, the absorption of PEDOT:PSTFSI was monitored during the EDOT polymerization. Figure 2.25 displays the temporal evolution of the absorption at 550nm, 720nm and 1300nm of PEDOT:PSTFSI during the EDOT polymerization in neutral and in acidified PSTFSI solution. As the UV/Vis monitoring was performed under the standard conditions, and not in dilute medium, the absorption of the dark blue dispersion reached the saturation of the instrument after 15 minutes of synthesis.

In contrast to the expected behavior, the polymerization kinetics were not significantly affected by the presence of the acid. Thus, the drastic change in opto-electronic performance can not be explained by changing reaction kinetics.

The comparison of the corresponding UV/Vis spectra (see figure 2.26) points out, that the change in the opto-electronic performance can be explained by a change in doping. With an increasing acid concentration in the synthesis medium the typical features correlated to poor doping were observed, namely a decrease in the bipolaronic absorption and a rise of the polaronic absorption of PEDOT:PSTFSI. In addition, PEDOT:PSTFSI$_{HCl0.01M}$ showed a non negligible absorption in the high energy regime of the spectrum. This could confirm the findings of Kirchmeyer *et al.* [15], who claimed

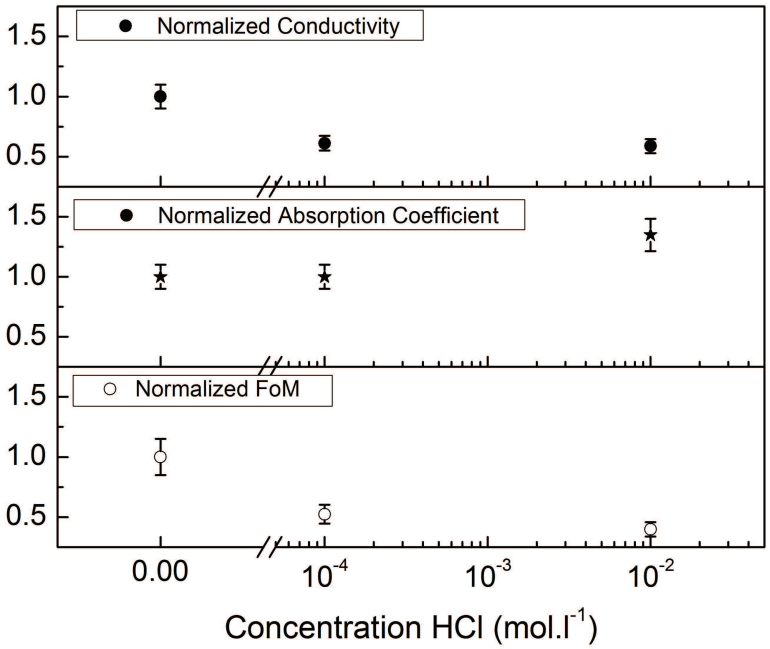

Fig. 2.24: Opto-electronic properties of PEDOT:PSTFSI synthesized in different pH, PSTFSIK solution at 9g.l^{-1}, equivalent to 0.025mol.l^{-1} STFSI nuits

that acids stabilize short oligomeric forms of PEDOT, which shows a characteristic absorption at 400nm and below. Therefore the observed drop in conductivity can be attributed to poor doping and possibly to the more important concentration of short PEDOT oligomers.

In order to clarify, if the changes in the opto-electronic properties of PEDOT:PSTFSI were really related to the acidity of the synthesis medium or to the general presence of ions in the solution, PEDOT:PSTFSI was synthesized from PSTFSIK solutions containing NaCl (PEDOT:PSTFSI$_{NaCl}$). Figure 2.27 displays the opto-electronic properties of the obtained PEDOT:PSTFSI dispersions.

Similarly to the PEDOT:PSTFSI synthesized in acidified solution (PEDOT:PSTFSI$_{HCl}$), also PEDOT:PSTFSI$_{NaCl}$ showed a decrease in conductivity, which was independent of the ionic concentration. However, the drop of the conductivity to around 75% of the initial value, due to the presence of NaCl, was considerably smaller than the drop caused by the presence of acid (55% of initial value). In contrast to the observation made for PEDOT:PSTFSI$_{HCl}$, the absorption coefficient of PEDOT:PSTFSI$_{NaCl}$ was unaffected over a wide range of salt concentrations. The marginal rise in the absorption coefficient of

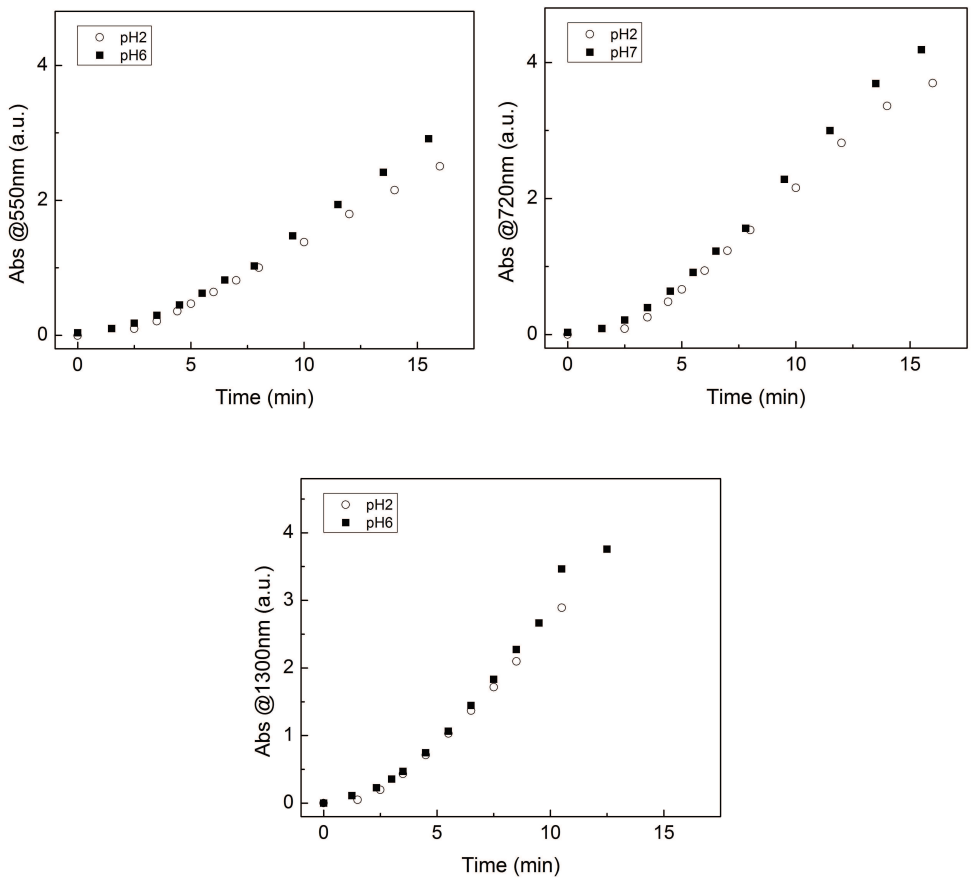

Fig. 2.25: Absorption at 550nm, 720nm and 1300nm of PEDOT:PSTFSI synthesised in pristine PSTFSI solution at pH6 and in acidified PSTFSI solution at pH2 as a funtion of time, $M_W(PSTFSIK) \approx 250kDa$

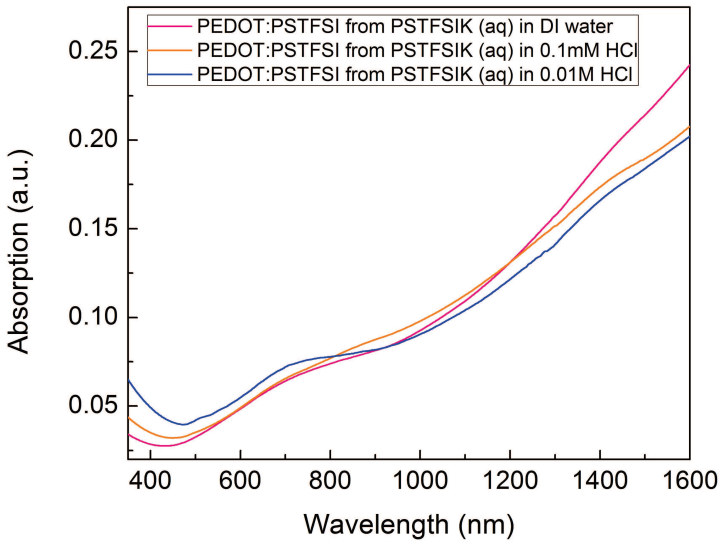

Fig. 2.26: UV/Vis spectra of PEDOT:PSTFSI films synthesized from PSTFSIK solutions with different concentrations of HCl; $M_W(PSTFSIK)$ ≈250kDa, PSTFSIK solution at 9g.l^{-1}, equivalent to 0.025mol.l^{-1} STFSIK units

PEDOT:PSTFSI$_{0.2M_NaCl}$ can be explained by the whitish aspect of the films, which was attributed to residual salt and which reduced the film transparency due to scattering.

The probing of PEDOT:PSTFSI$_{NaCl}$ by UV/Vis spectrometry (see figure 2.28) revealed a decrease of the bipolaronic absorption compared to the standard PEDOT:PSTFSI. Therefore, the loss of conductivity caused by the presence of NaCl in the synthesis medium can be attributed to a slight decrease of the doping level of PEDOT.

This leads to the conclusion, that high ion concentrations in the synthesis medium cause a decline of the doping level in PEDOT:PSTFSI. A possible explanation is the collapse of the PSTFSI chains in solutions with high ionic strength, which renders the formation of PEDOT on the PSTFSI template more difficult. In addition, the strong presence of ions could shield the electrostatic interactions between the STFSI$^-$ units and PEDOT, leading to a decrease in doping. Acidic synthesis conditions showed an even more drastic influence on the doping and conductivity of PEDOT:PSTFSI. Especially the increasing absorption of PEDOT:PSTFSI at 400 nm suggests, that acidic conditions favour the formation of PEDOT trimers, which further decreases the conductivity.

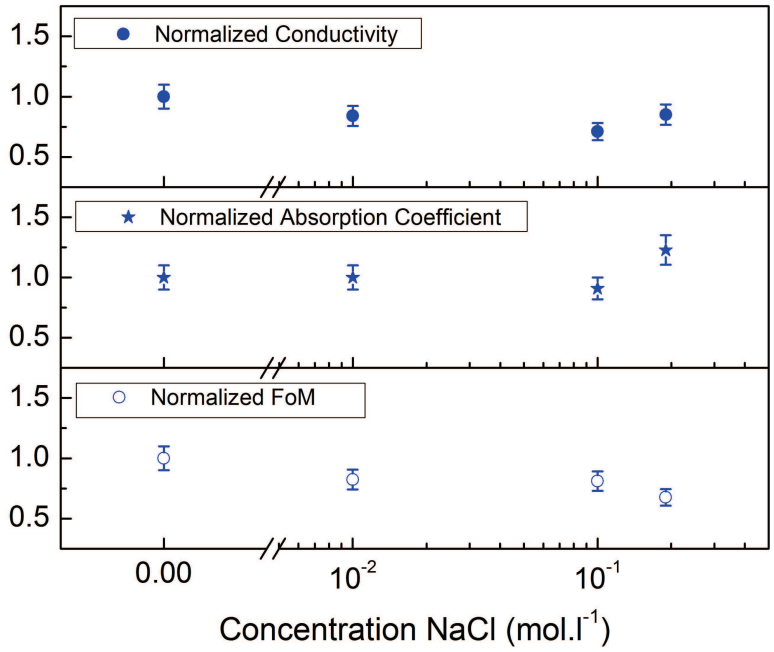

Fig. 2.27: Opto-electronic properties of PEDOT:PSTFSI synthesized in PSTFSIK solutions containing different concentrations of NaCl; PSTFSIK solution at 9g.l^{-1}, equivalent to 0.025mol.l^{-1} STFSI nuits

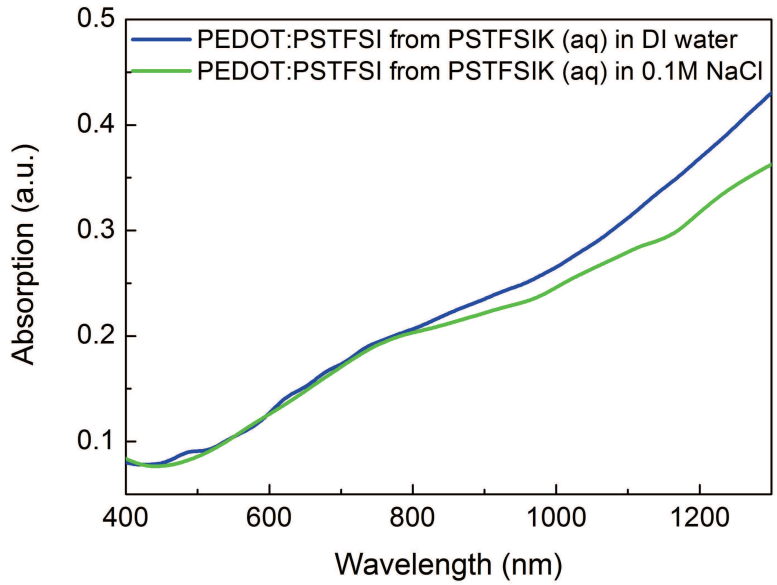

Fig. 2.28: UV/Vis spectra of PEDOT:PSTFSI dispersions synthesized from PSTFSIK soultions with different concentrations of NaCl; PSTFSIK solution at 9 g.l^{-1}, equivalent to 0.025mol.l^{-1} STFSIK units

To summarize, it was shown that the pH and the ion concentration of the PSTFSIK synthesis medium greatly affect the opto-electronic properties of the resulting PEDOT:PSTFSI. For PEDOT:PSTFSI synthesized in acidified PSTFSIK solutions, a drastic decrease of the conductivity was observed. It was shown that the lower pH did not affect the synthesis kinetics, however, the degree of doping was significantly lowered and signs for the presence of short PEDOT oligomers were found. Further investigations revealed that a similar decrease of the doping was observed upon the addition of NaCl to the synthesis medium. Therefore we can state, that high ion concentrations in the synthesis medium have a detrimental effect on the conductivity PEDOT:PSTFSI, which could be provoked by a change in the conformation of the PSTFSI chains and electrostatic screening effects that hinder the interaction of STFSI groups with PEDOT.

2.4.3 Synthesis of PEDOT:PSTFSI from Acidic PSTFSI Solution

As the polyelectrolyte PSTFSI shows an acid-base behaviour (see section 2.2), the pH of the synthesis medium can not only be lowered by the addition of an acid, but also by changing the counter ion of PSTFSI from potassium to hydrogen. In this way an acidic synthesis environment is created, without the presence of supplementary ions. The synthesis of PEDOT:PSTFSI from neutral PSTFSIK solution and from PSTFSIH solution at pH 2 allowed the comparative study of the kinetics, doping and morphology and their influence on the opto-electronic performance of the resulting PEDOT:PSTFSI. In addition, the properties of PEDOT:PSTFSI, synthesized from the potassium salt and from the acid form of PSTFSI, were compared to the ones of PEDOT:PSS, synthesized from the sodium salt or from the acid form of PSS.

Table 2.7 summarizes the opto-electronic properties of PEDOT:PSTFSI and PEDOT:PSS, synthesized from the salt and acid forms of the respective polyelectrolytes. PEDOT:PSTFSIH showed an average conductivity of 327S.cm^{-1}, which corresponds to 2.4 fold increase in conductivity with respect to PEDOT:PSTFSIK. As the absorption coefficient was found to be constant within the error bar, the FoM jumped from about 10 to almost 24. In case of PEDOT:PSS the use of the acidic form PSSH was beneficial

as well, and resulted in a 1.6 fold increase of the conductivity compared to PEDOT:PSSNa, from 196S.cm^{-1} to 305S.cm^{-1}. Together with a non negligible decrease in the absorption coefficient this led to a doubling of the FoM.

	Conductivity^{a,b} (S.cm^{-1})	Absorption Coefficient^{a} (10^3 cm^{-1})	FoM^{a}
PEDOT:PSTFSI K	134±15	2.1±0.3	10.1±1.5
PEDOT:PSTFSI H	327±21	2.2±0.2	23.7±1.9
PEDOT:PSS Na	196±18	3.2±0.3	9.8±0.6
PEDOT:PSS H	305±19	2.5±0.2	19.0±2.1

^{a} average on 8 measurements or more ^{b} determined by 4-point measurements

Tab. 2.7: Opto-electronic properties of PEDOT:PSTFSI and PEDOT:PSS dispersions, synthesized from the salt and acid form of the respective polyelectrolyte, under N_2, 625rpm mechanical stirring, at 10°C

In a first step it was investigated if the difference in counter ion of PSTFSI persisted in the PEDOT:PSTFSIH and PEDOT:PSTFSIK complex, as the presence of K^+ ions could affect the properties of PEDOT:PSTFSIK. The study of the literature regarding the presence of Na^+ in PEDOT:PSSNa does not allow to draw a clear conclusion on the question, as different results have been reported [28, 44]. In order to examine PEDOT:PSTFSIK for potential residual potassium ions, the K1s signal in the XPS spectra of PEDOT:PSTFSIK was analyzed. In PSTFSIK the K1s signal at 296 eV was clearly present, in PSTFSIH it was very low and it was absent in PEDOT:PSTFSIK/H, which indicates that the potassium concentration in both PEDOT:PSTFSI complexes was negligible (see figure 2.29).

The comparison of the XPS N1s spectra showed, that the spectra of PEDOT:PSTFSIK and PEDOT:PSTFSIH were almost congruent (see figure 2.29). By peak fitting it was found, that the peak at 398.5 eV, attributed to negatively charged STFSI groups, represented 38% and 36% of the total nitrogen atoms in PEDOT:PSTFSIK and in PEDOT:PSTFSIH, respectively (see table 2.8). This confirms the results discussed in the sections 2.2 and 2.3 of this work, which show, that under acidic conditions the polyelectrolyte stabilizes in a partially anionic and partially neutral state with approximatively 38% $STFSI^-$ units. Therefore the difference in counter ions of the PSTFSI template polymer can be considered as negligible in the PEDOT:PSTFSI complex and can be excluded as reason for the changing opto-electronic properties.

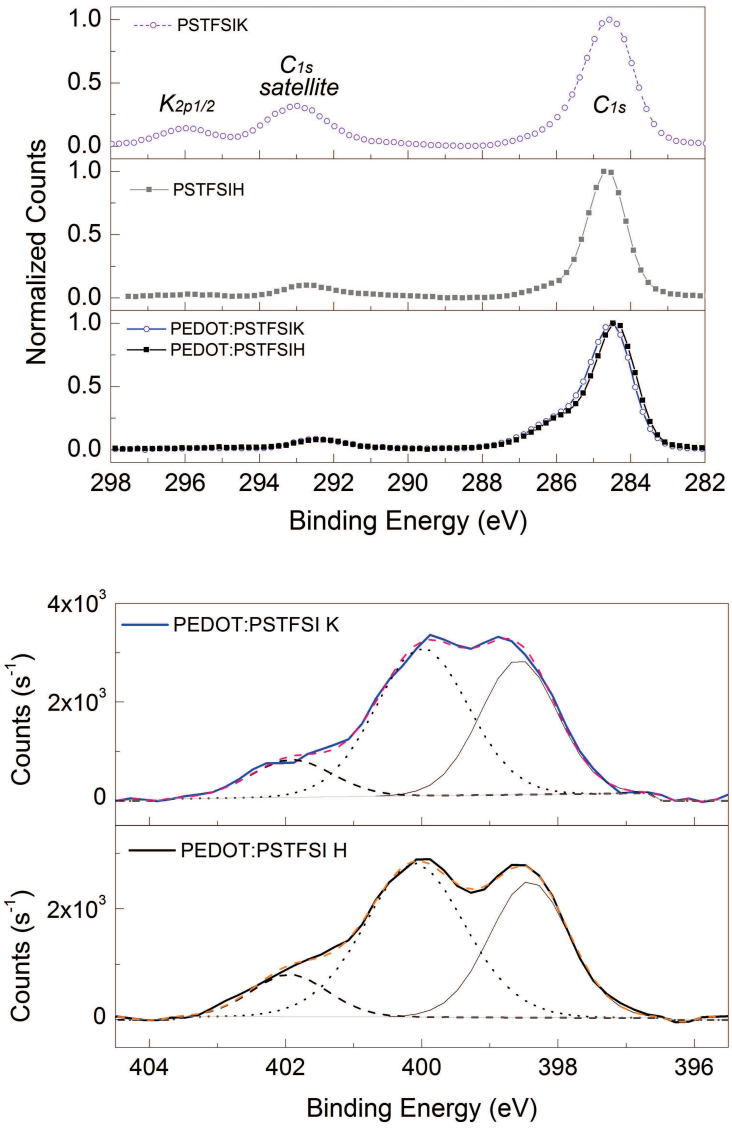

Fig. 2.29: XPS C1s/K2p1/2 spectra of PSTFSIK, PSTFSIH, PEDOT:PSTFSIK and PEDOT:PSTFSIH (left) and XPS N1s spectra of PEDOT:PSTFSIK and PEDOT:PSTFSIH with peak fitting

Peak Position		FWMH		Area	
PEDOT:PSTFSIK	PEDOT:PSTFSIH	PEDOT:PSTFSIK	PEDOT:PSTFSIH	PEDOT:PSTFSIK	PEDOT:PSTFSIH
398.6	398.4	1.3	1.4	38%	36%
400.0	400.1	1.6	1.7	51%	53%
401.9	401.9	1.4	1.3	11%	11%

Tab. 2.8: Peak positions, Full Width at Maximum Height (FWMH) and integrated area of the XPS N1s peak fit of PEDOT:PSTFSIK and PEDOT:PSTFSIH

One possibility to study the reaction kinetics of EDOT in the PSTFSI solution is the monitoring of the pH of the synthesis medium. As the polymerization of EDOT implies the generation of acidity, the pH is expected to decrease during the PEDOT synthesis. In a first step the oxidants were added to the PSTFSI solution, which caused a drop in the pH from 5.53 to 2.46 for the PSTFSIK solution and from 2.03 to 1.91 for the PSTFSIH solution. After the stabilization of the pH the EDOT monomer was added and the pH was monitored during the polymerization. Figure 2.30 displays the evolution of the pH during the EDOT polymerization in the aqueous solution of PSTFSIK and PSTFSIH. Upon the addition of the EDOT monomer the pH decreased steadily during 200min in both systems. Afterwards the pH stayed constant at around 2.07 in the PEDOT:PSTFSIK solutions, apart from small fluctuations within the measuring precision. In the case of PEDOT:PSTFSIH the pH stabilized first at pH 1.72 and at 800 min of polymerization time the pH decreased again until it stabilized at 1.65.
In order to explain this behavior the following hypothesis was developed using the assumption that the EDOT conversion was about 80% under the used polymerization conditions [45, 46]. From a EDOT concentration of 0.014 mol.l^{-1}

$$0.014 mol.l^{-1} \cdot 2 \cdot 0.08 = 0.022 mol.l^{-1} \tag{2.6}$$

of free H^+ will be generated. The PSTFSIK present in the solution will act as base for a pH smaller than its pK_a, which is 2.3. From the results presented in section 2.2 it is known that PSTFSI tends to stabilize in a partly protonated state comprising about 38% $STFSI^-$ units and 62% STFSI-H units. At the given concentration of 0.023 mol.l^{-1} STFSI functional units in the reaction medium, this results in

$$0.023 mol.l^{-1} \cdot 0.62 = 0.014 mol.l^{-1} \tag{2.7}$$

potentially basic $STFSI^-$ units. Upon the neutralization of these units with the generated protons an excess of

$$0.022 mol.l^{-1} - 0.014 mol.l^{-1} = 0.008 mol.l^{-1} \tag{2.8}$$

protons will be present in solution. The pH of such solution amounts to

$$pH = -log(c_{H^+}) = -log(0.008) = 2.10 \tag{2.9}$$

This estimated pH correlates very well with the experimentally measured value.
In the case of PSTFSIH the polyelectrolyte is already in the stable, partially protonated state, comprising about 38% of negatively charged $STFSI^-$ units and 62% protonated STFSI-H units, of which approximatively 11% are stabilized by strong inter-functional hydrogen bonding. As mentioned earlier in this chapter, the charge distribution on PSTFSI was not altered upon the synthesis of the PEDOT:PSTFSI complex. Therefore we assumed that no further acid base reaction takes place, which leaves the additional $0.022 mol.l^{-1}$ of H^+, generated during the polymerization of EDOT, un-neutralized. The pH of the solution can be estimated by

$$pH = -log(c_{H^+}) = -log(0.022) = 1.66 \tag{2.10}$$

which is coherent with the experimentally measured final pH of 1.65. However, this does not explain the stepwise change in the pH between 700min and 1200min.

In order to get a deeper insight in the reaction kinetics, the UV/Vis absorption of the PEDOT:PSTFSIK and PEDOT:PSTFSIH dispersions was monitored during the EDOT polymerization. The figure 2.31 shows the temporal evolution of the absorption spectra of PEDOT:PSTFSIK and PEDOT:PSTFSIH. To facilitate the analysis, the absorption of PEDOT:PSTFSIK and PEDOT:PSTFSIH at fixed wavelengths were plotted as a function of time (see figure 2.32). This allows a direct comparison of the absolute value of absorption, as well as of the rate of the change in absorption ($\partial(absorption)/\partial t$), which is related to the polymerization kinetics.

After an initially very slow increase of the absorption, correlated to the slow kinetics of the EDOT radical cation formation and the subsequent dimerisation [15], the absorption increased faster during fast chain growth. For PEDOT:PSTFSIK and PEDOT:PSTFSIH the evolution of the absorption was the same up to approximately 200min of synthesis, which shows that the initial reaction kinetics were not affected. At synthesis times longer than 250min ($\approx$ four hours) the absorption of PEDOT:PSTFSIH deviated from the absorption of PEDOT:PSTFSIK. During the EDOT polymerization

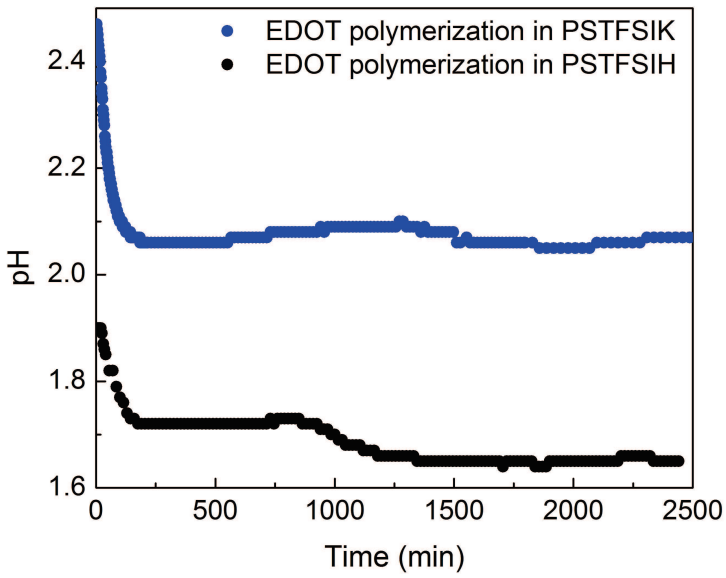

Fig. 2.30: Evolution of the pH during the EDOT polymerization in aqueous PSTFSIK and PSTFSIH solution; t=0min: EDOT monomer is added to the PSTFSI-oxidants solution

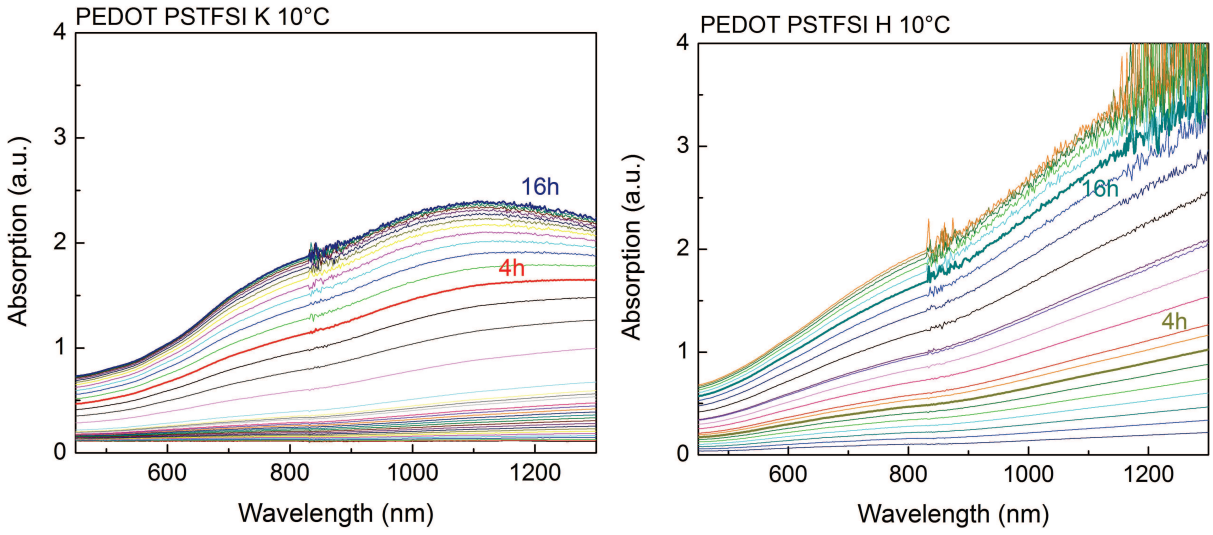

Fig. 2.31: UV/Vis absorption during the EDOT polymerization in PEDOT:PSTFSIK (left) and PEDOT:PSTFSIH (right) in dilute dispersion at 10°C

in PSTFSIK the absorption saturated after approximately 700min ($\approx$ 12 hours) of synthesis, whereas for PEDOT:PSTFSIH the reaction proceeded at the same rate and show a saturation only after about 1200min ($\approx$ 20 hours)(see figure 2.31 and figure 2.32). Thus, PEDOT:PSTFSIH showed a higher absolute value of absorption than PEDOT:PSTFSIK. This difference in absorption was particularly pronounced in the bipolaronic absorption regime ($\lambda > 1100$ nm), which indicates that it was the doping, that was further increased in PEDOT:PSTFSIH, whereas the conversion of EDOT was not significantly affected.

This was supported by the XPS S2p spectra, which did not display any difference in the composition of PEDOT:PSTFSIK and PEDOT:PSTFSIH (see figure 2.33). Therefore the higher conductivity of PEDOT:PSTFSIH can be attributed to a significant improve of doping. It is noteworthy, that this increase in bipolaronic absorption in PEDOT:PSTFSIH is observed simultaneously to the stepwise drop in the pH (compare figure 2.30). However, at this point no pertinent explanation for this phenomenon was found.

In PEDOT:PSS the same trends were observed (see figure 2.32 and figure A.8, appendix page 221). The initial reaction kinetics were not affected by the counter ion of PSS, on the long term, however, the absorption of PEDOT:PSSNa saturated earlier at a lower absolute value than for PEDOT:PSSH. However, the comparison of the PEDOT:PSS systems to PEDOT:PSTFSI revealed, that the reaction kinetics of the PEDOT synthesis were by far slower in PSS than in PSTFSI solutions and that the saturation was attained much later, at more than 4000min of synthesis.

In order to confirm the differences in doping, Raman spectroscopy with different excitation wavelengths was performed. Garreau *et al.* [47] reported, that due to resonance effects, the signatures of undoped PEDOT appear stronger in Raman spectra recorded at an excitation wavelength around 500nm, at which neutral PEDOT absorbs, whereas the signature of doped PEDOT are enhanced upon probing at higher wavelengths in the regime of polaronic and bipolaronic absorption. Therefore Raman spectra of PEDOT:PSTFSI and PEDOT:PSS were recorded at 532nm and at 785nm. The Raman spectra recorded at 532nm excitation wavelength of PEDOT:PSTFSIK and of PEDOT:PSTFSIH (see figure 2.34a) display the same main band at 1420cm^{-1} and at 1250cm^{-1}, which can be attributed to the symmetric C_α=C_β stretching mode and the

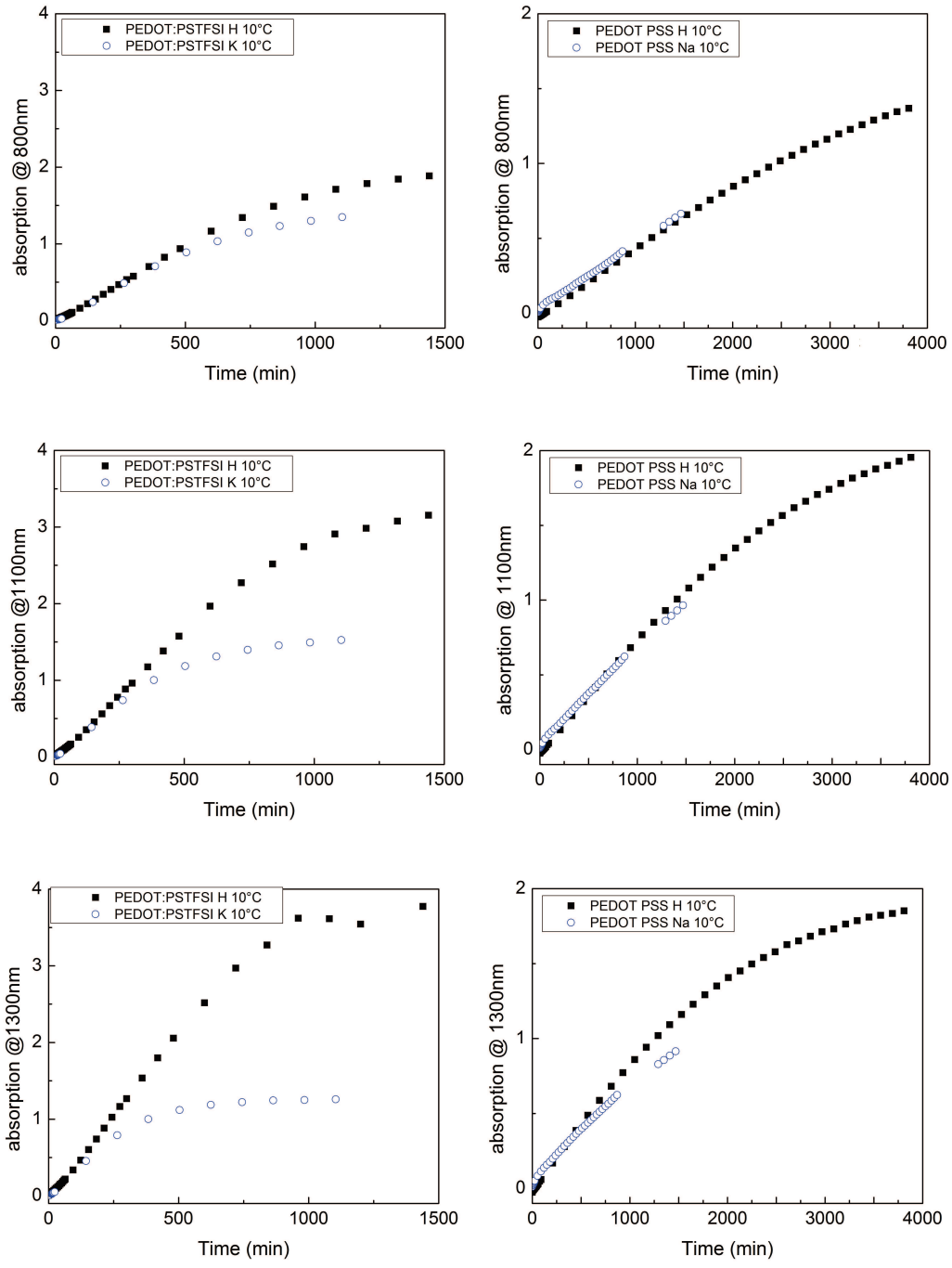

Fig. 2.32: Absorption of PEDOT:PSTFSIK, PEDOT:PSTFSIH, PEDOT:PSSNa and PEDOT:PSSH as a function of time at 800nm, 1100nm and 1300nm

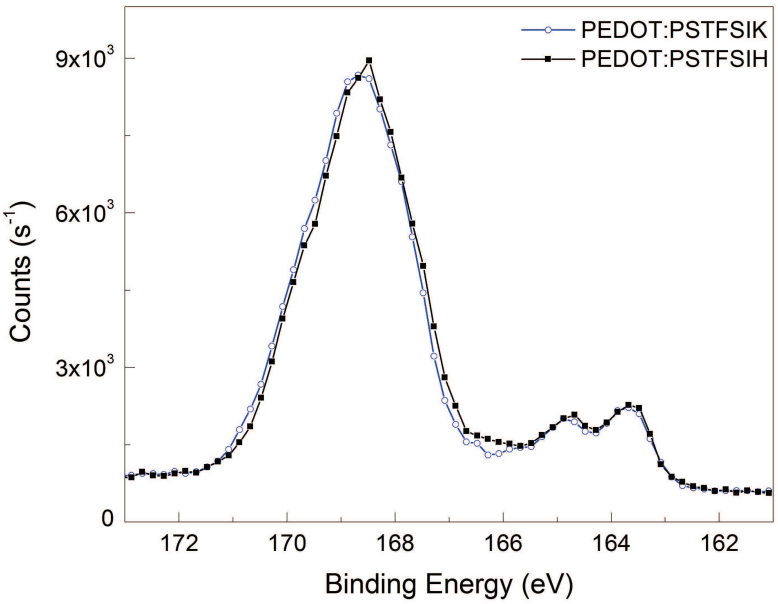

Fig. 2.33: XPS S2p spectrum of PEDOT:PSTFSIK and PEDOT:PSTFSIH

C_α-C_α stretching mode, respectively. However, PEDOT:PSTFSIH showed lower bands in the regime of the asymmetric C_α=C_β stretching at 1540cm^{-1} and at 1575cm^{-1} (see figure 2.34b). Studies of electro-polymerized PEDOT in literature showed that low assymmetric C_α=C_β bands can be correlated to high doping [47, 48], which confirms a higher degree of doping in PEDOT:PSTFSIH compared to PEDOT:PSTFSIK. The same trend can be seen in the Raman spectra recorded with an excitation wavelength of 785nm, in which PEDOT:PSTFSIH displayed a less pronounced shoulder at around 1529cm^{-1} than PEDOT:PSTFSIK (see figures 2.34b). The fact that the bands between 1500cm^{-1} and 1600cm^{-1} were more pronounced upon probing at 532nm, confirms that these bands are related to the undoped form of PEDOT. Therefore the less intense Raman bands of PEDOT:PSTFSIH in this regime are a sign for a higher degree of doping, which is perfectly in coherence with the conclusions drawn for UV/Vis spectroscopy.

The Raman spectrum ($\lambda_{excitation}$=785nm) of PEDOT:PSSH is very similar to the spectrum of PEDOT:PSTFSIH, indicating a similar doping as in PEDOT:PSTFSIH. At 532nm excitation wavelength the Raman spectra of PEDOT:PSS showed different characteristics in the asymmetric C_α=C_β stretching regime than PEDOT:PSTFSI, namely a more important peak at 1500cm^{-1} and lower bands at 1540cm^{-1} and

Sample	Radius 1 (nm)	Radius 2 (nm)
PEDOT:PSTFSIK	96 ± 15	582 ± 27
PEDOT:PSTFSIH	53 ± 10	607 ± 89

Tab. 2.9: Particle sizes in PEDOT:PSTFSIK and PEDOT:PSTFSIH dispersions, determined by dynamic light scattering

1575cm^{-1} (see figure A.9, appendix page 222). In addition, the main absorption band of PEDOT:PSTFSIH was shifted to higher wavenumbers, which was attributed to an increasing degree of doping of PEDOT in literature [47].
This proves that the use of the acidic polyelectrolyte results in a higher degree of doping of PEDOT:PSTFSIH, which is developed after more than 10 hours of polymerization.

Besides a good doping, also the morphology of the PEDOT:PSTFSIK and PEDOT:PSTFSIH complexes and films was studied. As the conformation of the polyelectrolyte is affected by the pH and its counter ion, such that PSTFSIH shows a smaller hydrodynamic radius in solution than PSTFSIK (see section 2.2), it was investigated if the different conformations of the polyelectrolyte template persisted in the morphology of the PEDOT:PSTFSI complex. In DLS experiments scattering from objects with a diameter of several hundreds of nanometers and from smaller scatterers with a diameter of 50nm to 100nm was observed for both PEDOT:PSTFSIK and PEDOT:PSTFSIH dispersions (see table 2.9). While the size of the bigger scatterers was about 600nm in both systems, the smaller particles in PEDOT:PSTFSIH were approximately half of the size of the ones in PEDOT:PSTFSIK.

Liquid AFM imaging on the dispersed complexes (see figure 2.35) revealed, that both, PEDOT:PSTFSIK and PEDOT:PSTFSIH, complexes were composed of long entangled polymer chains with thick nodal points. The diameter of the entangled complexes was in the sub-micrometer range and correlated well to the size of the bigger objects observed by DLS. A closer look on the shape of the polymer chains gave the impression that the chain segments in PEDOT:PSTFSIK were less straight and more randomly oriented than those of PEDOT:PSTFSIH. However, no experimental method was found to confirm this impression quantitatively.

In order to gain more information on the potential morphological differences of PEDOT:PSTFSIK and PEDOT:PSTFSIH films, the charge transport behavior was

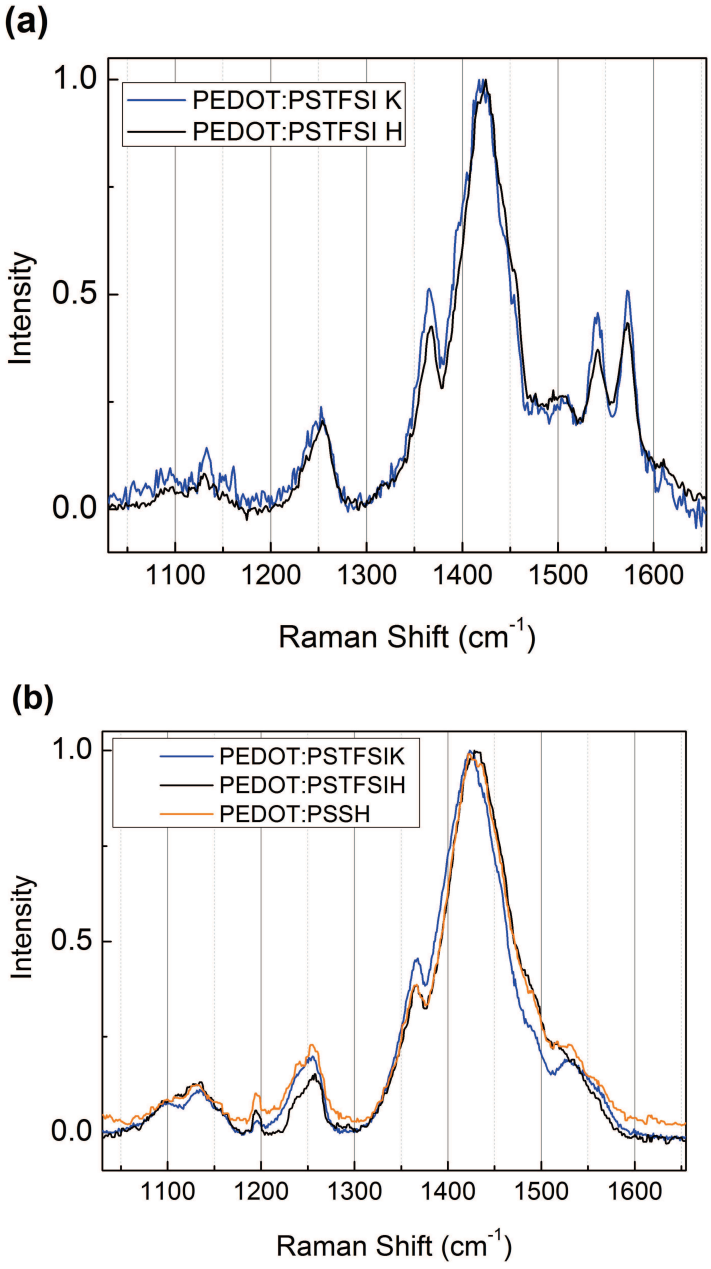

Fig. 2.34: Raman spectrum of PEDOT:PSTFSIK and PEDOT:PSTFSIH, with Raman excitation wavelength a)532nm and b)785nm

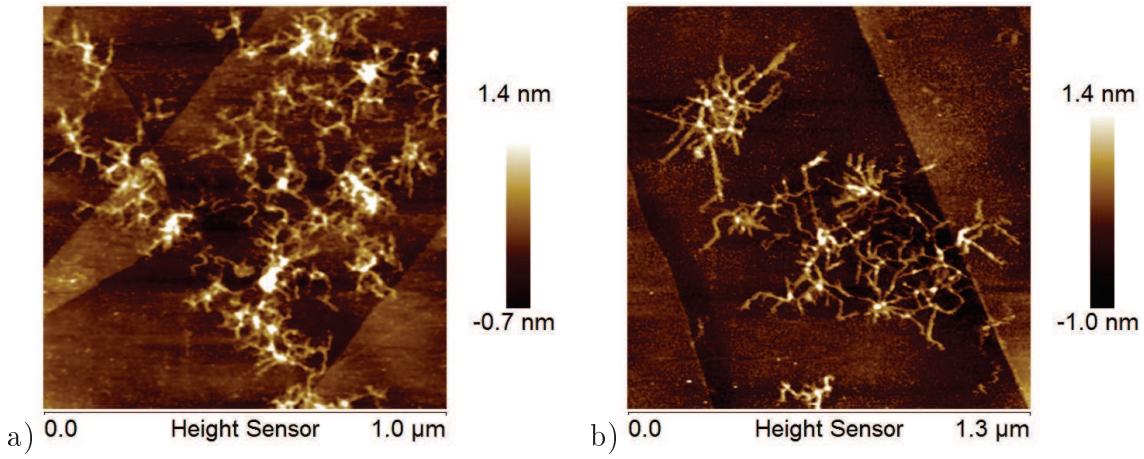

Fig. 2.35: a)PEDOT:PSTFSIK and b)PEDOT:PSTFSIH, imaged in aqueous dispersion by liquid AFM

studied with the help of temperature dependent resistance measurements. In both PEDOT:PSTFSI systems a decrease of the resistance with increasing temperature was observed, which was very pronounced in the low temperature regime (see figure 2.36). This corresponds to the commonly observed behavior of conducting polymers, in which the charge transport occurs by hopping between the highly conducting sites.
The plot of the reduced activation energy W,

$$W = \frac{\partial ln(\sigma(T))}{\partial ln(T)}, \tag{2.11}$$

over the temperature $\boldsymbol{T}$ in figure 2.36, shows that W decreases with increasing temperature ($\partial W/\partial T < 0$). Therefore the charge transport in both PEDOT:PSTFSI systems was in the insulating regime, as it was also reported for PEDOT:PSS in literature [25]. The plot of $R(\boldsymbol{T})$ was fitted with the one-dimensional variable range hopping model

$$R = R_0 exp(\frac{T_0}{T})^{\alpha} \tag{2.12}$$

with $\alpha = 0.5$ and R being the resistance, $\boldsymbol{T}$ being the temperature, $T_0 = \frac{16}{k_B N(E_F) L_{\parallel} L_{\perp}^2}$ being the energy barrier between localized states, $N(E_F)$ the density of states at the Fermi level, and $L_{\parallel}$ ($L_{\perp}$) the localization length of the charge carriers in the parallel (perpendicular) direction with respect to the measurement direction.

This allowed the extraction of the T_0, which corresponds to the effective energy barrier between two localized states [25, 49]. For PEDOT:PSTFSIK and PEDOT:PSTFSIH a T_0 of 359K and of 70K was found, respectively. This indicates, that the hopping barrier in PEDOT:PSTFSIH was drastically lower, which correlates to the higher conductivity in PEDOT:PSTFSIH. With the help of the VRH model developed by Shklovskii and Efros [50], the localization length a was calculated from T_0 to be 180nm for PEDOT:PSTFSIH and 35nm for PEDOT:PSTFSIK, using

$$T_0 = \frac{2.8e^2}{4\pi\epsilon_0\epsilon k_B a}. \tag{2.13}$$

The localization length of 35nm obtained for PEDOT:PSTFSIK corresponds well to the grain size of 40nm, visualized by AFM imaging of PEDOT:PSTFSIK films, on which the phase segregated PSTFSI layer was removed by one minute of CF_4 plasma etching (see figure 2.37). The calculated localization length of 180nm for PEDOT:PSTFSIH indicates, that the percolation of the PEDOT rich domains was improved. However, the change in localization length can not be correlated to the apparent grain size of PEDOT:PSTFSIH, which was identical to the grain size observed in the topographic AFM images of PEDOT:PSTFSIK.

In order to investigate the crystallinity of the PEDOT:PSTFSI systems differential scanning calometry was performed. From the DSC data (see figure A.10, apeendix page 222) no melting with corresponding re-crystallization peak was observed, which is a sign for the absence of crystallinity. This was confirmed by GIWAXS analysis on PEDOT:PSTFSIK thin films, which showed the characterisic scattering for amorphous materials in form of a broad halo (see figure D.7, appendix page 232). However, GIWAXS analysis has not been performed on PEDOT:PSTFSIH, but should elucidate if its higher conductivity is related to a higher degree of crystallinity.

In summary, we can assume the presence morphological differences between PEDOT:PSTFSIK and PEDOT:PSTFSIH, which lead to different charge transport characteristics in the PEDOT:PSTFSI films. This is supported by the differences in the object size observed by DLS and the qualitative differences in the morphology observed by liquid AFM imaging.

In conclusion, it was shown that the counter ion of the PSTFSI polyelectrolyte strongly affects the properties of the resulting PEDOT:PSTFSI complex. Upon the

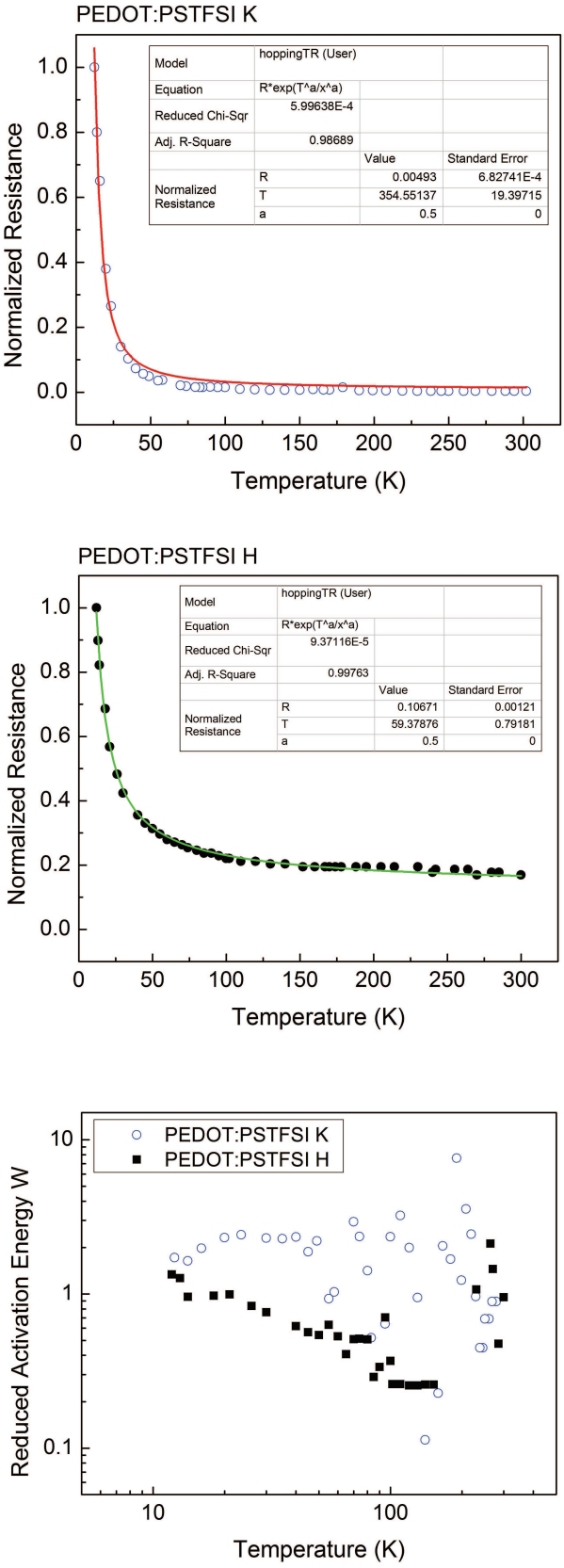

Fig. 2.36: Conductivity as a function of temperature for PEDOT:PSTFSIK (top) and PEDOT:PSTFSIH (middle) films with fit of the VRH model and plot of the reduced activation energy W versus the temperature T on a double logarithmic scale (bottom)

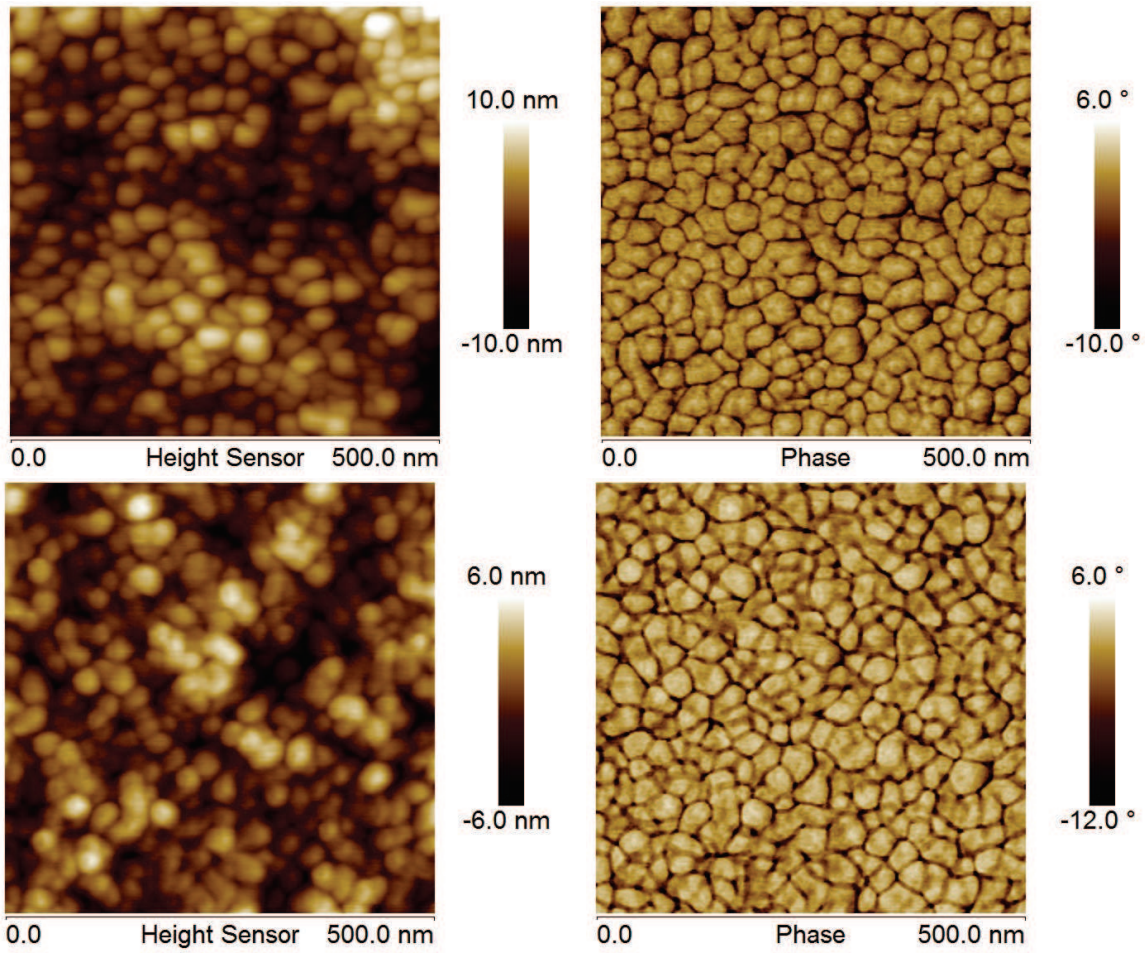

Fig. 2.37: AFM height and phase images of PEDOT:PSTFSIK (top) and PEDOT:PSTFSIH films after 1min CF_4 etch

polymerization of EDOT in the solution of the acidic PSTFSIH template polymer, a conductivity of about 330S.cm^{-1} for PEDOT:PSTFSIH was obtained, which corresponds to a 2.4 fold increase compared to PEDOT:PSTFSIK. The study of the synthesis kinetics revealed that the initial reaction kinetics, corresponding to the monomer oxidation and dimer formation, were not affected. However, the kinetics in PEDOT:PSTFSIH deviated after several hours of synthesis, which resulted in a drastic increase in doping. In addition, charge transport studies revealed a lower energy barrier for the charge transport in PEDOT:PSTFSIH, which is an indicator for better percolation of the conducting pathways in PEDOT:PSTFSIH. Therefore the gain in conductivity was correlated to a higher degree of doping and to a better percolation in the PEDOT:PSTFSIH films. However, the exact mechanism for the enhanced doping and the nature of the morphological changes could not be fully uncovered.

2.5 Optimization of the Synthesis Conditions

2.5.1 Oxidants

Based on the synthesis protocol for PEDOT:PSS patented by Bayer [12], for the synthesis of PEDOT:PSTFSI the EDOT monomer was dispersed in aqueous PSTFSI solution and polymerized using a mixture of $FeCl_3$ and $(NH_4)_2S_2O_8$ as oxidants (details see experimental section 203). Peroxides such as $(NH_4)_2S_2O_8$ are very strong oxidizing agents and will oxidise EDOT in aqueous solution. However, they also tend to oxidise the sulfur atom on the thiophene unit, which breaks the conjugation in PEDOT and limits its conductivity [51]. In contrast, $FeCl_3$ is able to oxidise EDOT only in the presence of PSTFSI, which acts a surfactant and lowers the oxidation potential of EDOT [52, 53, 54, 55, 56]. For better illustration, an overview of the oxidation potentials of the involved species in given in figure 2.39 [52, 53, 54, 55, 56].

The synthesis of PEDOT:PSTFSI with only $FeCl_3$ lead to an inhomogeneous two-phase system of dark blue agglomerates in an almost colorless aqueous medium. In contrast, the polymerization with only $(NH_4)_2S_2O_8$ resulted in a grayish blue dispersion with low viscosity. The strong aggregation of the polymer particles upon synthesis with $FeCl_3$ can be explained by the charge compensation of the anionic polyelectrolyte functionalities by the iron cations, which decreases the colloidal stability of the system [46] (see scheme in figure 2.38).

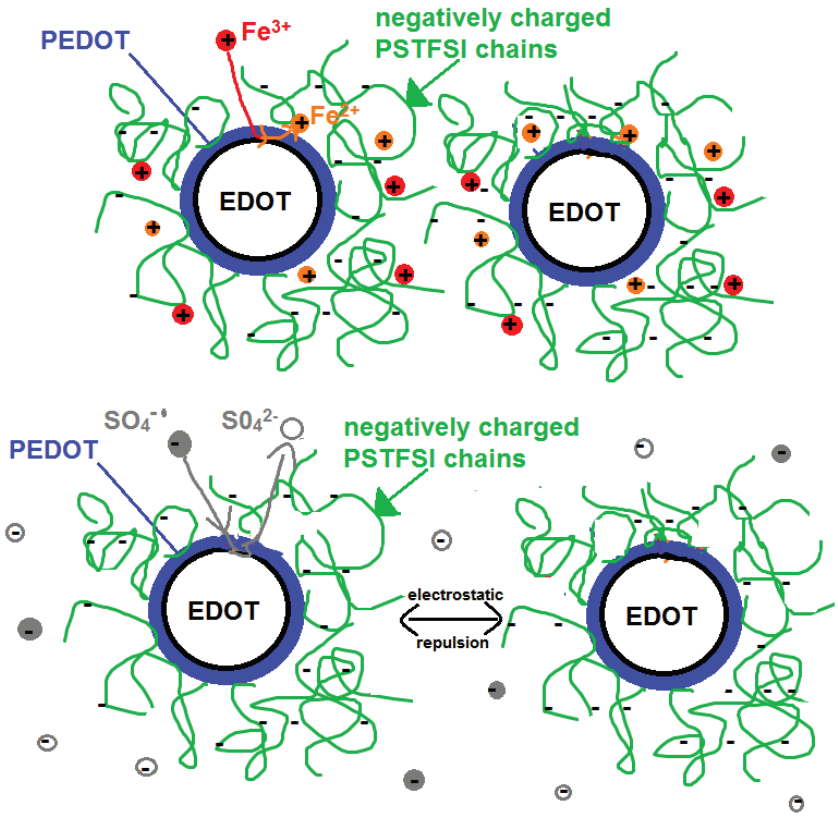

Fig. 2.38: Illustration of the decrease of the colloidal stability of PEDOT:PSTFSI due to the high concentration of Fe^{3+}/Fe^{2+} ions

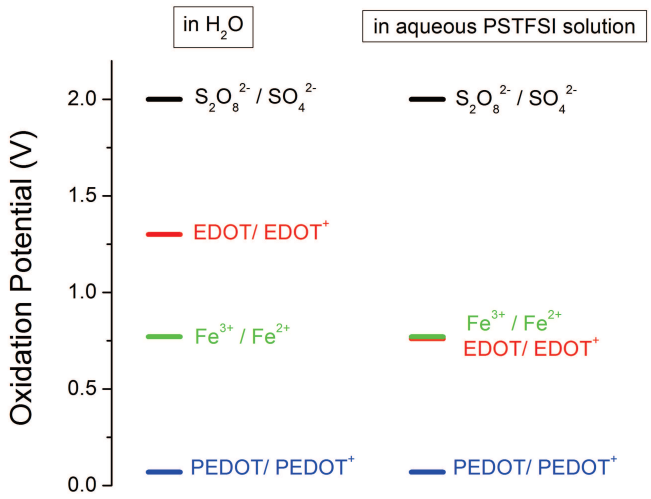

Fig. 2.39: Scheme illustrating the oxidation potentials of EDOT, PEDOT and the oxidants $Fe_3{}^+$ and $S_2O_8{}^{2-}$ [52, 53, 54, 55, 56]

By using a binary oxidant system of $Fe_3{}^+$ and $S_2O_8{}^{2-}$ the concentration of iron can be limited for the sake of colloidal stability and the conductivity and overall conversion is improved [46, 14]. The reactions during the EDOT polymerization using a mixture of iron and persulfalte salts can be described as in equations 2.14 and 2.15, in which $Fe_3{}^+$ serves as oxidant for the EDOT and is then regenerated due to a redox reaction with $S_2O_8{}^{2-}$:

$$2\,Fe^{3+} + 2\,EDOT \longrightarrow 2\,Fe^{2+} + EDOT_{dimer} + 2\,H^+ \tag{2.14}$$

$$S_2O_8{}^{2-} + 2\,Fe^{2+} \longrightarrow 2\,Fe^{3+} + 2\,SO_4{}^{2-} \tag{2.15}$$

In order to optimize the molar ratio of $FeCl_3$ and $(NH_4)_2S_2O_8$ for the synthesis of PEDOT:PSTFSI the oxidant composition was varied, while the molar ratio between oxidants and EDOT monomer was kept constant at 2.3. This oxidant concentration was chosen for two reasons. First, it allows, that every EDOT monomer is oxidized two times, which leads in theory to a continuous growth of the PEDOT chains and full conversion. Second, the excess oxidant allows the oxidation of about one third of the PEDOT repeat units, which corresponds to the optimal doping level of PEDOT [28, 33, 34].

Molar Ratio $S_2O_8^{2-}/Fe^{3+}$	Molar Ratio $Fe_3{}^+/EDOT$	Conductivity[a,b,c] ($S.cm^{-1}$)	Absorption Coefficient[a,c] ($10^3 cm^{-1}$)	FoM[a,c]
		wo DMSO/with DMSO		wo DMSO/with DMSO
16.0	0.07	0.5/158	2.5	0.03/10
4.9	0.21	1.2/252	2.5	0.07/16
2.7	0.35	2.6/240	2.5	0.14/15
1.8	0.49	4.0/263	2.6	0.21/17

[a] average on 8 measurements or more [b] determined by 4-point measurements [c] standard deviation of value ≈10%

Tab. 2.10: Opto-electronic performance of PEDOT:PSTFSI systems, synthesized with different molar ratios of ammonium persulfate to iron(III)chloride at 10°C, PSTFSIK 250kDa

The opto electronic properties of the obtained PEDOT:PSTFSI complexes are summarized in table 2.10. For pristine PEDOT:PSTFSI films the conductivity increased with higher $FeCl_3$ concentrations. Upon the addition of a co-solvent, such as DMSO, the differences in conductivity were cancelled out, except for PEDOT:PSTFSI synthesized with the smallest amount of $FeCl_3$, which showed lower conductivity. Taking into account that high boiling point solvents are known to induce morphological changes in the PEDOT:PSTFSI films, this indicates that the differences in conductivity were caused by different morphologies of the pristine PEDOT:PSTFSI complexes. A possible scenario is, that the higher iron concentration resulted in the formation of bigger or agglomerated particles due to the attractive electrostatic interactions and charge screening effects between Fe^{3+} and $PSTFSI^-$. With increasing size of the PEDOT particles in the PEDOT:PSTFSI film the hopping barriers are reduced and therefore the macroscopic conductivity should be increased. Upon the addition of DMSO this effect is wiped out by the induced morphology changes. However, imaging techniques and DLS measurements did not provide any conclusive information on this point.
From the UV/Vis absorption spectra (see figure 2.40) and the calculated absorption coefficients it can be seen, that the doping level and the degree of conversion of EDOT were scarcely affected by the changing oxidants ratio, which confirms that the differences in conductivity were not related to the degree of doping.

Furthermore, a combination of $(NH_4)_2S_2O_8$ and $Fe(Tos)_3$ was tested as oxidant. $Fe(Tos)_3$ was chosen, as it is widely used as oxidant for the preparation of in-situ polymerized PEDOT, in which the tosylate anions act as counter ion for the doped PEDOT. Therefore it was investigated, if the use of $Fe(Tos)_3$ was beneficial for the doping of PEDOT in PEDOT:PSTFSI. However, the obtained conductivities were about 60% of the conductivities obtained with $(NH_4)_2S_2O_8$ and $FeCl_3$ for the same

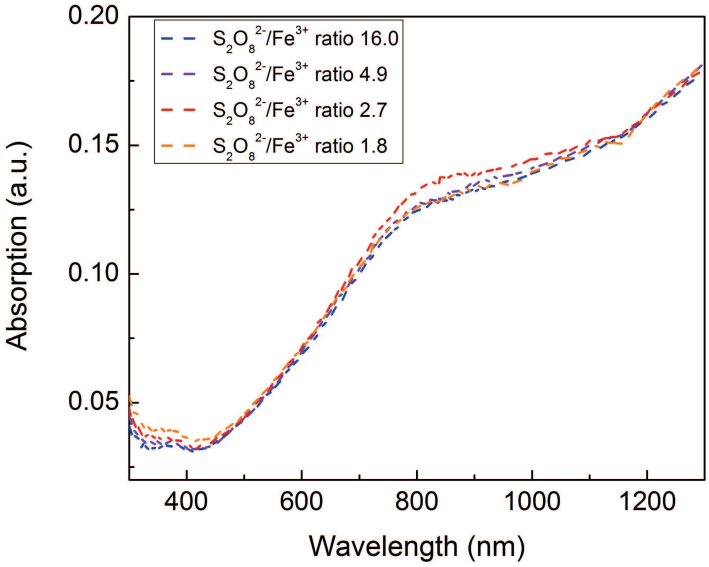

Fig. 2.40: UV/Vis absorption spectra of PEDOT:PSTFSI dispersion synthesized with different oxidant ratios

polyelectrolyte and under the same synthesis conditions (see table 2.11).

Fe^{3+}/EDOT	Conductivity^{a,b} (S.cm^{-1})	Absorption Coefficient^{a} (10^3 cm^{-1})	FoM^{a}
0.6	57 ± 5	2.0 ± 0.3	4.7 ± 0.4
0.8	64 ± 6	2.2 ± 0.3	4.7 ± 0.4
0.9	54 ± 5	2.0 ± 0.3	4.2 ± 0.4
1.1	35 ± 4	2.0 ± 0.3	3.1 ± 0.3

^{a} average on 8 measurements or more ^{b} determined by 4-point measurements

Tab. 2.11: Opto-electronic properties of PEDOT:PSTFSI synthesized with $(NH_4)_2S_2O_8$ and Fe(tosylate)$_3$ with Fe^{3+} to EDOT ratios of 0.6 to 1.1, at 10°C, PSTFSIK 100kDa

The Raman spectra of PEDOT:PSTFSI synthesized with Fe(Tos)$_3$ (see figure 2.41) showed more important bands at 1550cm^{-1} and 1575cm^{-1}, which are assigned to the asymmetric C_α=C_β stretching in PEDOT. It has been shown in literature, that these bands are dominantly present in PEDOT with a low degree of doping [47, 57]. The lower degree of doping of PEDOT:PSTFSI synthesized with Fe(Tos)$_3$ was confirmed by UV/Vis spectroscopy (see figure 2.41), which showed no shoulder at the polaronic absorption and lower bipolaronic absorption. Therefore, the lower conductivity of PEDOT:PSTFSI upon synthesis with Fe(Tos)$_3$ can be related to a lower degree of doping.

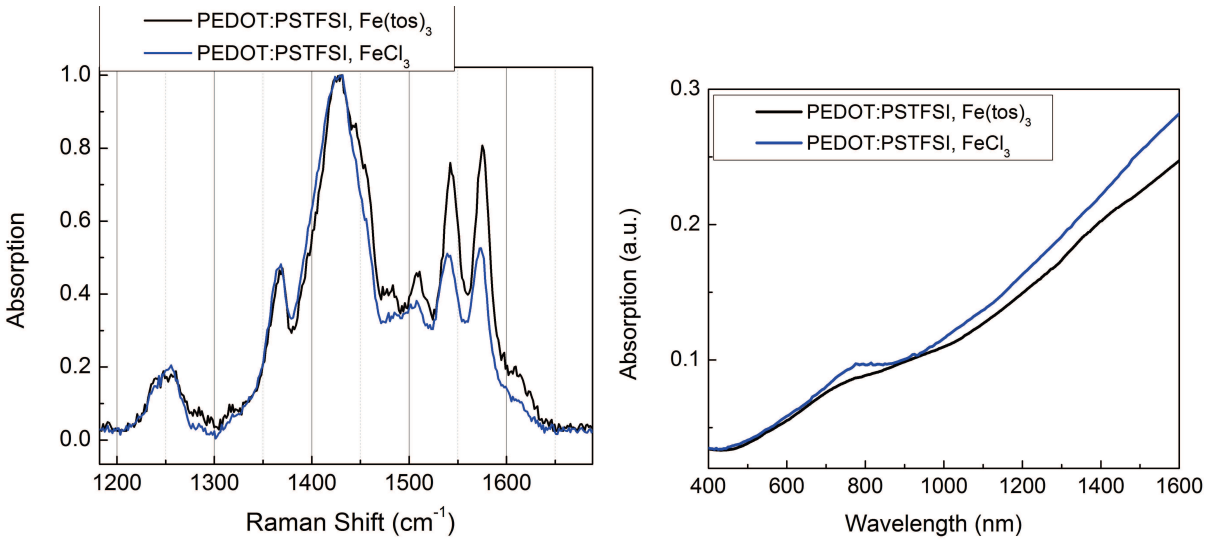

Fig. 2.41: Raman spectra and UV/Vis spectra of PEDOT:PSTFSI synthesized with $FeCl_3$ or $Fe(Tos)_3$

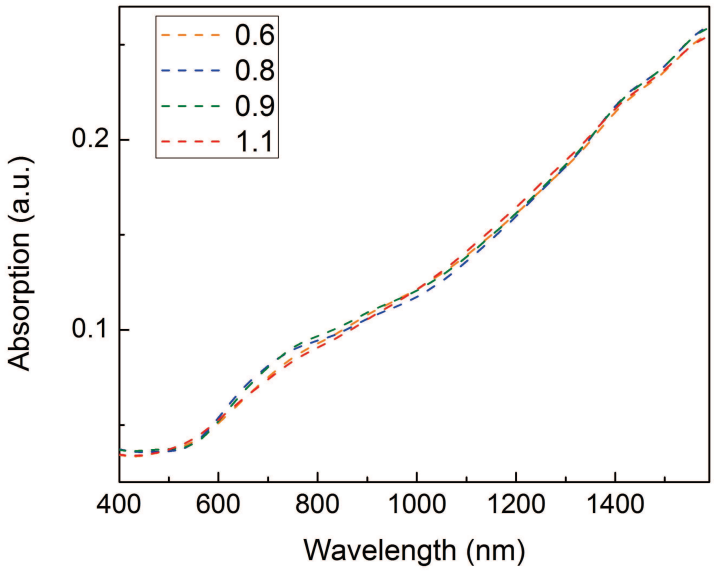

Fig. 2.42: UV/Vis spectra of PEDOT:PSTFSI synthesized with $(NH_4)_2S_2O_8$ and Fe(tosylate)$_3$ with Fe^{3+} to EDOT ratios of 0.6 to 1.1, at 10°C, PSTFSIK 100kDa

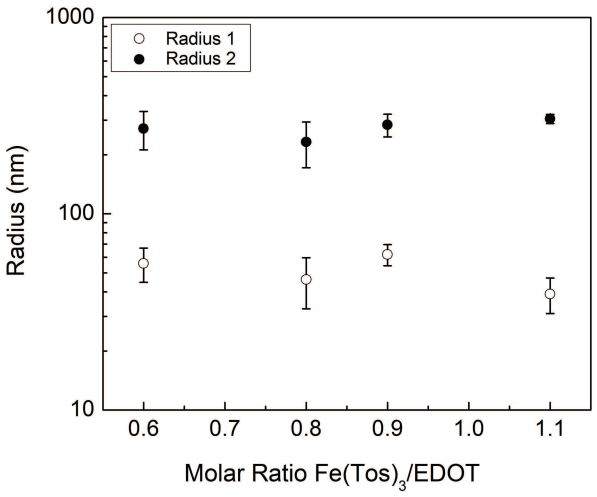

Fig. 2.43: Radii of objects in PEDOT:PSTFSI dispersion synthesized with different $Fe(Tos)_3$ concentrations, determined by DLS

In order to investigate if the doping could be improved by higher oxidant concentrations, the $Fe(Tos)_3$ concentration was stepwise increased, while the persulfate concentration was kept constant. From table 2.11 it can be seen that the polymerization was robust to changes of the iron concentration up to a Fe^{3+} to EDOT ratio of 0.9 and decreased upon further increase of the iron concentration. As the UV/Vis spectra of these inks do not show a clear difference for different iron concentrations (see figure 2.42), it can be assumed that the change in conductivity is not related to a change in doping, but to a change in morphology or particle size of PEDOT:PSTFSI. However, analysis of the PEDOT:PSTFSI dispersions by DLS did not reveal significant differences in the object size as a function of the $Fe(Tos)_3$ concentration (see figure 2.43, correlation functions figure A.11 , appendix page 223).

It has been reported for several PEDOT systems [14], that the nature and concentration of the oxidants affect the size and conductivity of PEDOT particles. However, no global trend for all PEDOT systems can be established, as the particle size and morphology do not only depend on the oxidants, which are used, but also on the nature of the polyelectrolyte and other synthesis conditions. In the case of $FeCl_3$ and $Fe(tosylate)_3$ the differences in doping of PEDOT:PSTFSI could be related to different acidity of HCl (pK_a -6.5) and *p*-toluenesulfonic acid (pK_a -2.8), which are present within the system upon the polymerization of EDOT, slight changes in the oxidation potentials

of the polymerization system or to the different size of the chloride and tosylate anions. However, no pertinent explanation for the differences in doping has been found.

In summary, we found that the binary oxidant system of Fe^{3+} and $(NH_4)_2S_2O_8$ allows the synthesis of homogeneous, conducting PEDOT:PSTFSI dispersions. Furthermore, it was shown that the synthesis is robust to small changes in the oxidant ratio and in the Fe^{3+} concentration around a molar $(NH_4)_2S_2O_8$: $FeCl_3$: EDOT ratio of 3.5 : 1 : 3.5, which was defined as standard composition for the PEDOT:PSTFSI synthesis.

2.5.2 Dispersion of the EDOT Monomer

As already mentioned, the PEDOT:PSTFSI complex is synthesized by polymerization of the EDOT monomer in an aqueous solution of PSTFSIK. The quality of the EDOT dispersion is supposed to considerably influence the monomer droplet size and thus to influence the interface between EDOT and the PSTFSI counter ion. This could affect the interaction between PEDOT and PSTFSI, the PEDOT:PSTFSI complex morphology, as well as the doping of PEDOT. As it is shown in chapter 6 all these characteristics are decisive for the opto-electronic properties of the PEDOT:PSTFSI polymer. Therefore, the influence of the dispersion of EDOT in the aqueous PSTFSIK solution on the doping, complex morphology, rheology and opto-electronic properties of PEDOT:PSTFSI has been studied by variation of the stirring speed during the synthesis. Furthermore, the influence of the EDOT dispersion on the optimum EDOT to PSTFSI ratio was investigated.
Figure 2.44 displays the opto-electronic properties of PEDOT:PSTFSI synthesized with different stirring speeds from 55rpm to 625rpm.

Independently of the stirring speed, all PEDOT:PSTFSI systems showed an increase of the absorption coefficient with increasing EDOT concentration, as it has been shown in section 2.3. Also the evolution of the conductivity was very similar for all stirring speeds, showing an initial increase with increasing EDOT concentration, attributed to better percolation of the conducting PEDOT rich domains, follow by a drop of the conductivity, which results from a saturation of the stabilizer PSTFSI with PEDOT (discussion see section 2.3). However, for high stirring speeds a three-fold increased of the maximum conductivity was observed, as well as a shift of the maximum conductivity to a higher EDOT to STFSI ratio (from 0.6 to 0.9).

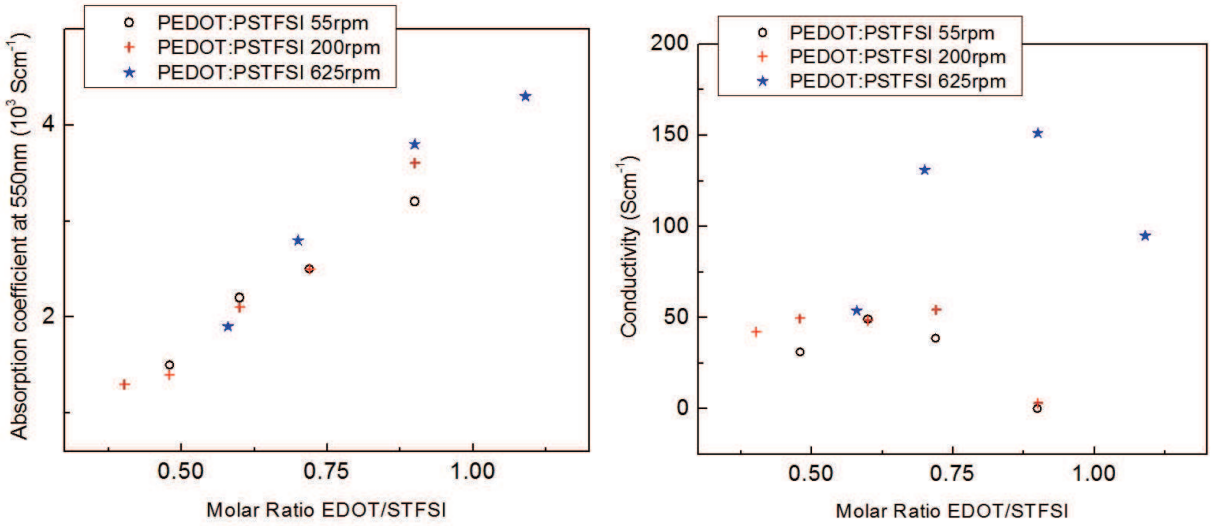

Fig. 2.44: Absorption coefficient and conductivity of PEDOT:PSTFSI and PEDOT:PSS dispersions, synthesized at different stirring speeds under N_2 for 50 hours

UV/Vis spectroscopy revealed, that the synthesis at higher stirring speeds, which was linked to a better dispersion of EDOT in PSTFSI, lead to a considerably higher bipolaronic absorption of the resulting PEDOT:PSTFSI dispersion (see figure 2.45). This indicates an improved doping of the PEDOT:PSTFSI complex upon good EDOT dispersion and is in coherence with the observed increase in conductivity.

Furthermore, the influence of the stirring speed on the complex morphology was investigated by microscopy. By scanning transmission electron microscopy (STEM) of PEDOT:PSTFSI with low EDOT concentrations, big and sponge like objects of up to 1μm in diameter were visualized (see figure 2.46a). These big objects contained very small particles ($<$ 10nm) with higher contrast, which can be interpreted as PEDOT rich areas. This morphology is fundamentally different from the agglomerated particles of about 100nm, which were observed for PEDOT:PSTFSI complexes synthesized at low stirring speeds (see figure 2.19, in section 2.3, page 78). For PEDOT:PSTFSI with high PEDOT concentrations (EDOT to STFSI ratio of 1.10), the objects appeared denser and less well defined (see figure 2.46b). This is analogous to the observations made for PEDOT:PSTFSI synthesized at low stirring speeds, for which high PEDOT concentrations resulted in ill-defined complexes. However, the critical PEDOT concentration, at which the formation of these ill-defined complexes was observed, was

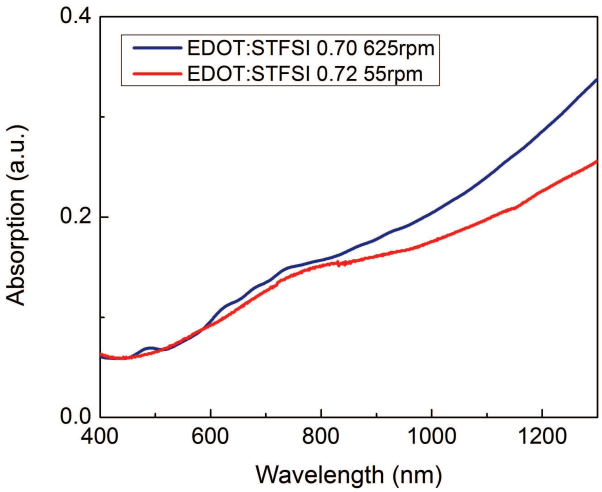

Fig. 2.45: UV/Vis absorption spectra of PEDOT:PSTFSI with EDOT to STFSI ratio of 0.7 synthesized at 55rpm and 625rpm stirring, respectively

higher upon faster stirring. This indicates that a higher degree of dispersion of the EDOT monomer was favorable for an efficient stabilization of PEDOT by PSTFSI.

The difference of the PEDOT:PSTFSI complex morphology as a function of the EDOT dispersion was confirmed by rheological characterization.
PEDOT:PSTFSI dispersions with a low PEDOT concentration (EDOT/STFSI<0.6) synthesized at 625rpm stirring displayed the characteristics of a viscoelastic fluid, which is composed of weakly interacting separate colloidal particles (see figure 2.47 and figure A.6, appendix page 220). The measured rheological properties were similar to those of PEDOT:PSTFSI with low PEDOT concentrations synthesized at low stirring speed. This indicates, that for low PEDOT concentrations the dispersion of the EDOT monomer did not decisively influence the rheological properties of PEDOT:PSTFSI.
For higher PEDOT concentrations (EDOT/STFSI>0.6), however, the PEDOT:PSTFSI synthesized at 625rpm showed the characteristics of a gel, for which G' and G" are independent of the frequencies and G'>G" (see figure 2.47). This is an indicator for strong colloidal forces or the formation of three dimensional network. In addition, the yield stress was determined to be 0.06Pa (see figure A.5, appendix page 219), which is three times higher than the yield stress measured for PEDOT:PSTFSI synthesized at slow stirring, and affirms the higher structural strength. The observed gel character is in perfect coherence with the three-dimensional network structure of these complexes

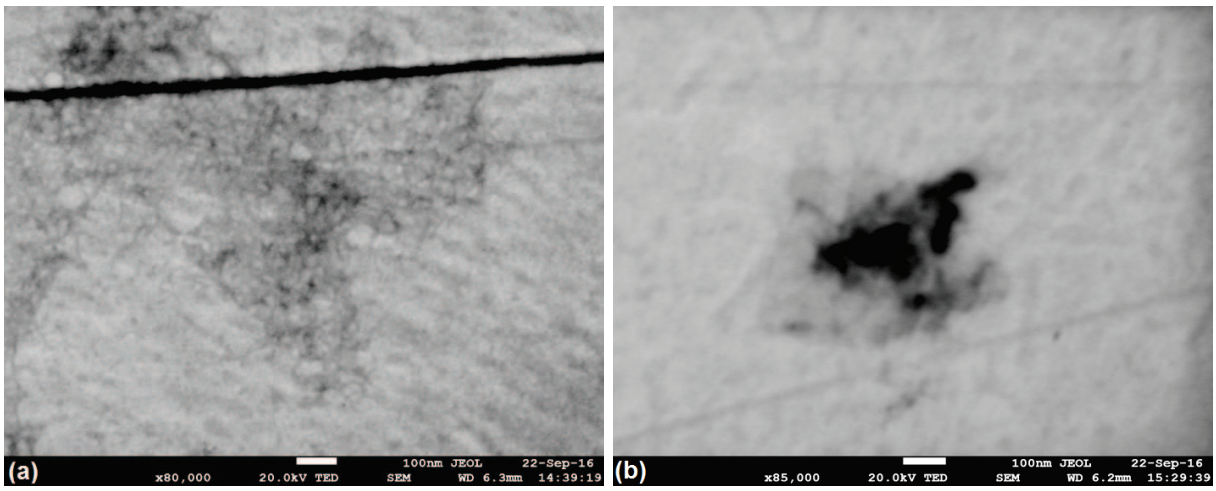

Fig. 2.46: STEM images of PEDOT:PSTFSI with a)EDOT/STFSI=0.70 and b)EDOT/STFSI=1.10, synthesized at 625rpm

observed by imaging (see figure 2.46a).

A further increase of the EDOT to STFSI ratio (EDOT/STFSI>0.9) resulted in a loss of viscosity (see figure A.5, appendix page 219) and in the destabilization of the dispersions, for which the gel character is lost upon application of 0.2% shear strain (see figure A.6, appendix page 220) or shear frequencies higher than 20rad.s^{-1} (see figure 2.47). This indicates, that the PSTFSI poyelectrolyte is saturated with PEDOT, which results in the destabilization of the solution and which is coherent with the formation of ill-defined complexes imaged by STEM (see figure 2.46b).

Independently of the EDOT to STFSI ratio or the stirring speed, no or negligible thixotropy was observed in the PEDOT:PSTFSI systems (see figure A.7, appendix page 221), which indicates that after its break down the structure was not recovered with time.

The strong influence of the monomer dispersion on the rheology of the final ink can be explained by changes in the complex morphology. In the case of big monomer droplets the interface with the PSTFSI stabilizer is small and PEDOT is stabilized in form of few big, separated agglomerates, which are surrounded by PSTFSI. Therefore these PEDOT:PSTFSI inks show the viscous flow behavior of dispersed, weakly interacting latex particles. Good dispersion of EDOT leads to a high interface with PSTFSI and many small PEDOT rich domains in a three dimensional network of PSTFSI are formed (see scheme figure 2.48). These PEDOT rich domains act as nodal

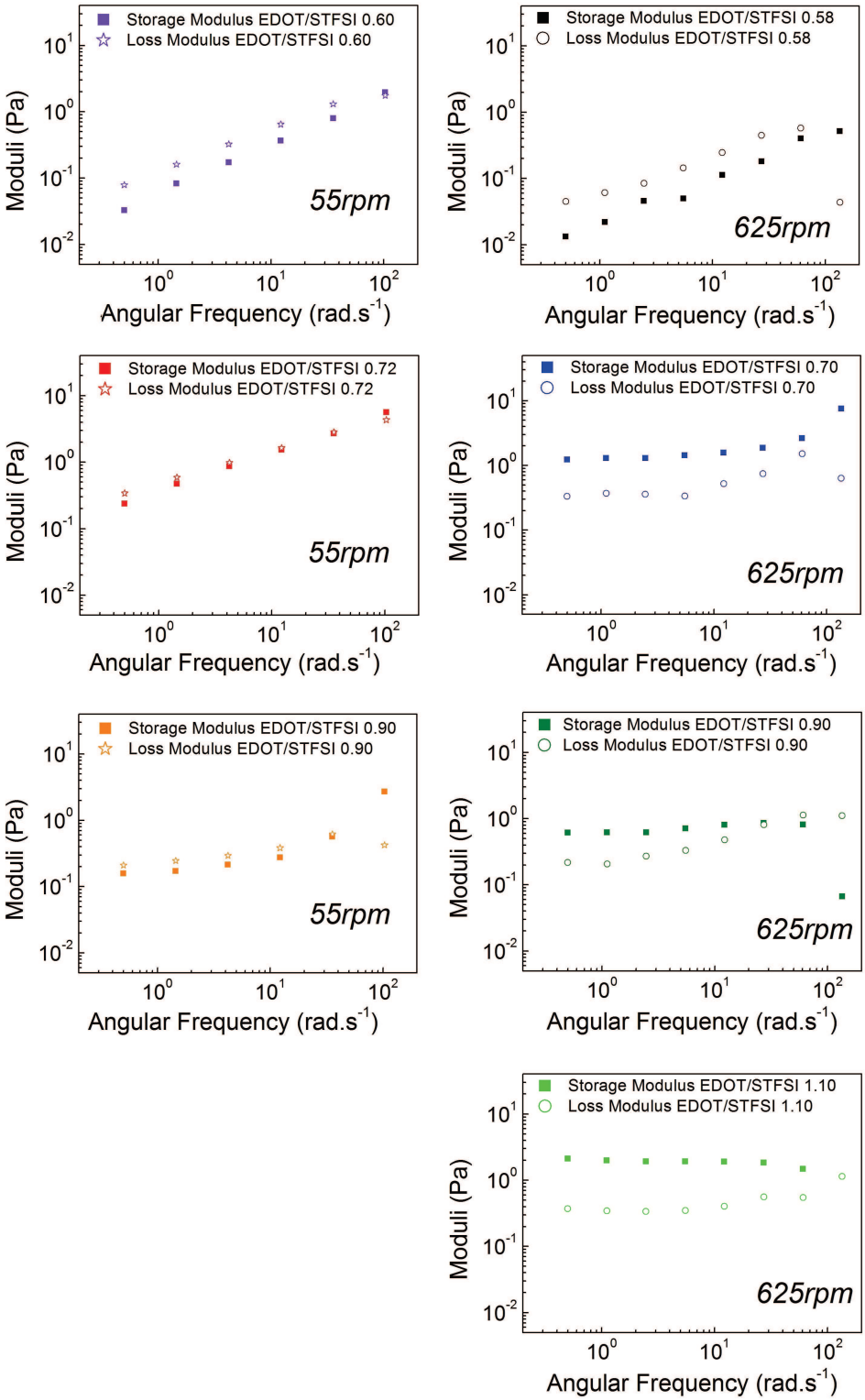

Fig. 2.47: Storage and Loss Moduli as a function of angular frequency at 2% shear strain of PEDOT:PSTFSI with different EDOT to STFSI ratios and stirring at 55rpm and at 625rpm

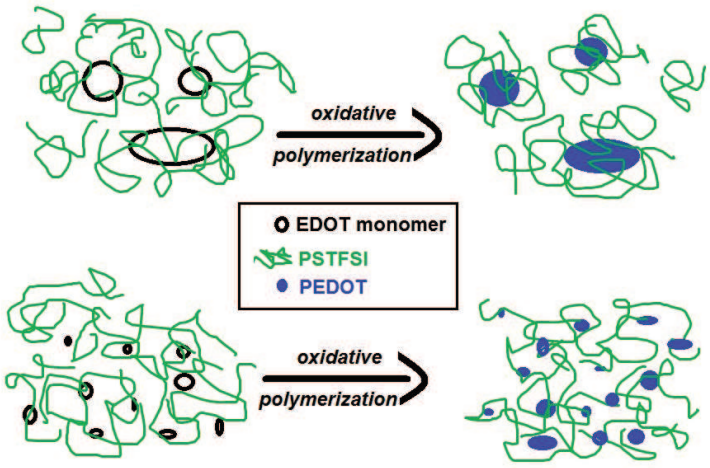

Fig. 2.48: Scheme illustrating the influence of the EDOT monomer dispersion on the morphology of the PEDOT:PSTFSI complex

points between several PSTFSI chains and a three dimensional PEDOT:PSTFSI network is formed. Hence, the rheology of these dispersions is dominated by the elastic properties of the interconnected polymer gel. This is in coherence with the structural differences imaged by TEM (see figure 2.19, page 78, figure 2.46, page 116 and figure 2.10, page 70).

In addition, the larger interface between PEDOT and PSTFSI is most likely favorable for better PEDOT-PSTFSI interactions, which can explain the higher degree of doping upon improved dispersion. Furthermore, a multitude of small PEDOT rich domains should be advantageous for the formation of a percolated conducting network in the PEDOT:PSTFSI films. As both, doping and percolation, are decisive factors for the conductivity of a film, this could explain the drastic increase in conductivity upon better dispersion of the EDOT monomer.
The important influence of the stirring speed during the PEDOT synthesis on the conductivity of the PEDOT:PSTFSI complex was confirmed by supplementary experiments, which are summarized in table 2.12 (see page 120).

In conclusion, it was found, that a good dispersion of the EDOT monomer is crucial for a good complexation, stabilization and doping of the PEDOT by PSTFSI and influences decisively the morphology, rheology and conductivity of the PEDOT:PSTFSI system.

Upon improved dispersion of the EDOT monomer the PEDOT:PSTFSI inks displayed a strong gel character and a three-fold increase in conductivity of the PEDOT:PSTFSI films was observed.

2.5.3 Temperature

The temperature is a crucial parameter for most chemical reactions as it affects the thermodynamics and kinetics. In radical polymerizations the dissociation of certain initiators, such as persulfates, is thermally activated and consequently the initiation step is accelerated at high temperatures. Therefore increasing synthesis temperatures result in polymers with higher dispersity and a lower average chain length. In most protocols for the synthesis of aqueous PEDOT:PSS dispersion, the polymerization of EDOT is performed at room temperature [58]. However, the patents hold by Bayer for the synthesis of pi-conjugated water soluble polymers [12] and processing of polythiophenes [51] cover temperature ranges from 20°C to 100°C. Corradi and Armes [59] and Jiang *et al.* [45] reported, that by increasing the synthesis temperature the yield of the oxidative polymerization of EDOT in water using Fe_3^+ salts could be improved. However, the faster reaction kinetics resulted in lower colloidal stability of the PEDOT particles, which caused a drop of their conductivity. Therefore the influence of the temperature on the doping, kinetics and opto-electronic properties of PEDOT:PSTFSI was investigated.

From figure 2.49 it can be seen, that the FoM decreased exponentially with increasing synthesis temperature. The comparison of the opto-electronic properties of PEDOT:PSTFSI dispersions synthesized at 13°C and at 23°C shows, that the drop of the FoM with increasing temperature is caused by a loss of conductivity and a concurrent rise of the absorption (see table 2.12). For temperatures below 13°C (lowest temperature studied: 9°C) no further change of the opto-electronic properties was observed.

The beneficial effect of low synthesis temperatures on the conductivity of PEDOT:PSTFSI can be related to the slower reaction kinetics and the formation of longer PEDOT chains, which are crucial for good doping and charge transport. This is confirmed by the comparison of the UV/Vis spectra of PEDOT:PSTFSI synthesized at 13°C and at 23°C in figure 2.49b, in which the PEDOT:PSTFSI synthesized at lower temperatures clearly shows a stronger bipolaronic absorption, which is a sign for a high

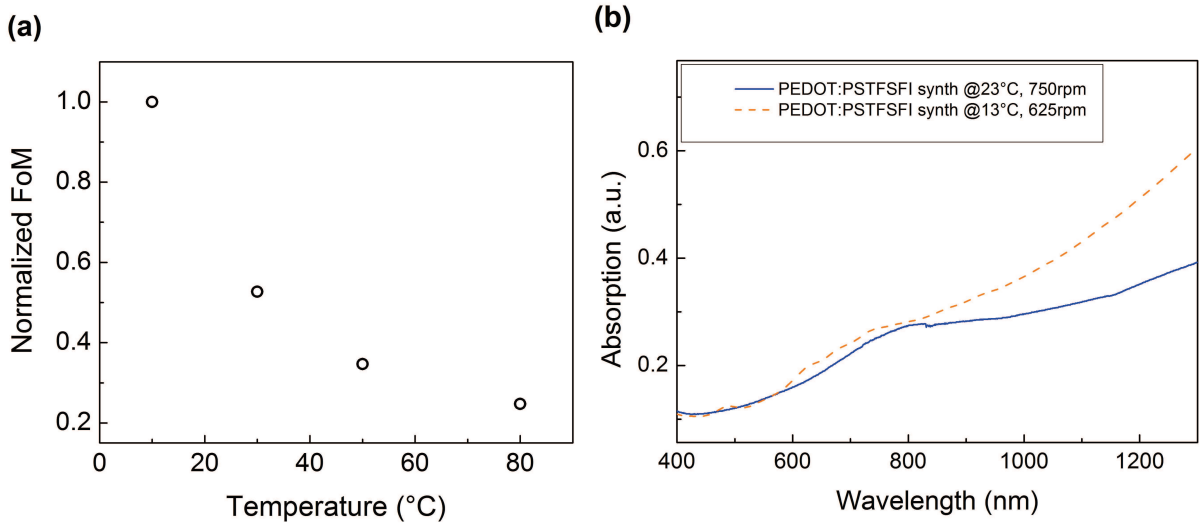

Fig. 2.49: a)Dependancy of the FoM on the polymerization temperature and b)UV/Vis spectra of PEDOT:PSTFSI synthesized at 13°C and at 23°C

Stirring Speed (rpm)	Temperature (°C)	Conductivity[a,b] (S.cm^{-1})	Absorption Coefficient[a] (cm^{-1})	FoM[a]	Particle Size[c] (nm)
55	13	39±4	2.5±0.4	2.5±0.3	297 ± 37
200	13	55±6	2.5±0.3	3.4±0.3	288 ± 16
625	13	131±10	2.8±0.4	7.1±0.4	294 ± 90
100	23	11±3	4±0.4	0.5±0.1	380 ± 90
375	23	33±5	7±0.6	0.7±0.2	304 ± 11
750	23	46±5	7±0.5	1.0±0.2	360 ± 13

[a] average on 8 measurements or more [b] determined by 4-point measurements
[c] bigger diameter of bimodal scattering determined by DLS, correlation function see figure A.13 in appendix page 225

Tab. 2.12: Opto-electronic properties of PEDOT:PSTFSI synthesized at 13°C and at 23°C and at different stirring speeds

degree of doping and a good delocalization of the charges. However, no experimental method was found, which allowed the determination of the chain length of PEDOT in the PEDOT:PSTFSI.

The increased absorption coefficient for higher synthesis temperatures could be explained by an increase in the EDOT conversion [59, 45]. Also the formation of big, agglomerated complexes, caused by fast reaction kinetics, could lead to a decreasing transparency of the PEDOT:PSTFSI films due to increased scattering. However, it can be seen from table 2.12, the particle size of the PEDOT:PSTFSI complexes was not drastically affected by the increase in temperature.

Furthermore, an increase in the dispersity of the PEDOT:PSTFSI complexes could be expected with increasing synthesis temperature. However, this could not be confirmed by DLS analysis or imaging.

In order to confirm the influence of the synthesis temperature on the kinetics of the EDOT polymerization, the UV/Vis absorption of the PEDOT:PSTFSI dispersion was monitored during the EDOT polymerization at different synthesis temperatures (see figure A.12, appendix page 224). To facilitate the analysis, the absorption at a fixed wavelength (800 nm, 1100 nm and 1300 nm, respectively) and for a constant temperature (10°C, 25°C and 50°C, respectively) was traced as a function of time (see figure 2.50a-c).

From these plots it can be seen that, at first, the absorption increased fast and linearly with time, until after a certain time a saturation of the absorption was reached. The rate of the change in absorption (equal to the slope ∂(absorption)/∂t of the plots 2.50a-c) was used to compare the reaction kinetics of the PEDOT formation. As it can be seen from figure 2.50d, the absorption rate increased almost linearly with temperature, which confirms the acceleration of the reaction kinetics with increasing temperatures.

However, the absorption spectra obtained during the monitoring of the synthesis (see figure A.12, appendix page 224) and the spectra of the PEDOT:PSTFSI systems, synthesized under standard conditions (see figure 2.49 for instance), show completely different features. This can be explained by the special experimental conditions of the UV/Vis monitoring, which had to be performed in a ten times diluted system compared to the standard and without stirring. Therefore we can conclude, that the doping of

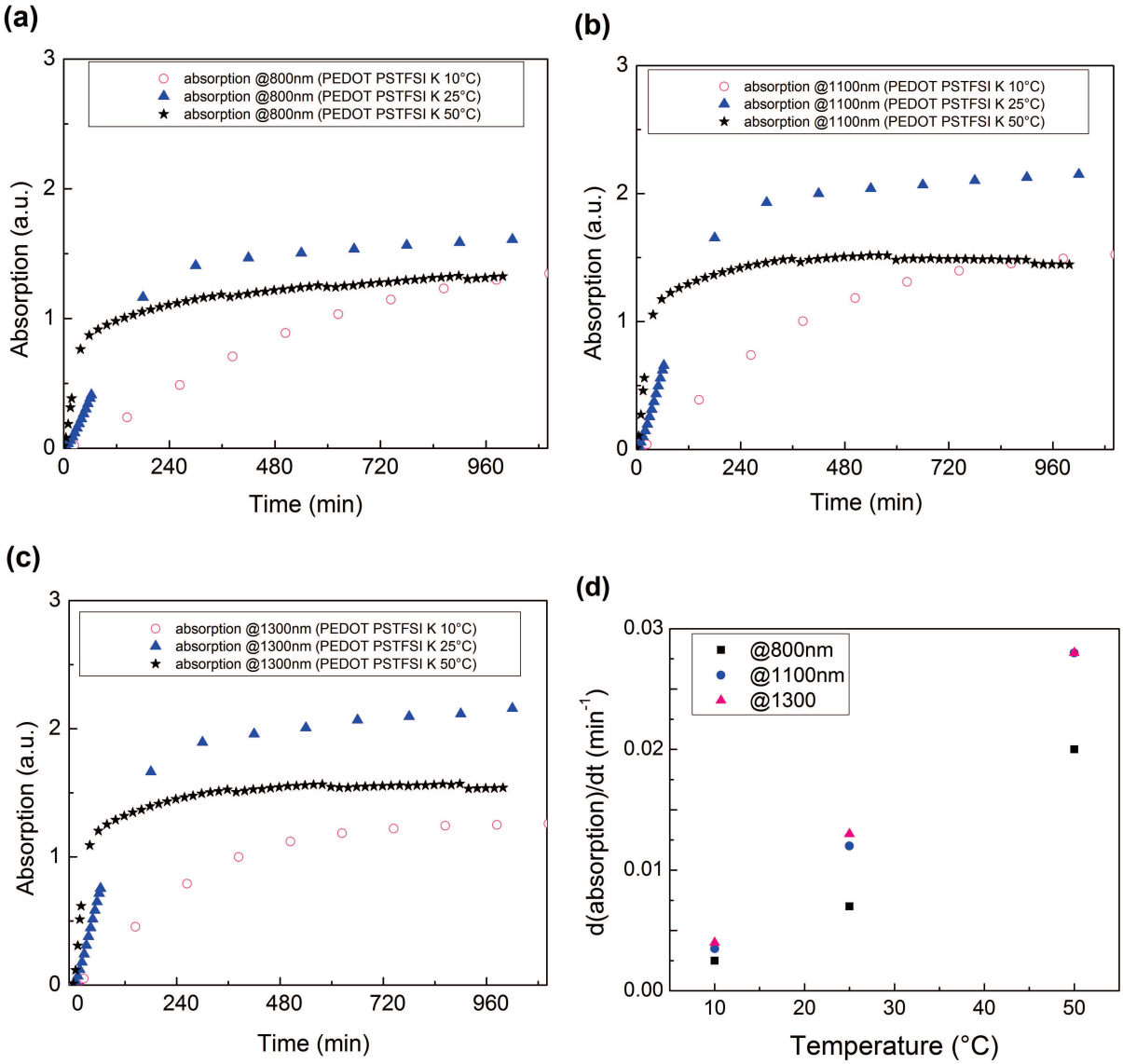

Fig. 2.50: Absorption of PEDOT:PSTFSI at a)800nm, b)1100nm and c)1300nm as a function of polymerization time for T= 10°C, 25°C and 50°C and d)rate of increasing absoprtion as a function of synthesis time

PEDOT:PSTFSI is indeed affected by the temperature, but depends in equal measure on other synthesis parameters.
In conclusion it was shown that the synthesis temperature has a drastic influence on the opto-electronic performance of the PEDOT:PSTFSI complexes. The highest conductivities were obtained for a synthesis temperatures between 10°C and 13°C. A possible explanation is, that the slower reaction kinetics at low synthesis temperatures lead to the formation of longer PEDOT chains, which are favourable for good doping and charge transport. However, this assumption could not be proven by experimental data.

2.5.4 Synthesis Time

Once the oxidants and the synthesis temperature for the standard synthesis protocol of PEDOT:PSTFSI were defined, the influence of the synthesis time on the opto-electronic properties was investigated. The right choice of the synthesis time is crucial to ensure that a sufficiently high degree of EDOT conversion has been reached. In order to study the temporal evolution of the opto-electronic properties and the doping of PEDOT:PSTFSI, samples were taken from the same batch of PEDOT:PSTFSI at different times of the synthesis.
Figure 2.51 displays the opto-electronic properties of PEDOT:PSTFSI dispersion, which were purified and characterized after 17 hours to maximum 234 hours of reaction time.

For the further discussion it is important to remember, that the absorption coefficient takes only into account the absorption at 550nm, which corresponds to the absorption of neutral PEDOT, and is not affected by changes in the polaronic and bipolaronic absorption regime.
As it can be seen from figure 2.51 the FoM increased until roughly 70 hours of synthesis and decreased then for synthesis times longer than 200 hours. The initial increase in the FoM was caused by a simultaneous gain in conductivity and a drop in the absorption at 550nm. This is related to an increasing degree of polymerization of EDOT and a increasing degree of doping, as it can be seen from the UV/Vis spectra in figure 2.51. For longer synthesis times the absorption coefficient stayed constant, which indicates that the polymerization of EDOT did not proceed further. The conductivity, however, decreased for synthesis times longer than 150 hours. From the UV/Vis spectrum (see

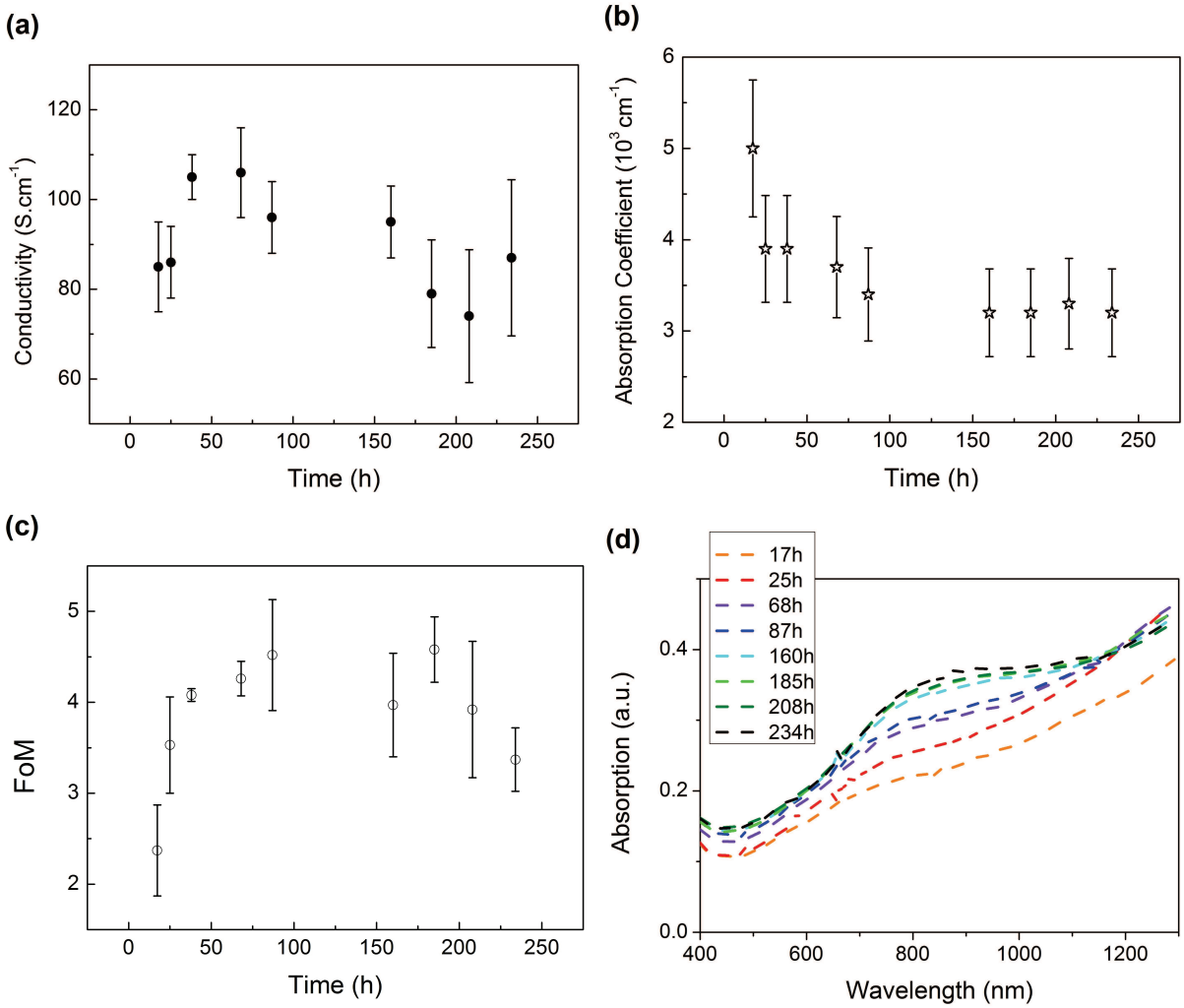

Fig. 2.51: Conductivity, absorption coefficient (at 550nm), FoM and UV/Vis spectra of PEDOT:PSTSFI at different times of the synthesis at T=10°C

figure 2.51) it can be seen, that the polaronic absorption at 800nm increased drastically for long synthesis times, whereas the absorption in the bipolaronic regime decreased slightly. Therefore, the decrease in conductivity for reaction times longer than 150 hours was attributed to a change in doping. This change could be either explained by an over-doping of PEDOT, which would result in a high density of more and more localized charges, or by the formation of sulfate functionalities on the PEDOT due to side reactions with persulfate radicals, which would lead to a break of the conjugation and therefore to a confinement of the charges. To clarify this question, XPS spectroscopy could be performed, which should give information on the presence of sulfate functionalities on PEDOT.

In summary, it was shown, that for the synthesis of PEDOT:PSTFSI at 10°C, the dispersion should be purified after 48 to 70 hours, in order to obtain the maximum conductivity and Figure of Merit. It was found that for shorter synthesis times the EDOT polymerization and doping was not completed, whereas for longer synthesis time degradation of the PEDOT doping was observed.

2.6 Conclusion

In conclusion we can state, that PEDOT:PSTFSI is a complex system, whose opto-electronic properties are highly dependent on intrinsic properties of the PSTFSI polyelectrolyte and at the same time on multiple synthesis parameters. It was shown, that the opto-electronic properties of PEDOT:PSTFSI are decisively influenced by the molar ratio of EDOT to STFSI units. On one hand, the PEDOT concentration has to be high enough to allow the percolation of conducting pathways in the film. On the other hand, the PSTFSI template polymer becomes saturated with PEDOT at molar EDOT to STFSI ratios higher than 0.9, which leads to a decrease in doping and colloidal instability. It seems, that the saturation behavior can be correlated to the amount of negative charges on PSTFSI, which can act as a base and becomes partially protonated in acidic medium, with an equilibrium at approximately 38% $STFSI^-$ units and 62% STFSIH units. As acidity is generated upon the polymerization of EDOT, the PSTFSI polyanion is partially neutralized during the PEDOT synthesis, which lowers the density of negative charges on the PSTFSI and affects its ability for charge compensation of PEDOT.

Parameter	Major Influence On	Best Opto-Electronic Performance For
Composition PEDOT/PSTFSI	Conductivity, Transparency, Rheology	σ_{max}at EDOT/STFI=0.9 FoM$_{max}$at EDOT/STFI=0.6
pH - Counter Ion of PSTFSI	Conductivity	PSTFSI-H
pH- Additional Base/Acid/Salt	Conductivity	no additional Base/Acid/Salt
Oxidants	Conductivity	$(NH_4)_2S_2O_8$:$FeCl_3$ at 3.5 : 1
Monomer Dispersion	Conductivity, Rheology	good dispersion (stirring>625rpm)
Temperature	Conductivity, Transparency	10°-13°C
Synthesis Time	Conductivity	50 hours

The synthesis of PEDOT:PSTFSI from the acid form of PSTFSI lead to an increase of the doping of PEDOT and morphological changes in the PEDOT:PSTFSI films, which resulted in a 2.4-fold increase of the conductivity. As the acidification of the synthesis medium with HCl did dot show the same effect, this could be caused by a different conformation or dissociation of PSTFSIH compared to PSTFSIK and changes in the chain growth of PEDOT. However, the underlying mechanism was not uncovered.

Furthermore it was found, that a good dispersion of the EDOT monomer in the PSTFSI solution is crucial for the efficient stabilization and doping of PEDOT through PSTFSI, as well as for the formation of a highly structured PEDOT:PSTFSI network with gel characteristics. By improvement of the dispersion of the EDOT monomer a three-fold increase of the conductivity was obtained.

The optimization of the synthesis parameters showed that the highest conductivity of about 330S.cm^{-1} (absorption coefficient=2200cm^{-1}, FoM=24) was obtained for PEDOT:PSTFSIH (M_W(PSTFSIH)≈350kDa) after about 50 hours of synthesis at 10°C under magnetic stirring at 625rpm by using a binary oxidant system of $FeCl_3$ and $(NH_4)_2S_2O_8$ with a molar ratio between oxidants and EDOT monomer of $(NH_4)_2S_2O_8$: $FeCl_3$: EDOT ratio of 3.5 : 1 : 3.5. PEDOT:PSS (M_W(PSSH)=1000kDa), which was synthesized using exactly the same protocol, displayed a conductivity of 305S.cm^{-1}, an absorption coefficient of 2500cm^{-1} and a FoM of 19.

Bibliography

[1] R. Meziane, J.-P. Bonnet, M. Courty, K. Djellab, and M. Armand, "Single-ion polymer electrolytes based on a delocalized polyanion for lithium batteries," *Electrochimica Acta*, vol. 57, pp. 14–19, Dec. 2011.

[2] S. Feng, D. Shi, F. Liu, L. Zheng, J. Nie, W. Feng, X. Huang, M. Armand, and Z. Zhou, "Single lithium-ion conducting polymer electrolytes based on poly[(4-styrenesulfonyl)(trifluoromethanesulfonyl)imide] anions," *Electrochimica Acta*, vol. 93, pp. 254–263, 2013.

[3] J. Li, H. Zhu, X. Wang, M. Armand, D. R. MacFarlane, and M. Forsyth, "Synthesis of Sodium Poly[4-styrenesulfonyl(trifluoromethylsulfonyl)imide]-co-ethylacrylate] Solid Polymer Electrolytes," *Electrochimica Acta*, vol. 175, pp. 232–239, Sept. 2015.

[4] M. Ullner and C. E. Woodward, "Simulations of the Titration of Linear Polyelectrolytes with Explicit Simple Ions: Comparisons with Screened Coulomb Models and Experiments," *Macromolecules*, vol. 33, pp. 7144–7156, Sept. 2000.

[5] J. D. Ziebarth and Y. Wang, "Understanding the Protonation Behavior of Linear Polyethylenimine in Solutions through Monte Carlo Simulations," *Biomacromolecules*, vol. 11, pp. 29–38, Jan. 2010.

[6] C. Barthet, M. Guglielmi, and P. Baudry, "A polyaniline + polyethylene oxide mixture as a composite polymer positive electrode in solid-state secondary batteries," *Journal of Electroanalytical Chemistry*, vol. 431, pp. 145–152, July 1997.

[7] M. Porté-Durrieu, F. Guillemot, S. Pallu, C. Labrugère, B. Brouillaud, R. Bareille, J. Amédée, N. Barthe, M. Dard, and C. Baquey, "Cyclo-(DfKRG) peptide grafting onto Ti–6al–4v: physical characterization and interest towards human osteoprogenitor cells adhesion," *Biomaterials*, vol. 25, pp. 4837–4846, Aug. 2004.

[8] H. Hanibah, A. Ahmad, and N. H. Hassan, "A New Approach in Determining Limiting Molar Conductivity value for Liquid Electrolyte," *Electrochimica Acta*, vol. 147, pp. 758–764, Nov. 2014.

[9] C. Holm, J. F. Joanny, K. Kremer, R. R. Netz, P. Reineker, C. Seidel, T. A. Vilgis, and R. G. Winkler, "Polyelectrolyte Theory," in *Polyelectrolytes with Defined Molecular Architecture II* (M. Schmidt, ed.), no. 166 in Advances in Polymer Science, pp. 67–111, Springer Berlin Heidelberg, 2004. DOI: 10.1007/b11349.

[10] Z. Luo and G. Zhang, "Sedimentation of polyelectrolyte chains in solutions: From dilute to semidilute," *Polymer*, vol. 52, pp. 5846–5850, Nov. 2011.

[11] L. Wang and H. Yu, "Chain conformation of linear polyelectrolyte in salt solutions: sodium poly (styrenesulfonate) in potassium chloride and sodium chloride," *Macromolecules*, vol. 21, no. 12, pp. 3498–3501, 1988.

[12] T. Cloots, L. D. Groenendaal, F. D. Jonas, and F. D. Louwet, "Method for making pi-conjugated water soluble polymers," Aug. 2001. International Classification H05K1/09, H01B1/12, C08G61/12; Cooperative Classification H01G11/56, H01G11/48, H01B1/127, C08G61/126, Y02E60/13, H01G9/028; European Classification H01B1/12H4, C08G61/12D1F.

[13] F. Louwet, L. Groenendaal, J. Dhaen, J. Manca, J. Van Luppen, E. Verdonck, and L. Leenders, "PEDOT/PSS: synthesis, characterization, properties and applications," *Synthetic Metals*, vol. 135-136, pp. 115–117, Apr. 2003.

[14] N. Paradee and A. Sirivat, "Synthesis of poly(3,4-ethylenedioxythiophene) nanoparticles via chemical oxidation polymerization: Synthesis of PEDOT nanoparticles," *Polymer International*, pp. n/a–n/a, May 2013.

[15] S. Kirchmeyer and K. Reuter, "Scientific importance, properties and growing applications of poly(3,4-ethylenedioxythiophene)," *Journal of Materials Chemistry*, vol. 15, pp. 2077–2088, May 2005.

[16] L. Groenendaal, F. Jonas, D. Freitag, H. Pielartzik, and J. R. Reynolds, "Poly(3,4-ethylenedioxythiophene) and Its Derivatives: Past, Present, and Future," *Advanced Materials*, vol. 12, pp. 481–494, Apr. 2000.

[17] J. Rivnay, S. Inal, B. A. Collins, M. Sessolo, E. Stavrinidou, X. Strakosas, C. Tassone, D. M. Delongchamp, and G. G. Malliaras, "Structural control of mixed ionic and electronic transport in conducting polymers," *Nature Communications*, vol. 7, p. 11287, Apr. 2016.

[18] X. Crispin, F. L. E. Jakobsson, A. Crispin, P. C. M. Grim, P. Andersson, A. Volodin, C. van Haesendonck, M. Van der Auweraer, W. R. Salaneck, and M. Berggren, "The Origin of the High Conductivity of Poly(3,4-ethylenedioxythiophene)−Poly(styrenesulfonate) (PEDOT−PSS) Plastic Electrodes," *Chemistry of Materials*, vol. 18, pp. 4354–4360, Sept. 2006.

[19] A. W. M. Diah, C. I. Holdsworth, J. L. Holdsworth, W. Belcher, and J. P. Quirino, "Capillary electrophoresis with photodiode array detection of processable poly(3,4-ethylenedioxythiophene)/polystyrene sulfonate aqueous dispersions," *Journal of Chromatography A*, vol. 1267, pp. 246–251, Dec. 2012.

[20] A. W. Diah, J. P. Quirino, W. Belcher, and C. I. Holdsworth, "An investigation of the doping efficiency of poly(styrene sulfonic acid) in poly(3,4-ethylenedioxythiophene)/ poly(styrene sulfonic acid) dispersions by capillary electrophoresis," *ELECTROPHORESIS*, pp. n/a–n/a, Apr. 2014.

[21] G. Zotti, S. Zecchin, G. Schiavon, F. Louwet, L. Groenendaal, X. Crispin, W. Osikowicz, W. Salaneck, and M. Fahlman, "Electrochemical and XPS Studies toward the Role of Monomeric and Polymeric Sulfonate Counterions in the Synthesis, Composition, and Properties of Poly(3,4-ethylenedioxythiophene)," *Macromolecules*, vol. 36, pp. 3337–3344, May 2003.

[22] K. Z. Xing, M. Fahlman, X. W. Chen, O. Inganäs, and W. R. Salaneck, "The electronic structure of poly(3,4-ethylene-dioxythiophene): studied by XPS and UPS," *Synthetic Metals*, vol. 89, pp. 161–165, Sept. 1997.

[23] H. Yan and H. Okuzaki, "Effect of solvent on PEDOT/PSS nanometer-scaled thin films: XPS and STEM/AFM studies," *Synthetic Metals*, vol. 159, pp. 2225–2228, Nov. 2009.

[24] G. Greczynski, T. Kugler, and W. R. Salaneck, "Characterization of the PEDOT-PSS system by means of X-ray and ultraviolet photoelectron spectroscopy," *Thin Solid Films*, vol. 354, pp. 129–135, Oct. 1999.

[25] J. Y. Kim, J. H. Jung, D. E. Lee, and J. Joo, "Enhancement of electrical conductivity of poly(3,4-ethylenedioxythiophene)/poly(4-styrenesulfonate) by a change of solvents," *Synthetic Metals*, vol. 126, pp. 311–316, Feb. 2002.

[26] S. Jönsson, J. Birgerson, X. Crispin, G. Greczynski, W. Osikowicz, A. Denier van der Gon, W. Salaneck, and M. Fahlman, "The effects of solvents on the morphology and sheet resistance in poly(3,4-ethylenedioxythiophene)–polystyrenesulfonic acid (PEDOT–PSS) films," *Synthetic Metals*, vol. 139, pp. 1–10, Aug. 2003.

[27] S. Marciniak, X. Crispin, K. Uvdal, M. Trzcinski, J. Birgerson, L. Groenendaal, F. Louwet, and W. Salaneck, "Light induced damage in poly(3,4-ethylenedioxythiophene) and its derivatives studied by photoelectron spectroscopy," *Synthetic Metals*, vol. 141, pp. 67–73, Mar. 2004.

[28] X. Crispin, S. Marciniak, W. Osikowicz, G. Zotti, A. W. D. van der Gon, F. Louwet, M. Fahlman, L. Groenendaal, F. De Schryver, and W. R. Salaneck, "Conductivity, morphology, interfacial chemistry, and stability of poly(3,4-ethylene dioxythiophene)–poly(styrene sulfonate): A photoelectron spectroscopy study," *Journal of Polymer Science Part B: Polymer Physics*, vol. 41, pp. 2561–2583, Nov. 2003.

[29] T.-W. Lee and Y. Chung, "Control of the Surface Composition of a Conducting-Polymer Complex Film to Tune the Work Function," *Advanced Functional Materials*, vol. 18, no. 15, pp. 2246–2252, 2008.

[30] S. Ulrich, A. Laguecir, and S. Stoll, "Complexation of a Weak Polyelectrolyte with a Charged Nanoparticle. Solution Properties and Polyelectrolyte Stiffness Influences," *Macromolecules*, vol. 38, pp. 8939–8949, Oct. 2005.

[31] S. Ulrich, M. Seijo, and S. Stoll, "The many facets of polyelectrolytes and oppositely charged macroions complex formation," *Current Opinion in Colloid & Interface Science*, vol. 11, pp. 268–272, Nov. 2006.

[32] A. Laguecir and S. Stoll, "Adsorption of a weakly charged polymer on an oppositely charged colloidal particle: Monte Carlo simulations investigation," *Polymer*, vol. 46, pp. 1359–1372, Feb. 2005.

[33] W. W. Chiu, J. Travaš-Sejdić, R. P. Cooney, and G. A. Bowmaker, "Spectroscopic and conductivity studies of doping in chemically synthesized poly(3,4-ethylenedioxythiophene)," *Synthetic Metals*, vol. 155, pp. 80–88, Oct. 2005.

[34] T. A. Skotheim and J. Reynolds, *Conjugated Polymers: Processing and Applications*. CRC Press, Dec. 2006.

[35] A. Elschner, S. Kirchmeyer, W. Lovenich, U. Merker, and K. Reuter, *PEDOT: Principles and Applications of an Intrinsically Conductive Polymer*. CRC Press, Nov. 2010.

[36] G.-H. Kim, L. Shao, K. Zhang, and K. P. Pipe, "Engineered doping of organic semiconductors for enhanced thermoelectric efficiency," *Nature Materials*, vol. 12, pp. 719–723, May 2013.

[37] J. Ouyang, ""Secondary doping" methods to significantly enhance the conductivity of PEDOT:PSS for its application as transparent electrode of optoelectronic devices," *Displays*, vol. 34, pp. 423–436, Dec. 2013.

[38] Y. Xia and J. Ouyang, "Significant Conductivity Enhancement of Conductive Poly(3,4-ethylenedioxythiophene): Poly(styrenesulfonate) Films through a Treatment with Organic Carboxylic Acids and Inorganic Acids," *ACS Applied Materials & Interfaces*, vol. 2, pp. 474–483, Feb. 2010.

[39] U. Lang, E. Müller, N. Naujoks, and J. Dual, "Microscopical Investigations of PEDOT:PSS Thin Films," *Advanced Functional Materials*, vol. 19, pp. 1215–1220, Apr. 2009.

[40] E. Vitoratos, S. Sakkopoulos, E. Dalas, N. Paliatsas, D. Karageorgopoulos, F. Petraki, S. Kennou, and S. A. Choulis, "Thermal degradation mechanisms of PEDOT:PSS," *Organic Electronics*, vol. 10, pp. 61–66, Feb. 2009.

[41] J. S. Choi, J.-H. Yim, D.-W. Kim, J.-K. Jeon, Y. S. Ko, and Y. Kim, "Effects of various imidazole-based weak bases and surfactant on the conductivity and transparency of poly(3,4-ethylenedioxythiophene) films," *Synthetic Metals*, vol. 159, pp. 2506–2511, Dec. 2009.

[42] J. H. Chen, C.-A. Dai, and W.-Y. Chiu, "Synthesis of highly conductive EDOT copolymer films via oxidative chemicalin situ polymerization," *Journal of Polymer Science Part A: Polymer Chemistry*, vol. 46, pp. 1662–1673, Mar. 2008.

[43] Y.-H. Ha, N. Nikolov, S. Pollack, J. Mastrangelo, B. Martin, and R. Shashidhar, "Towards a Transparent, Highly Conductive Poly(3,4-ethylenedioxythiophene)," *Advanced Functional Materials*, vol. 14, pp. 615–622, June 2004.

[44] G. Greczynski, T. Kugler, M. Keil, W. Osikowicz, M. Fahlman, and W. R. Salaneck, "Photoelectron spectroscopy of thin films of PEDOT–PSS conjugated polymer blend: a mini-review and some new results," *Journal of Electron Spectroscopy and Related Phenomena*, vol. 121, no. 1, pp. 1–17, 2001.

[45] C. Jiang, G. Chen, and X. Wang, "High-conversion synthesis of poly(3,4-ethylenedioxythiophene) by chemical oxidative polymerization," *Synthetic Metals*, vol. 162, pp. 1968–1971, Dec. 2012.

[46] C.-H. Wu, T.-M. Don, and W.-Y. Chiu, "Characterization and conversion determination of stable PEDOT latex nanoparticles synthesized by emulsion polymerization," *Polymer*, vol. 52, pp. 1375–1384, Mar. 2011.

[47] S. Garreau, J. L. Duvail, and G. Louarn, "Spectroelectrochemical studies of poly(3,4-ethylenedioxythiophene) in aqueous medium," *Synthetic Metals*, vol. 125, pp. 325–329, Dec. 2001.

[48] S. Garreau, G. Louarn, J. P. Buisson, G. Froyer, and S. Lefrant, "In Situ Spectroelectrochemical Raman Studies of Poly(3,4-ethylenedioxythiophene) (PEDT)," *Macromolecules*, vol. 32, pp. 6807–6812, Oct. 1999.

[49] Y. Xia, K. Sun, and J. Ouyang, "Solution-Processed Metallic Conducting Polymer Films as Transparent Electrode of Optoelectronic Devices," *Advanced Materials*, vol. 24, pp. 2436–2440, May 2012.

[50] B. I. Shklovskii and A. L. Efros, *Electronic Properties of Doped Semiconductors*, vol. 45. Springer, 2013. Google-Books-ID: OZXsCAAAQBAJ.

[51] K. Reuter and S. Kirchmeyer, "Process for preparing polythiophenes," June 2010. US-Klassifikation 252/500, 528/378; Internationale Klassifikation H01B1/12, C08G61/12; Unternehmensklassifikation H01G11/56, C08G61/126, H01G11/48, Y02E60/13; Europäische Klassifikation C08G61/12D1F.

[52] N. Sakmeche, E. Bazzaoui, M. Fall, S. Aeiyach, M. Jouini, J. Lacroix, J. Aaron, and P. Lacaze, "Application of sodium dodecylsulfate (SDS) micellar solution as an organized medium for electropolymerization of thiophene derivatives in water," *Synthetic Metals*, vol. 84, pp. 191–192, Jan. 1997.

[53] N. Sakmeche, S. Aeiyach, J.-J. Aaron, M. Jouini, J. C. Lacroix, and P.-C. Lacaze, "Improvement of the Electrosynthesis and Physicochemical Properties of Poly(3,4-ethylenedioxythiophene) Using a Sodium Dodecyl Sulfate Micellar Aqueous Medium," *Langmuir*, vol. 15, pp. 2566–2574, Mar. 1999.

[54] A. Lima, P. Schottland, S. Sadki, and C. Chevrot, "Electropolymerization of 3, 4-ethylenedioxythiophene and 3, 4-ethylenedioxythiophene methanol in the presence of dodecylbenzenesulfonate," *Synthetic metals*, vol. 93, no. 1, pp. 33–41, 1998.

[55] X. Du and Z. Wang, "Effects of polymerization potential on the properties of electrosynthesized PEDOT films," *Electrochimica Acta*, vol. 48, pp. 1713–1717, May 2003.

[56] T.-W. Chen, T.-H. Tsai, S.-M. Chen, and K.-C. Lin, "Using PEDOT Film Modified Electrode to Monitor Iodide and Its Enhancement of Arsenite Sensing," *Int. J. Electrochem. Sci*, vol. 6, pp. 2043–2057, 2011.

[57] S. G. Im and K. K. Gleason, "Systematic Control of the Electrical Conductivity of Poly(3,4-ethylenedioxythiophene) via Oxidative Chemical Vapor Deposition," *Macromolecules*, vol. 40, pp. 6552–6556, Sept. 2007.

[58] J. Wang, G. Cai, X. Zhu, and X. Zhou, "Oxidative chemical polymerization of 3, 4-ethylenedioxythiophene and its applications in antistatic coatings," *Journal of Applied Polymer Science*, vol. 124, pp. 109–115, Apr. 2012.

[59] R. Corradi and S. P. Armes, "Chemical synthesis of poly (3, 4-ethylenedioxythiophene)," *Synthetic metals*, vol. 84, no. 1, pp. 453–454, 1997.

3 Formulation and Processing of PEDOT:PSTFSI

From the aqueous PEDOT:PSTFSI dispersions, transparent and homogeneous conducting films can be fabricated using different coating techniques such as doctor blading, spin coating or spray coating. By formulation of the PEDOT:PSTFSI dispersions the opto-electronic properties of the resulting inks can be decisively influenced. It was found, that the conductivity could be drastically enhanced by the addition of high boiling point solvents or salts, whereas the transparency was increased through additional PSTFSIK polymer. Furthermore, the influence of the ink concentration and composition, as well as the influence of coating parameters such as temperature and blading speed on the film properties were investigated.

Les dispersions aqueuses de PEDOT:PSTFSI ont permis la fabrication de films conducteurs et transparents via des techniques d'enduction différentes, comme le 'spin coating', le 'spray coating' ou le 'doctor blading'. Les propriétés opto-électroniques des films PEDOT:PSTFSI peuvent être modifiées par formulation des encres, à partir desquelles ils sont élaborés. Il a été montré que la conductivité peut être améliorée de plusieurs ordres de grandeur grâce à la formulation de l'encre avec certains solvants ou sels, tandis que la transmittance et l'épaisseur des films ont par exemple pu être augmentées par formulation avec du PSTFSI utilisé comme additif. En outre, l'influence de la concentration et de la composition de l'encre, ainsi que l'influence des paramètres d'enduction ont été étudiées.

3.1 Introduction

One of the key advantages of conducting polymers as electrode materials, compared to thin metal films or inorganic oxides, is their printability. The easy processing of conducting inks at low temperatures and on large scales allows the cost efficient production of electronic devices. Nonetheless, the printability of polymer dispersions depends strongly on their rheological behavior, such as viscosity, drop formation, or filament break up, as well as their wetting behavior on the subjacent layer. These characteristics are affected by the polymer structure, molecular weight, the solvent and the concentration of the ink, but they can be adjusted by formulation with additives. In addition, it is known, that pristine PEDOT:PSS shows a conductivity of less than $1 S.cm^{-1}$, which is not sufficient for the application as transparent electrode. However, by formulation with high boiling point solvents, which are miscible with water, such as DMSO or EG, the conductivity of the PEDOT:PSS films can be increased for more than two orders of magnitude [1, 2, 3, 4, 5, 6, 7, 8, 9, 10]. Therefore the effect of different additives and co-solvents on PEDOT:PSTFSI was studied, in order to define a formulation which allows the fabrication of homogeneous thin PEDOT:PSTFSI films with high conductivities on glass and plastic substrates.

3.2 Increasing the Conductivity by Formulation with Small Molecule Additives and High Boiling Point Solvents

Exactly as in the case of PEDOT:PSS, the conductivity of the pristine PEDOT:PSTFSI films is rather low with about $1 S.cm^{-1}$ (see table 3.1), but can be drastically increased by the treatment with high boiling point solvents. Upon the the addition of 5% DMSO (or EG) as co-solvent and drying at 120°C an almost 200-fold increase of the conductivity was observed, while the absorption coefficient of the films was not affected (see table 3.1). Therefore the Figure of Merit of the films was drastically increased (see table 3.1).

For higher concentrations of DMSO co-solvent, the opto-electronic properties stayed unchanged (see table 3.1). However, the film roughness increased slightly, as it can be

Concentration DMSO (wt%)	Conductivity[a,b] (S.cm^{-1})	Absorption Coefficient[a] (10^3 cm^{-1})	FoM	R_q [c] (nm)
0	0.7± 0.5	2.3± 0.1	0.1± 0.05	0.6
5	130± 13	2.4± 0.1	8.0± 0.5	1.0
10	122± 10	2.2± 0.1	8.3± 0.5	1.1
15	123± 12	2.3± 0.1	8.2± 0.6	1.4

[a] average on 8 measurements or more [b] determined by 4-point measurements [c] determined from AFM height images

Tab. 3.1: Opto-electronic properties and surface roughness of PEDOT:PSTFSI cast with different concentrations of DMSO co-solvent, M_W(PSTFSIK)≈200kDa, synthesis at 11°C, ∼400rpm

seen from AFM height images in figure 3.2. Thus, we chose to work with 5% DMSO co-solvent, which also allowed good processing and minimized the potentially residual DMSO in the films. In literature the effect of high boiling point solvents on PEDOT:PSS is commonly explained by a phase separation of PEDOT and PSS, leading to a growth of the PEDOT rich domains [3, 4, 5], better percolation [6, 3] and an increase in crystallinity [7, 8, 9, 10]. The mechanism leading to this phase separation is not fully understood, but is probably related to the high dipole moments of the solvents, which interact with the charged PEDOT and PSS moieties, softens the electrostatic interactions between PEDOT and PSS and facilitates the rearrangement of the chains [11].

AFM phase images of PEDOT:PSTFSI films without and with DMSO (see figure 3.2) confirmed a change in the surface structure of PEDOT:PSTFSI films, which could be attributed to a phase separation of PEDOT and the PSTFSI polyelectrolyte.

Surface analysis of pristine films and DMSO containing films by XPS revealed, that the surface composition is affected by the DMSO co-solvent. In the XPS S2p spectrum (see figure 3.1) it can be seen, that due to the use of DMSO co-solvent the intensity of the doublet at 163.6eV, which is assigned to the sulfur atoms in polythiophenes, increased, whereas the intensity of the peak at around 168eV, which corresponds to sulfur atoms in sulfonyl groups, decreased. This signifies an increasing PEDOT concentration at the film surface of PEDOT:PSTFSI deposited with DMSO co-solvent, which is coherent with the results presented for PEDOT:PSS in literature [6, 12, 5].

Furthermore, it has been reported that the use of high boiling point solvents leads to an increase in crystallinity of PEDOT:PSS [7, 8, 9, 10]. This was not confirmed for PEDOT:PSTFSI. In the case of of PEDOT:PSTFSI (M_W(PSTFSI)>10kDa) DSC and GIWAXS analysis did not show any sign of crystallinity for both pristine and DMSO

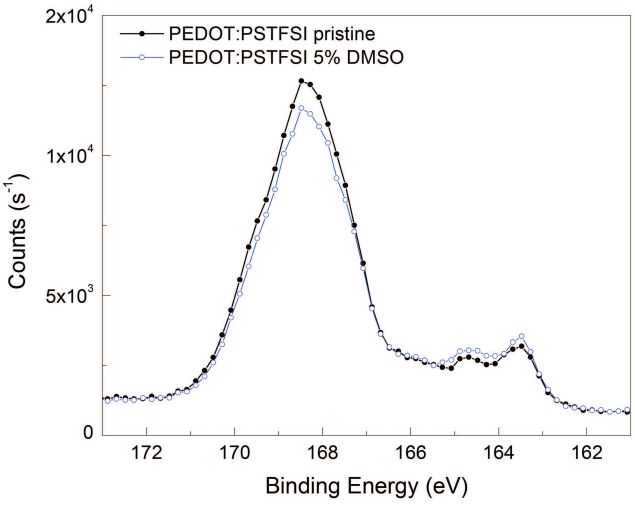

Fig. 3.1: XPS S2p spectrum of films cast from pristine PEDOT:PSTFSI and from PEDOT:PSTFSI with 5% DMSO co-solvent

treated PEDOT:PSTFSI (see figure D.7, appendix page 232, and figure B.1, appendix page 226).

Ouyang and co-workers reported, that the conductivity of PEDOT:PSS can also be increased by the addition of certain salts [13]. Furthermore, a synergetic effect of the treatment with high boiling point solvents and salts was observed [14]. In analogy to the mechanism discussed for polar solvents, this effect could be explained by the charge screening of the salt ions, which helps the rearrangement of polymer chains.
For this work, we chose to study the formulation of PEDOT:PSTFSI with lithium bis(trifluoromethanesulfonyl)imide (LiTFSI) and with para toluene sulfonic acid (pTSA). LiTFSI could be seen as the monomeric equivalent to the STFSI functional unit of PSTFSI and pTSA is known as good counter ion for in situ polymerized PEDOT and has been studied as plasticizer in poly(4-vinylpyridine) [15]. Therefore these small ionic molecules are supposed to be well miscible with the PEDOT:PSTFSI system and to interact with charged PEDOT.

Upon the addition of pTSA to PEDOT:PSTFSI, a drastic increase in its conductivity was observed, which surpassed the conductivity obtained upon formulation with DMSO (see table 3.2). However, the presence of pTSA made the films appear whitish, which was attributed to microscopic inhomogeneities in the film caused by domains of crystallizing pTSA and which lead to a decrease of the film transparency. Therefore, the

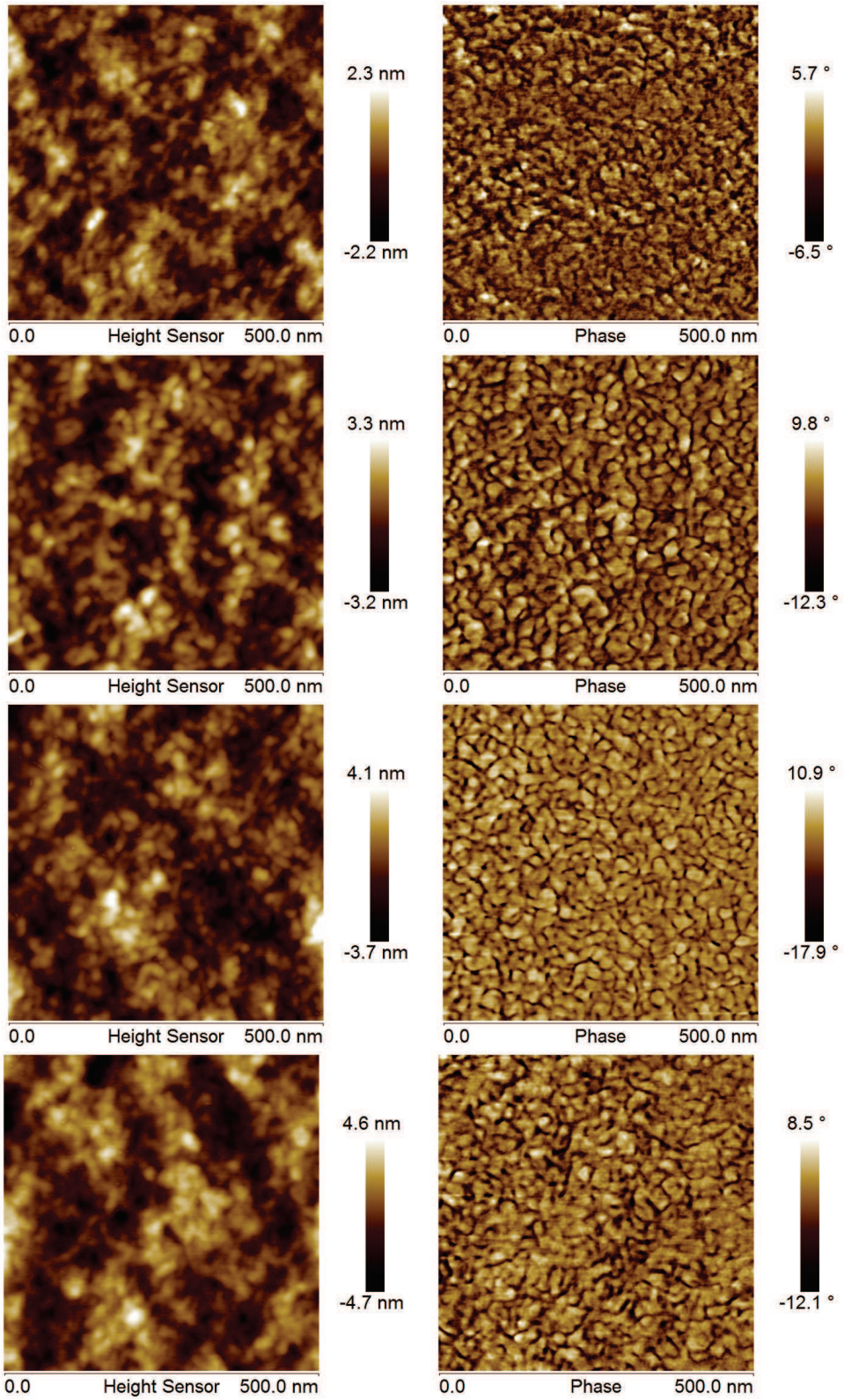

Fig. 3.2: AFM height images (left) and phase images (right) of pristine PEDOT:PSTFSI films and films cast with 5%, 10% and 15% DMSO (from top to bottom)

Salt	DMSO (vol%)	Conductivity[a,b] (S.cm^{-1})	Absorption Coefficient[a] (10^3 cm^{-1})	FoM[a]
-	0	1±0.3	3.7±0.5	< 1
	5	151±18	3.8±0.4	6.4±0.6
LiTFSI	0	110±12	2.6±0.0	6.4±0.5
	5	133±11	3.8±1.0	6.3±1.2
pTSA	0	191±23	3.8±0.6	7.7±0.3
	5	230±42	4.3±0.9	8.1±0.6

[a] average on 8 measurements or more [b] determined by 4-point measurements

Tab. 3.2: Opto-electronic properties of PEDOT:PSTFSI formulated with DMSO and/or with 6g.l^{-1} LiTFSI or 14g.l^{-1} pTSA

FoM of pTSA formulated films was not much higher than the FoM of DMSO formulated films, despite their higher conductivity. The highest FoM was obtained for about 1.7g pTSA for 1g dry PEDOT:PSTFSI polymer, which is equivalent to 2.4wt% pTSA in PEDOT:PSTFSI dispersion of 1.4% solid content (see figure 3.3). At this pTSA concentration a partial precipitation of the PEDOT:PSTFSI complexes was observed. This decrease in colloidal stability could be explained by the replacement of the polymeric counter ion PSTFSI by the small anion pTSA, which can act as counter ion for PEDOT, but can not stabilized PEDOT particles in dispersion. A similar ion exchange behavior in PEDOT:PSS dispersion, from PSSH to PSS$^-$Cation complexes, has been reported by Mecerreyes and co-workers [16]. UV/Vis spectroscopy revealed, that PEDOT:PSTFSI films containing pTSA showed higher bipolaronic absorption than pristine or DMSO treated films, the latter showing exactly the same absorption spectrum (see figure 3.3). This confirms, that pTSA affects the doping, whereas DMSO only affects the morphology of PEDOT:PSTFSI films. In addition, the AFM height and phase images of PEDOT:PSTFSI films with pTSA did not display clear differences to the surface of pristine PEDOT:PSTFSI films (see figure 3.4), which is opposed to the observation made upon the treatment of PEDOT:PSTFSI with DMSO (see figure 3.2).

Upon addition of both pTSA and DMSO to the PEDOT:PSTFSI dispersions, a small synergistic effect was observed regarding the conductivity of the PEDOT:PSTFSI films. However, these films showed an increased surface roughness and a much lower transparency.

As the FoM obtained by the addition of pTSA, DMSO co-solvent or pTSA and DMSO was very similar, the use of only DMSO was preferred for two reasons. First, pTSA

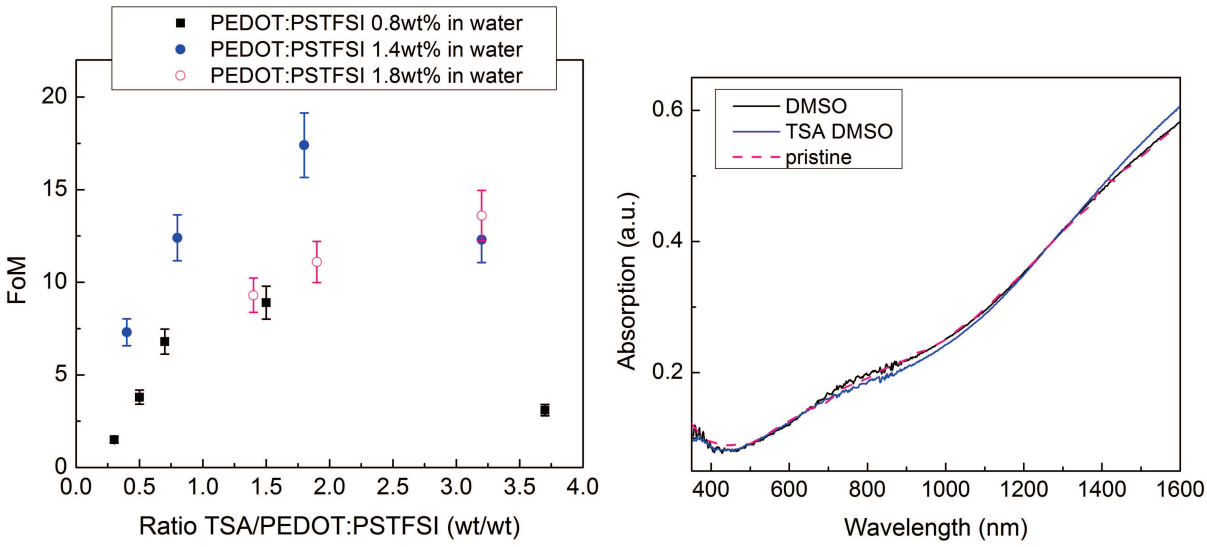

Fig. 3.3: Figure of Merit of PEDOT:PSTFSI dispersions with different solid contents as a function of the toluene sulfonic acid concentration (left) and UV/Vis spectra of PEDOT:PSTFSI films cast from pristine ink, ink with 5%DMSO co-solvent and ink with 5%DMSO cosolvent and 1.4wt%pTSA

formed a whitish layer on top of the PEDOT:PSTFSI films which had to be removed by washing, whereas DMSO could be removed by simple heating of the films. Second, PEDOT:PSTFSI films containing pTSA were slightly hygroscopic, which lead to instabilities of the opto-electronic properties on a time scale of several months.

As already mentioned, another salt, which was tested as additive for PEDOT:PSTFSI in this work, is LiTFSI. The addition of small quantities of LiTFSI to PEDOT:PSTFSI did not affect the opto-electronic properties of the PEDOT:PSTFSI films. Only upon the addition of about 6g.l^{-1} LiTFSI, a considerable increase of the conductivity was observed (see figure 3.5). However, the absolute conductivity obtained through the formulation with LiTFSI was lower than via the formulation with DMSO or pTSA (see table 3.2). It is noteworthy, that the PEDOT:PSTFSI-LiTFSI films were very homogeneous on the macroscopic scale and showed a shiny aspect, which is in coherence with the low absorption coefficient of these films (see table 3.2).

In the presence of DMSO, the effect of LiTFSI was ruled out and the opto-electronic properties of PEDOT:PSTFSI were determined by the influence of the DMSO co-solvent (see table 3.2 and figure 3.5).

UV/Vis spectroscopy revealed, that the presence of LiTFSI affected the absorption of

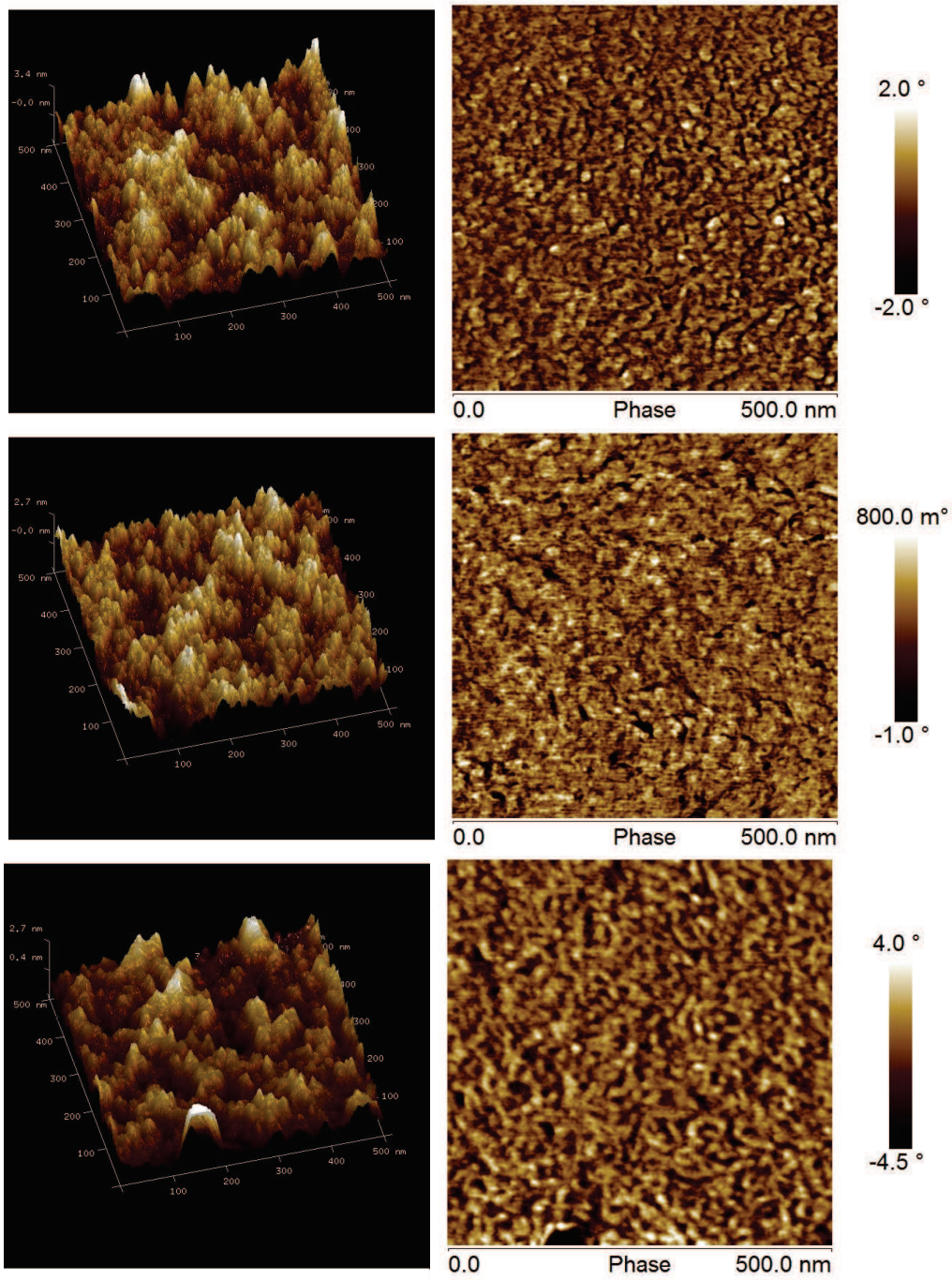

Fig. 3.4: AFM 3D height and 2D phase images of a pristine PEDOT:PSTFSI film (top) and of films of PEDOT:PSTFSI containing 14g.l^{-1} pTSA (middle) and of PEDOT:PSTFSI containing 6g.l^{-1} LiTFSI

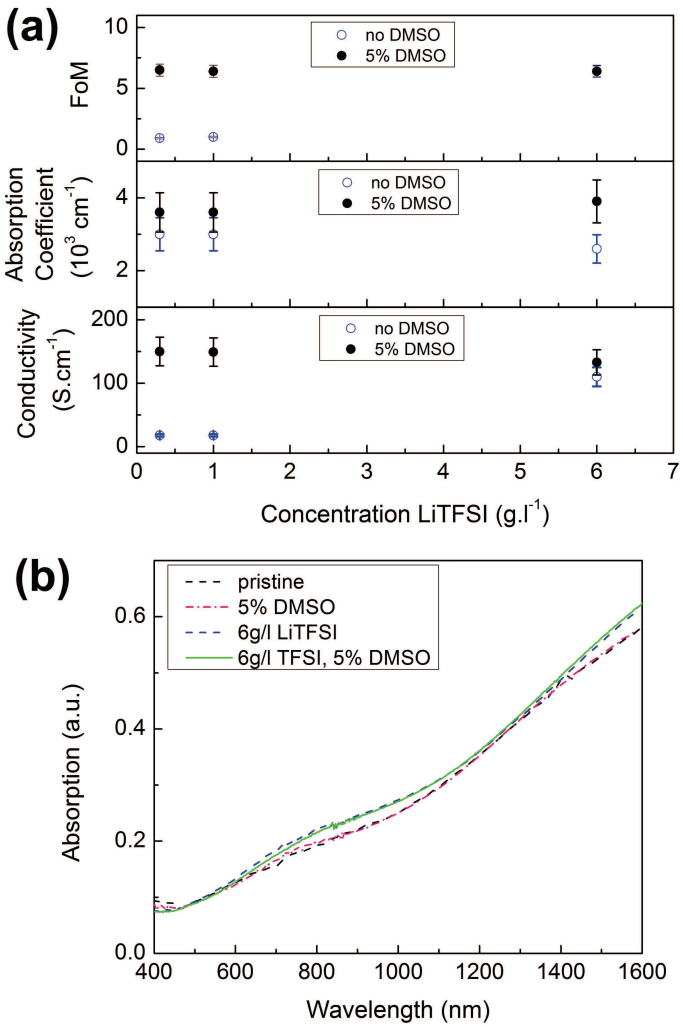

Fig. 3.5: a)Opto-electronic properties and b)UV/Vis absorption spectra of PEDOT:PSTSFI formulated with LiTFSI and with LiTFSI+5% DMSO

PEDOT:PSTFSI in the polaronic and bipolaronic regime, which indicates, that LiTFSI influences the doping of the PEDOT:PSTFSI system. This is in analogy to the observation made for pTSA and could be explained by the small and mobile $TFSI^-$ anions acting as supplementary counter ions for the doped PEDOT. Unlike in the case of pTSA, no precipitation was observed in the PEDOT:PSTFSI-LiTFSI dispersions, even for high LiTFSI concentrations. However, at LiTFSI concentrations higher than 25g.l^{-1} the obtained PEDOT:PSTFSI-LiTFSI films did not dry properly, which was attributed to the hygroscopic nature of LiTFSI.

In a last step, the PEDOT:PSTFSI film homogeneity was improved by the formulation of the inks with surfactants. The use of sodium dodecyl sulfate (SDS) lead

to very homogeneous films, but also to a decrease in the conductivity. However, the formulation with the fluoro-surfactant Zonyl allowed the deposition of films with excellent homogeneity [17] and did not affect the measured conductivity. Therefore, in this work 0.04wt% of Zonyl was added to all PEDOT:PSTFSI dispersions before film deposition.

In conclusion, we found, that the conductivity of PEDOT:PSTFSI can be increased by a factor of 200 due to the use of 5% DMSO as co-solvent. The increase of conductivity was attributed to a change of the film morphology, in analogy to the mechanism described for PEDOT:PSS. A similar increase of the figure of merit was obtained by formulation with LiTFSI or pTSA. However, for reasons of simple processing DMSO was defined as the additive of choice for the study of PEDOT:PSTFSI. To ensure homogeneous film formation, the formulation with 0.04wt% Zonyl fluorosurfactant was elaborated, which did not affect the opto-electronic properties of the PEDOT:PSTFSI film.

3.3 Increasing the Transparency by Formulation of PEDOT:PSTFSI with PSTFSI

For certain applications, such as invisible anti electrostatic coatings or nanowire - polymer composite electrodes, "extremely" transparent conducting polymers are needed. PEDOT:PSTFSI displays a higher transparency in the visible range than PEDOT:PSS and by simple formulation the transparency can be further increased without the complete loss of conductivity.

The main strategy to achieve extremely high transparencies was to incorporate additional transparent PSTFSIK polymer in the conducting PEDOT:PSTFSI inks. As PSTFSI is a component of the PEDOT:PSTFSI system, it is perfectly miscible with the dispersion. The amount of additional PSTFSIK is reported in wt% with respect to the total mass of dry PEDOT:PSTFSI polymer.

From figure 3.6 it can be seen, that upon the addition of PSTFSIK to PEDOT:PSTFSI both the absorption coefficient and the conductivity of the polymer films decreased. A closer look on the evolution of the absorption coefficient reveals, that already upon the addition of small amounts of PSTFSIK the absorption dropped to 30% to 40% of the initial value. For higher amounts of additional PSTFSIK, the decrease of

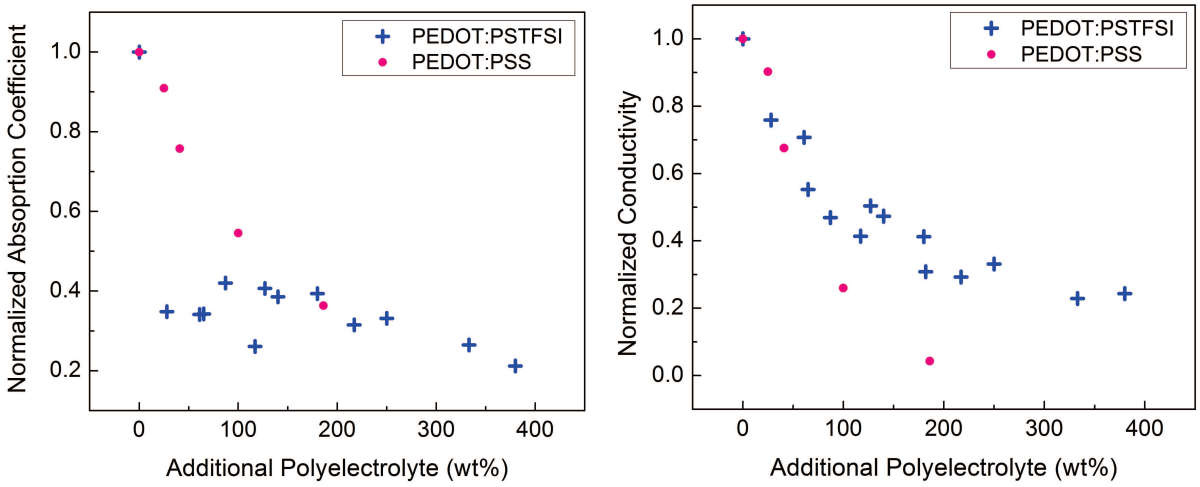

Fig. 3.6: Normalized absorption coefficient and conductivity of PEDOT:PSTFSI (PEDOT:PSS) as a function of PSTFSIK (PSSNa) added to the dispersion

the absorption coefficient was insignificant. In the same time, the conductivity of the PEDOT:PSTFSI films decreased continuously and seemed to stabilize at about 20% of the initial value.

The abrupt drop of the absorption coefficient and the much smaller decrease of the conductivity upon the addition of less than 100wt% PSTFSIK to PEDOT:PSTFSI dispersions, allows the fabrication of extremely transparent films with decent conductivity. Figure 3.7 illustrates, that a film of unformulated PEDOT:PSTFSI with 120nm thickness showed the same transmittance as the 550nm thick film made of the ink, which was formulated with 87wt% PSTFSIK (see green arrow). In the same time, the sheet resistance of the thicker film, made of formulated PEDOT:PSTFSI, was lower, despite the loss in conductivity. Therefore the calculated FoM increased upon the addition of PSTFSIK to PEDOT:PSTFSI (see figure 3.8). However, it has to be taken into account, that for extremely highly transparent films with T $>$ 97% the FoM diverges due to its strong dependency on T (see figure 3.8) and can not serve as valuable measure for the opto-electronic performance of the films.

In comparison, the addition of PSSNa to PEDOT:PSS resulted in a steady, but slow decrease of the absorption coefficient and the conductivity decreased steadily until the films became insulating for more than 200wt% of additional PSSNa. The formulation of PEDOT:PSS with PSSNa also allowed to increase the film thickness by keeping the

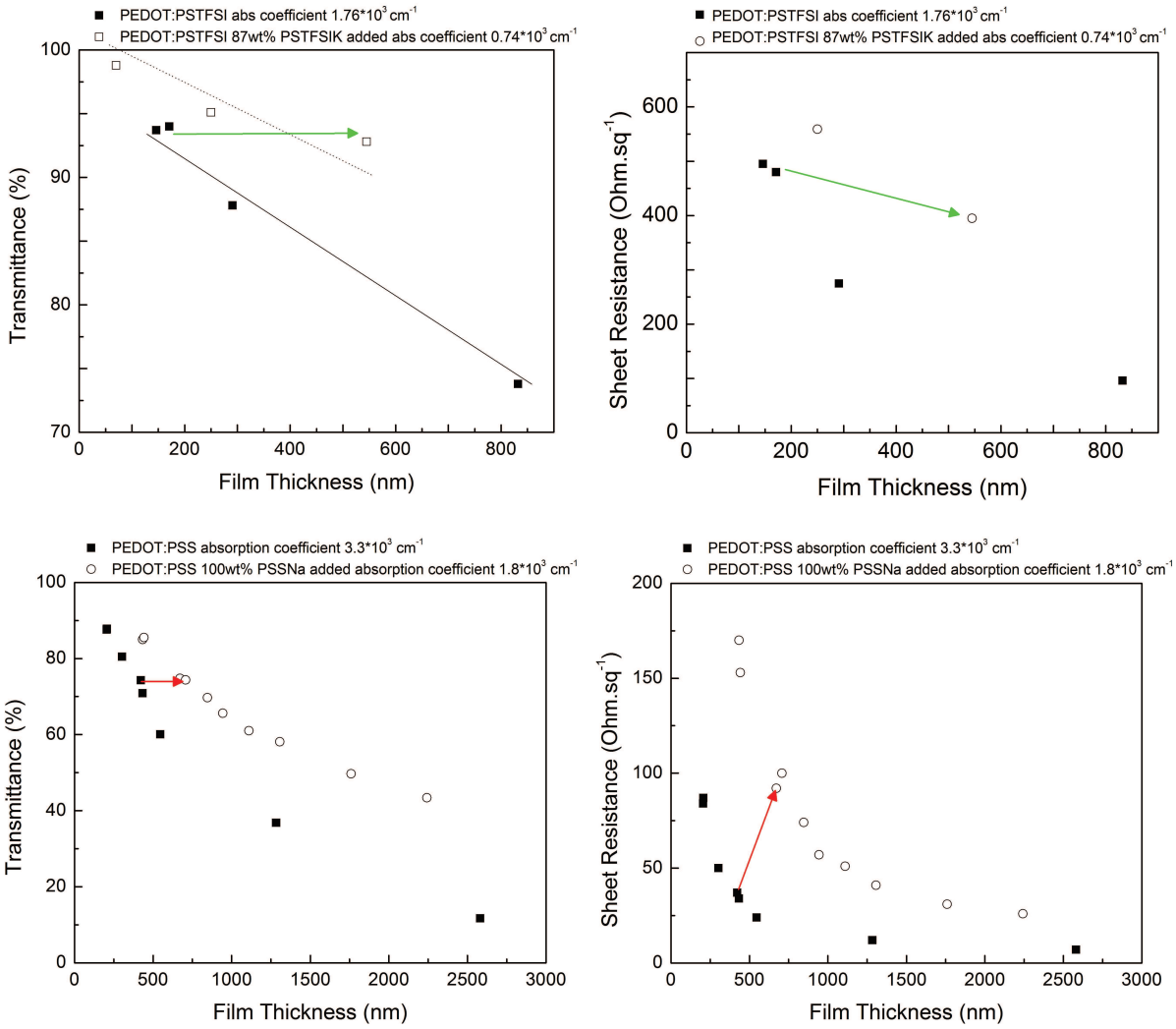

Fig. 3.7: Transmittance and sheet resistance as a function of film thickness of films cast from pristine PEDOT:PSTFSI (PEDOT:PSS) and from PEDOT:PSTFSI (PEDOT:PSS) formulated with PSTFSIK (PSSNa)

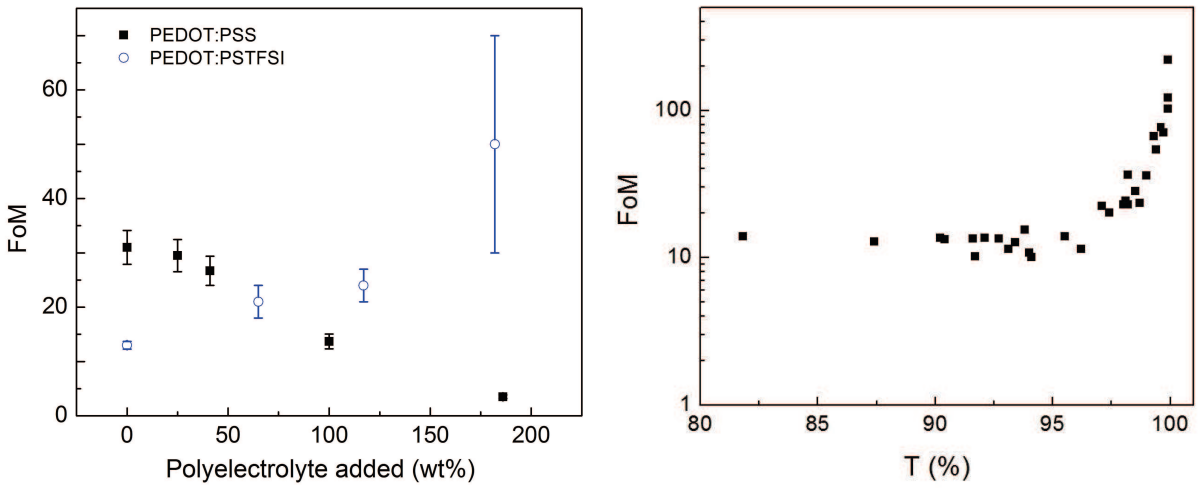

Fig. 3.8: The FoM for PEDOT:PSTFSI and PEDOT:PSS fomulated with PSTFSIK and PSS, respectively and dependency of the FoM of PEDOT:PSTFSI on the transparency T

transmittance constant (see red arrow figure 3.7). However, the sheet resistance of the thicker film of formulated PEDOT:PSS was substantially higher and the FoM decreased (see figure 3.8). Therefore the gain in transparency was not big enough to compensate the loss in conductivity and the opto-electronic properties of PEDOT:PSS were worsened by formulation.

From figure 3.9 and figure 3.10 it can be seen, that the increase of the amount of PSTFSIK during the synthesis of PEDOT:PSTFSI did not lead to the same effect. With increasing PSTFSI concentration the absorption coefficient of the resulting PEDOT:PSTFSI decreased linearly and less drastically. For the double amount of PSTFSI, which corresponds to about 75wt% of added PSTFSIK in the case of formulation, the absorption coefficient was at 70% of the initial value, compared to 35% of the initial absorption in case of formulation. By contrast, the decrease in conductivity was faster than in the case of formulation. Therefore the decrease in absorption was not important enough to compensate the loss of conductivity (see figure 3.10) and the FoM was drastically decreased.

The underlying mechanism for the formulation process was not further investigated. However, a possible explanation for the different effect of formulation on the conductivity of PEDOT:PSTFSI and on PEDOT:PSS, is the network character of PEDOT:PSTFSI, which can not be observed in the commercial PEDOT:PSS (see figure 3.11). Upon the addition of PSTFSIK, PSTFSIK rich domains can be formed, which inter-penetrate the

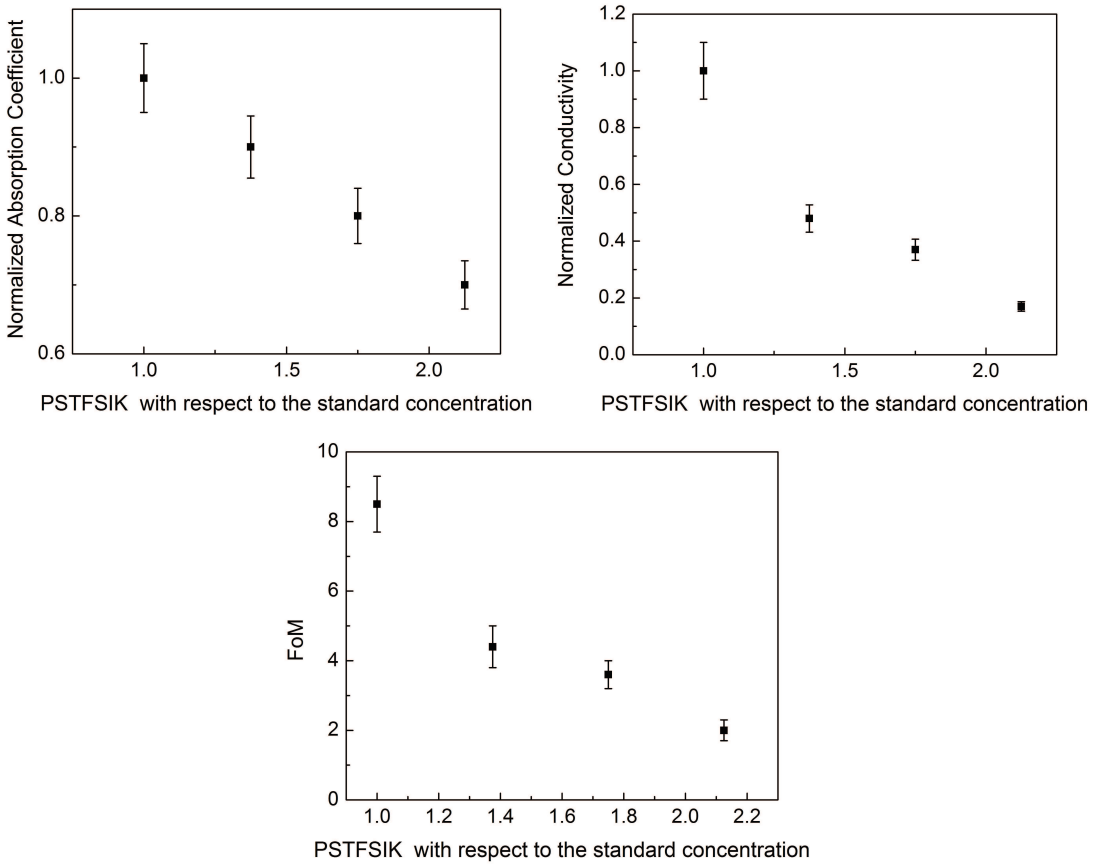

Fig. 3.9: Normalized absorption coefficient, normalized conductivity and FoM of PEDOT:PSTFSI, synthesized with increased PSTFSI concentration

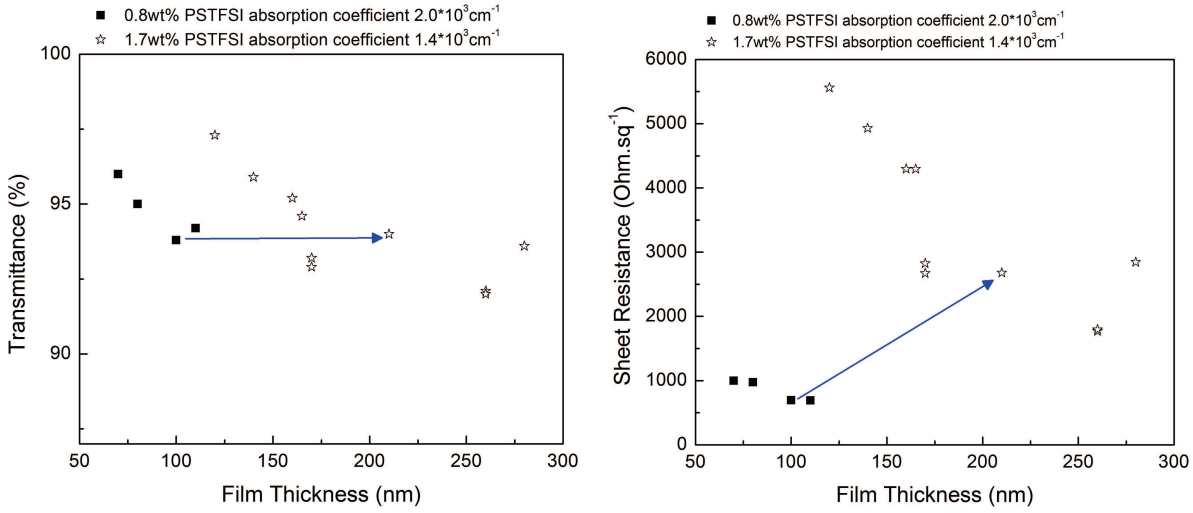

Fig. 3.10: Transmittance and sheet resistance as a function of film thickness for PEDOT:PSTFSI, synthesized with increasing concentrations of PSTFSI

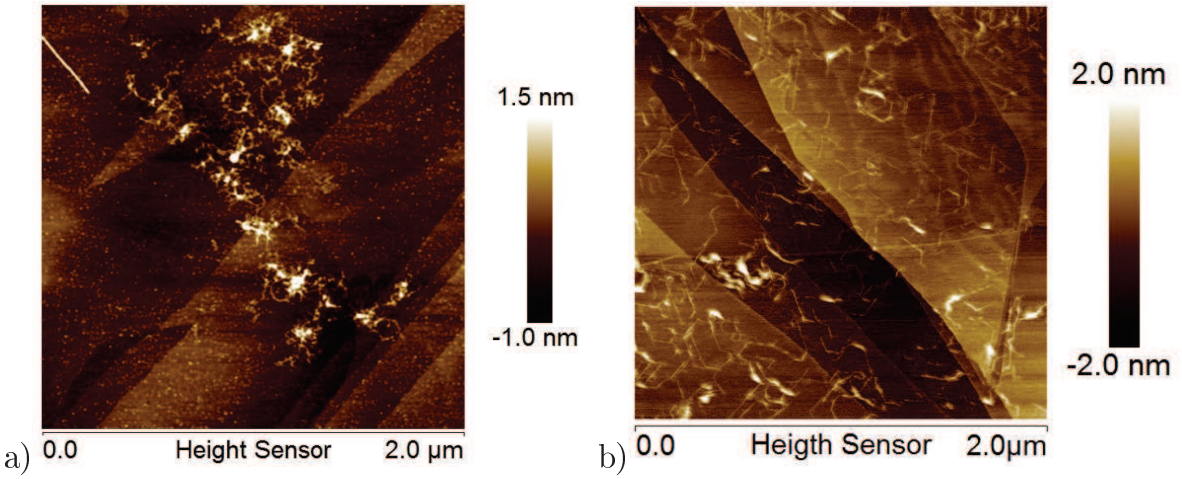

Fig. 3.11: a)PEDOT:PSTFSI and b)commercial PEDOT:PSS imaged by liquid AFM

network of PEDOT:PSTFSI without interrupting the percolation of the PEDOT rich domains and allow the persistence of conductivity. The isolated PEDOT:PSS complexes, however, can be assumed to form isolated domains in a PSS rich matrix, which leads to a disruption of the conducting, percolated network.

In summary, it was shown that the Figure of Merit for PEDOT:PSTFSI films can be increased by simple formulation with PSTFSIK. This formulation method allowed the fabrication of thick PEDOT:PSTFSI - PSTFSIK films with high transmittance and decent sheet resistance (thickness 550nm, T = 93%, R = 400Ohm.sq^{-1}), which are suitable for applications in composite electrodes. However, this principle was not applicable to the formulation of commercial PEDOT:PSS.

3.4 Fabrication of PEDOT:PSTFSI Thin Films

PEDOT:PSTFSI films were deposited by spin coating, spray coating or doctor blading. Due to its high viscosity and gel character, PEDOT:PSTFSI was easily processable by doctor blading, which resulted in homogeneous films with film thickness of up to 600nm. Very thin and homogeneous films were obtained by spin coating. In order to render spray coating possible, the PEDOT:PSTFSI dispersion had to be diluted with water to avoid complete plugging of the nozzle. The spray coated films were inhomogeneous and showed a high surface roughness (see figure 3.12). Therefore, spin coating and doctor blading were the coating techniques of choice for PEDOT:PSTFSI and the opto-electronic properties of the films were the same for both these coating techniques.

As doctor blading allowed the casting of rather large films with very variable thickness from 80nm to 600nm on glass and on plastic substrates, the doctor blading process was studied more closely in correlation with the rheology of PEDOT:SPTFSI dispersion.

It was found, that PEDOT:PSTFSI dispersions with a solid content higher than 0.8wt% resulted in more homogeneous films than the same dispersions with lower solid content. This can be explained by the increase in viscosity of the dispersion for higher solid contents (see figure 3.13), which is favorable for the processing by spin coating and doctor blading. Dispersions with a solid content of 1.4wt% were highly viscous, comparable to pastes. A clear influence of the solid content on the opto-electronic properties in the range of 0.8 wt% to 1.4% was not observed.

As described in literature [18], the increase in viscosity with increasing dispersion concentration is not linear. This is related to the hydrodynamic interaction between the particles and depends on multiple factors, including the particle size distribution and geometry. The fact, that the flow curve was not identical for increasing and decreasing shear rates (see figure 3.13), indicates that the structure of the polymer complex is altered by the applied shear. To investigate the structure breakdown further amplitude sweeps were performed. From figure 3.14 it can be seen, that for all dispersion concentrations the storage modulus G' was higher than the loss modulus G", which indicates high colloidal forces between the polymer particles. The critical strain, which is defined as the maximum strain before the polymer structure is disrupted, was determined to be between 2 and 3% for all dispersions. The measurement of the storage and loss moduli over a wide range of frequencies (see figure 3.15) confirmed the gel character of the dispersions. Interestingly, the gel characteristics can be already found for mass contents low as 0.63wt% in water. Therefore we can state, that an increase in the total concentration of PEDOT:PSTFSI lead to higher viscosity, but did not drastically alter the gel behavior.

In order to obtain homogeneous films, it is crucial, that the critical shear rate and the critical strain are not exceeded during the coating process. For PEDOT:PSTFSI dispersions coating speeds between $4mm.s^{-1}$ to $24mm.s^{-1}$ were used. From figure 3.16 it can be seen, that the opto-electronic properties were not dependant on the blade speed in the studied regime. Therefore we can state that the rheological properties of

PEDOT:PSTFSI allow a wide range of coating conditions. However, colloidal instabilities of PEDOT:PSTFSI dispersions with high EDOT concentrations, became apparent during processing (see figure 3.17). With increasing blading speed (from right to left in figure 3.17) the shear rate increases and the dispersions became instable.

For PEDOT:PSTFSI inks with different concentrations and different formulations or in order to control drying it might be desirable to adapt the temperature of the substrate during coating. As it can be seen from figure 3.18 the opto-electronic properties of PEDOT:PSTFSI films were not affected by the coating temperature in the range of 40°C to 80°C.

In conclusion we can state that the rheological properties of PEDOT:PSTFSI allow the coating of PEDOT:SPTFSI dispersions with a solid content of higher than about 0.8wt% in a wide range of coating speeds and temperatures. Therefore the processing parameters can be adapted to the viscosity of each ink and to the target film thickness, without affecting the opto-electronic properties of the dry film.

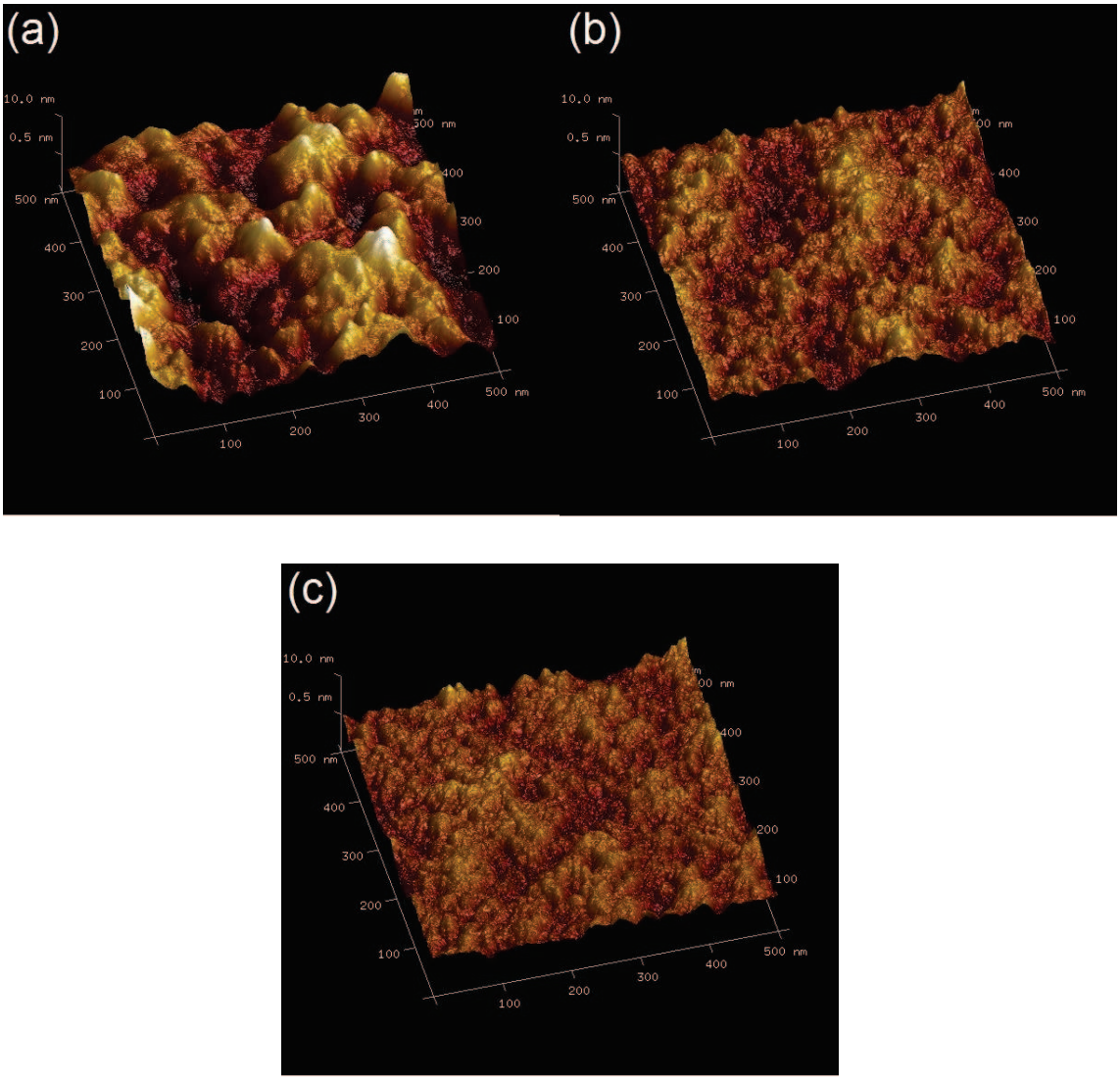

Fig. 3.12: 3D representation of AFM height images of a)spray coated PEDOT:PSTFSI, R_q=2.7nm, b)of doctor bladed PEDOT:PSTFSI R_q=1.3nm and c)of spin coated PEDOT:PSTFSI, R_q=1.0nm

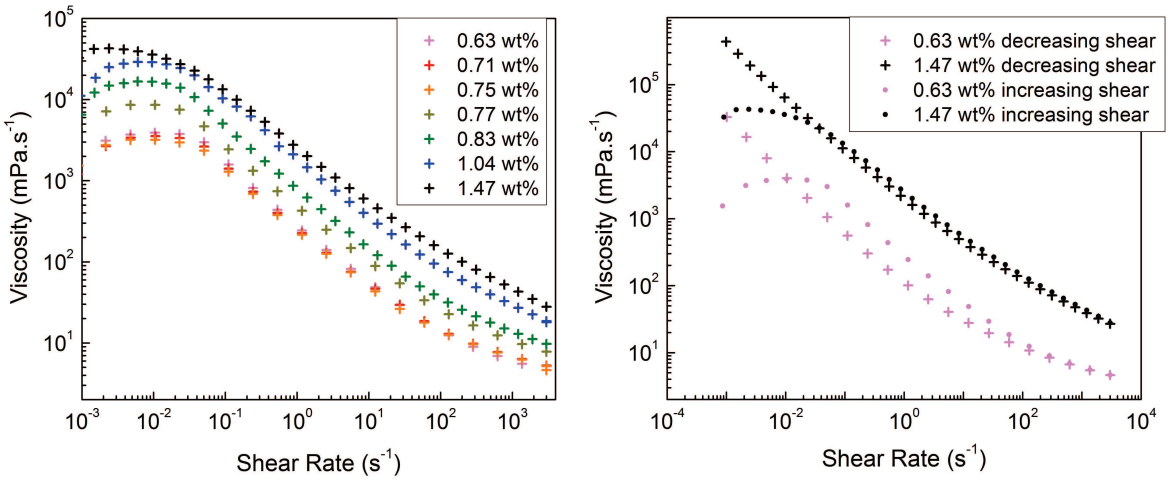

Fig. 3.13: Flow curves as a function of applied strain for PEDOT:PSTFSI dispersions with different solid contents from 0.64wt% to 1.47wt%

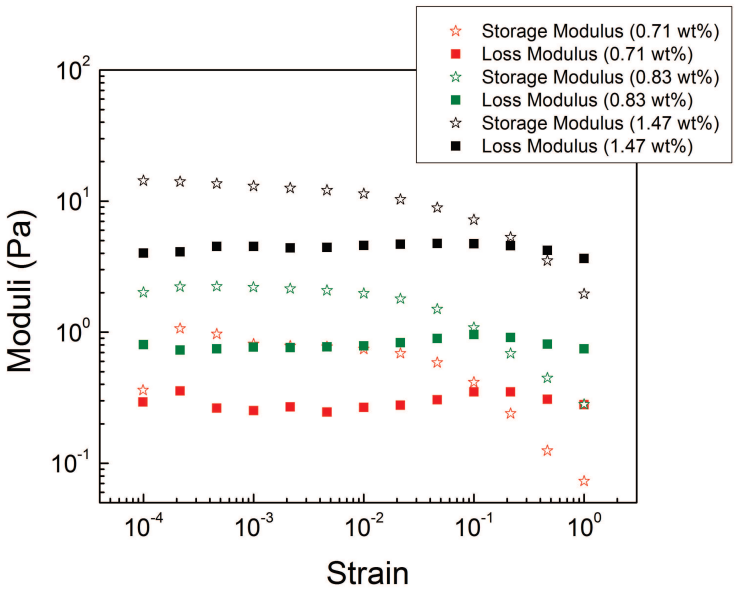

Fig. 3.14: Elastic moduli as a function of applied strain for PEDOT:PSTFSI dispersions with different solid contents from 0.64wt% to 1.47wt%

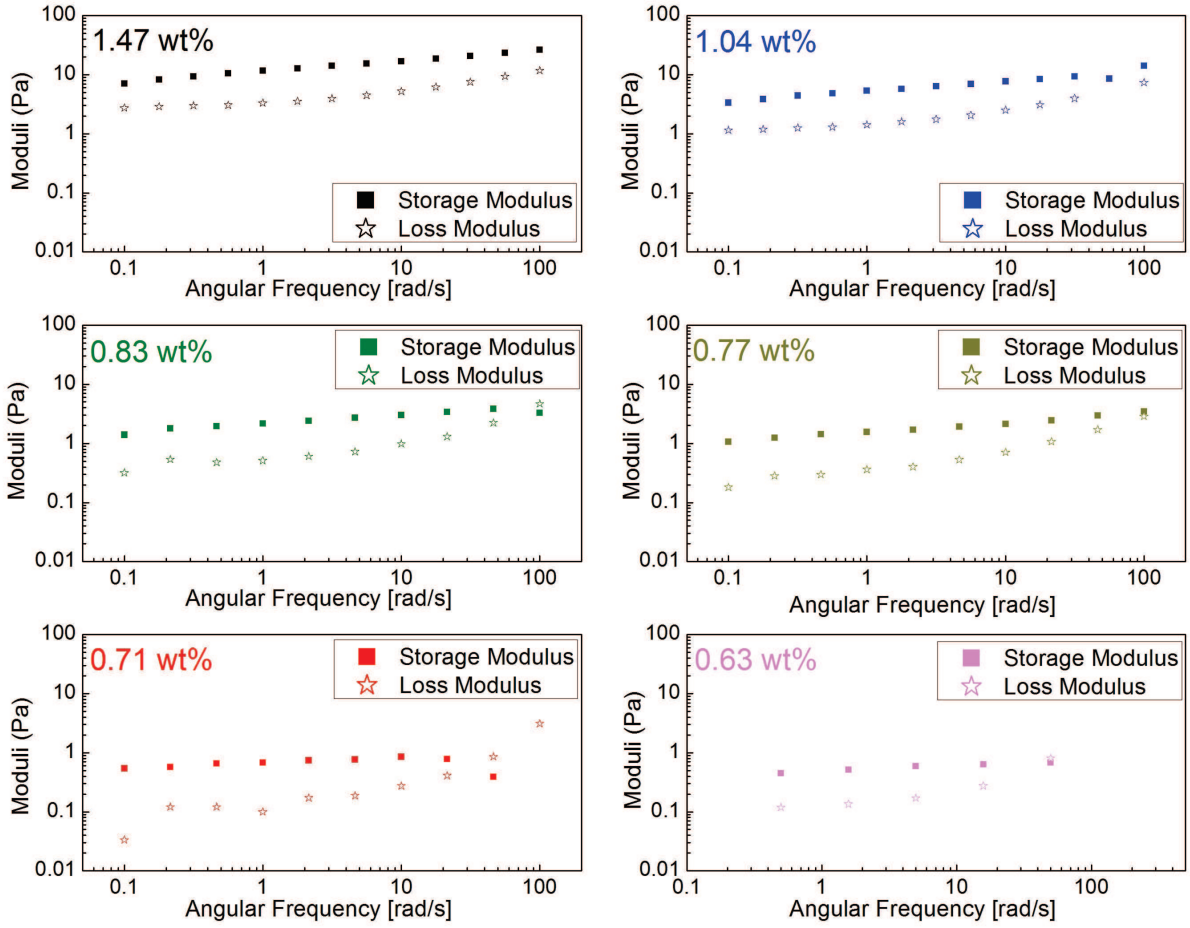

Fig. 3.15: Elastic moduli as a function of frequency for PEDOT:PSTFSI dispersions with different solid contents from 0.64wt% to 1.47wt%

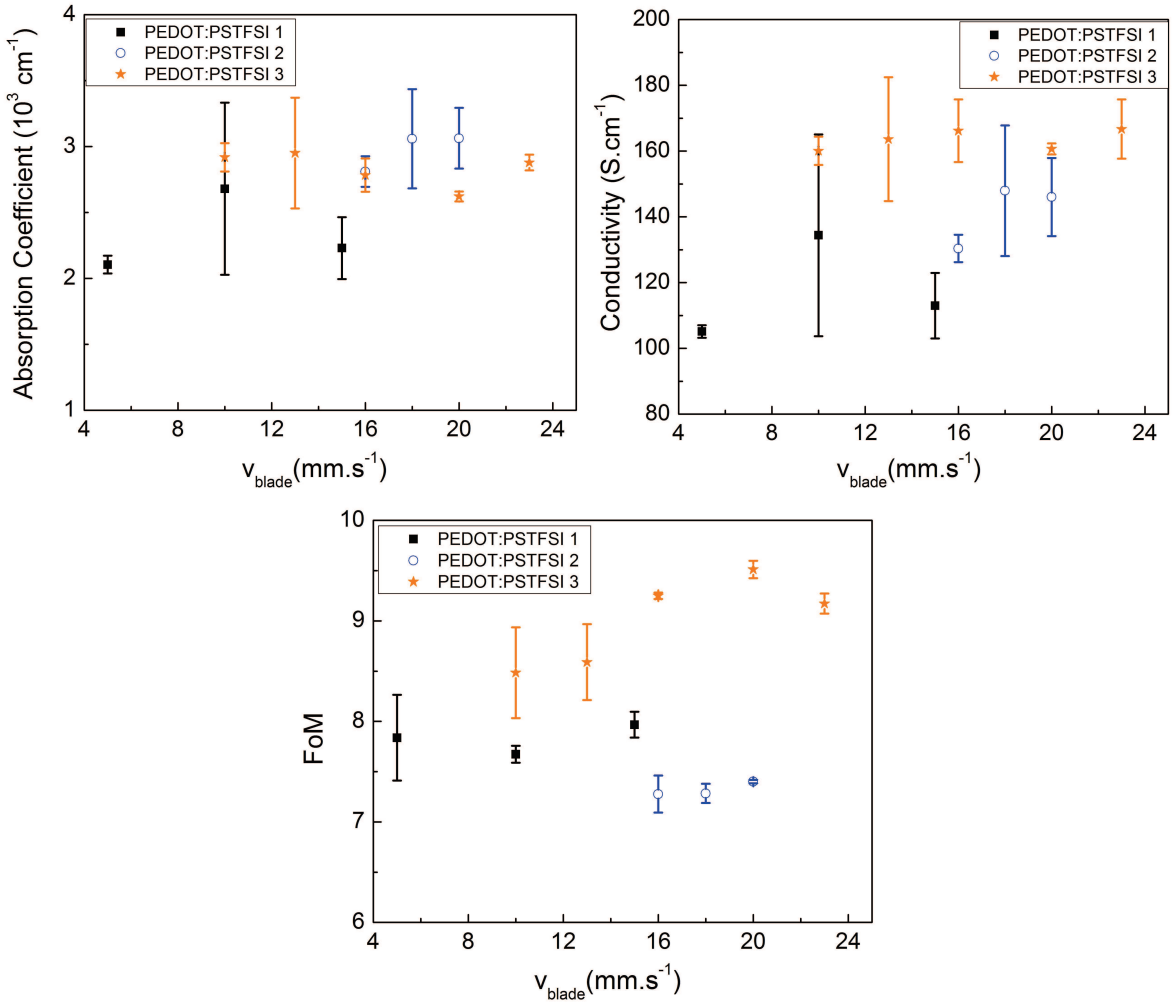

Fig. 3.16: Opto-electronic properties of PEDOT:PSTFSI films deposited by doctor blading at 70°C with different blade speeds

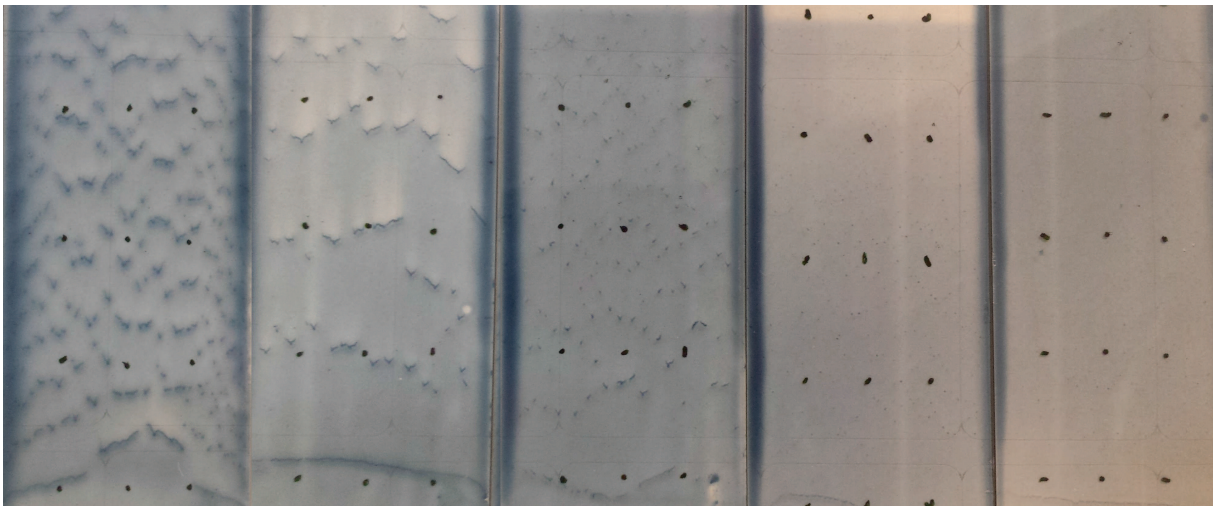

Fig. 3.17: PEDOT:PSTFSI films cast by doctor blading from a PEDOT rich dispersion with increasing blading speed from right to left

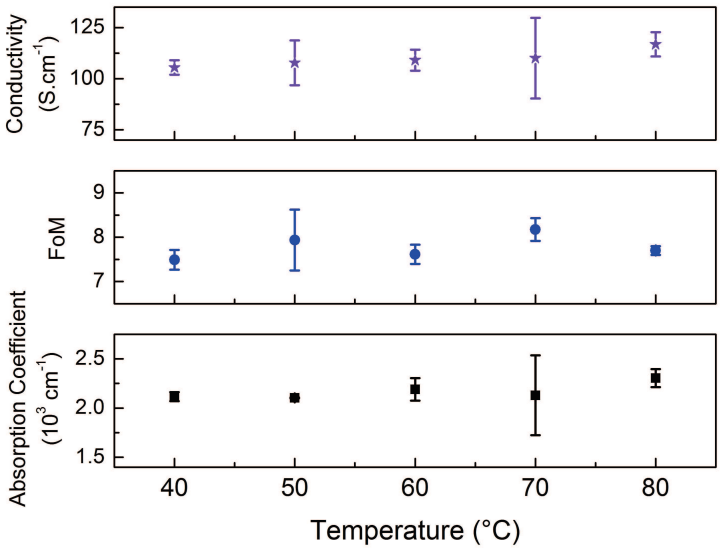

Fig. 3.18: Opto-electronic properties of PEDOT:PSTFSI films deposited by doctor blading at different temperatures with a constant blade speed of 10mm.s^{-1}

3.5 Conclusion

It has been demonstrated, that the opto-electronic properties of PEDOT:PSTFSI films can be drastically changed upon formulation of the PEDOT:PSTFSI dispersions. In analogy to the behavior of PEDOT:PSS, the addition of high boiling point solvents, such as DMSO, to the PEDOT:PSTFSI dispersions, results in an increase of the film conductivity of several orders of magnitude. This effect was attributed to changes in the film morphology, which facilitate the charge transport. Similar conductivities have been obtained upon admixing of certain salts or acids, such as LiTFSI or pTSA. In order to increase the transparency of PEDOT:PSTFSI films, supplementary PSTFSI can be admixed to PEDOT:PSTFSI. The addition of 50 to 100wt% PSTFSIK to PEDOT:PSTFSI allows the fabrication of thick conducting films with an extremely high transparency and an increased FoM.

Furthermore it has been shown, that PEDOT:PSTFSI dispersions with solid contents of about 0.8% can be easily processed by doctor blading at various blading speeds and temperatures without any impact on the opto-electronic properties of the resulting films. By changing the dispersion concentration, the viscosity of PEDOT:PSTFSI can be adjusted for the processing by other coating techniques, such as slot die coating or screen printing.

Bibliography

[1] J. Ouyang, Q. Xu, C.-W. Chu, Y. Yang, G. Li, and J. Shinar, "On the mechanism of conductivity enhancement in poly(3,4-ethylenedioxythiophene):poly(styrene sulfonate) film through solvent treatment," *Polymer*, vol. 45, pp. 8443–8450, Nov. 2004.

[2] Y. Xia and J. Ouyang, "PEDOT:PSS films with significantly enhanced conductivities induced by preferential solvation with cosolvents and their application in polymer photovoltaic cells," *Journal of Materials Chemistry*, vol. 21, no. 13, p. 4927, 2011.

[3] A. M. Nardes, R. A. J. Janssen, and M. Kemerink, "A Morphological Model for the Solvent-Enhanced Conductivity of PEDOT:PSS Thin Films," *Advanced Functional Materials*, vol. 18, pp. 865–871, Mar. 2008.

[4] J. Rivnay, S. Inal, B. A. Collins, M. Sessolo, E. Stavrinidou, X. Strakosas, C. Tassone, D. M. Delongchamp, and G. G. Malliaras, "Structural control of mixed ionic and electronic transport in conducting polymers," *Nature Communications*, vol. 7, p. 11287, Apr. 2016.

[5] H. Yan and H. Okuzaki, "Effect of solvent on PEDOT/PSS nanometer-scaled thin films: XPS and STEM/AFM studies," *Synthetic Metals*, vol. 159, pp. 2225–2228, Nov. 2009.

[6] S. Jönsson, J. Birgerson, X. Crispin, G. Greczynski, W. Osikowicz, A. Denier van der Gon, W. Salaneck, and M. Fahlman, "The effects of solvents on the morphology and sheet resistance in poly(3,4-ethylenedioxythiophene)–polystyrenesulfonic acid (PEDOT–PSS) films," *Synthetic Metals*, vol. 139, pp. 1–10, Aug. 2003.

[7] J. Zhou, D. H. Anjum, G. Lubineau, E. Q. Li, and S. T. Thoroddsen, "Unraveling the Order and Disorder in Poly(3,4-ethylenedioxythiophene)/Poly(styrenesulfonate) Nanofilms," *Macromolecules*, vol. 48, pp. 5688–5696, Aug. 2015.

[8] C. M. Palumbiny, F. Liu, T. P. Russell, A. Hexemer, C. Wang, and P. Müller-Buschbaum, "The Crystallization of PEDOT:PSS Polymeric Electrodes Probed In Situ during Printing," *Advanced Materials*, vol. 27, pp. 3391–3397, June 2015.

[9] C. M. Palumbiny, C. Heller, C. J. Schaffer, V. Körstgens, G. Santoro, S. V. Roth, and P. Müller-Buschbaum, "Molecular Reorientation and Structural Changes in Cosolvent-Treated Highly Conductive PEDOT:PSS Electrodes for Flexible Indium Tin Oxide-Free Organic Electronics," *The Journal of Physical Chemistry C*, vol. 118, pp. 13598–13606, June 2014.

[10] Q. Wei, M. Mukaida, Y. Naitoh, and T. Ishida, "Morphological Change and Mobility Enhancement in PEDOT:PSS by Adding Co-solvents," *Advanced Materials*, vol. 25, no. 20, pp. 2831–2836, 2013.

[11] L. A. A. Pettersson, S. Ghosh, and O. Inganäs, "Optical anisotropy in thin films of poly(3,4-ethylenedioxythiophene)–poly(4-styrenesulfonate)," *Organic Electronics*, vol. 3, pp. 143–148, Dec. 2002.

[12] X. Crispin, S. Marciniak, W. Osikowicz, G. Zotti, A. W. D. van der Gon, F. Louwet, M. Fahlman, L. Groenendaal, F. De Schryver, and W. R. Salaneck, "Conductivity, morphology, interfacial chemistry, and stability of poly(3,4-ethylene dioxythiophene)–poly(styrene sulfonate): A photoelectron spectroscopy study," *Journal of Polymer Science Part B: Polymer Physics*, vol. 41, pp. 2561–2583, Nov. 2003.

[13] Y. Xia and J. Ouyang, "Salt-Induced Charge Screening and Significant Conductivity Enhancement of Conducting Poly(3,4-ethylenedioxythiophene):Poly(styrenesulfonate)," *Macromolecules*, vol. 42, pp. 4141–4147, June 2009.

[14] Z. Yu, Y. Xia, D. Du, and J. Ouyang, "PEDOT:PSS Films with Metallic Conductivity through a Treatment with Common Organic Solutions of Organic Salts and Their Application as a Transparent Electrode of Polymer Solar Cells," *ACS Applied Materials & Interfaces*, vol. 8, pp. 11629–11638, May 2016.

[15] R. V. Rao and M. H. Shridhar, "Effect of P-toluene sulphonic acid on the dielectric properties of poly(4-vinylpyridine)," *Materials Science and Engineering: A*, vol. 325, pp. 73–78, Feb. 2002.

[16] M. Döbbelin, R. Marcilla, C. Tollan, J. A. Pomposo, J.-R. Sarasua, and D. Mecerreyes, "A new approach to hydrophobic and water-resistant poly(3,4-ethylenedioxythiophene):poly(styrenesulfonate) films using ionic liquids," *Journal of Materials Chemistry*, vol. 18, pp. 5354–5358, Nov. 2008.

[17] F. Louwet, L. Groenendaal, J. Dhaen, J. Manca, J. Van Luppen, E. Verdonck, and L. Leenders, "PEDOT/PSS: synthesis, characterization, properties and applications," *Synthetic Metals*, vol. 135-136, pp. 115–117, Apr. 2003.

[18] U. Bröckel, W. Meier, and G. Wagner, *Product design and engineering: formulation of gels and pastes*. John Wiley & Sons, 2013.

4 Stability of PEDOT:PSTFSI

In this chapter the chemical and colloidal stability of the PEDOT:PSTFSI dispersions was investigated. Using UV/Vis, Raman and XPS spectroscopy techniques, as well as rheological characterization the long term stability of the PEDOT:PSTFSI inks was confirmed. Furthermore, the stability of the PEDOT:PSTFSI films and their opto-electronic properties under ambient conditions, as well as at elevated temperatures up to 190°C was demonstrated.

L'utilisation de techniques de spectroscopie UV/Vis, Raman et XPS, ainsi que des analyses rhéologiques ont permis de mettre en évidence de bonnes stabilités chimique et colloïdale des encres de PEDOT:PSTFSI. De plus, les films de PEDOT:PSTFSI ont montré une bonne stabilité (conservation des caractéristiques opto-électroniques) sous atmosphère ambiante et à température élevée jusqu'à 190° C.

4.1 Introduction

For the integration of any new material in devices a good stability is crucial. Even if the quality of the encapsulation of the devices is more and more improved, the electrode material will be subjected to ageing processes due to chemical oxidation, humidity, irradiation or heat. Therefore the stability of the polymer under ambient conditions, this is the stability to chemical oxidation or humidity, is crucial. The thermal stability and degradation plays not only a role for the life time of the devices under harsh thermal conditions, such as for solar cells, which are naturally exposed to the heat of direct sunlight, but also for the processing, which might require annealing steps for other layers to which the potential electrode material has to withstand. In the case of conducting polymer inks, such as PEDOT:PSTFSI, also the colloidal stability of the dispersion is important to guarantee a long shelf life and unaltered rheological and opto-electronic properties over time. Therefore some fundamental aspects of the colloidal and chemical stability of the PEDOT:PSTFSI system have been investigated.

4.2 Stability Under Ambient Conditions

For the application and processing of PEDOT:PSTFSI in the lab scale, but especially for potential up-scaling, the colloidal and chemical stability of the polymer complex in dispersion is detrimental in order to ensure that for the same processing parameters the same film properties are obtained. For commercial PEDOT:PSS, such as Clevios PH1000 (Heraeus, Germany) the shelf life is given as nine month. Practical experience in the lab shows that commercial PEDOT:PSS dispersions were used for about two years without a change in the processing or opto-electronic properties.

Table 4.1 displays the opto-electronic properties of different PEDOT:PSTFSI samples, measured on films, which were cast directly after the synthesis, and on films, which were cast from the aged dispersion three to eleven months after the synthesis. For all dispersions the opto-electronic properties stayed unchanged over time.

In order to investigate possible changes in doping, UV/Vis and Raman spectroscopy of the freshly synthesized inks and from the aged inks were recorded. From figure 4.1 it can be seen that the absorption of PEDOT:PSTFSI dispersions did not change over time, independently of the initial shape of the spectra and doping. Therefore it can be

Sample	Day after Synthesis	Conductivity[a,b] (S.cm^{-1})	Absorption Coefficient[a] (cm^{-1})
1	2	140 ± 12	3.0±0.4
	96	140 ± 10	3.0±0.3
2	2	93 ± 9	2.2±0.2
	111	128 ± 13	2.2±0.2
3	30	263 ± 27	3.1±0.6
	189	260 ± 26	2.5±0.5
4	2	229 ± 18	1.8±0.6
	344	211 ± 20	2.0±0.5

[a] average on 8 measurements or more [b] determined by 4-point measurements

Tab. 4.1: Opto-electronic properties of PEDOT:PSTFSI films cast directly after synthesis of the inks and after several months

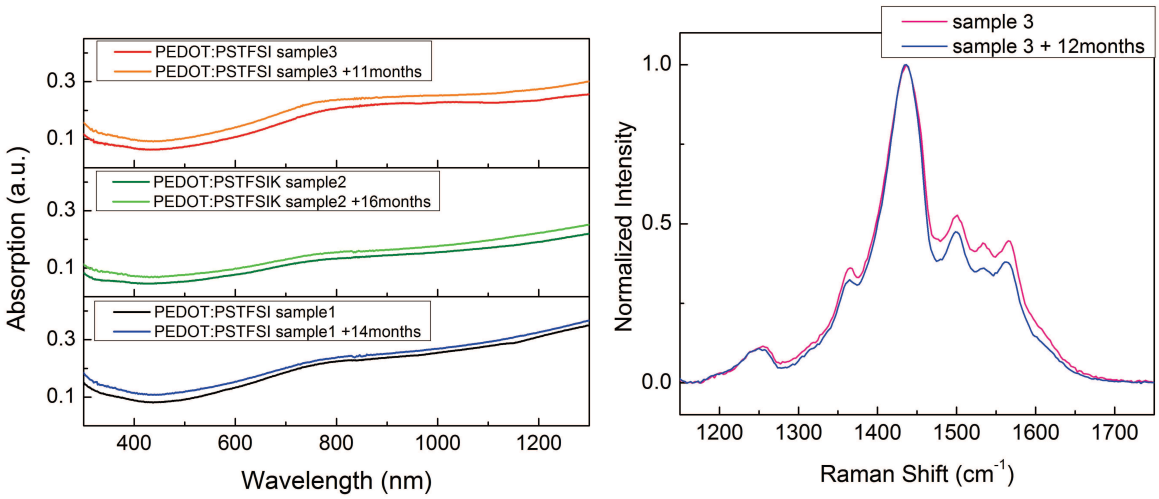

Fig. 4.1: UV/Vis spectra (left) and Raman spectra (right) of PEDOT:PSTFSI dispersions directly after synthesis and several month later, with sample 1: EDOT/STFSIK 0.6, M_W(PSTFSIK)=100kDa, 500rpm at 10°C, σ=103S.cm^{-1}, sample 2: EDOT/STFSIK 0.48, M_W(PSTFSIK)=350kDa, 55rpm at 10°C, σ=31S.cm^{-1} and sample 3: EDOT/STFSIK 0.6, M_W(PSTFSIK)=350kDa, 625rpm at 10°C, σ=205S.cm^{-1}

assumed that the doping of PEDOT:PSTFSI is not affected by aging phenomena within 16 months. This was confirmed by the recorded Raman spectra, which showed only little deviations that were attributed to differences in the background subtraction.

It is known from literature, that changes in the chemical structure of PEDOT:PSS, which are caused by degradation reactions, can be characterized by XPS [1, 2]. The photo-oxidation of PEDOT, for instance, leads to the appearance of an new contribution in the sulfur S2p spectrum of PEDOT which can be attributed to the formation of sulfone groups, whereas the formation of carboxyl groups due to chain scission reactions results in changes of the carbon C1s spectrum [1, 2]. Figure 4.2 displays the C1s, S2p, N1s, and

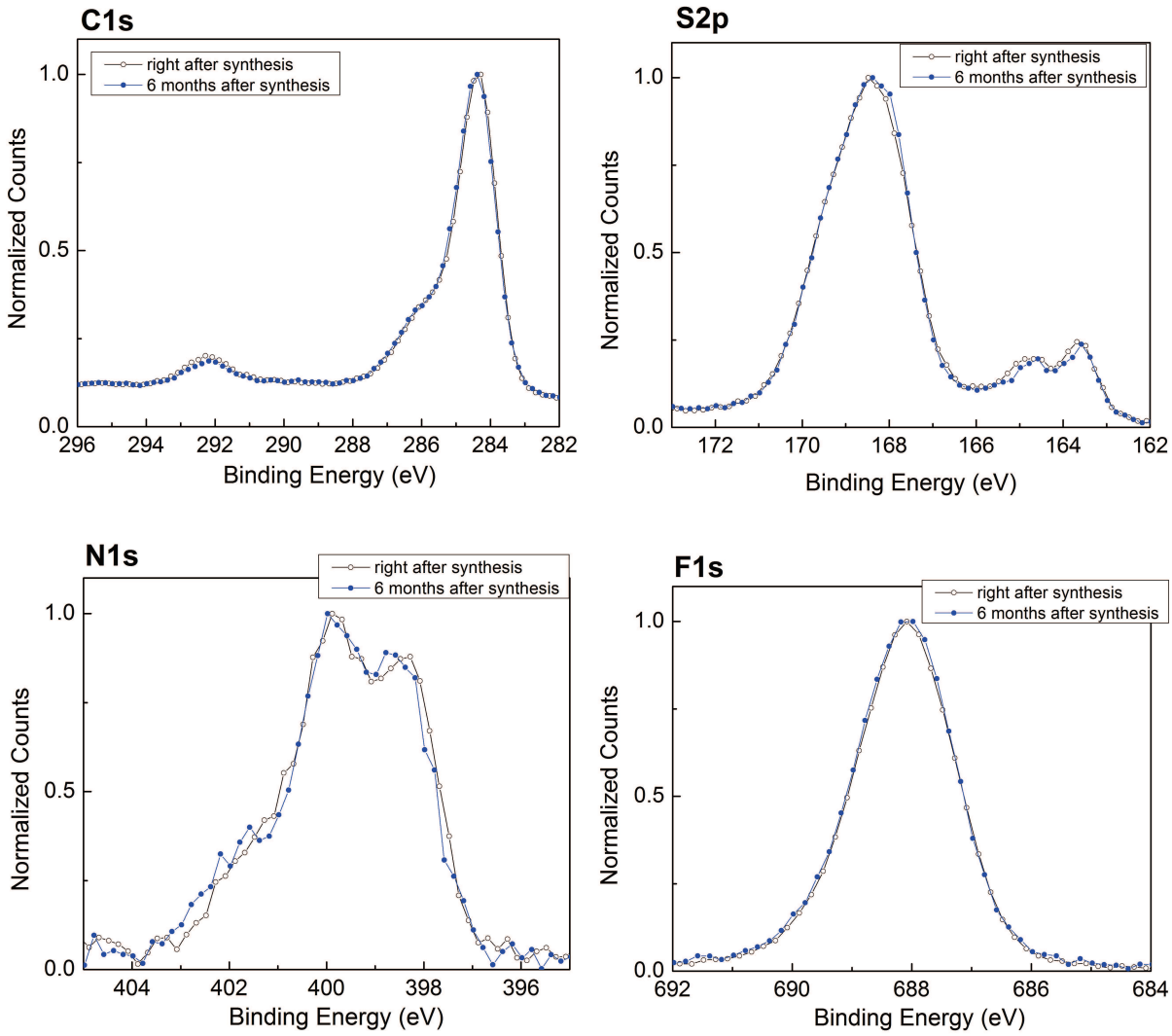

Fig. 4.2: XPS C1s, S2p, N1s and F1s spectra of a new and an aged PEDOT:PSTFSI system

F1s XPS spectra of a PEDOT:PSTFSI film, which was cast directly after synthesis, and the spectra of a film cast from the same PEDOT:PSTFSI ink, which has been stored under ambient conditions in a brown tinted glass vial for six months. The carbon, sulfur, nitrogen and fluorine spectra are identical for both samples, which indicates that the chemical structure of the PEDOT:PSTFSI complex was unchanged. Therefore we can state that the PEDOT:PSTFSI dispersion is chemically stable for at least six months under ambient conditions and when protected against UV light.

In order to study the colloidal stability of PEDOT:PSTFSI, comparative rheology measurements on a PEDOT:PSTFSI dispersion shortly after synthesis and several months later have been performed. For PEDOT:PSTFSI dispersions with a viscoelastic behavior

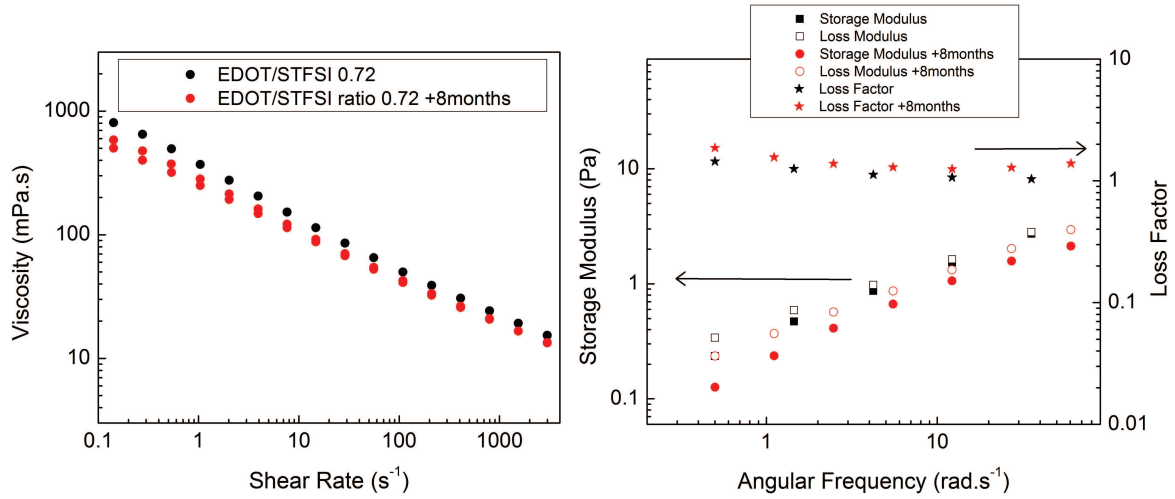

Fig. 4.3: Flow curve (left) and storage modulus, loss modulus and loss factor of PEDOT:PSTFSI (EDOT to STFSI ratio 0.72, stirring 55rpm) shortly after synthesis and 8 months later

close to the gel point ($tan\delta = \frac{G''}{G'} \approx 1$), a slight decrease in viscosity and a small increase of the loss factor $tan\delta$, related to a decreasing storage modulus G', was observed after several months of aging (see figure 4.3). This signifies a reduction of the internal structure of the dispersion, which is coherent with moderate colloidal interactions. However, the observed changes were marginal and the dispersions can be considered as stable. Even less change in the rheological properties was observed for PEDOT:PSTFSI systems with pronounced gel character, obtained *e.g.* via better dispersion of the EDOT monomer or in PEDOT:PSTFSIH, which retained their gel character for more than one year after the synthesis.

The excellent stability was confirmed by the analysis of PEDOT:PSTFSI using a turbiscan, which allowed the monitoring of the sample transmittance over the whole sample length at 30°C for four weeks. The measured change in transmittance (see figure C.1, appendix page 227) was marginal and constant throughout the sample, except for a higher increase of transmittance close to the meniscus of the sample. This indicates a slight increase of the particle size in the dispersion and an insignificant clarification close to the sample meniscus over time. However, these changes are negligible and the dispersion can be considered as stable.

In order to investigate the stability of PEDOT:PSTFSI conducting films, which were stored under ambient conditions at room temperature and protected from sun light, the

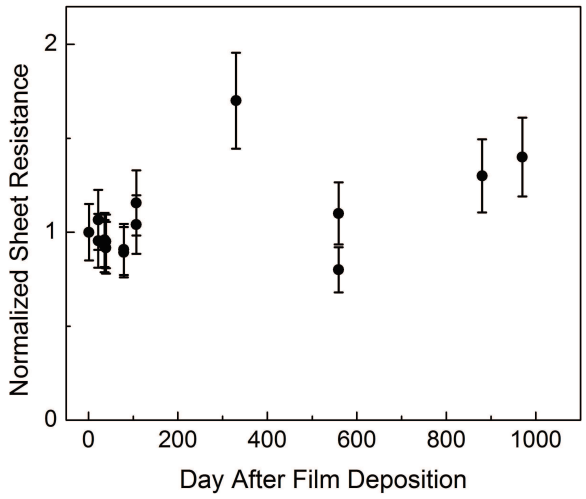

Fig. 4.4: Development in time of the sheet resistance of two PEDOT:PSTFSI films

sheet resistance of several films was monitored for more than two years. From Figure 4.4 it can be seen, that the measured sheet resistance was stable for about 3 years within the error bars of the measurement. Interestingly, the tendencies of the fluctuations of the measured sheet resistance were the same for different samples and films, which indicates that the influence of the measurement conditions such as the ambient temperature and humidity was not negligible.

To summarize, PEDOT:PSTFSI dispersions have been shown to be stable for about one year, when stored under ambient conditions and protected from sun light. Dry PEDOT:PSTFSI films, stored under ambient conditions at room temperature and protected from sun light, were demonstrated to retain their conductivity for approximately three years.

4.3 Thermal Stability

As mentioned earlier, the thermal stability of PEDOT:PSTFSI is not only of interest to ensure a long life time of the electrode once the material is integrated in devices, but also for the device processing, during which the electrode can be subjected to high temperatures due to the processing of other layers of the device.

Thermal gravimetric analysis shows that PEDOT:PSTFSI is stable up to 200 °C under

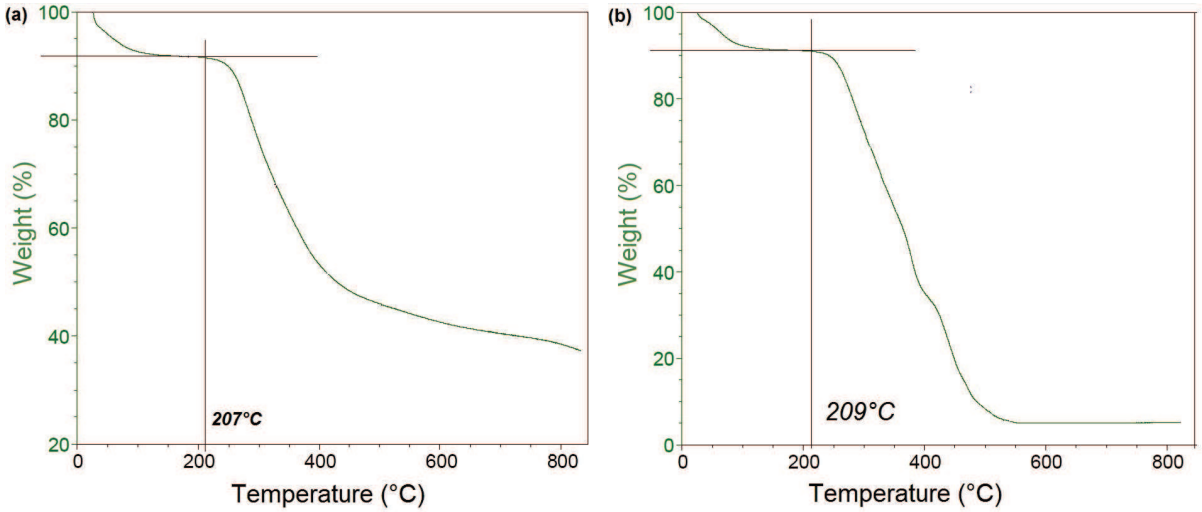

Fig. 4.5: Thermo-gravimetric analysis of PEDOT:PSTFSI under a)N_2 and b)in air

nitrogen atmosphere and in air (see figure 4.5). Similar values have been reported for PEDOT:PSS in literature [3, 4].

The measurement of the sheet resistance of PEDOT:PSTFSI films a function of the annealing temperature showed, that the electronic properties of the PEDOT:PSTFSI films were unaffected up to 130°C and dropped significantly only upon degradation of the polymer at temperatures higher than 200°C (see figure 4.6).

In the case of PEDOT:PSS it has been reported, that the films can be annealed at up to 100°C for up to 1000h with no change in conductivity [5] and that for annealing at 120°C the conductivity of PEDOT:PSS decreases with annealing time [6]. For PEDOT:PSTFSI films annealed at 120°C for 340h, no change in the sheet resistance was observed over time.

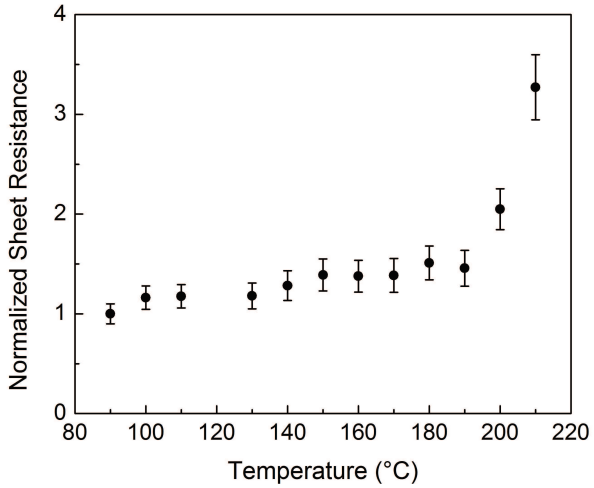

Fig. 4.6: Normalized sheet resistance of PEDOT:PSTFSI, averaged over three samples, as a function of the annealing temperature

4.4 Conclusion

In summary, it was shown that PEDOT:PSTFSI dispersions are stable for more than one year with unchanged rheological, chemical and opto-electronic properties. Thermal analysis proved that PEDOT:PSTFSI is stable up to 200°C and shows stable conductivities up to annealing temperatures of 190 °C and is therefore a promising candidate for the application in printed organic electronics.

Bibliography

[1] X. Crispin, S. Marciniak, W. Osikowicz, G. Zotti, A. W. D. van der Gon, F. Louwet, M. Fahlman, L. Groenendaal, F. De Schryver, and W. R. Salaneck, "Conductivity, morphology, interfacial chemistry, and stability of poly(3,4-ethylene dioxythiophene)–poly(styrene sulfonate): A photoelectron spectroscopy study," *Journal of Polymer Science Part B: Polymer Physics*, vol. 41, pp. 2561–2583, Nov. 2003.

[2] S. Marciniak, X. Crispin, K. Uvdal, M. Trzcinski, J. Birgerson, L. Groenendaal, F. Louwet, and W. Salaneck, "Light induced damage in poly(3,4-ethylenedioxythiophene) and its derivatives studied by photoelectron spectroscopy," *Synthetic Metals*, vol. 141, pp. 67–73, Mar. 2004.

[3] A. Nardes, M. Kemerink, M. de Kok, E. Vinken, K. Maturova, and R. Janssen, "Conductivity, work function, and environmental stability of PEDOT:PSS thin films treated with sorbitol," *Organic Electronics*, vol. 9, pp. 727–734, Oct. 2008.

[4] J. Y. Kim, J. H. Jung, D. E. Lee, and J. Joo, "Enhancement of electrical conductivity of poly(3,4-ethylenedioxythiophene)/poly(4-styrenesulfonate) by a change of solvents," *Synthetic Metals*, vol. 126, pp. 311–316, Feb. 2002.

[5] L. Groenendaal, F. Jonas, D. Freitag, H. Pielartzik, and J. R. Reynolds, "Poly(3,4-ethylenedioxythiophene) and Its Derivatives: Past, Present, and Future," *Advanced Materials*, vol. 12, pp. 481–494, Apr. 2000.

[6] E. Vitoratos, S. Sakkopoulos, E. Dalas, N. Paliatsas, D. Karageorgopoulos, F. Petraki, S. Kennou, and S. A. Choulis, "Thermal degradation mechanisms of PEDOT:PSS," *Organic Electronics*, vol. 10, pp. 61–66, Feb. 2009.

5 Application of PEDOT:PSTFSI Electrodes in Devices

L'utilisation de techniques de spectroscopie UV/Vis, Raman et XPS, ainsi que des analyses rhéologiques ont permis de mettre en évidence de bonnes stabilités chimique et colloïdale des encres de PEDOT:PSTFSI. De plus, les films de PEDOT:PSTFSI ont montré une bonne stabilité (conservation des caractéristiques opto-électroniques) sous atmosphère ambiante et à température élevée jusqu'à 190°C.

Des films de PEDOT:PSTFSI ont été intégrés avec succès en tant qu'électrodes transparentes dans des dispositifs électroniques comme des cellules solaires organiques et des diodes électroluminescentes organiques montrant des performances égales ou supérieures à celles des dispositifs de référence disposant d'une électrode en PEDOT:PSS ou en ITO dans le cas des dispositifs flexibles. Enfin, des électrodes de PEDOT:PSTFSI ont montré de bons résultats dans des transistors électrochimiques organiques lorsqu'ils étaient utilisés comme conducteurs ambivalents de trous et d'ions.

5.1 Transparent Electrodes in OLEDs and OPVs

Electronic devices become more and more present in almost every aspect of our daily lives, such as entertainment, communication, energy supply and health. However, questions about the environmental impact, costs and sustainability have been raised regarding the production processes and the raw materials used for these electronic devices. The development of organic electronics might not only be a way for a more cost efficient and eco-friendly production of electronic devices on a large scale, but allows also the design of flexible and light weight devices. Since their development in the 1980s organic electronic light emitting diodes (OLEDs) have attracted a great deal of attention and OLED displays and lighting systems have recently been commercialized. Organic photovoltaics are less widely used, mainly due to their limited stability and power conversion efficiencies. However, OPVs show a big potential for applications where traditional solar panels can not be used because of their weight, brittleness and high production costs. A crucial component of OLEDs and OPVs devices is the transparent electrode. Due to its good opto-electronic properties, but also due to the lack of alternatives, the most used material for flexible and printable transparent electrodes is the conducting polymer PEDOT:PSS. However, PEDOT:PSS is known to be acidic and hygroscopic, which affects the device stability. Therefore, new conducting polymers such as PEDOT:PSTFSI are of interest for the application as transparent electrode in order to further improve device performance and stability.

In order to evaluate the potential of PEDOT:PSTFSI for transparent electrodes, OLED and OPV devices with PEDOT:PSTFSI electrodes were fabricated and compared to devices with benchmark PEDOT:PSS and ITO electrodes. This work was done in collaboration with the Fraunhofer Institute for Organic Electronics in Dresden, Germany.

The average opto-electronic properties of the PEDOT:PSTFSI, PEDOT:PSS and ITO electrode materials are displayed in table 5.1.

Figure 5.1 displays the structure of a monochrome orange OLED stack, of an organic solar cell device, both fabricated with either PEDOT:PSTFSI or ITO electrodes, and of a 3-color-white OLED stack, fabricated with either PEDOT:PSTFSI or PEDOT:PSS electrodes. The details of the device fabrication are given in the experimental section page 209.

Electrode	Sheet Resistance[a] (Ohm.sq^{-1})	Transmittance (%)	FoM[b]
PEDOT:PSTFSI	90-180	70-85	11.5±2.5
PEDOT:PSS	32-80	70-85	30±1
ITO	12	>95	>600

[a] determined by 4-point measurements [b] average value on 10 films or more

Tab. 5.1: Sheet resistance, transmittance and FoM of PEDOT:PSTFSI, commercial PEDOT:PSS (Clevios PH1000) and ITO electrode materials

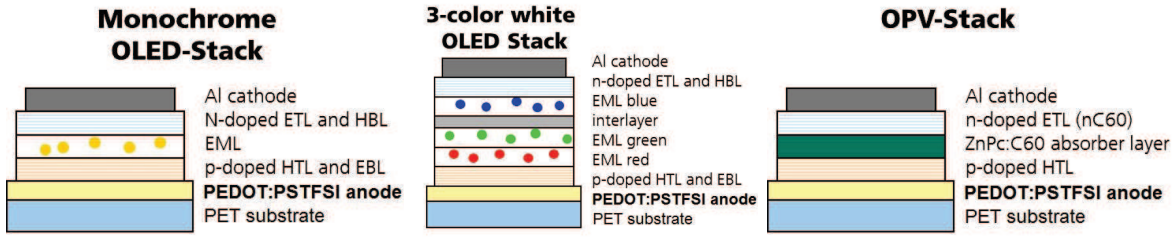

Fig. 5.1: Structure of orange monochrome and 3-color-white OLED stacks and the organic solar cell device. ETL: electron transporting layer, HTL: hole transport layer, EBL: electron blocking layer, HBL: hole blocking layer, EML: emitting layer

For the characterization of the OLEDs the current density J and the luminance L were recorded as a function of the applied voltage V. From the resulting L-I-V curves the current efficiency γ (defined as the ratio of the luminance L to the current density J), the power efficiency η (defined as the ratio of the luminous flux output to the corresponding electrical power $\eta = \frac{\pi \times L}{J \times V}$) and the leakage current $J_{leakage}$ were determined and served as key parameters for the evaluation of the device performance.

Figure 5.2 displays a picture of a white OLED stack with a PEDOT:PSS electrode and a white OLED stack with a PEDOT:PSTFSI electrode. For both electrode materials the devices seem homogeneous and no difference can be seen by inspection under the optical microscope. Typical L-I-V curves of the white OLEDs are shown in figure 5.3 and the key characteristics are summarized in table 5.2. From the L-I-V curves it can be seen that for both types of electrodes the turn on voltage of the devices was at about 2V. In order to reach the same luminance, the devices with PEDOT:PSTFSI electrodes required a slightly higher voltage than the devices with PEDOT:PSS electrodes. However, the current density J in devices with PEDOT:PSTFSI was considerably lower, which resulted in a higher current efficiency of γ=39.49cd.A^{-1} (γ=36.06cd.A^{-1} for PEDOT:PSS electrodes) and a higher power efficiency η=25.24lm.W^{-1} (η=24.28lm.W^{-1} for PEDOT:PSS electrodes). In addition,

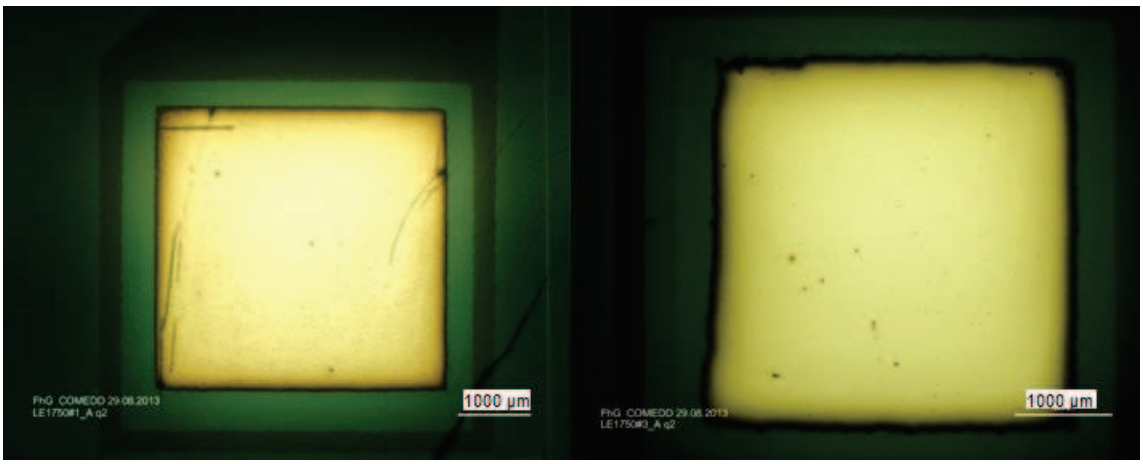

Fig. 5.2: White OLEDs with PEDOT:PSS electrode (left) and PEDOT:PSTFSI electrode (right)

Electrode	Voltage (V)	Current Density ($mA.cm^{-2}$)	Current Efficiency[a] ($cd.A^{-1}$)	Power Efficiency[a,b] ($lm.W^{-1}$)	Leakage Current[a] ($mA.cm^{-2}$)
PEDOT:PSS	4.67	2.81	36.06±3.89	24.28±2.69	0.24
PEDOT:PSTFSI	4.92	2.53	39.49±5.18	25.24±5.07	0.01

[a] average over 6 devices [b] calculated from forward direction, assuming lambertian emission

Tab. 5.2: Key characteristics of 3-color-white OLED stacks with PEDOT:PSS and PEDOT:PSTFSI electrodes at 1000cd.m^{-2} luminance

the leakage current in PEDOT:PSTFSI devices was more than one order of magnitude lower than in the PEDOT:PSS reference devices, which is an indicator for less defects and better device stability.

For orange OLED stacks with PEDOT:PSTFSI an average current efficiency of γ=(11.57 ± 1.09)$cd.A^{-1}$ and an average power efficiency of η=(13.95 ± 1.54)$lm.W^{-1}$ were obtained, which were slightly lower than the efficiencies of the ITO bench mark devices (γ=(15.08 ± 6.52)$cd.A^{-1}$, η=(16.97 lm.W± 8.36)$lm.W^{-1}$). However, the reproducibility was far higher for the purely organic devices, as it can be seen from the much lower standard deviations. This is affirmed by the high yield of functional devices (39/40) for the OLED series with PEDOT:PSTFSI electrodes (8/8 for ITO electrodes). Bending tests confirmed the superiority in terms of flexibility of the all organic orange OLED devices, which showed stable performance down to a bending radius of 10mm, whereas the performance of the ITO benchmark devices decreased starting from a bending radius of 40nm (see figure 5.4).

For the characterization of the OPV device a voltage sweep was applied and the current response of the solar cell was measured. To define the performance of a solar cell four key parameters are used, namely the open circuit voltage V_{OC}, the short circuit current I_{SC},

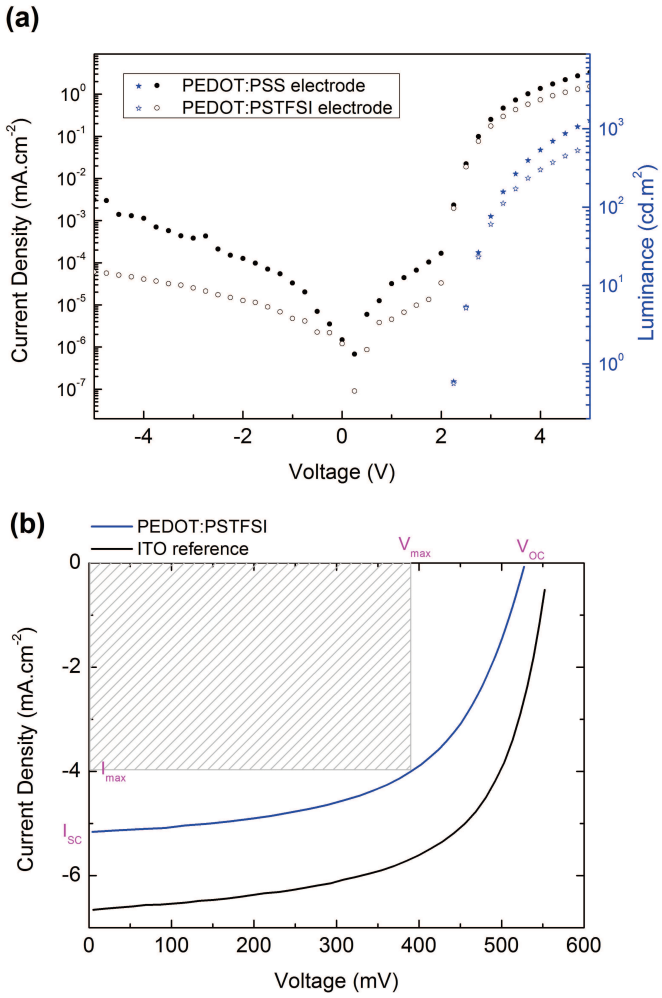

Fig. 5.3: a)LIV characteristics of 3-color-white OLED stacks with PEDOT:PSTFSI and PEDOT:PSS electrodes and b)IV characteristics of organic solar cells with PEDOT:PSTFSI and ITO electrodes

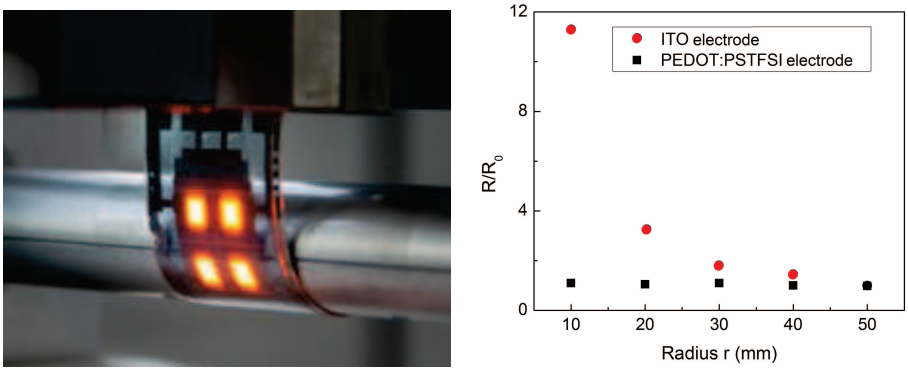

Fig. 5.4: Picture of an orange OLED stack undergoing a bending test (left) and the change in sheet resistance R with respect to the initial sheet resistenace R_0 due to bending as a function of the bending radius r for orange OLEDs with PEDOT:PSTFSI and ITO electrodes on PET substrates

Electrode	V_{OC} (mV)	I_{SC} (mA.cm^{-2})	FF (%)	PCE (%)
PEDOT:PSTFSI	531[a]	5.8[a]	57.74[a]	1.76[a]
ITO	542[b]	7.3[b]	50.94[b]	2.6[b]

[a] average over 36 devices [b] average over 8 devices

Tab. 5.3: Characteristics of OPV devices with PEDOT:PSTFSI and ITO electrodes

the fill factor (FF) and the power conversion efficiency (PCE). The fill factor is related to the maximum power of the cell and defined as:

$$FF = \frac{I_{max}V_{max}}{I_{SC}V_{OC}} \tag{5.1}$$

whereas the PCE is defined as the ratio of the generated electricity over the power of the incoming irradiation:

$$PCE = \frac{I_{SC}V_{OC}FF}{P_{light}} \tag{5.2}$$

Figure 5.3 shows typical IV curves recorded for a device with a PEDOT:PSTFSIK electrode (blue line) in comparison to an ITO reference device (black line) and the key parameters are summarized in table 5.3. The difference in V_{OC} is small (5%). However, the devices made with PEDOT:PSTFSI electrodes show a 20% lower I_{SC} with respect to the reference cells. The fill factor is considerably higher for solar cells with PEDOT:PSTFSI electrode, which could be an indicator for lower series or shunt resistance in the devices. The PCE, however, is significantly lower than for the ITO reference devices. This can be related to the lower transparency of the PEDOT:PSTFSI electrode in the visible regime compared to ITO. As in the case of OLED devices the yield of functional devices for PEDOT:PSTFSI electrodes is very high (86.1%), especially in comparison to the low yield with ITO electrodes (25%).

One of the critical parameters for organic electronics is their limited life time due to intrinsic degradation and insufficient encapsulation [1, 2, 3, 4, 5]. As the main objective of this collaboration was a first evaluation of the new material PEDOT:PSTFSI as transparent electrode, systematic stability test have not been performed. However, testing of the orange OLED devices after three years revealed a high degree of degradation. The residual emission of the devices was not strong enough for proper characterization (see figure 5.5). Taking into account the quality of the encapsulation

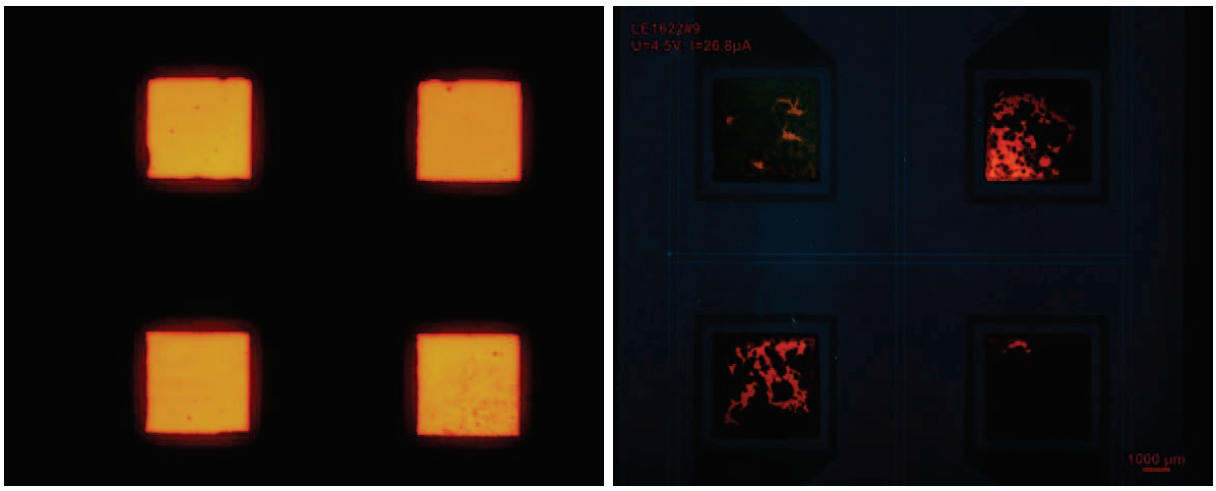

Fig. 5.5: Yellow OLED devices measured directly after fabrication (left) and three years after fabrication (right)

and the fact that the devices were stored under ambient conditions, the main cause of degradation can be attributed to diffusion of oxygen and humidity into the device.

In summary, PEDOT:PSTFSI was succefully integrated as transparent electrode in OLED and OPV devices. In 3-color-white OLED devices PEDOT:PSTFSI electrodes slightly outperformed PEDOT:PSS electrodes. Compared to ITO reference devices monochrome orange OLEDs with PEDOT:PSTFSI electrodes showed about 20% lower efficiencies. Organic solar cells with PEDOT:PSTFSI electrodes showed a higher fill factor than the ITO reference devices, but a considerably lower power conversion efficiency, which could be explained by higher absorption of PEDOT:PSTFSI in the visible. The key advantages of the PEDOT:PSTFSI electrodes were a low leakage current in OLED devices and very high reproducibility for all types of devices. This indicates that PEDOT:PSTFSI films were very homogeneous with few defects. Therefore we can state that PEDOT:PSTFSI is a promising material for transparent electrodes, which competes with PEDOT:PSS electrodes, especially for OLED applications.

5.2 Mixed Electron Ion Conductor in OECTs

Conducting polymers are important materials for the development of new biomedical devices for smart drug delivery or sensing [6, 7, 8, 9, 10]. PEDOT:PSS has been widely used for such applications, due to its flexibility, its biocompatibility and its hole and ion

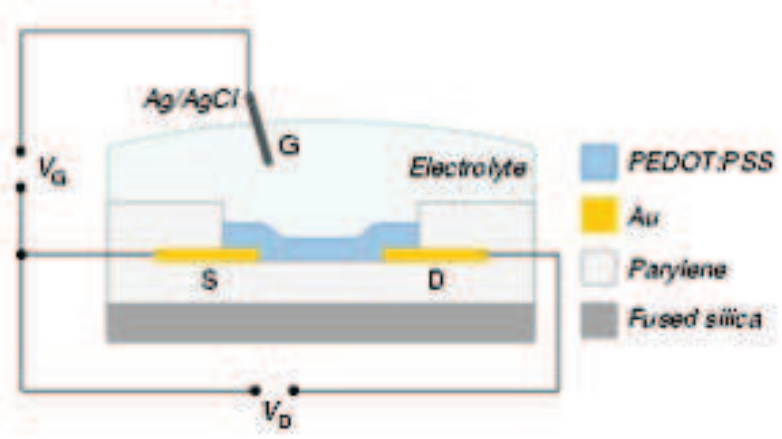

Fig. 5.6: Scheme of an OECT [15]

conducting properties . One of the bio-electronic devices, which lately has attracted a lot of attention for *in vitro* and *in vivo* diagnostics and electrophysiological recordings, is the organic electrochemical transistor (OECT) [8, 10, 11, 12, 13]. OECTs are ion to electron transducers, which rely on active channel materials, which combine ionic and electronic conductivity, such as PEDOT:PSS [10, 14]. The mixed conductivity of the PEDOT:PSS originates from the hole conducting properties of PEDOT and the PSS polyelectrolyte phase, which provides channels for ion migration. Figure 5.6 displays the schematic structure of an OECT device fabricated with PEDOT:PSS. The PEDOT:PSS film is deposited between the source and the drain electrode and is in direct contact with the electrolyte solution, into which the gate electrode is immersed. Upon application of a positive gate voltage, the cations of the electrolyte solution are injected into the PEDOT:PSS layer. This results in a decrease of the hole density of the PEDOT, leading to a drastic decrease of its conductivity and of the drain current in the device. The de-doping process is fully reversible once the gate voltage is switched off.

For this work the PEDOT:PSTFSI, synthesized with PSTFSILi and PSTFSIK salt (M_W(PSTFSI)= 100kDa or 250kDa), and PEDOT:PMaTFSI (M_W(PMaTFSI)= 80kDa) were tested as active material in OECT devices and compared to a reference device fabricated with PEDOT:PSS (structure and properties of PEDOT:PSTFSI and PEDOT:PMaTFSI see chapter 6, page 179). For the characterization of the OECT devices the drain current I_D was measured upon application of a series of drain voltage V_D and gate voltage V_G sweeps. In order to define the performance of an OECT, two key parameters were used. First, the transconductance g_m, which is defined as the

polyelectrolyte	g_m (mS)	τ (μs)	σ ($S.cm^{-1}$)	Swelling (%)
PSS	3.51 ± 0.17	49 ± 24	270	160
PSTFSI K 20kDa	3.05 ± 0.16	45 ± 5	45	90
PSTFSI K 250kDa	2.58 ± 0.21	34 ± 4	95	60
PSTFSI Li 100kDa	3.41 ± 0.32	90 ± 25	40	110
PMaTFSI Li 80kDa	1.65 ± 0.23	178 ± 3	8	50

Tab. 5.4: Transconductance g_m and response time τ of OECTs with different PEDOT:polyelectrolyte active layers and hole conductivity σ and swelling of the different PEDOT:polyelectrolyte systems

change of the drain current as response to changes in the gate voltage ($g_m = \partial I_D/\partial V_G$) and which is obtained from the $I_D - V_G$ transfer curve. A high transconductance at low gate voltages is important for the design of highly sensitive devices. Second, the response time τ, which characterizes the switching speed of the drain current upon the application of a pulsed gate bias and which was determined by fitting the exponential decay of the drain current over time upon application of a gate bias. As expected, the obtained characteristics of OECTs fabricated with PEDOT:polyelectrolytes correspond to the behavior of OECTs operating in the depletion mode, in which the drain current decreases as a result of the application of a positive gate voltage. Figure 5.7 displays the I_D-V_D curve, the I_D-V_G transfer characteristics, the transconductance (V_D=-0.8V) and the temporal response of the drain current of an OECT with PEDOT:PSS as active material and of an OECT with PEDOT:PSTFSI (M_W(PSTFSI)=100kDa) as active material. The transconductance and time response values obtained for all devices with different PEDOT:polyelectrolytes are summarized in table 5.4.

By far the poorest performance was obtained for PEDOT:PMaTFSI, which was the least conducting material (σ=8S.cm^{-1}) and showed the lowest degree of swelling, a low transconductance of 1.65mS and a long response time of 178μs. Among the PEDOT:PSTFSI materials the best characteristics were obtained for PEDOT:PSTFSI with M_W(PSTFSI Li)= 100kDa, which showed a transconductance of 3.41mS and a response time of 90μs. These values are close to the characteristics obtained for state-of-the-art OECTs [14]. The other PEDOT:PSTFSI systems showed similar performances, which were only slightly inferior to the performance of PEDOT:PSS in terms of response time and transconductance, indicating that the PEDOT:PSTFSI

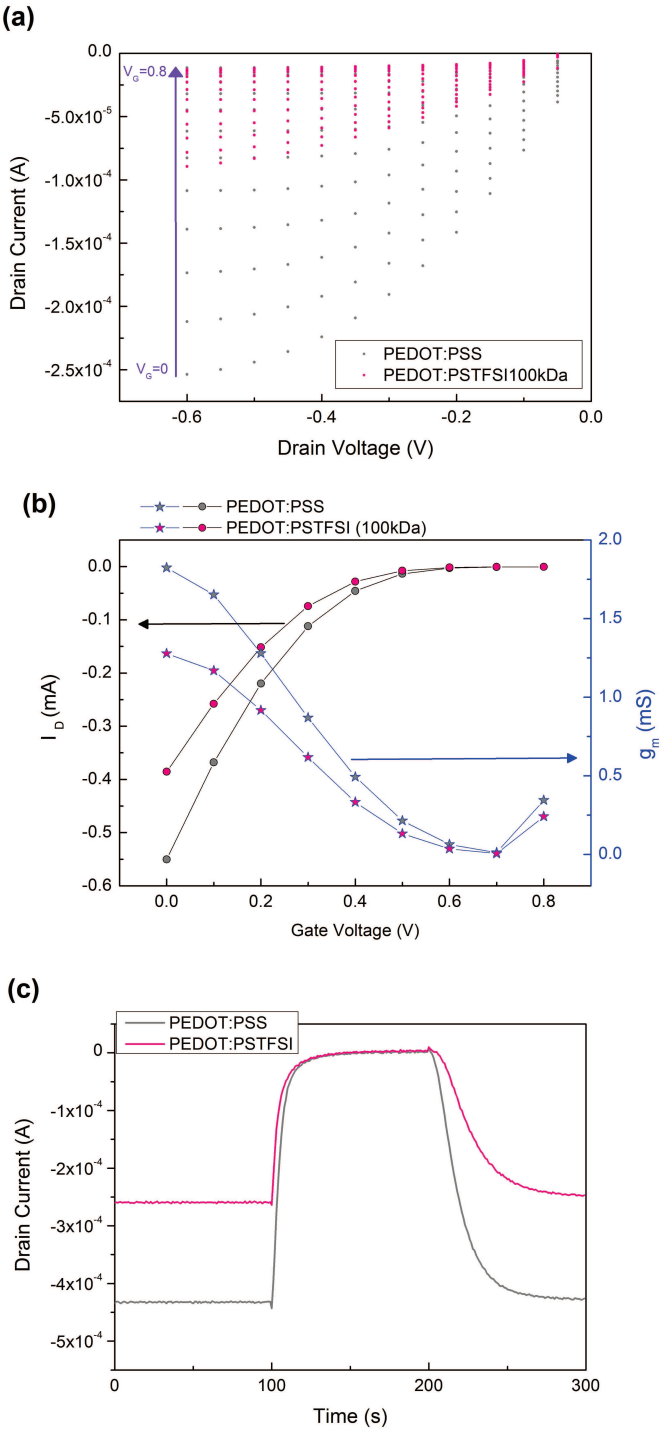

Fig. 5.7: a)I_D-V_D curve, b)I_D-V_G transfer characteristics, transconductance (V_D=-0.8V) and c)temporal response of the drain current of OECTs with a PEDOT:PSS or a PEDOT:PSTFSI (M_W(PSTFSI)=100kDa) electrode

systems are an interesting alternative to PEDOT:PSS as active material in OECTs.

From table 5.4 it can be seen that neither the molar mass nor the counter ion of the PSTFSI polyelectrolyte seemed to have an influence on the performance of the PEDOT:PSTFSI films in OECT devices. Also the hole conductivity of the active material could not be directly correlated to the transconductance of the OECT device. However, the transconductance seemed to depend strongly on the ability for swelling of the active material. PEDOT:PSS and PEDOT:PSTFSI (M_W(PSTFSI)=100kDa), which showed the most important swelling, resulted in the highest transconductance in OECTs, whereas PEDOT:PMaTFSI showed the lowest degree of swelling and the lowest transconductance. Interestingly, the response time did not correlate to the degree of swelling. Though, it has been reported, that the response time depends on the ionic conductivity of the active material, which in turn depends on the swelling [16]. This is an indicator for the presence of a barrier to ion injection in the PEDOT:PSTFSI film or for an anomalous ion transport behavior. In summary, the good performance of PEDOT:PSTFSI (M_W(PSTFSI)=100kDa) in OECT devices reveals that a polymer with rather mediocre hole or electron conductivity but with a high degree of swelling can yield high transconductance OECTs.

It was shown in literature, that the ion mobility in PEDOT:polyelectrolyte films is strongly related to the swelling of the material [17]. This indicates, that the performance of an OECT is decisively influenced by the ion transport behaviour of the active material. Therefore the ion transport in PEDOT:PSTFSI was investigated and compared to the one of PEDOT:PSS. In planar electrolyte-PEDOT:polyelectrolyte junctions the optical transmission of the PEDOT:polyelectrolyte films was monitored over time while the injected cations propagate in the film, leading to a de-doping and color change of the PEDOT:PSTFSI complex. Figure 5.8 displays the evolution of the moving front of the injected potassium cations in the PEDOT:polyelectrolyte films over time. The data confirmed, that the ion mobility in PEDOT:polyelectrolyte films was strongly correlated to the degree of swelling of the material. In PEDOT:PSS, which showed the highest degree of swelling, the highest ion mobility was measured. With decreasing degree of swelling of the PEDOT:polyelectrolytes also the ion mobility decreased. Therefore, in PEDOT:PSTFSI (M_W(PSTFSI)=250kDa), which is the least swellable polymer, the ion front had barely moved after 20min of applied bias, which

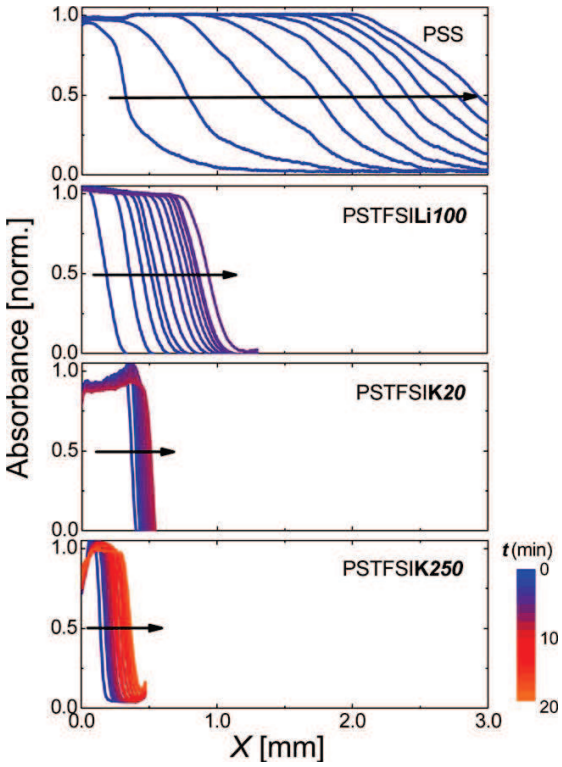

Figure 5.8: Change in optical absorption of the PEDOT:polyelectrolyte films as potassium cations propagate within the film length x. The color code corresponds to the time window of the experiment, with t=0s being the time when 1V bias is applied

shows that the ion mobility in the film was very low. It is noteworthy, that the ion drift in PEDOT:PSS followed a square root dependence with time, which was not the case for the PEDOT:PSTFSI polymers. This is another indicator for the presence of an ion injection barrier and a different ion transport mechanism than in PEDOT:PSS. A possible explanation could be, that the excess PSTFSI units in PEDOT:PSTFSI are predominantly protonated and that their acidity is limited due to the stabilization of hydrogens in the structure via hydrogen bonding with neighboring groups (see section 2.3, page 68). In contrast, it is known from literature, that in PEDOT:PSS the excess PSS units are partly protonated and partly in the sodium salt form [18, 19]. It seems plausible that PSS^{-}-Na^{+} sites are helpful for ion injection and transport, whereas neutral PSTFSI-H sites, in which the protons are stabilized by hydrogen bonding to the neighboring groups, are detrimental to ion injection and transport. This hyphothesis is supported by the XPS N1s data of the PEDOT:PSTFSI inks used for this experiments (see figure 5.9), which show that PEDOT:PSTFSI with M_W(PSTFSIK)=20kDa and M_W(PSTFSILi)=100kDa, which show higher swelling and ion mobility, had a higher percentage of negatively charged STFSI units than PEDOT:PSTFSI M_W(PSTFSIK)=250kDa.

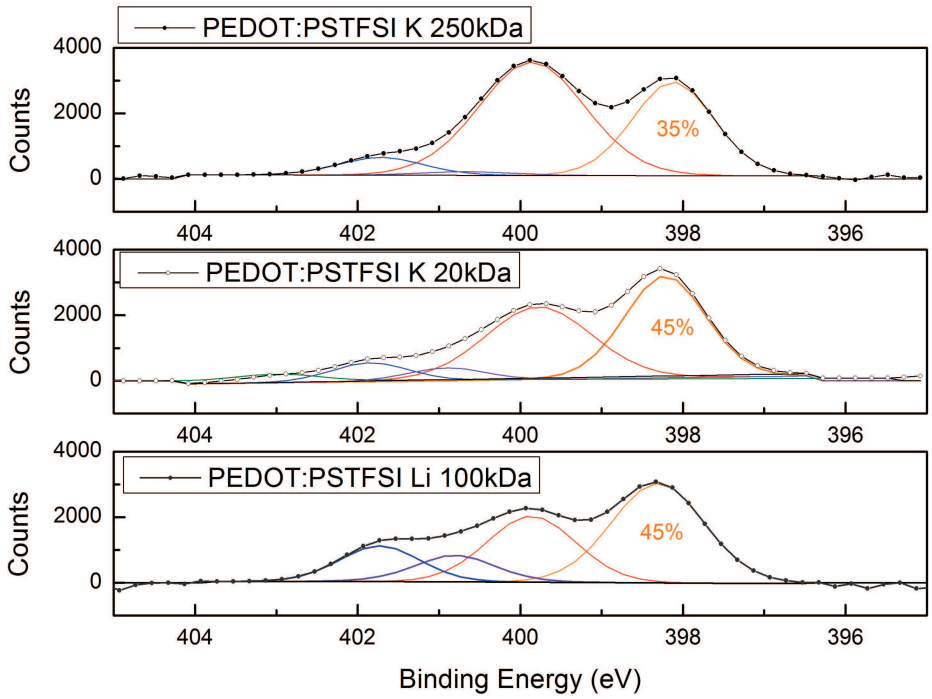

Fig. 5.9: XPS N1s spectra with peak fitting of PEDOT:PSTFSI films with M_W(PSTFSIK)=20kDa, M_W(PSTFSIK)=250kDa and M_W(PSTFSILi)=100kDa. The respective percentage of negatively charged functional units obtained by peak fitting is indicated in orange

In summary, different PEDOT:polysulfonylimide type polymers were tested as active material in OECT devices and compared to commercial PEDOT:PSS. The methacrylate based PEDOT:PMaTFSI, which has a very low conductivity and a low capacity for swelling, results in poorly performing OECTs. All PEDOT complexes synthesized with PSTFSI, which bears sulfonylimide units on a styrenic backbone, showed performance close to the state-of-the-art. This proves that the choice of the polyelectrolyte for the PEDOT:polyelectrolyte complex is a mean to control the OECT performance. Furthermore it was shown that the performance of the OECTs is not much affected by the hole conductivity of the PEDOT:polyelectrolyte films, but is strongly correlated to the swelling ability of the material. Therefore poor electron conducting materials can yield in high performance OECTs, if their high swelling capacity leads to high ion mobilities. This opens up the search for new PEDOT:polyelectrolyte systems, which show optimized swelling behaviour and high ion mobilities in combination with a adequate hole conductivity.

Bibliography

[1] B. Geffroy, P. le Roy, and C. Prat, "Organic light-emitting diode (OLED) technology: materials, devices and display technologies," *Polymer International*, vol. 55, pp. 572–582, June 2006.

[2] P. E. Burrows, V. Bulovic, S. R. Forrest, L. S. Sapochak, D. M. McCarty, and M. E. Thompson, "Reliability and degradation of organic light emitting devices," *Applied Physics Letters*, vol. 65, pp. 2922–2924, Dec. 1994.

[3] H. Aziz, Z. D. Popovic, N.-X. Hu, A.-M. Hor, and G. Xu, "Degradation Mechanism of Small Molecule-Based Organic Light-Emitting Devices," *Science*, vol. 283, pp. 1900–1902, Mar. 1999.

[4] J. S. Lewis and M. S. Weaver, "Thin-film permeation-barrier technology for flexible organic light-emitting devices," *IEEE Journal of Selected Topics in Quantum Electronics*, vol. 10, pp. 45–57, Jan. 2004.

[5] M. Jørgensen, K. Norrman, and F. C. Krebs, "Stability/degradation of polymer solar cells," *Solar Energy Materials and Solar Cells*, vol. 92, pp. 686–714, July 2008.

[6] P. Lin and F. Yan, "Organic Thin-Film Transistors for Chemical and Biological Sensing," *Advanced Materials*, vol. 24, pp. 34–51, Jan. 2012.

[7] G. Wallace and G. Spinks, "Conducting polymers - bridging the bionic interface," *Soft Matter*, vol. 3, no. 6, p. 665, 2007.

[8] D. Khodagholy, T. Doublet, P. Quilichini, M. Gurfinkel, P. Leleux, A. Ghestem, E. Ismailova, T. Hervé, S. Sanaur, C. Bernard, and G. G. Malliaras, "In vivo recordings of brain activity using organic transistors," *Nature Communications*, vol. 4, p. 1575, Mar. 2013.

[9] D. T. Simon, S. Kurup, K. C. Larsson, R. Hori, K. Tybrandt, M. Goiny, E. W. H. Jager, M. Berggren, B. Canlon, and A. Richter-Dahlfors, "Organic electronics for precise delivery of neurotransmitters to modulate mammalian sensory function," *Nature Materials*, vol. 8, pp. 742–746, Sept. 2009.

[10] J. Rivnay, P. Leleux, M. Ferro, M. Sessolo, A. Williamson, D. A. Koutsouras, D. Khodagholy, M. Ramuz, X. Strakosas, R. M. Owens, C. Benar, J.-M. Badier, C. Bernard, and G. G. Malliaras, "High-performance transistors for bioelectronics through tuning of channel thickness," *Science Advances*, vol. 1, p. e1400251, May 2015.

[11] X. Strakosas, M. Bongo, and R. M. Owens, "The organic electrochemical transistor for biological applications," *Journal of Applied Polymer Science*, vol. 132, pp. n/a–n/a, Apr. 2015.

[12] L. H. Jimison, S. A. Tria, D. Khodagholy, M. Gurfinkel, E. Lanzarini, A. Hama, G. G. Malliaras, and R. M. Owens, "Measurement of Barrier Tissue Integrity with an Organic Electrochemical Transistor," *Advanced Materials*, vol. 24, pp. 5919–5923, Nov. 2012.

[13] A. Campana, T. Cramer, D. T. Simon, M. Berggren, and F. Biscarini, "Electrocardiographic Recording with Conformable Organic Electrochemical Transistor Fabricated on Resorbable Bioscaffold," *Advanced Materials*, vol. 26, pp. 3874–3878, June 2014.

[14] D. Khodagholy, J. Rivnay, M. Sessolo, M. Gurfinkel, P. Leleux, L. H. Jimison, E. Stavrinidou, T. Herve, S. Sanaur, R. M. Owens, and G. G. Malliaras, "High transconductance organic electrochemical transistors," *Nature Communications*, vol. 4, July 2013.

[15] S. Inal, J. Rivnay, A. I. Hofmann, I. Uguz, M. Mumtaz, D. Katsigiannopoulos, C. Brochon, E. Cloutet, G. Hadziioannou, and G. G. Malliaras, "Organic electrochemical transistors based on PEDOT with different anionic polyelectrolyte dopants," *Journal of Polymer Science Part B: Polymer Physics*, vol. 54, pp. 147–151, Oct. 2015.

[16] D. A. Bernards and G. G. Malliaras, "Steady-State and Transient Behavior of Organic Electrochemical Transistors," *Advanced Functional Materials*, vol. 17, pp. 3538–3544, Nov. 2007.

[17] E. Stavrinidou, P. Leleux, H. Rajaona, D. Khodagholy, J. Rivnay, M. Lindau, S. Sanaur, and G. G. Malliaras, "Direct Measurement of Ion Mobility in a Conducting Polymer," *Advanced Materials*, vol. 25, pp. 4488–4493, Aug. 2013.

[18] G. Greczynski, T. Kugler, and W. R. Salaneck, "Characterization of the PEDOT-PSS system by means of X-ray and ultraviolet photoelectron spectroscopy," *Thin Solid Films*, vol. 354, pp. 129–135, Oct. 1999.

[19] G. Zotti, S. Zecchin, G. Schiavon, F. Louwet, L. Groenendaal, X. Crispin, W. Osikowicz, W. Salaneck, and M. Fahlman, "Electrochemical and XPS Studies toward the Role of Monomeric and Polymeric Sulfonate Counterions in the Synthesis, Composition, and Properties of Poly(3,4-ethylenedioxythiophene)," *Macromolecules*, vol. 36, pp. 3337–3344, May 2003.

6 Polyelectrolytes for Aqueous PEDOT Complexes

By using different polysaccharide and polysulfonylimide type polyelectrolytes for the synthesis of aqueous PEDOT:polyelectrolyte dispersions, the influence of polyelectrolyte backbone and of the anionic groups on the properties of the resulting PEDOT:polyelectrolyte complex is studied. The obtained PEDOT:polyelectrolyte systems are characterized regarding the doping and the morphology of the polymer complexes in dispersion, as well as regarding the opto-electronic properties and the morphology of the dry PEDOT:polyelectrolyte films. The use of polysaccharide type electrolytes is promising for the development of low cost and highly bio-compatible PEDOT complexes, whereas polysulfonylimide type polyelectrolytes allow the synthesis of highly transparent still conductive PEDOT:polyelectrolyte films.

Dans l'objectif de moduler les caractéristiques opto-électroniques des films à base de dispersions aqueuses de PEDOT:polyélectrolyte nous avons étudié toute une série de polyélectrolytes de types polysaccharides et polystyrenes substitués par des groupements bissulfonylimides. L'influence du groupement anionique (charge et nature chimique) ainsi que les structures/rigidité des polyélectrolytes sur les complexes PEDOT:polyélectrolyte et donc sur les caractéristiques finales de leurs films minces ont été étudiées. Il ressort notamment que le complexe de type PEDOT:Poly(p-styrene bissulfonylimide) donne les meilleurs résultats en terme de compromis transmittance/conductivité électronique et que les complexes bio-sourcés à base de sulfate de dextrane sont très prometteurs montrant des conductivités de l'ordre de 15 S/cm.

6.1 Introduction

Over the last decade conducting polymers attracted more and more attention in the scientific community. The development of aqueous dispersions of conducting polymers, such as PEDOT:PSS, makes it possible to print flexible, transparent and biocompatible thin conducting films, which allow the development of a new generation of flexible electronics with a wide range of applications in energy [1, 2, 3, 4, 5, 6, 7] , entertainment [8, 9, 10, 11, 12] and the biomedical field [13, 14, 15]. For now the material of choice for these applications is PEDOT:PSS, which is mainly due to its good opto-electronic properties and biocompatibility [16], but also due to a lack of alternatives. Given the huge variety of applications it would be preferable to design aqueous PEDOT:polyelectrolyte systems which meet better the specific requirements of each application. To do so a better understanding of the stabilization and doping mechanism of PEDOT is needed. Therefore, different PEDOT:polyelectrolyte systems were studied in this chapter, in order to investigate the influence of the rigidity of the polyelectrolyte chain, different acid functionalities and the density of the charges on the opto-electronic properties of the PEDOT:polyelectrolyte complex. The palette of the studied polyelectrolytes for the synthesis of PEDOT complexes comprised synthetic polyanions bearing bisulfonylimide groups, which lead to highly transparent films, as well as polyanionic polysaccharides, which could allow the cost efficient production of highly bio-compatible conducting PEDOT:polyelectrolyte films.

In the PEDOT:polyelectrolyte complex the anionic polyelectrolyte acts as counter ion for the positively charged, doped PEDOT and allows the dispersion of the insoluble PEDOT in water. Therefore the nature of the anionic groups, the charge density and the morphology of the polyelectrolyte play a crucial role for the doping and stabilization of PEDOT. In nature a huge variety of polyanionic biopolymers, such as polysaccharides, bearing a different amount of carboxylic or sulfate groups can be found. Figure 6.1 displays the chemical structure of the different anionic polysaccharides which were chosen for this work. Pectin (see figure 6.1), which is commercially used as gelling agent and food stabilizer, consists of linear chains of α-(1–4)-linked D-galacturonic acid units and of very complex branched derivatives [17]. It bears one carboxylic group on every repeat unit, of which 60-70% are esterified and which can be hydrolyzed in acidic medium. Sodium

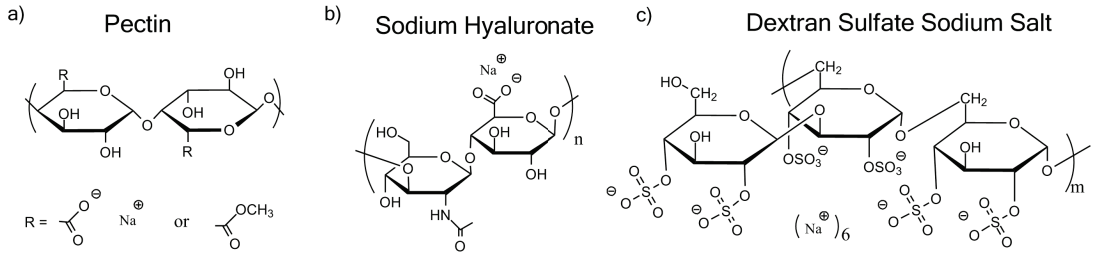

Fig. 6.1: Chemical structure of a)Pectin, b)Hyaluronic acid (HLA) and c)Dextran sulfate (DS)

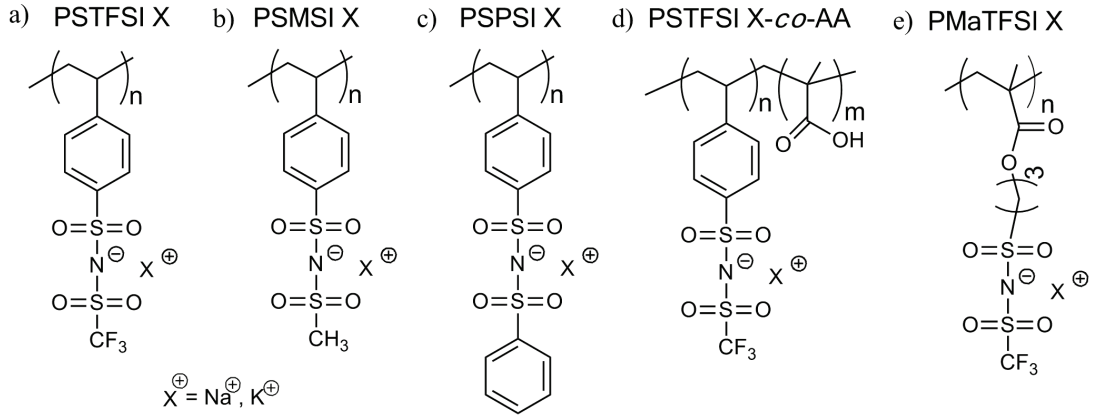

Fig. 6.2: Chemical structure of synthesized a)PSTFSI, b)PSMSI, c)PSPSI, d) PMaTFSI and e) PSTFSI-co-AA (m:n=1)

hyaluronate (see figure 6.1) is a linear polysaccharide composed of D-glucuronic acid and D-N-acetylglucosamine units, linked via alternating β-1,4 and β-1,3 glycosidic bonds and bears one carboxylic group on every second repeating unit [18, 19]. It is known for its biomedical application and component in skin care products. Dextran sulfate (see figure 6.1), known as coagulant, is a branched d-glucose polymer, which is highly charged due to two sulfate groups per repeating unit.

These three polysaccharides mentioned above were compared to bissulfonylimide-based polyelectrolytes regarding their ability to "dope" and disperse PEDOT in water [20]. All polymers studied in this work bear at least one negatively charged group per repeating unit and differ either in backbone, such as poly(4-styrene trifluoromethyl(bissulfonylimide)) (PSTFSI) and poly(methacrylate trifluoromethyl(bissulfonylimide)) (PMaTFSI), in side group, such as poly(4-styrene phenyl(bissulfonylimide)) (PSPSI) and poly(4-styrene methyl(bissulfonylimide) (PSMSI), or in both (PSTFSI-co-poly(acrylic acid), (PSTFSI-co-AA)(see figure 6.2)).

All PEDOT:polyelectrolyte dispersions were synthesized by oxidative polymerization of EDOT in the aqueous polyelectrolyte solutions under nitrogen atmosphere at 10 °C,

using a binary oxidant system of $FeCl_3$ and $(HN_4)_2S_2O_8$) (details see experimental section, page 203).

6.2 Opto-Electronic Properties

Table 6.1 displays the opto-electronic properties of the different PEDOT:polyelectrolyte films, deposited with 5% DMSO co-solvent. All three polysaccharides tested were able to stabilize PEDOT in aqueous medium and dark blue dispersions were obtained. The PEDOT:Dextran sulfate (PEDOT:DS) complex showed a maximum conductivity of 15S.cm^{-1} for a molar ratio of dextran sulfate to EDOT of 2.2, which is similar to the conductivity for a PEDOT:DS reported by Harman *et al.*[21]. However, neither the PEDOT:Hyaluronate (PEDOT:HLA) nor the PEDOT:Pectin films were conducting. With an absorption coefficient a at 550nm of about 2000cm^{-1} PEDOT:DS showed a good transparency in the visible range, which was higher than the one of PEDOT:PSS.
As reported before [20], the synthesized PEDOT:PSTFSI and home made PEDOT:PSS showed good conductivities up to 300S.cm^{-1} with PEDOT:PSTFSI being considerably more transparent (a≈2) than PEDOT:PSS (a≈3.5). For both, PEDOT:PSS and PEDOT:PSTFSI, the use of higher molar mass polyelectrolytes resulted in a higher transparency and conductivity, but did not fundamentally change the characterisitcs of the PEDOT:polyelectrolyte complexes (see figure 6.3). Interestingly, the conductivity of the PEDOT:polyelectrolyte complex did not increase gradually with increasing molar mass of the polyelectrolyte, but was constant over a range of molar masses and only jumped up when a certain "threshold" molar mass was reached.
PEDOT:PSMSI and PEDOT:PSTFSI-*co*-AA showed a considerably lower conductivity of 12S.cm^{-1} and 5S.cm^{-1}, respectively, and both PEDOT:PMaTFSI and PEDOT:PSPSI showed negligible conductivity. The absorption coefficients a of those polymers ranged between 2200cm^{-1} and 3000cm^{-1}, which indicates that were less transparent in the green regime than PEDOT:PSTFSI, but more transparent than PEDOT:PSS.

6.3 Doping of the PEDOT:polyelectrolyte complexes

In order to obtain information on the doping of PEDOT, UV/Vis spectra of all PEDOT:polyelectrolyte complexes were recorded. It is known from literature that neutral PEDOT absorbs at around 500nm, whereas the polaronic and bipolaronic

System	Molar Mass Polyelectrolyte (kDa)	Molar Ratio Polyelectrolyte Repeating Unit /EDOT[a]	Molar Ratio Negative Charge /EDOT[a]	Conductivity[b,c] (S.cm^{-1})	Absorption Coefficient[b] at 550nm (10^3 cm^{-1})	Work Function[d] (eV)	T_g Polyelectrolyte (°C)
PEDOT:HLA	-	2.5	1.0	< 0.01	1.4±0.2	5.2	14[18]
		2.0	1.25	< 0.01	1.0±0.2		
PEDOT:Pec	-	2.4	< 2.4	< 0.01	2.9±0.3	5.0	35[22]
		1.8	< 1.8	< 0.01	5.9±0.8		
PEDOT:DS	-	3.3	6.6	8±2	-	-	-
		3.0	6.0	8±2	2.2±0.3	5.1	
		2.4	4.8	7±2	1.9±0.2	-	
		2.2	4.4	15±4	1.9±0.2	5.1	
		2.0	4.0	8±3	-	-	
		1.7	3.4	x	x	x	
PEDOT:PSS	1000	1.7	1.7	205±16	3.2±0.2	5.2	-
	70	1.7	1.7	127±13	3.7±0.3		-
PEDOT:PSTFSI	350[a]	1.7	1.7	210±20	1.8±0.2	5.3	-
	20[a]	1.7	1.7	112±12	3.1±0.3		59[e]
PEDOT:PMaTFSI	80[a]	1.7	1.7	< 0.01	3.0±0.5	5.3	44[e]
PEDOT:PSPSI	100[a]	1.7	1.7	< 0.01	2.7±0.3	4.9	-
PEDOT:PSMSI	20[a]	1.7	1.7	12±2	2.2±0.2	5.2	-
PEDOT:PSTFSI-*co*-AA	40[a]	3.4	3.4	3±1	1.6±0.2	5.2	60[e]
		1.7	1.7	5±2	3.0±0.4		

[a] theoretical value [b] average on 8 measurements or more [c] determined by 4-point measurements
[d] determined by Kelvin Probe AFM [e] determined by DSC, 2nd cycle, heating/cooling rate 10°C/min

Tab. 6.1: Opto-electronic properties of PEDOT:polyelectrolytes

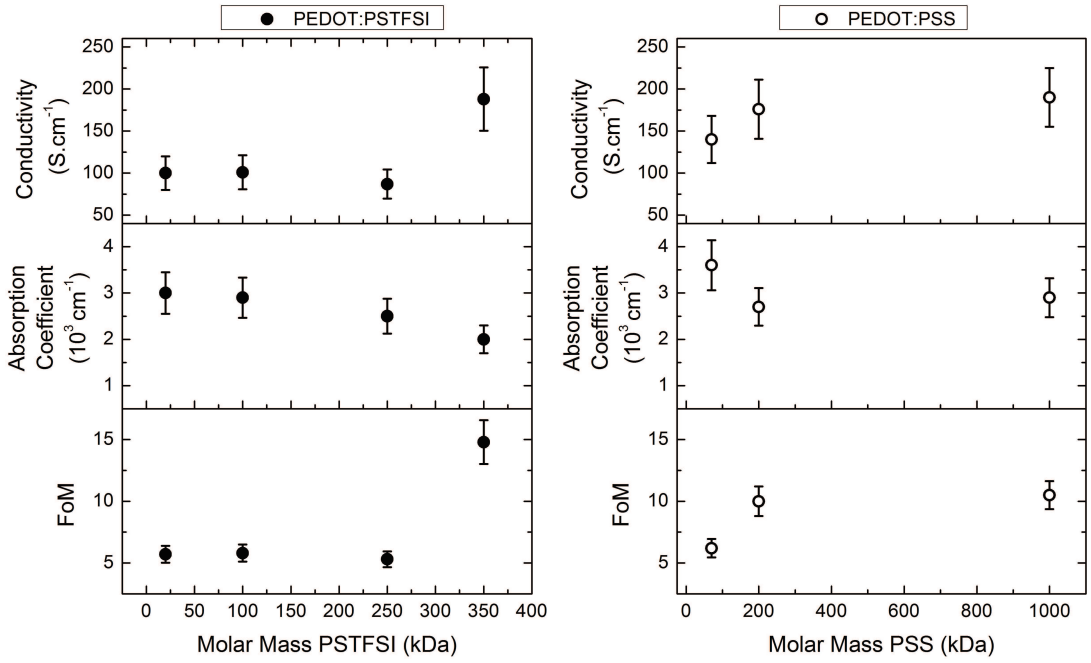

Fig. 6.3: Opto-electronic properties of PEDOT:PSTFSI and PEDOT:PSS as a function of the molar mass of the polyelectrolyte

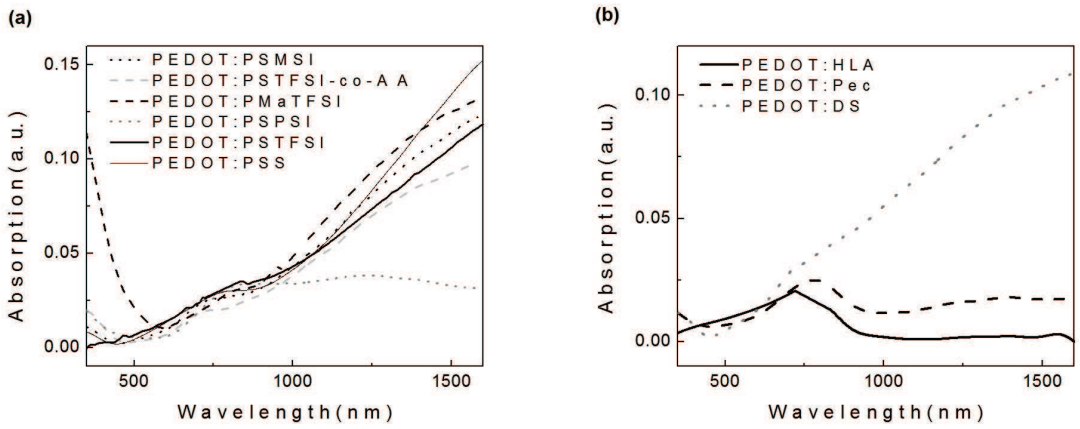

Fig. 6.4: UV Vis spectra of PEDOT:polyelectrolyte films

absorption can be found at 800nm and at wavelengths longer than 1300nm, respectively [23, 24, 25, 26]. Highly doped PEDOT typically shows a monotonically increasing absorption towards higher wavelengths, as it can be seen for PEDOT:PSS in figure 6.4. A very similar spectrum was observed for PEDOT:PSTFSI, with the exception of a lower bipolaronic contribution at high wavelengths. The comparison of the absorption spectra of PEDOT:PSTFSI systems made from PSTFSIK with different molar masses revealed no clear differences as function of the molar mass of the PSTFSI polyelectrolyte. Therefore it was assumed, that the absorption spectra were characteristic for each PEDOT:polyelectrolyte system, which justifies the comparison of the spectra of the different PEDOT:polyelectrolyte systems.

The absorption characteristics of PEDOT:PSMSI, PEDOT:PSTFSI-*co*-AA, PEDOT:PMaTFSI and PEDOT:DS resemble these of PEDOT:PSS, but display a strongly flattened and curved slope in the bipolaronic absorption regime. Studies of PEDOT in literature show, that lower bipolaronic absorption is a sign of an inferior degree of doping [23, 24, 25]. From the shape of the UV/Vis spectra of PEDOT:PSPSI, PEDOT:Hyaluronic acid and PEDOT:Pectin it is evident that these PEDOT complexes are very poorly doped, which explains the lack of conductivity of these polymers.

The difference in doping was confirmed by Raman spectroscopy (see figure 6.5). The spectra of PEDOT:PSTFSI, PEDOT:PSS and PEDOT:PSMSI are very similar and show a broad band centered at 1425cm^{-1}, 1427cm^{-1} and 1441cm^{-1}, respectively, which can be assigned to the symmetric $c_\alpha = c_\beta$ stretching [25, 27] (assignment of c_α and c_β see figure 6.6). PEDOT:DS, PEDOT:PMaTFSI and PEDOT:PSTFSI-*co*-AA show a

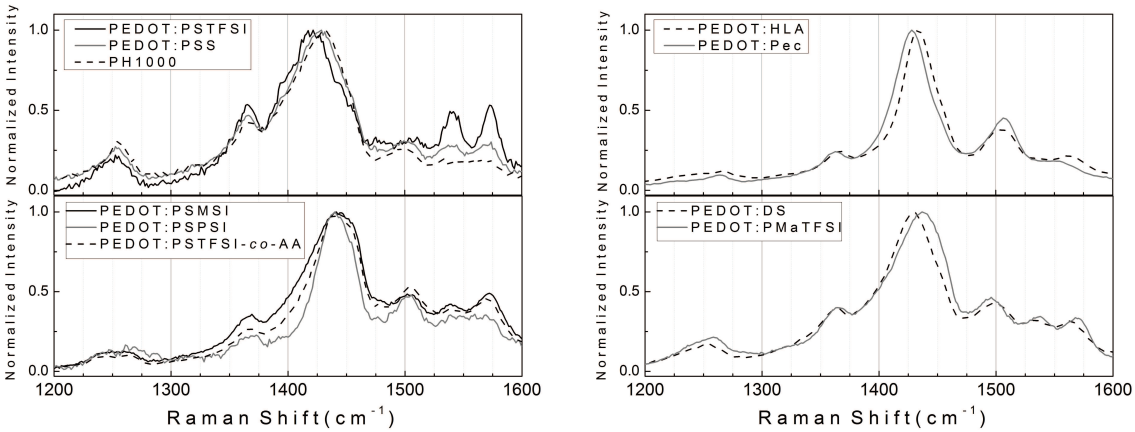

Fig. 6.5: Raman spectra of PEDOT:polyelectrolyte dispersions, excitation wavelength 532nm

slightly less broad band, centered at 1430cm^{-1}, 1436cm^{-1} and 1439cm^{-1}, respectively. In the case of PEDOT:Pectin, PEDOT:HLA and PEDOT:PSPSI, however, the corresponding band is narrow and located at 1427cm^{-1}, 1433cm^{-1} and 1439cm^{-1}, respectively. It has been shown, that for highly doped PEDOT the $c_\alpha = c_\beta$ band is very broad, resulting from the superposition of the different contributions of PEDOT in the benzoidic and quinoidic conformation [25, 28]. This confirms the high doping in PEDOT:PSS, PEDOT:PSTFSI and PEDOT:PSMSI, slightly lower doping in PEDOT:DS, PEDOT:PMaSTFSI and PEDOT:PSTFSI-*co*-AA and very low doping for PEDOT:Pectin, PEDOT:HLA and PEDOT:PSPSI. Im and Gleason [26] observed a shift of the $c_\alpha = c_\beta$ band from 1444cm^{-1} to 1428cm^{-1} with increasing doping and conductivity of CVD deposited PEDOT. This is coherent with our findings for the PEDOT:polyelectrolyte systems, for which broad $c_\alpha = c_\beta$ bands are observed. The $c_\alpha = c_\beta$ bands of PEDOT:PSS and PEDOT:PSTFSI, which show the highest bipolaronic absorption in UV/Vis and the highest conductivity, are located at lower frequencies than 1430cm^{-1}, whereas the $c_\alpha = c_\beta$ bands of the PEDOT:polyelectrolytes, which show flattened absorption in the bipolaronic regime in the UV/Vis and low conductivity, are located at frequencies above 1430cm^{-1}. However, in literature the inverse shift has also been observed [25, 28]. Therefore the correlation of the peak position of the $c_\alpha = c_\beta$ band to the doping of PEDOT in the PEDOT:polyelectrolyte complexes cannot be conclusive enough.

Both PEDOT:PSTFSI and PEDOT:PSS show a high band at 1255cm^{-1}, which can be assigned to the $c_\alpha - c_\alpha$ inter ring stretching, as well as a high $c_\beta - c_\beta$ stretching band at 1365cm^{-1}. These bands have been observed in highly doped PEDOT [25, 27] and the

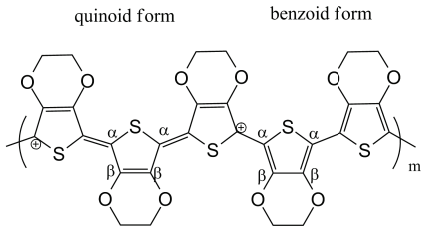

Fig. 6.6: Chemical structure of doped PEDOT

intense $c_\alpha - c_\alpha$ signal can also be an indicator for the presence of long benzoidic PEDOT chains in PEDOT:PSS and PEDOT:PSTFSI. By contrast, PEDOT:DS and PEDOT:PMaTFSI show less intense absorption bands at 1250cm^{-1} and at 1365cm^{-1} and the spectra of PEDOT:PSPSI, PEDOT:HLA and PEDOT:Pectin are characterized by extremely low and broad peaks at 1250cm^{-1}. This is in agreement with data from literature on Raman spectra of PEDOT with a low doping level or of undoped PEDOT [25, 26, 27]. Furthermore, the low intensity of $c_\alpha - c_\alpha$ bands is a sign for the absence of long PEDOT chains. The PEDOT being in the form of short and poorly oxidized oligomers in PEDOT:Pectin, PEDOT:HLA and PEDOT:PSPSI could explain the lack of bipolaronic absorption in their UV/Vis spectra (see figure 6.4), as bipolarons are stabilized by their delocalization over several repeating units [29, 30]. The absence of sufficiently long PEDOT chains, which are crucial for the delocalization and the transport of charges, in PEDOT:Pectin, PEDOT:HLA and PEDOT:PSPSI is coherent with the absence of conductivity.

By varying the polyelectrolyte to EDOT ratio it can be shown, that the use of an excess of polyelectrolyte or a higher density of anionic groups on the backbone does not increase the doping of the complexed PEDOT, as it is exemplary shown for PEDOT:DS (see table 6.1). A detailed discussion of the influence of the polyelectrolyte to PEDOT ratio on the opto-electronic properties of PEDOT:PSTFSI can be found in chapter 2.3, page 68. However, when a certain PEDOT concentration is reached the polyelectrolyte becomes saturated with PEDOT, the doping decreases and the PEDOT:polyelectrolyte complex precipitates. The decrease in doping of PEDOT:DS with increasing PEDOT concentration was confirmed by UV/Vis spectrometry, which revealed a decreasing bipolaronic absorption ($\lambda > 1300nm$) for molar EDOT to DS ratios >0.45 (see figure 6.7). In addition, PEDOT:DS dispersions became unstable for a molar ratio of EDOT units to DS units of 0.5 or higher, which resulted in the formation of agglomerates and

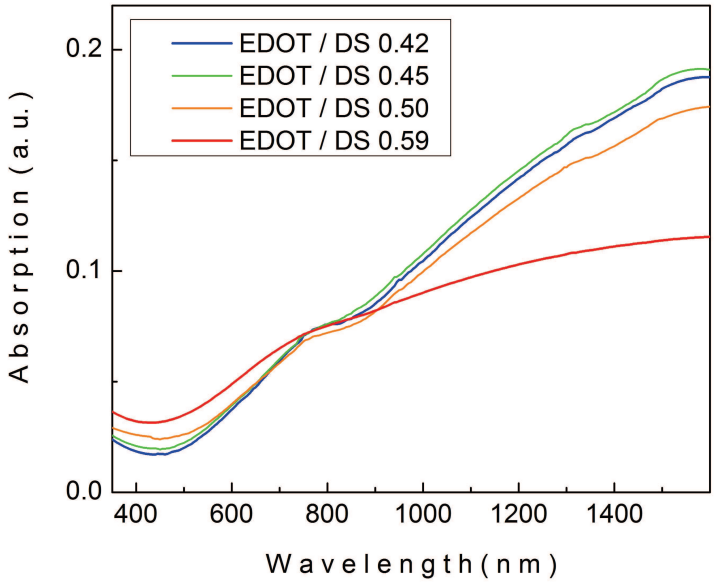

Fig. 6.7: UV/Vis absorption spectra of PEDOT:DS systems with different molar ratio of EDOT to DS repeating unit

partial precipitation of the polymer complex from the dispersion and rendered the fabrication of homogeneous films impossible.

As both PEDOT:HLA and PEDOT:Pectin resulted in insulating complexes due to insufficient doping and charge delocalization, we can state that carboxylate groups do not stabilize PEDOT properly. Due to their relatively weak acidity the carboxylate groups can be protonated in the acidic environment of the EDOT polymerization and the neutral carboxylic acid groups cannot stabilize the positive charges on the growing PEDOT chain. In addition, pectin is known to be hydrolized in acidic conditions over time [17], resulting in less branched and shorter polymeric chains, which can also decrease the ability to stabilize PEDOT in aqueous dispersion. This trend is confirmed by the fact that PEDOT stabilized by the PSTFSI-acrylic acid co-polymer shows a lower degree of doping than PEDOT in the PEDOT:PSTFSI complex. A similar reasoning can be done for PSPSI and PSMSI. By replacing the highly electron withdrawing trifluoromethyl group of PSTFSI by a phenyl (PSPSI) or methyl (PSMSI) group the acidity of the functional group is slightly lowered, which could lead to lower doping of the PEDOT:PSPSI and PEDOT:PSMSI complexes. Therefore we can conclude that a highly acidic functionality on the polyanionic stabilizer is indispensable for an efficient doping of PEDOT.

The difference in doping between PEDOT:DS and PEDOT:PMaTFSI cannot be explained

by the nature of the acid groups, as DS and PMaTFSI bear almost the same acid groups as PSS and PSTFSI, respectively. Therefore it has to be related to the differences in the polymer backbone and to the different position of the functional groups on the backbone. These differences will lead to a different conformation of the polyelectrolyte chains in solution, affecting the 3D distribution of charges. Hartree-Fock simulations on PEDOT oligomers done by Bredas and co-workers [30] indicate, that the position of the counter ions does have an influence on the charge distribution on PEDOT and the stability of the PEDOT:counter ion complex. Polymers with a styrenic backbone are known to be stiff and display a glass transition temperature far above room temperature [31]. Due to the bulky side chains of PSS and PSTFSI the barrier for segmental motion is further increased. It is known, that PSSNa does not show a glass transition and also for PSTFSIK with a molar mass higher than 20kDa no glass transition was observed between -80°C and 200°C (see DSC data in figure D.1, appendix page 227). It is known from literature [32, 33, 34, 35], that at low ionic strength PSS adopts an extended coil conformation in aqueous solution. From DLS measurements on PSTFSI solutions with different molar masses, hydrodynamic radii of 60nm (PSTFSIK 10kDa) to more than 300nm (PSTFSIK 350kDa) were obtained, which exceed the size of the maximal theoretical chain length. This indicates that PSTFSI was not fully solubilized and thus, no information on the chain configuration of PSTFSIK can be retrieved from the DLS data. However, PSTFSIK chains depicted by Atomic Force Microscopy (AFM) (see figure 6.8) on a mica surface clearly showed a wormlike chain conformation. In contrast, the T_g of PMaTFSI was measured to be 44°C (see figure D.1), suggesting a much more flexible backbone, which is in coherence with results from literature for polyacrylates and polymethacrylates [31, 34] and the coiled PMaTFSI chains depicted by AFM imaging (see figure 6.8). DS does not show a T_g, however, the slope of 0.5 in the conformation plot, determined by size exclusion chromatography (see figure D.2, appendix page 228), points out that DS adopts a random coil conformation in water. As both flexible polyelectrolytes resulted in PEDOT complexes with lower doping and conductivity, we can assume that rigid polyelectrolytes facilitate the formation of long and well doped PEDOT chains, serving as better templates for the conjugated and linear PEDOT.

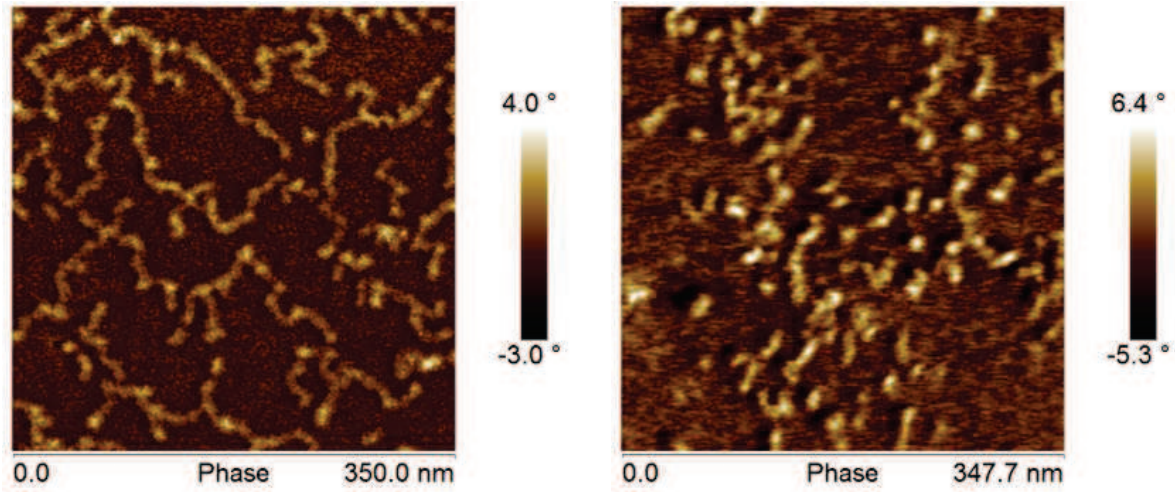

Fig. 6.8: AFM phase images of PSTFSI, M_W ≈300kDa (left) and PMaTFSI, M_W ≈80kDa (right) on a mica surface

6.4 Morphology of the PEDOT:polyelectrolyte complexes

Besides the doping, the morphology of the PEDOT:polyanion complex also plays a crucial role for its conductivity. For PEDOT:PSS it has been shown that the macroscopic conductivity depends not only on the size [36, 37] and crystallinity [38, 39] of the PEDOT rich domains, but also on the percolation of the conducting network [39, 40, 41, 42] and the energy barrier for inter chain and inter domain charge hopping [7]. Considering that the polyanions act as templates for the PEDOT oligomers/polymers we can expect that the flexibility of the polyanion chains influences the morphology of the final PEDOT:polyanion complex.

In order to get more insight in the meso-scale morphology of the PEDOT complexes, AFM on solid films and on the complexes in aqueous dispersion was performed. As it can be seen from figure 6.9, the dispersed PEDOT:PSS, PEDOT:PSTFSI and PEDOT:PSMSI complexes form a three dimensional network with thick nodal points, probably corresponding to PEDOT rich domains, with an average height of 6nm, 3nm and 3nm, respectively. The chains around the nodes in PEDOT:PSS are very thin and adopt a random coil shape whereas the free chains around the nodes in PEDOT:PSTFSI and PEDOT:PSMSI appear thicker and more linear. During drying the three dimensional network collapses and forms a film composed of particle like objects, which

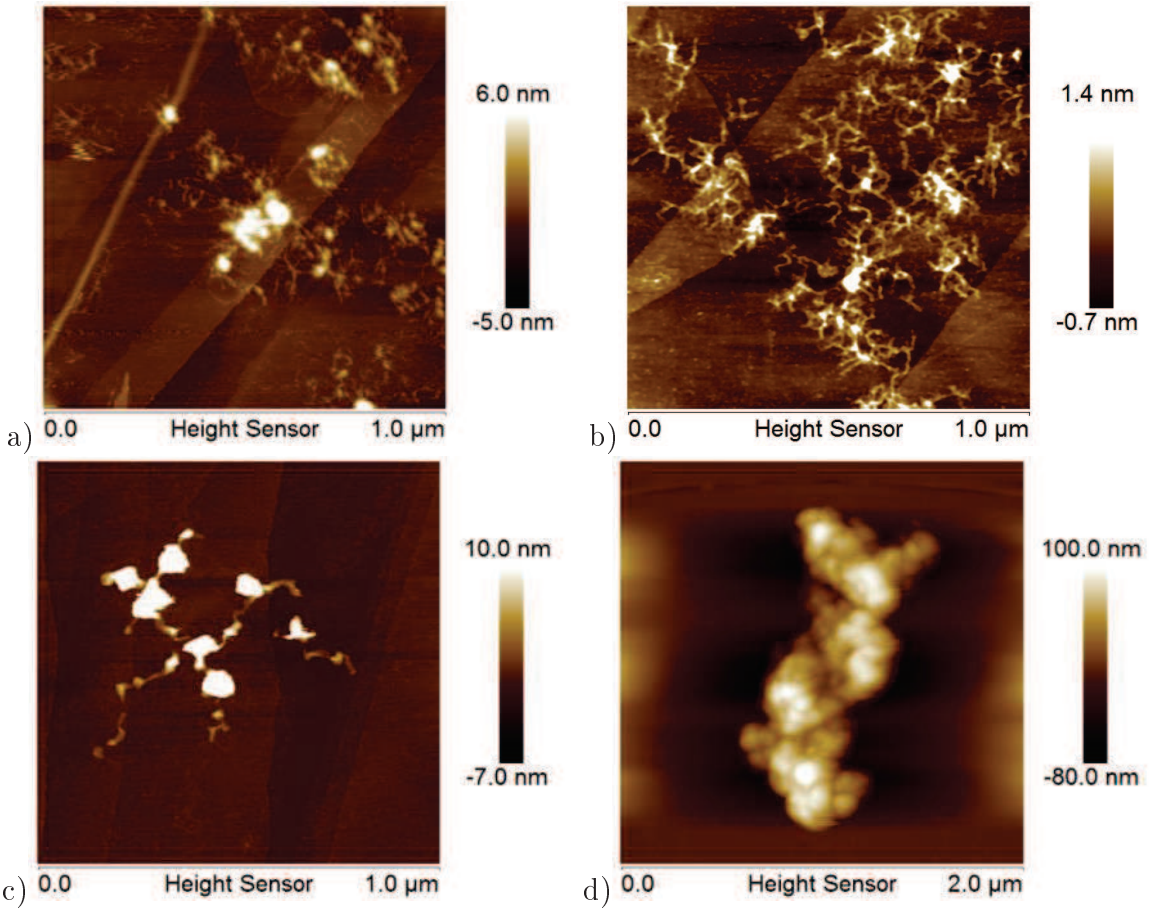

Fig. 6.9: Liquid AFM images of a)PEDOT:PSS, b)PEDOT:PSTFSI, c)PEDOT:DS and d)PEDOT:PMaTFSI

can be visualized by AFM imaging (see figure 6.10 and figures D.4 and D.6). The average size of the domains in PEDOT:PSTFSI containing DMSO co-solvent is 40nm, which is similar to the findings for PEDOT:PSS in literature [36][37][43]. For the AFM image shown in figure 6.10c the surface layer, which is known to be rich in excess polyanion[43, 44], was removed by CF_4 plasma etching in order to picture the bulk morphology. It is well known from literature that the treatment of PEDOT:PSS films with high boiling point solvents leads to an important increase of the macroscopic conductivity. The same effect of solvent treatment on the conductivity can be observed for PEDOT:PSTFSI and PEDOT:PSMSI (see chapter 3.2, page 132). Commonly, this phenomenon is explained by a growth of PEDOT rich domains [36][37] and an increase in their crystallinity [39][45][46][47]. In the case of PEDOT:PSTFSI, however, no crystallinity could be observed by grazing incidence wide angle x-ray scattering (GIWAXS) (see figure D.7, appendix page 232) or by differential scanning calorimetry (see figure B.1 in section 3.2, page 226). Interestingly, the conductivity of the other PEDOT:polyanion systems presented in this work was not affected by the addition of co-solvents such as DMSO or ethyleneglycol. This suggests that the ability for phase separation in the film is linked to the three dimensional corona of chains which can be found around nanometer sized particles in PEDOT:PSS, PEDOT:PSTFSI and PEDOT:PSMSI. Amongst the conductivities of the pristine films, PEDOT:dextran sulfate shows the highest one. Only after a treatment with ethylene glycol or DMSO the conductivities of PEDOT:PSS and PEDOT:PSTFSI show an increase of two orders of magnitude and therefore the treated PEDOT:PSS and PEDOT:PSTFSI outperform PEDOT:dextran sulfate.

In comparison to PEDOT:PSS and PEDOT:PSTFSI, PEDOT:DS complexes in dispersion show bigger nodal points of up to 30nm and fewer surrounding chains and form a less dense network (see figure 6.9). The morphology of the resulting PEDOT:DS films is similar to the one of PEDOT:PSTFSI. However, the grain size increases to about 65nm and the surface roughness is drastically increased to R_q=12nm (see figure 6.10 and figure D.4 in the appendix page 230). It has been reported that the conductivity of PEDOT:PSS increases with increasing domain size [36][37][43], because this implies an improved percolation of the PEDOT rich domains and the reduction of hopping barriers[36]. In order to investigate the effect of the structure of PEDOT:DS

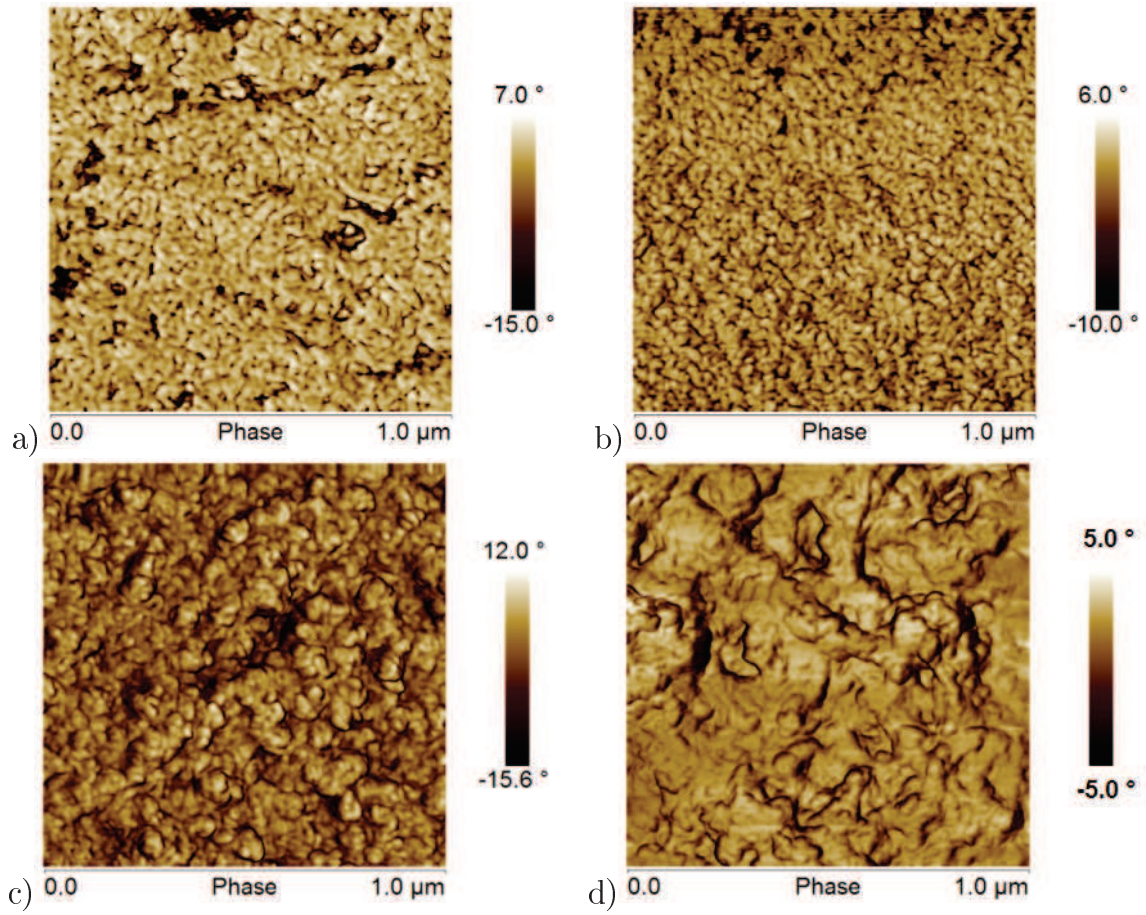

Fig. 6.10: AFM phase images of a)PEDOT:PSS, b)PEDOT:PSTFSI, c)PEDOT:DS and d)PEDOT:PMaTFSI

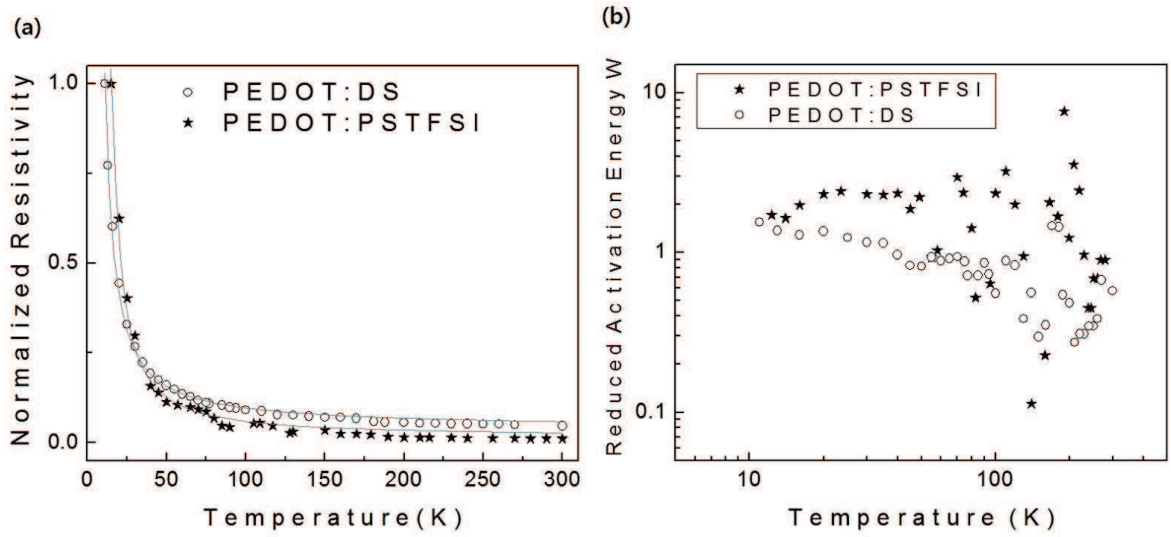

Fig. 6.11: Temperature dependency of the resistivity of PEDOT:PSTFSI and PEDOT:DS films and b) reduced activation energy W versus temperature for PEDOT:PSTFSI and PEDOT:DS

and PEDOT:PSTFSI on their conductivities, the charge transport mechanism was studied. For this purpose the resistance of the polymer films was measured as a function of temperature in the range of 300K to 10K and fitted with the variable range hopping model[48][49]

$$R(T) = R_0 exp[(\frac{T_0}{T})^{\alpha}] \tag{6.1}$$

with R being the resistance, T being the temperature, $T_0 = \dfrac{16}{k_B N(E_F) L_{\parallel} L_{\perp}^2}$ being the energy barrier between localized states, $N(E_F)$ the density of states at the Fermi level, and $L_{\parallel}$ ($L_{\perp}$) the localization length of the charge carriers in the parallel (perpendicular) direction with respect to the measurement direction. The exponent α is related to the transport process and is equal to $1/(1+d)$, where d is the dimensionality of the hopping transport in the system.

As it can be seen in figure 6.11a the resistivity decreased drastically with increasing temperature. The plot of the reduced activation energy $W = \dfrac{\partial ln\sigma}{\partial lnT}$ as function of the temperature T showed negative slopes for both PEDOT complexes (see figure 6.11b). This signifies that both systems were in the insulating regime, which is in accordance with the charge transport characteristics of PEDOT:PSS reported in literature [50, 51]. By fitting of the resistivity with the one dimensional VRH model ($\alpha = 0.5$), the energy barrier T_0 for PEDOT:PSTFSI (with DMSO) and for PEDOT:DS (with DMSO) was

determined as 354K and 138K, respectively. These values are coherent with T_0 values of 1700K [50] to 1900K [7], reported for pristine PEDOT:PSS, and of 20K to 80K [7, 52] reported for highly conducting PEDOT:PSS. The lower energy barrier for PEDOT:DS could be explained by a longer localization length, which is coherent with the increased grain size of the PEDOT rich domains [36] observed by AFM imaging. Using the Efros-Shklovski VRH model [49, 53] the localization length a was estimated from

$$T_0 = \frac{2.8e^2}{4\pi\epsilon\epsilon_0 k_B a} \tag{6.2}$$

with ϵ being the dielectric constant. With an approximated dielectric constant for the PEDOT complexes of 3.5 [54], localization lengths of 35nm and of 90nm were found for PEDOT:PSTFSI and PEDOT:DS, respectively. These calculated localization length are in good agreement with the grain sizes observed on the PEDOT:PSTFSI and PEDOT:DS film surface by AFM imaging (see figure 6.10 and figure D.5, appendix, page 230), and with the localization lengths between 33nm and 44nm in sorbitol treated PEDOT:PSS reported by Nardes *et al.* [36]. However, the bigger domain size in PEDOT:DS should enhance the macroscopic conductivity, as it has been observed, that big PEDOT rich domains were favorable for the charge transport in heterogeneous PEDOT systems [36, 37]. Therefore the lower conductivity of PEDOT:DS cannot be explained by a structural aspect, which limits the charge transport, but is related to insufficient doping. In contrast, the drastic difference in morphology is a plausible explanation for the absence of conductivity in the case of PEDOT:PMaTFSI. From figure 6.9 and figure 6.10 it can be seen, that the PEDOT:PMaTFSI complex formed micrometer size randomly shaped aggregates in dispersion and results in rough solid films without any discernable domains. TEM imaging (see figure 6.12) confirmed the three dimensional network structure of PEDOT:PMaTFSI, in which no PEDOT rich domains could be distinguished, whereas for PEDOT:PSTFSI particles of 35nm size were observed. The micro morphology can be directly linked to the flexibility of the PMaTFSI chain, which allows the polymer chains to coil and entangle. Consequently, after the PEDOT synthesis the entangled PEDOT:PMaTFSI chains are less mobile and even with the use of a co-solvent phase separation cannot take place during drying. The lack of percolation of PEDOT rich domains in the homogeneous phase hinders the charge transport and can explain the absence of conductivity of PEDOT:PMaTFSI.

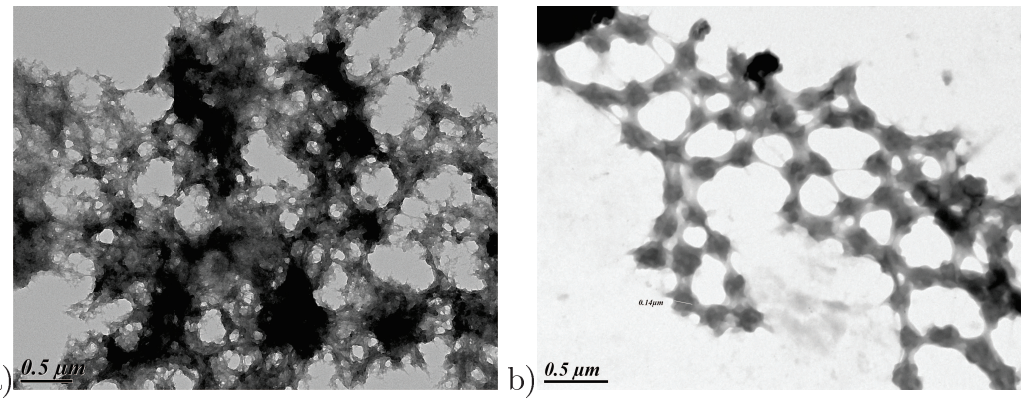

Fig. 6.12: TEM images of a)PEDOT:PMaSTFSI and b)PEDOT:PSTFSI

6.5 Conclusion

Several PEDOT:polyelectrolyte complexes, based on bissulfonylimide-type and polysaccharide-type polyelectrolytes, were synthesized by oxidative dispersion polymerization and characterized regarding their doping, morphology and opto-electronic properties. Furthermore, the relation between the polyelectrolyte characteristics such as the nature of the charged groups and the chain flexibility on the properties of the final PEDOT:polyelectrolyte complex was investigated. It was found, that PEDOT can be stabilized in aqueous dispersion with both, bissulfonylimide-type and polysaccharide-type polyelectrolytes. However, strongly acidic groups, which are not protonated in the strongly acidic environment of the EDOT polymerization, were shown to be crucial for an efficient doping of PEDOT. Interestingly, a higher density of anionic units on the polyelectrolyte or the excess of polyelectrolyte did not improve the doping. PEDOT:dextran sulfate showed the highest conductivity (15S.cm^{-1}) among all pristine PEDOT complexes. The highest absolute conductivities were obtained for PEDOT:PSS and PEDOT:PSTFSI (210S.cm^{-1}) after formulation with the high boiling point solvent DMSO. This can be explained by the high doping of PEDOT and a good stabilization of bipolarons in PEDOT:PSS and PEDOT:PSTFSI, which seemed to be related to the high rigidity of the styrenic polyelectrolyte backbone. By liquid AFM nanometer sized particles, embedded in a three dimensional network of stabilizing chains, were observed. After drying, a solid film with granular morphology with a domain size of about 40nm was formed. In contrast, PEDOT complexes with polyelectrolytes with the same acid groups, but flexible backbone, showed lower doping, formed bigger particles and resulted

in films with less clearly defined domains and lower conductivity.

Furthermore, PEDOT:PSTFSI and PEDOT:DS films displayed high transparencies, with an about 30% lower absorption coefficient than PEDOT:PSS, which renders PEDOT:PSTFSI and PEDOT:DS interesting alternatives to the omnipresent PEDOT:PSS.

We can conclude, that very rigid polyelectrolytes, based on either a polysaccharide or a fully synthetic backbone, which bear highly acidic functionalities, are promising candidates for new conducting PEDOT:polyelectrolyte complexes and are therefore of interest for future studies and the development of conducting polymer inks.

Bibliography

[1] H. Do, M. Reinhard, H. Vogeler, A. Puetz, M. F. Klein, W. Schabel, A. Colsmann, and U. Lemmer, "Polymeric anodes from poly(3,4-ethylenedioxythiophene):poly(styrenesulfonate) for 3.5% efficient organic solar cells," *Thin Solid Films*, vol. 517, pp. 5900–5902, Aug. 2009.

[2] A. J. Heeger, "Semiconducting and Metallic Polymers: The Fourth Generation of Polymeric Materials (Nobel Lecture)," *Angewandte Chemie International Edition*, vol. 40, no. 14, pp. 2591–2611, 2001.

[3] F. C. Krebs, "All solution roll-to-roll processed polymer solar cells free from indium-tin-oxide and vacuum coating steps," *Organic Electronics*, vol. 10, pp. 761–768, Aug. 2009.

[4] E. Ahlswede, W. Mühleisen, M. W. bin Moh Wahi, J. Hanisch, and M. Powalla, "Highly efficient organic solar cells with printable low-cost transparent contacts," *Applied Physics Letters*, vol. 92, pp. 143307–143307–3, Apr. 2008.

[5] C. Brabec, N. Sariciftci, and J. Hummelen, "Plastic solar cells," *Advanced Funtional Materials*, vol. 11, no. 1, pp. 15–26, 2001.

[6] S. K. Hau, H.-L. Yip, J. Zou, and A. K.-Y. Jen, "Indium tin oxide-free semi-transparent inverted polymer solar cells using conducting polymer as both bottom and top electrodes," *Organic Electronics*, vol. 10, pp. 1401–1407, Nov. 2009.

[7] Y. Xia, K. Sun, and J. Ouyang, "Solution-Processed Metallic Conducting Polymer Films as Transparent Electrode of Optoelectronic Devices," *Advanced Materials*, vol. 24, pp. 2436–2440, May 2012.

[8] Y. Kim, J. Lee, S. Hofmann, M. Gather, L. Müller-Meskamp, and K. Leo, "Achieving high efficiency and improved stability in ITO-free transparent organic light-emitting diodes with conductive polymer electrodes," *Advanced Functional Materials*, vol. 23, no. 30, pp. 3763–3769, 2013.

[9] L. Groenendaal, F. Jonas, D. Freitag, H. Pielartzik, and J. R. Reynolds, "Poly(3,4-ethylenedioxythiophene) and Its Derivatives: Past, Present, and Future," *Advanced Materials*, vol. 12, pp. 481–494, Apr. 2000.

[10] A. K. Havare, M. Can, S. Demic, M. Kus, and S. Icli, "The performance of OLEDs based on sorbitol doped PEDOT:PSS," *Synthetic Metals*, vol. 161, pp. 2734–2738, Jan. 2012.

[11] A. Argun, A. Cirpan, and J. Reynolds, "The First Truly All-Polymer Electrochromic Devices," *Advanced Materials*, vol. 15, pp. 1338–1341, Aug. 2003.

[12] J. Kawahara, P. A. Ersman, I. Engquist, and M. Berggren, "Improving the color switch contrast in PEDOT:PSS-based electrochromic displays," *Organic Electronics*, vol. 13, pp. 469–474, Mar. 2012.

[13] D. Khodagholy, J. Rivnay, M. Sessolo, M. Gurfinkel, P. Leleux, L. H. Jimison, E. Stavrinidou, T. Herve, S. Sanaur, R. M. Owens, and G. G. Malliaras, "High transconductance organic electrochemical transistors," *Nature Communications*, vol. 4, July 2013.

[14] S. Inal, J. Rivnay, A. I. Hofmann, I. Uguz, M. Mumtaz, D. Katsigiannopoulos, C. Brochon, E. Cloutet, G. Hadziioannou, and G. G. Malliaras, "Organic electrochemical transistors based on PEDOT with different anionic polyelectrolyte dopants," *Journal of Polymer Science Part B: Polymer Physics*, vol. 54, pp. 147–151, Oct. 2015.

[15] D. Khodagholy, T. Doublet, P. Quilichini, M. Gurfinkel, P. Leleux, A. Ghestem, E. Ismailova, T. Hervé, S. Sanaur, C. Bernard, and G. G. Malliaras, "In vivo recordings of brain activity using organic transistors," *Nature Communications*, vol. 4, p. 1575, Mar. 2013.

[16] M. Berggren and A. Richter-Dahlfors, "Organic Bioelectronics," *Advanced Materials*, vol. 19, pp. 3201–3213, Oct. 2007.

[17] A. N. Round, N. M. Rigby, A. J. MacDougall, and V. J. Morris, "A new view of pectin structure revealed by acid hydrolysis and atomic force microscopy," *Carbohydrate Research*, vol. 345, pp. 487–497, Feb. 2010.

[18] V. Dave, M. Tamagno, B. Focher, and E. Marsano, "Hyaluronic acid-(hydroxypropyl) cellulose blends: A solution and solid state study," *Macromolecules*, vol. 28, no. 10, pp. 3531–3539, 1995.

[19] M. K. Cowman and S. Matsuoka, "Experimental approaches to hyaluronan structure," *Carbohydrate Research*, vol. 340, pp. 791–809, Apr. 2005.

[20] A. I. Hofmann, W. T. T. Smaal, M. Mumtaz, D. Katsigiannopoulos, C. Brochon, F. Schütze, O. R. Hild, E. Cloutet, and G. Hadziioannou, "An Alternative Anionic Polyelectrolyte for Aqueous PEDOT Dispersions: Toward Printable Transparent Electrodes," *Angewandte Chemie International Edition*, pp. 8506–8510, June 2015.

[21] D. G. Harman, R. Gorkin, L. Stevens, B. Thompson, K. Wagner, B. Weng, J. H. Chung, M. in het Panhuis, and G. G. Wallace, "Poly(3,4-ethylenedioxythiophene):dextran sulfate (PEDOT:DS) – A highly processable conductive organic biopolymer," *Acta Biomaterialia*, vol. 14, pp. 33–42, Mar. 2015.

[22] M. Iijima, K. Nakamura, T. Hatakeyama, and H. Hatakeyama, "Phase transition of pectin with sorbed water," *Carbohydrate Polymers*, vol. 41, pp. 101–106, Jan. 2000.

[23] J. Hwang, D. B. Tanner, I. Schwendeman, and J. R. Reynolds, "Optical properties of nondegenerate ground-state polymers: Three dioxythiophene-based conjugated polymers," *Physical Review B*, vol. 67, Mar. 2003.

[24] N. Massonnet, A. Carella, O. Jaudouin, P. Rannou, G. Laval, C. Celle, and J.-P. Simonato, "Improvement of the Seebeck coefficient of PEDOT:PSS by chemical reduction combined with a novel method for its transfer using free-standing thin films," *Journal of Materials Chemistry C*, vol. 2, pp. 1278–1283, Jan. 2014.

[25] S. Garreau, G. Louarn, J. P. Buisson, G. Froyer, and S. Lefrant, "In Situ Spectroelectrochemical Raman Studies of Poly(3,4-ethylenedioxythiophene) (PEDT)," *Macromolecules*, vol. 32, pp. 6807–6812, Oct. 1999.

[26] S. G. Im and K. K. Gleason, "Systematic Control of the Electrical Conductivity of Poly(3,4-ethylenedioxythiophene) via Oxidative Chemical Vapor Deposition," *Macromolecules*, vol. 40, pp. 6552–6556, Sept. 2007.

[27] J. Ouyang, Q. Xu, C.-W. Chu, Y. Yang, G. Li, and J. Shinar, "On the mechanism of conductivity enhancement in poly(3,4-ethylenedioxythiophene):poly(styrene sulfonate) film through solvent treatment," *Polymer*, vol. 45, pp. 8443–8450, Nov. 2004.

[28] W. W. Chiu, J. Travaš-Sejdić, R. P. Cooney, and G. A. Bowmaker, "Spectroscopic and conductivity studies of doping in chemically synthesized poly(3,4-ethylenedioxythiophene)," *Synthetic Metals*, vol. 155, pp. 80–88, Oct. 2005.

[29] T. A. Skotheim, *Handbook of Conducting Polymers, Second Edition,*. CRC Press, Nov. 1997.

[30] A. Dkhissi, D. Beljonne, R. Lazzaroni, F. Louwet, L. Groenendaal, and J. L. Brédas, "Density functional theory and Hartree–Fock studies of the geometric and electronic structure of neutral and doped ethylenedioxythiophene (EDOT) oligomers," *International Journal of Quantum Chemistry*, vol. 91, pp. 517–523, Jan. 2003.

[31] K. Kunal, C. G. Robertson, S. Pawlus, S. F. Hahn, and A. P. Sokolov, "Role of Chemical Structure in Fragility of Polymers: A Qualitative Picture," *Macromolecules*, vol. 41, pp. 7232–7238, Oct. 2008.

[32] B. Jachimska, T. Jasiński, P. Warszyński, and Z. Adamczyk, "Conformations of poly(allylamine hydrochloride) in electrolyte solutions: Experimental measurements and theoretical modeling," *Colloids and Surfaces A: Physicochemical and Engineering Aspects*, vol. 355, pp. 7–15, Feb. 2010.

[33] Z. Adamczyk, B. Jachimska, T. Jasiński, P. Warszyński, and M. Wasilewska, "Structure of poly (sodium 4-styrenesulfonate) (PSS) in electrolyte solutions: Theoretical modeling and measurements," *Colloids and Surfaces A: Physicochemical and Engineering Aspects*, vol. 343, pp. 96–103, July 2009.

[34] Z. Adamczyk, A. Bratek, B. Jachimska, T. Jasiński, and P. Warszyński, "Structure of Poly(acrylic acid) in Electrolyte Solutions Determined from Simulations and Viscosity Measurements," *The Journal of Physical Chemistry B*, vol. 110, pp. 22426–22435, Nov. 2006.

[35] L. Wang and H. Yu, "Chain conformation of linear polyelectrolyte in salt solutions: sodium poly (styrenesulfonate) in potassium chloride and sodium chloride," *Macromolecules*, vol. 21, no. 12, pp. 3498–3501, 1988.

[36] A. M. Nardes, R. A. J. Janssen, and M. Kemerink, "A Morphological Model for the Solvent-Enhanced Conductivity of PEDOT:PSS Thin Films," *Advanced Functional Materials*, vol. 18, pp. 865–871, Mar. 2008.

[37] J. Rivnay, S. Inal, B. A. Collins, M. Sessolo, E. Stavrinidou, X. Strakosas, C. Tassone, D. M. Delongchamp, and G. G. Malliaras, "Structural control of mixed ionic and electronic transport in conducting polymers," *Nature Communications*, vol. 7, p. 11287, Apr. 2016.

[38] T. Takano, H. Masunaga, A. Fujiwara, H. Okuzaki, and T. Sasaki, "PEDOT Nanocrystal in Highly Conductive PEDOT:PSS Polymer Films," *Macromolecules*, vol. 45, pp. 3859–3865, May 2012.

[39] J. Zhou, D. H. Anjum, G. Lubineau, E. Q. Li, and S. T. Thoroddsen, "Unraveling the Order and Disorder in Poly(3,4-ethylenedioxythiophene)/Poly(styrenesulfonate) Nanofilms," *Macromolecules*, vol. 48, pp. 5688–5696, Aug. 2015.

[40] T. Stöcker, A. Köhler, and R. Moos, "Why does the electrical conductivity in PEDOT:PSS decrease with PSS content? A study combining thermoelectric measurements with impedance spectroscopy," *Journal of Polymer Science Part B: Polymer Physics*, vol. 50, pp. 976–983, July 2012.

[41] S. Jönsson, J. Birgerson, X. Crispin, G. Greczynski, W. Osikowicz, A. Denier van der Gon, W. Salaneck, and M. Fahlman, "The effects of solvents on the morphology and sheet resistance in poly(3,4-ethylenedioxythiophene)–polystyrenesulfonic acid (PEDOT–PSS) films," *Synthetic Metals*, vol. 139, pp. 1–10, Aug. 2003.

[42] X. Crispin, S. Marciniak, W. Osikowicz, G. Zotti, A. W. D. van der Gon, F. Louwet, M. Fahlman, L. Groenendaal, F. De Schryver, and W. R. Salaneck, "Conductivity, morphology, interfacial chemistry, and stability of poly(3,4-ethylene dioxythiophene)–poly(styrene sulfonate): A photoelectron spectroscopy study," *Journal of Polymer Science Part B: Polymer Physics*, vol. 41, pp. 2561–2583, Nov. 2003.

[43] S. Timpanaro, M. Kemerink, F. J. Touwslager, M. M. De Kok, and S. Schrader, "Morphology and conductivity of PEDOT/PSS films studied by scanning–tunneling microscopy," *Chemical Physics Letters*, vol. 394, pp. 339–343, Aug. 2004.

[44] L. Ouyang, C. Musumeci, M. J. Jafari, T. Ederth, and O. Inganäs, "Imaging the Phase Separation Between PEDOT and Polyelectrolytes During Processing of Highly Conductive PEDOT:PSS Films," *ACS Applied Materials & Interfaces*, p. 150825124148009, Aug. 2015.

[45] C. M. Palumbiny, C. Heller, C. J. Schaffer, V. Körstgens, G. Santoro, S. V. Roth, and P. Müller-Buschbaum, "Molecular Reorientation and Structural Changes in Cosolvent-Treated Highly Conductive PEDOT:PSS Electrodes for Flexible Indium Tin Oxide-Free Organic Electronics," *The Journal of Physical Chemistry C*, vol. 118, pp. 13598–13606, June 2014.

[46] C. M. Palumbiny, F. Liu, T. P. Russell, A. Hexemer, C. Wang, and P. Müller-Buschbaum, "The Crystallization of PEDOT:PSS Polymeric Electrodes Probed In Situ during Printing," *Advanced Materials*, vol. 27, pp. 3391–3397, June 2015.

[47] Q. Wei, M. Mukaida, Y. Naitoh, and T. Ishida, "Morphological Change and Mobility Enhancement in PEDOT:PSS by Adding Co-solvents," *Advanced Materials*, vol. 25, no. 20, pp. 2831–2836, 2013.

[48] N. F. Mott and E. A. Davis, *Electronic processes in non-crystalline materials*. Oxford: Clarendon, 1979.

[49] B. I. Shklovskii and A. L. Efros, *Electronic Properties of Doped Semiconductors*, vol. 45. Springer, 2013. Google-Books-ID: OZXsCAAAQBAJ.

[50] J. Y. Kim, J. H. Jung, D. E. Lee, and J. Joo, "Enhancement of electrical conductivity of poly(3,4-ethylenedioxythiophene)/poly(4-styrenesulfonate) by a change of solvents," *Synthetic Metals*, vol. 126, pp. 311–316, Feb. 2002.

[51] C. S. S. Sangeeth, M. Jaiswal, and R. Menon, "Charge transport in transparent conductors: A comparison," *Journal of Applied Physics*, vol. 105, no. 6, p. 063713, 2009.

[52] Z. Yu, Y. Xia, D. Du, and J. Ouyang, "PEDOT:PSS Films with Metallic Conductivity through a Treatment with Common Organic Solutions of Organic Salts and Their Application as a Transparent Electrode of Polymer Solar Cells," *ACS Applied Materials & Interfaces*, vol. 8, pp. 11629–11638, May 2016.

[53] D. Talukdar, U. N. Nandi, K. K. Bardhan, C. C. Bof Bufon, T. Heinzel, A. De, and C. D. Mukherjee, "Nonlinearity exponents in lightly doped conducting polymers," *Physical Review B*, vol. 84, Aug. 2011.

[54] M. R. Abidian and D. C. Martin, "Experimental and theoretical characterization of implantable neural microelectrodes modified with conducting polymer nanotubes," *Biomaterials*, vol. 29, pp. 1273–1283, Mar. 2008.

General Conclusion and Perspectives

In this work several conducting aqueous PEDOT:polyelectrolyte dispersions, based on anionic polysaccharides and on synthetic polyelectrolytes bearing a bissulfonylimide functionality, have been synthesized and characterized regarding their doping, complex morphology, rheology and opto-electronic properties.

The systematic study of the different PEDOT:polyelectrolyte complexes allowed to relate the polyelectrolyte characteristics such as the nature of the charged groups and the chain flexibility on the properties of the final PEDOT:polyelectrolyte complex. It was found, that high molar mass polyelectrolytes with a rigid backbone and bearing highly acidic groups, resulted in the most conducting PEDOT:polyelectrolyte complexes. By using the anionic polyelectrolyte poly(4- styrenetrifluoromethyl(bissulfonylimide) (PSTFSI) as template polymer for poly (3,4-ethylenedioxythiophene) (PEDOT), colloidally and chemically stable dispersions were obtained. The PEDOT:PSTFSI dispersion displayed gel characteristics, which facilitated the processing by spin coating or doctor blading. Upon formulation with high boiling point solvents, such as DMSO, transparent films with conductivities of up to 300S.cm^{-1} and a figure of merit (FoM) of 23 were obtained. It is noteworthy, that the transparency of these PEDOT:PSTFSI systems was considerably higher than the one of PEDOT:PSS with the same composition and comparable conductivity. Therefore, PEDOT:PSTFSI is a promising candidate to replace PEDOT:PSS, particularly for applications which require extremely high transparent conducting films.

The fundamental study of the PEDOT:PSTFSI system and of various synthesis parameters allowed the definition of an optimized synthesis protocol. It was shown, that the composition of the PEDOT:PSTFSI complex had a decisive influence on the opto-electronic and rheological properties of PEDOT:PSTFSI. On one hand, the PEDOT concentration had to be high enough to allow percolation of the conducting PEDOT domains. On the other hand, at a certain PEDOT concentration a saturation of the PSTFSI template was reached, which resulted in a decrease of the conductivity and of the colloidal stability.

Furthermore, it was shown, that the counter ion of PSTFSI, the quality of the EDOT dispersion, the synthesis temperature, as well as the synthesis time had a decisive

influence on the opto-electronic properties and on the rheology of the final PEDOT:PSTFSI. The highest conductivities were obtained for PEDOT:PSTFSIH (M_W(PSTFSIH)≈350kDa) after 50 hours of polymerization at 10°C under magnetic stirring at 625rpm by using a binary oxidant system of $FeCl_3$ and $(NH_4)_2S_2O_8$ with a molar ratio between oxidants and EDOT monomer of $(NH_4)_2S_2O_8$: $FeCl_3$: EDOT ratio of 3.5 : 1 : 3.5.

Owing to its good opto-electronic properties PEDOT:PSTFSI films were successfully integrated in OPV and OLED devices, which performed as well as the reference devices or even out-performed the reference devices. Furthermore, the integration of PEDOT:PSTFSI electrodes in OECT devices confirmed the mixed ion-hole conducting properties of these films.

For future work it would be of interest to develop new PEDOT:polyelectrolyte systems based on highly acidic and rigid polyelectrolytes. A promising approach would be the functionalization of linear an rigid biopolymers with highly acidic groups, which could allow the development of cheap and highly bio-compatible conducting systems. Also the study of polyelectrolyte co-polymers could be of interest for the development of PEDOT:polyelectrolyte complexes with the objective to introduce new functionalities and properties into the complex or to reduce the acidity of the dispersion.

Taking into account, that the PEDOT:PSS synthesized in this work was outperformed by PEDOT:PSTFSI and that it displayed in the same time largely inferior opto-electronic properties to the commercial PEDOT:PSS, allows the assumption, that the opto-electronic properties of PEDOT:PSTFSI can be further increased. This could be achieved by a further optimization of the synthesis process or post-treatments, such as sonication or mechanical shearing, which alter the morphology of the dispersed complexes.

The basic rheological study on PEDOT:PSTFSI performed during this work showed, that these dispersions display interesting rheological properties, which could be of interest for fundamental studies and for their application in different processing techniques.

Experimental Details

E.1 Synthesis of PSTFSIK

The STFSI monomer was synthesized as follows: Under Ar atmosphere Oxalyl Chloride (8ml) and DMF (0.348g) were added to 160ml of dry Acetonitrile. Upon formation of a Vilsmeier-Haack complex the solution turned yellow and sodium 4-vinylbenzenesulfonate (16g) was added under vigorous stirring to the solution. After 24 hours the solution of the formed 4-styrenesulfonyl chloride in acetonitrile was filtered to remove the precipitated NaCl. In a separate reactor 32.4ml triethylamine and 11.56g trifluoromethanesulfonamide are admixed to 120ml dry acetonitrile and left under stirring. After 1 hour the triethylamine/trifluoromethanesulfonamide/acetonitrile solution was introduced under vigorous stirring into the cooled (T=0°C) 4-styrenesulfonyl chloride/acetonitrile solution in vacuum atmosphere. Thereafter the mixture was allow to warm up to room temperature and was left under stirring for 16h. The obtained monomer was transferred to dichloromethane and was washed two times with an aqueous solution of $NAHCO_3$ (4%) and one time with 1M HCl, in order to remove salts. Subsequently the dichloromehtane was removed and an ion exchange reaction in aqueous solution was performed using an excess of K_2CO_3, in order to obtain the potassium salt form STFSIK.

The PSTFSIK polyelectrolyte was synthesized by reversible addition-fragmentation chain-transfer (RAFT) polymerization by mixing, according to the target molar mass, the proper quantity of the STFSIK monomer, chain transfer agent (see figure E.1) and azobisisobutyronitrile (AIBN) in dimethylformimide. After several freeze-thaw cycles, the mixture was left to polymerize at 65°C from several hours to few weeks, depending on the molar mass that should be obtained. The polymer was ready after precipitation in tetrahydrofuran (THF), filtration, washing with THF and drying in vacuum oven at 65°C for at least one day.

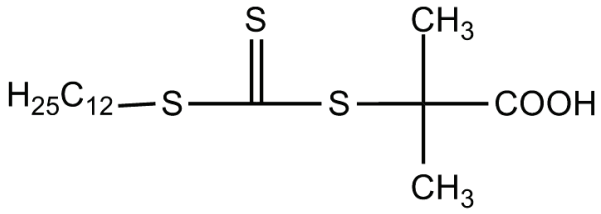

Fig. E.1: Chemical structure of the chain transfer agent used in the RAFT polymerization of STFSIK

E.2 Synthesis of PEDOT:PSTFSI and PEDOT:PSS

The PEDOT:polyelectrolyte complexes were obtained by a oxidative polymerization of EDOT in the aqueous PSTFSI solution in DI water (resistance <15MOhm). Different amounts of EDOT were dispersed in the aqueous PSTFSI solutions (PSTFSI K 9.1g.l^{-1} , PSTFSI H 8.4g.l^{-1}) under nitrogen atmosphere and vigorous stirring. For the standard synthesis $(NH_4)_2S_2O_8$ and $FeCl_3$ at a molar ratio of 3.5 were used as oxidants with a molar ratio oxidants to EDOT monomer of 2.3. After 48h at 10°C the polymer dispersions were purified using Lewatit S100KR/H and Lewatit MP62WS ion exchange resins (60mg resin per 1ml ink).

E.3 Formulation and Film Preparation

Prior to the film deposition all PEDOT:polyelectrolyte dispersions were formulated with 5%DMSO and less than 0.05wt% Zonyl FS300 fluorosurfactant (Sigma Aldrich), which improves film formation but does not influence conductivity. The films were deposited under ambient conditions by spin-coating, doctor blading or spray coating onto glass substrates, which were previously cleaned under sonication in acetone and isopropanol. The films were dried for 30min at 120°C on a hotplate under ambient conditions.

Typical parameters for spin coating (SPS-Europe Spin150): 800-2200rpm, 200-400rpm.s^{-1} for 60s.

Typical parameters for doctor blading (Erichsen coatmaster 510): blading speed 5-20mm.s^{-1}, with the gap blade-substrate being 50-120μm.

Spray coating (non commercial setup): diameter of nozzel 0.2mm, distance to substrate 20-30cm, substrate temperature 120°C, manual regulation of flux.

E.4 Characterization

Determination of the Opto-Electrronic Properties The sheet resistance was determined by the four point probe technique, using a Keithley 4200 system and by applying a voltage sweep over several orders of magnitude in order to ensure that the measurement was conducted in the ohmic regime. The film thickness was measured with a Brucker Dektak XT profilometer. The film transmittance at 550nm was determined using a Shimadzu UV3600 UV/VIS/NIR spectrometer. The Conductivity σ and the absorption coefficient a were calculated using

$$\sigma = \frac{1}{R_S d} \tag{E.3}$$

$$a = \frac{A}{d} = \frac{-log_{10}(T)}{d} \tag{E.4}$$

Temperature dependent Conductivity Measurements For the temperature dependent conductivity measurements gold electrodes (7mmx2mm, thickness 120nm, spacing 500μm) were evaporated on the PEDOT:polyelectrolyte films. The resistivity of the cooled films in the Helium cryostat was determined in the ohmic regime of the IV curves, measured with a Keithley.

Atomic Force Microscopy Atomic force microscopy (AFM Dimension FastScan, Bruker) was used in tapping mode to characterize the surface morphology of PEDOT:polyelectrolyte dry films. Silicon cantilevers (Fastscan-A) with a typical tip radius of about 5nm, a spring constant of 18N.m^{-1} and a cantilever resonance frequency of about 1.4MHz were used. To image the polyelectrolyte chains, the polymers were drop casted from very dilute solutions (0.005g.l^{-1}) onto a cleaved mica surface and dried at 40°C. AFM imaging in aqueous medium was performed using a Dimension FastScan SPM (Bruker) operated in PeakForce Tapping mode with silicon cantilevers (Fastscan-C) with a typical tip radius of 5nm, a spring constant of 0.8N.m^{-1} and a cantilever resonance frequency of about 300kHz. A droplet of polymer dispersion was deposited on freshly cleaved highly oriented pyrolytic graphite (HOPG, Ted Pella, grade ZYB) and the morphology of molecules adsorbed on HOPG surface under aqueous medium were observed.

Capillary Electrophoresis (CE) Capillary electrophoresis measurements were performed on a Wyn-CE (WynSep) instrument at a separation voltage of 15kV and at 20°C (see schematic setup in figure E.2). Fused silica capillaries (Polymicro Technologies) with an interior radius of 50μm, a total length of 45cm to 50cm distance to the detection window were used. The detection window was generated by removing of the polyimide coating. For the conditioning the new capillaries were washed with 0.5M NaOH for 20min, followed by a washing step with DI water for 10 min. Between every measurement the capillary was flushed with 0.5M NaOH, DI water and separation buffer (20mM borate buffer at pH9.2) for 1min each. The optical detector was set at 230nm or 550nm, respectively. The PEDOT:PSTFSI dispersions were diluted by a factor 20 in MiliQ water, sonicated at with pulses of 3 times 5 seconds and then filtered with a 1μ PTFE filter.

All capillary electrophoresis measurements were performed in collaboration with Professor A. Kuhn at the ISM, Université Bordeaux.

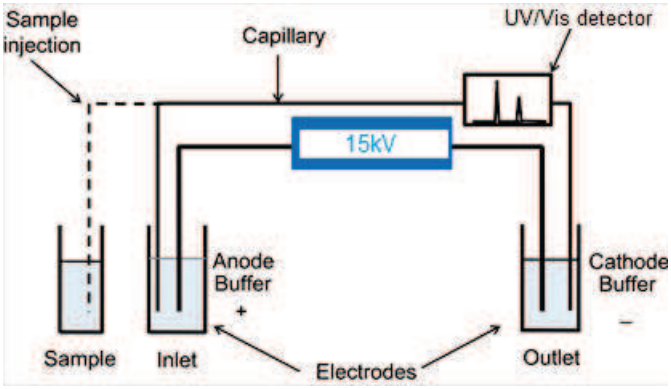

Fig. E.2: Scheme of capillary electrophoresis setup

DFT simulations Simulations on the charge distribution on PSTFSI were performed using a DFT – B3LYP/631-G*/ED3 data set and implicit water as solvent(CPCM, g09), $\Delta RT \approx 0.5$kcal/mol.

All simulations were performed by Gali S. Manoj, PhD student at LCPO, Universisté Bordeaux.

Differential Scanning Calorimetry (DSC) DSC measurements were performed under nitrogen using a Q100 from TA Instruments with a heating and cooling rates of 10°C.min^{-1}. The weight of all samples was superior to 5mg.

Dynamic Light Scattering (DLS) DLS measurements were performed using a DLS setup with a laser at λ=633nm, an AVL/CGS-3 goniometer and an AVL/ LSE-5004 detector. The scattering intensity was measured at θ=90° for four times 15s. By fitting of the measured correlation function with $g(t) = B + A_(1)e^{(-\Theta_1 t)} + A_(2)e^{(-\Theta_2 t)}$ the hydrodynamic radii R_h were obtained using the Stokes-Einstein relation $R_h = kT/6\pi\eta D$ with the viscosity η_{H_2O}= 1.0mPa.s and the diffusion coefficient D=Θ/q^2 , with Θ being the decay rate and the scattering vector $q = \frac{4\pi n}{\lambda} sin(\frac{\theta}{2})$.

Grazing Incidence Wide Angle X-Ray Scattering (GIWAXS) GIWAXS measurements were performed on the Dutch-Belgian Beamline (DUBBLE CRG), station BM26B, at the European Synchrotron Radiation Facility (ESRF), Grenoble, France. The energy of the X-rays was 10keV, the sample-to-detector distance and the angle of incidence, α_i, were set at 20cm and 0.1°, respectively. The diffracted intensity was recorded by a Frelon CCD camera and was normalized by the incident photon flux and the acquisition time (30s). Flat field, polarization, solid angle and efficiency corrections were subsequently applied to the 2D GIWAXS images. No modification of the scattering patterns were observed for five consecutive acquisitions allowing us to conclude that the samples are stable to radiation damage during measurements. The scattering vector q was defined with respect to the center of the incident beam and has a magnitude of $q = (4\pi/\lambda)sin(\theta)$, where 2θ is the scattering angle and λ is the wavelength of the X-ray beam.

Transmission Electron Microscopy (TEM) The 50 times diluted PEDOT:polyelectrolyte dispersions were allowed to dry at room temperature on Formvar coated TEM grids. Imaging was performed on a Hitachi H7650 electron transmission microscope operating at 80kV.
TEM imaging was performed at the Bordeaux Imaging Center (UMS 3420 CNRS - University of Bordeaux / Inserm US4) with the help of S. Lacomme.

UV/Vis and Raman Spectroscopy UV/Vis spectra were recorded from the dry PEDOT:polyelectrolyte films on glass with a glass reference sample for background subtraction, using a Shimadzu UV3600 UV/VIS/NIR spectrometer. Raman spectra were also measured on the dry PEDOT:polyelectrolyte samples with an excitation

wavelength of 532nm.

Raman spectroscopy was performed at the SAFIRR platform (ISM-UMR 5255 / Université Bordeaux 1) with the help of J.L. Bruneel.

Rheology Rheology measurements were performed in clean room environment at 20°C on an Anton Paar MCR 302 Rheometer using a CP50-1 cone-plate geometry with a diameter of 49.98mm, 10.2μm truncation and a cone angle of 1°. Flow curves were measured starting from low to high shear rates and back ($0.01s^{-1}$-$3000s^{-1}$-$0.01s^{-1}$). Amplitude sweeps were measured between 0.05% and 50% strain at $10rad.s^{-1}$. Frequency sweeps were performed at 0.2% and at 2% strain from $300rad.s^{-1}$ to $0.5rad.s^{-1}$.

X-ray photoelectron spectroscopy (XPS) XPS specra were recorded using an Escalab VG 200i-XL spectrometer. The measurements were performed on PEDOT:polyelectrolyte films, which were deposited on clean ITO-glass substrates. The power of the monochromatized AlKα source was 100W and a flood gun was used for charge compensation and a constant pass energy of 10eV was used. Fitting was performed using the Advantage software provided by Thermo Scientific and the spectra were referenced to the carbon peak at 284.8eV.

Transparent Electrodes in OLEDs and OPVs

Fabrication of devices:

PEDOT:PSTFSI and PEDOT:PSS electrodes of 35mm×50mm were coated on a PET substrate, purchased from OIKE, with a thickness of 175μm and a water permeability of 10^{-3} g.m^2 per day in a clean room class 10 000. Transparency of films between 75% and 85% with a FoM of 12±2. Laser patterning of the polymer electrodes using a 3D-Micromac microSTRUCT ps355 laser tool, followed by printing of the metallization and a passivation layer (printing tool EKRA X4 Professional) and subsequent drying at 110°C for one hour. The OLED structures were deposited using a Sunicel200 cluster system and the OPV structures were fabricated in the Bestec system. Figure E.3 shows the scheme of the standard test layouts with four devices per substrate with a surface area of 14.9 mm^2 for each device. As final step the devices were encapsulated by manual lamination of a self sticking barrier foil on both sides of the devices. The yield of functional devices for the white OLED stacks for PEDOT:PSTFSI and PEDOT:PSS electrodes was 100% out of six.

The deposition and characterization of the PEDOT:PSTFSI transparent electrodes was done in the LCPO (University of Bordeaux, CNRS UMR5629, INP Bordeaux) in Pessac, France. All device fabrication and characterization was performed at the Fraunhofer Institue for Organic Electronics, Dresden, Germany.

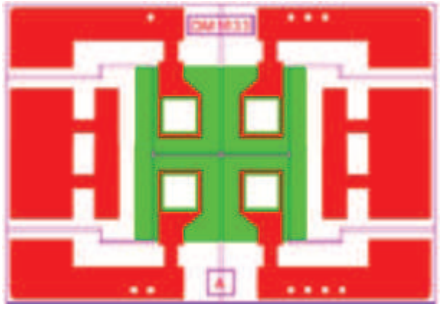

Figure E.3: Test layout of OLED and OPV devices consisting of four devices with a surface area of 14.99mm^2 each

Mixed Electron-Ion Conductor in OECTs

Materials and Device Preparation: PEDOT:PSS PH1000 was purchased from H.C. Stark. PEDOT:PSTFSI and PEDOT:PMaTFSI were synthesized as described in section 2.3. On a glass substrate transistors with gold interconnects and gold source and drain electrodes were patterned by photolithography. In a following step a parylene-c layer was deposited by vapour polymerization in order to insulate the interconnects from the electrolyte. The insulating parylene layer and the active channel were simultaneously patterned using a second, sacrificial parylene layer. In order to obtain homogeneous, conducting PEDOT:polyelectrolyte films, which resist to the immersion in an aqueous electrolyte, the PEDOT:polyelectrolyte inks were formulated with 0.04wt% of the surfactant Zonyl, 5vol% DMSO and 1wt% of the cross linking agent glycidoxypropyltrimethoxysilane (GOPS). In order to determine the conductivity of the PEDOT:polyelectrolyte systems, films were prepared on glass substrates under the same conditions as the OECT devices. As gate electrode a Ag/AgCl pellet was used, which was immersed in the aqueous 0.1M NaCl solution, which served as electrolyte.

Device Characterization: The IV-characteristics were measured with a National Instruments PXIe-1062Q system. An NI-PXI-4071 digital multimeter was used to measure drain current, and a NI-PXI 6289 measured drain and gate voltage. All the measurements were triggered through the built-in PXI architecture. The recorded signals were saved and analyzed using customized LabVIEW software.

Swelling measurements: The swelling capacity of the PEDOT:polyelectrolyte materials was studied using a quartz crystal microbalance with dissipation module and a q-sense E4 system. PEDOT:polyelectrolyte films were deposited on the quartz crystal sensors and immersed in deionized water for an extended period. The sample chamber containing an uncoated quartz crystal as reference was flushed with deionized water at a flow rate of 30ml.min^{-1} for 100min. The water uptake results in a change of the frequency and dissipation, which can be related to mass coupled to the quartz crystal. By modelling the drop in vibration frequency caused by water uptake using the Sauerbrey relation, the change in thickness of the PEDOT:polyelectrolyte films due to the swelling can be estimated. The percentage of swelling was calculated by relating the

increase in film thickness to the initial film thickness.

Ion transport measurements: Ion transport measurements were performed as described by Stavrinidou *et al.*. The PEDOT:polyelectrolyte dispersions were spin cast onto parylene coated glass substrates and an Au contact was evaporated on one side of the film. Subsequently 4μm thick layer of SU-8 was deposited on top, which served as ion barrier. By photolithography a well was created and filled with 0.01M KCl electrolyte solution, in which an Ag/AgCl counter electrode was immersed. While applying a positive bias of 1V at the Ag/AgCl electrode, the current flow through the film and the color changes of the film, associated with the propagation of the dedoping front, were recorded simultaneously. The color change was measured using an inverted Carl Zeiss Axio Observer Z1 in the bright field mode. Image reduction and analysis was performed using customized MATLAB tools.

For more experimental details see Inal *et al.* [14]. *All experiments were performed at the Center of Microelectronics of Provence CMP-EMSE (Gardanne, France), in collaboration with the group of Professor G. Malliaras.*

Appendices

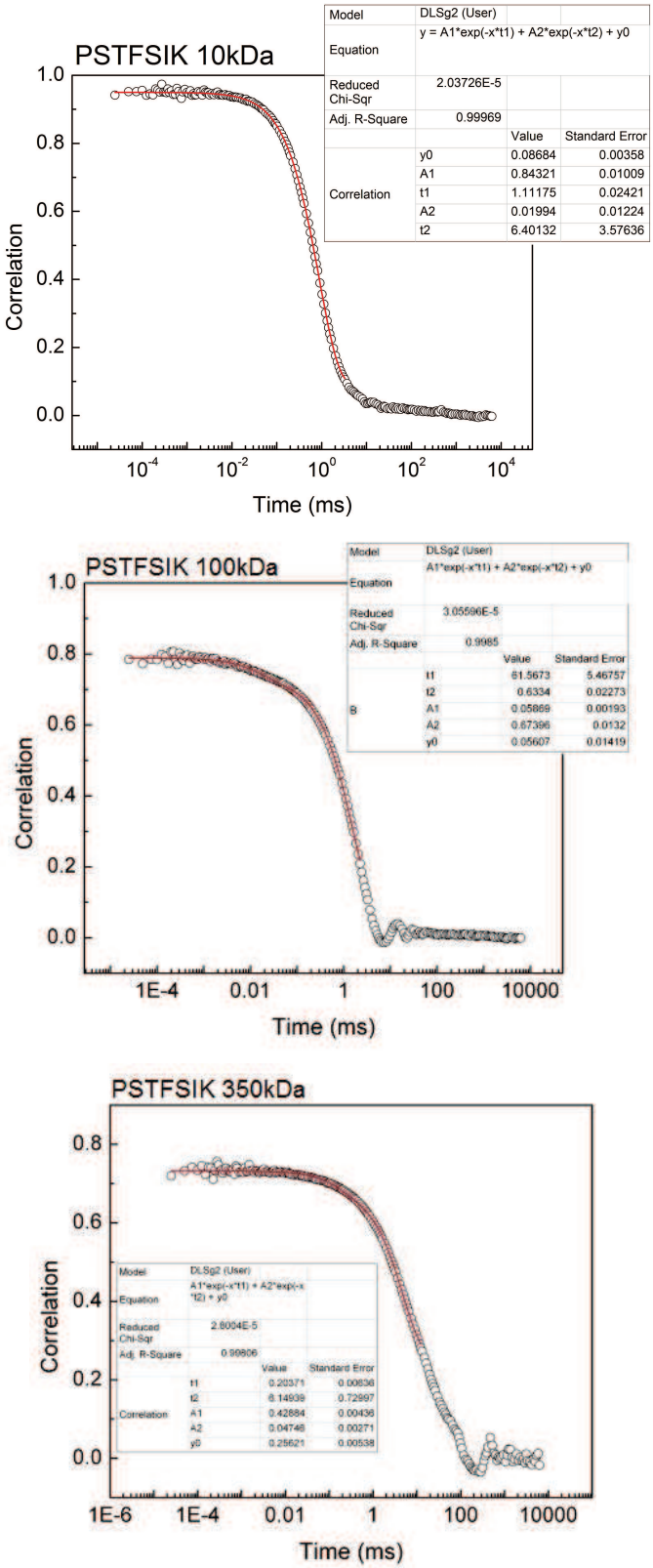

Fig. A.1: DLS correlation function of PSTFSIK in aqueous solution ($15g.l^{-1}$) for M_W(PSTFSIK)=10kDa, 100kDa and 350kDa

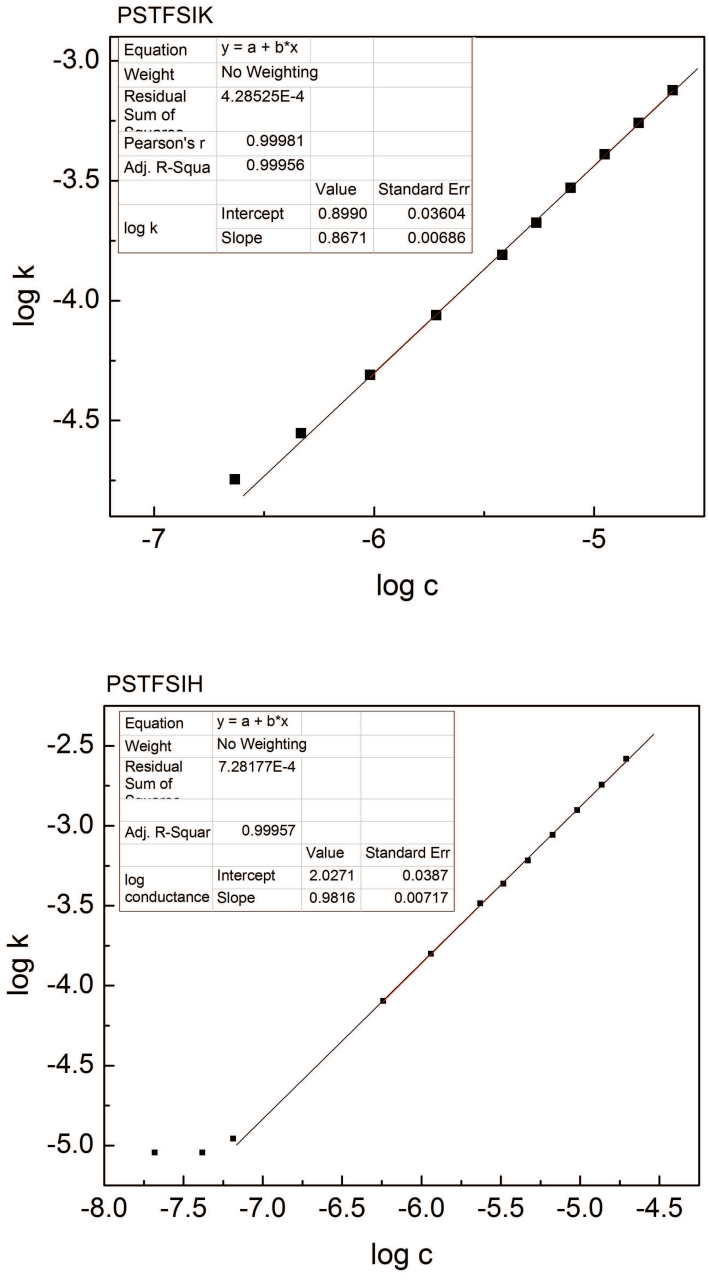

Fig. A.2: Logarithmus of the conductance k vs logarithmus of the molar STFSIX concentration with fit of the linear regime

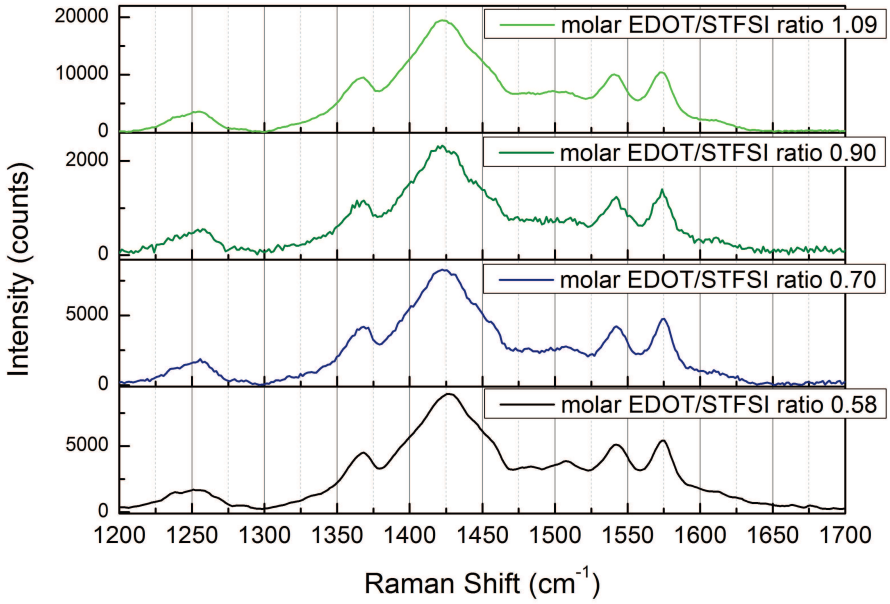

Fig. A.3: Raman spectra of PEDOT:PSTFSI as a function of the molar EDOT to STFSI ratio, synthesis under N_2, magnetic stirring 6250rpm, M_W(PSTFSIK)=350kDa

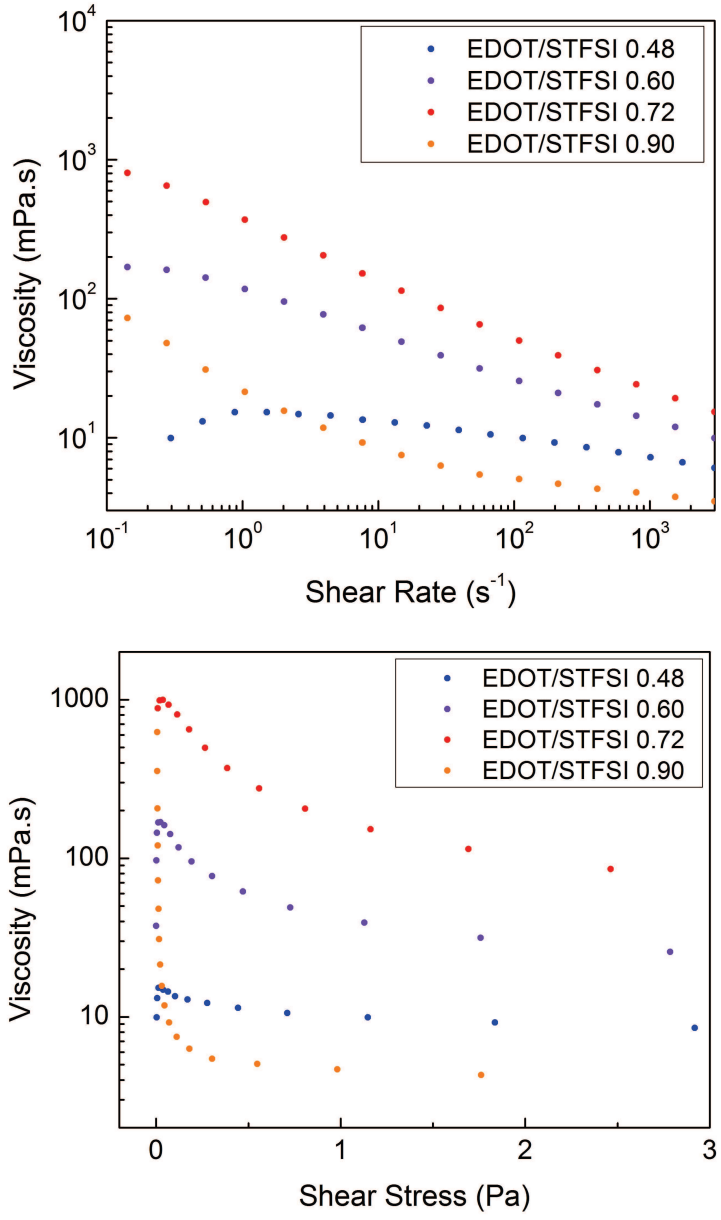

Fig. A.4: Flow curve (left) and viscosity as a function of the shear stress of PEDOT:PSTFSI with different EDOT to STFSI ratios, stirring at 55rpm

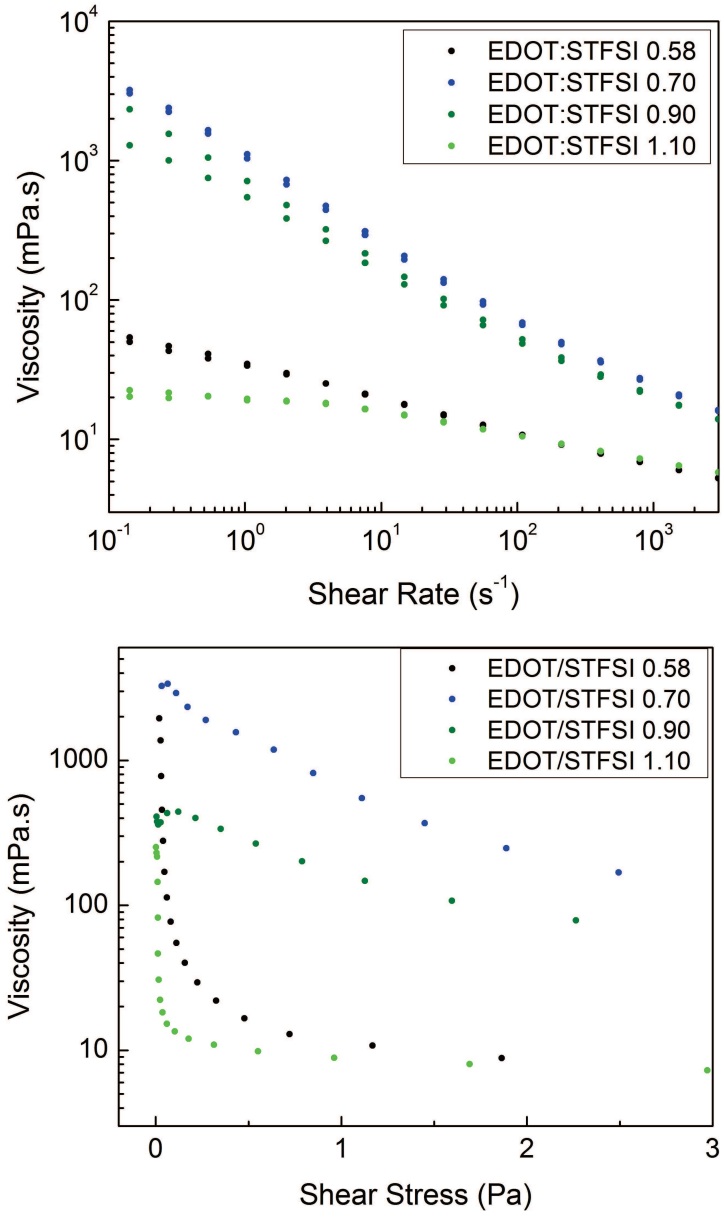

Fig. A.5: Flow curve (left) and viscosity as a function of the shear stress of PEDOT:PSTFSI with different EDOT to STFSI ratios, stirring at 625rpm

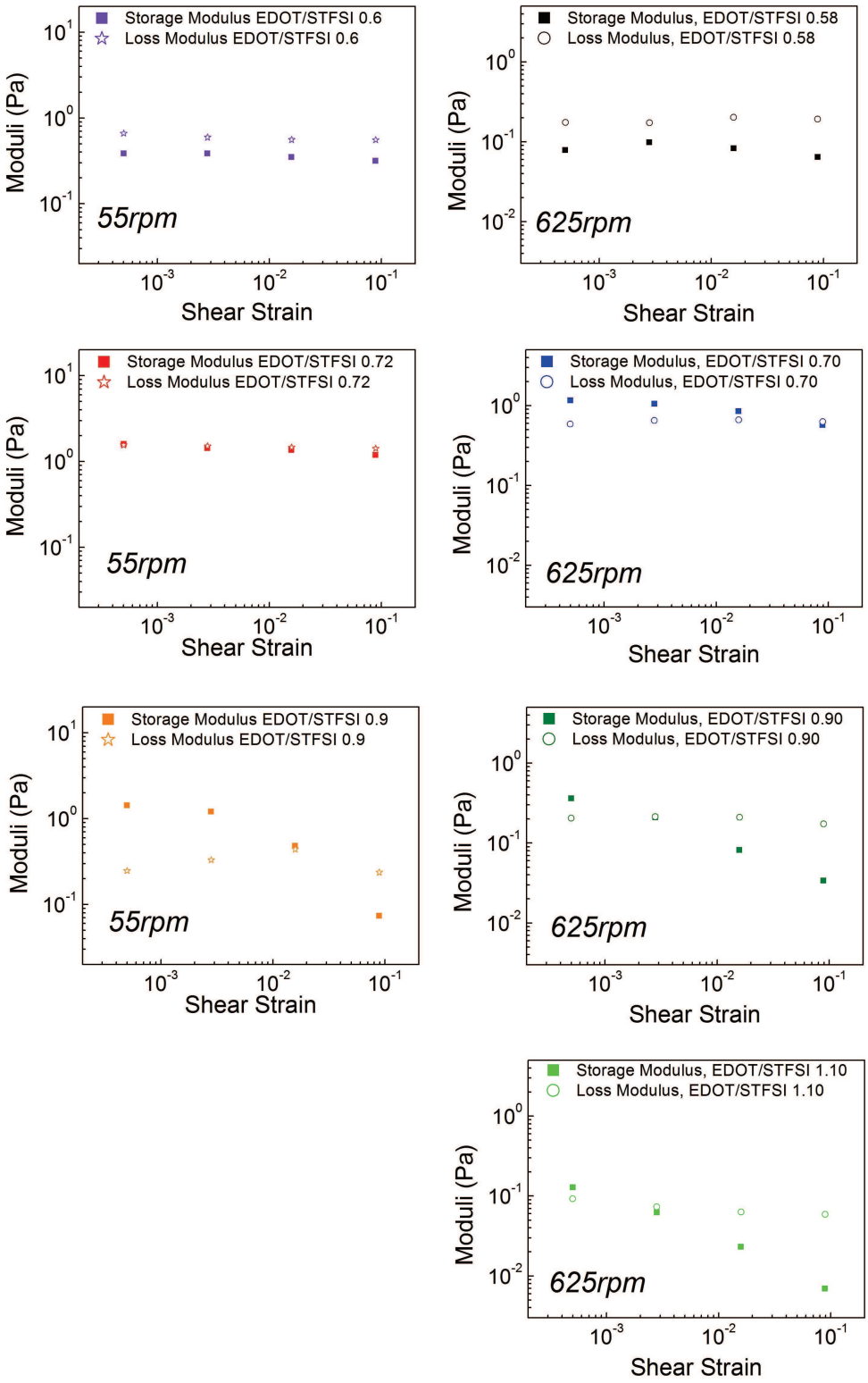

Fig. A.6: Storage and Loss Moduli as a function of shear strain at 10rad.s^{-1} of PEDOT:PSTFSI with different EDOT to STFSI ratios and stirring at 55rpm and at 625rpm

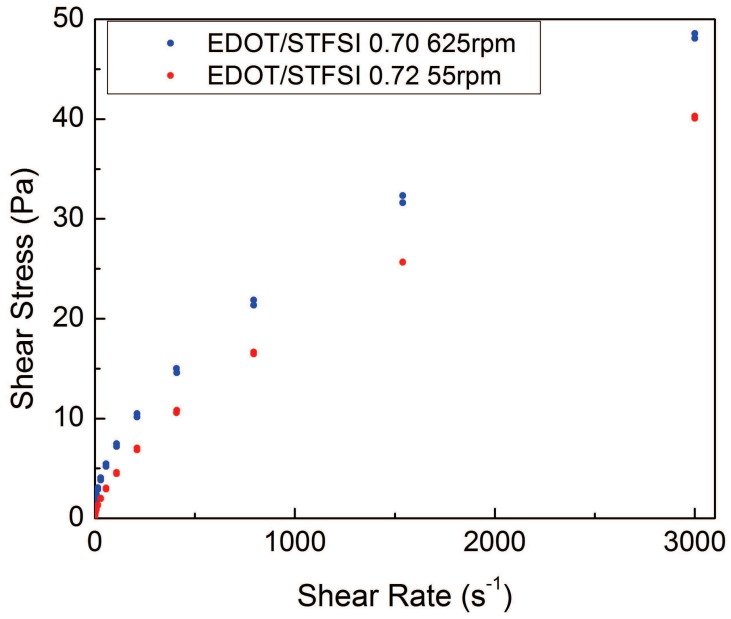

Fig. A.7: Shear stress as a function of the shear rate of PEDOT:PSTFSI with an EDOT to STFSI ratio of 0.7, stirring at 55rpm or 625rpm

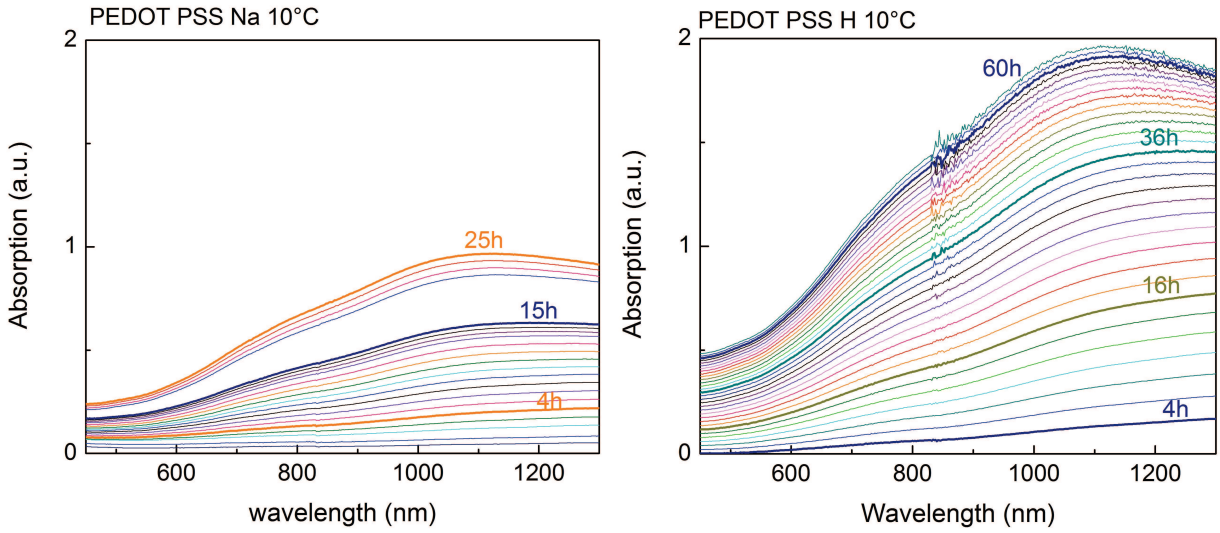

Fig. A.8: UV/Vis absorption during the EDOT polymerization in PEDOT:PSSNa and PEDOT:PSSH in dilute dispersion at 10°C

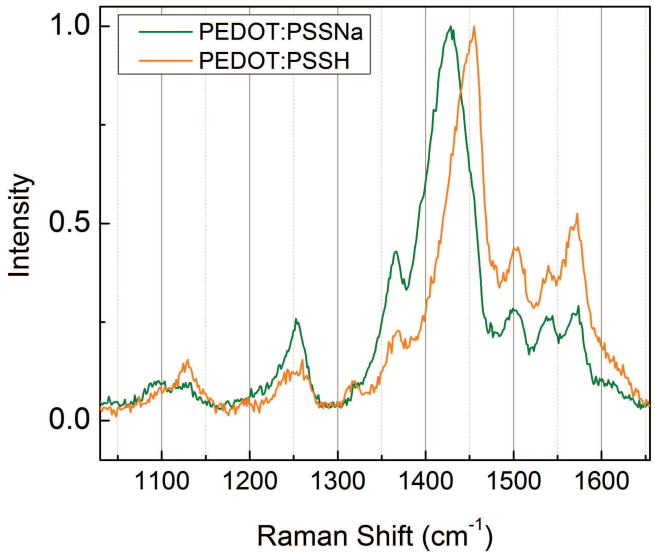

Fig. A.9: Raman spectrum of PEDOT:PSSNa and PEDOT:PSSH with excitation wavelength 532nm

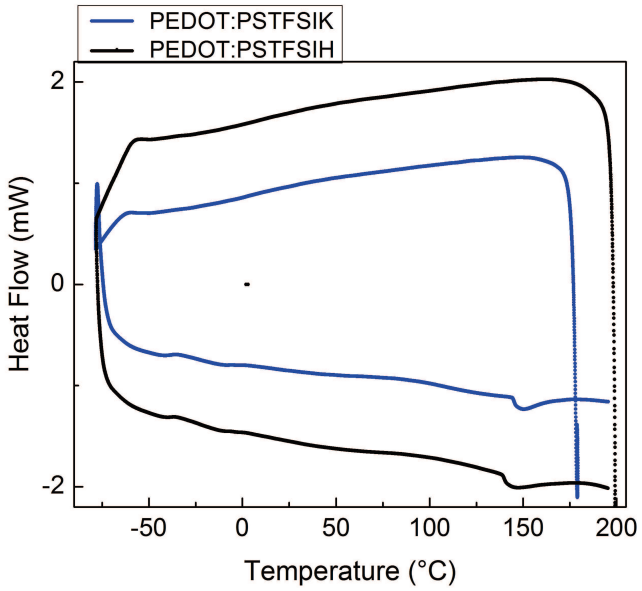

Fig. A.10: DSC data of PEDOT:PSTFSIK and PEDOT:PSTFSIH powder obtained from PEDOT:PSTFSI dispersions containing 5% DMSO co-solvent

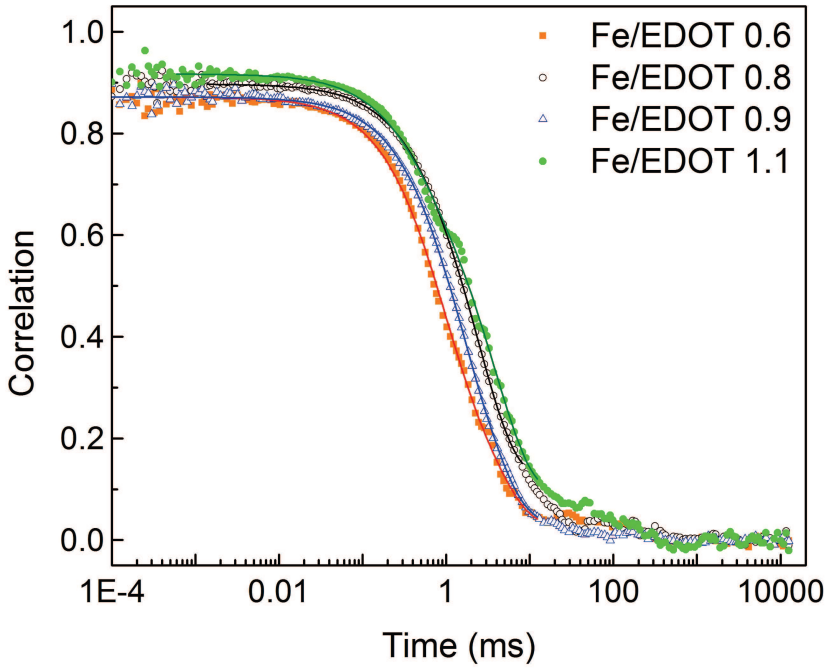

Fig. A.11: Correlation function of DLS measurements of PEDOT:PSTFSI dispersions synthesized with different concentrations of $Fe(Tos)_3$

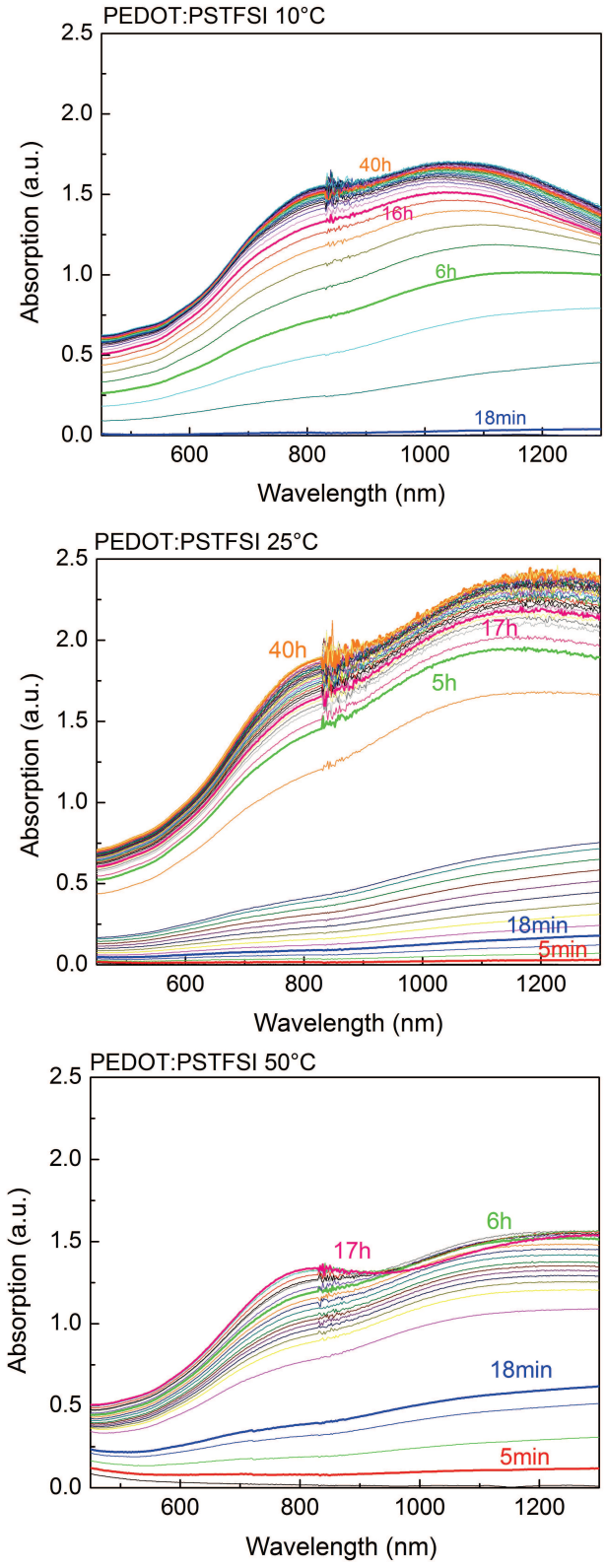

Fig. A.12: UV/Vis monitoring of the EDOT polimerization process at 10°C, 25°C and at 50°C

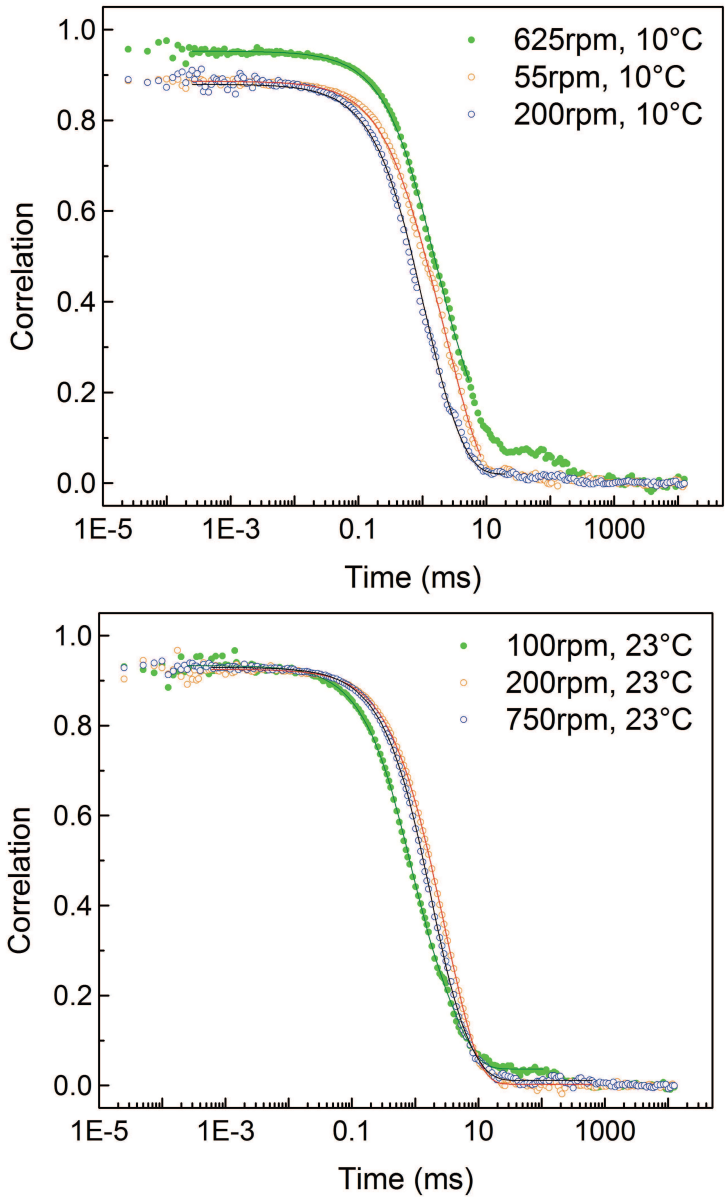

Fig. A.13: Correlation function of DLS measurements of PEDOT:PSTFSI dispersions synthesized at different temperatures and stirring speeds, molar ratio EDOT/STFSI=0.6

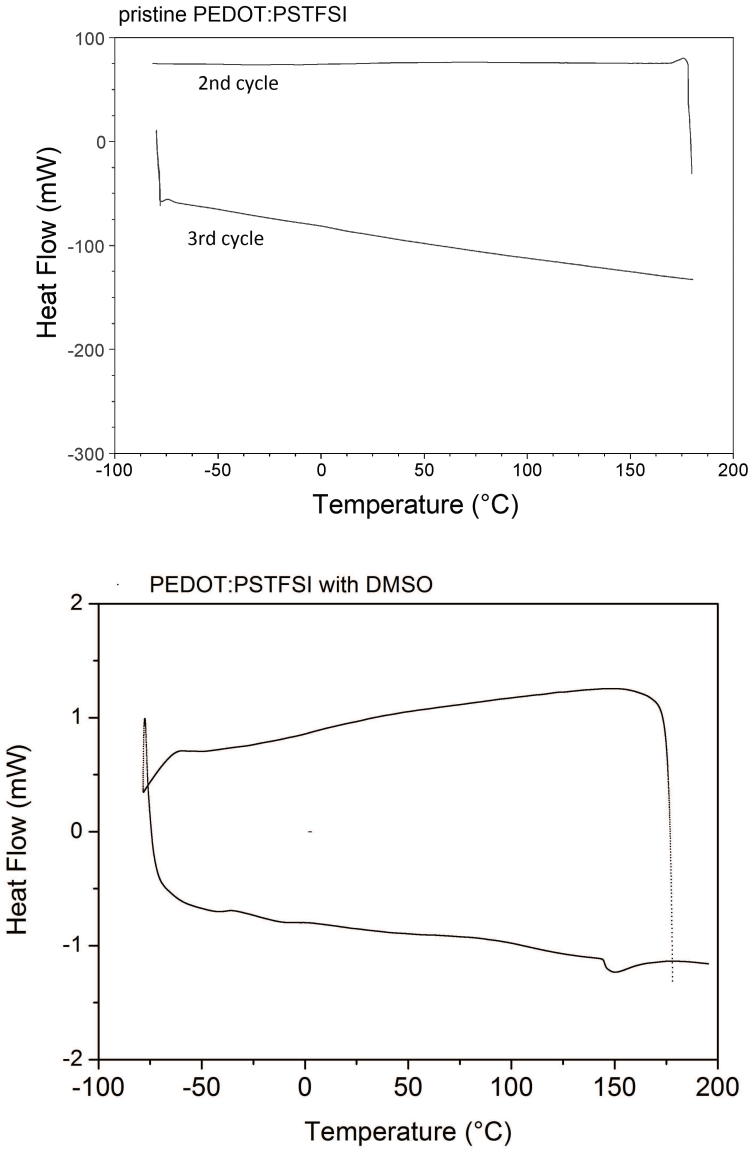

Fig. B.1: DSC analysis of pristine PEDOT:PSTFSI (top) and of PEDOT:PSTFSI with 5% DMSO co-solvent (bottom), the latter showing the melting and evaporation of residual DMSO

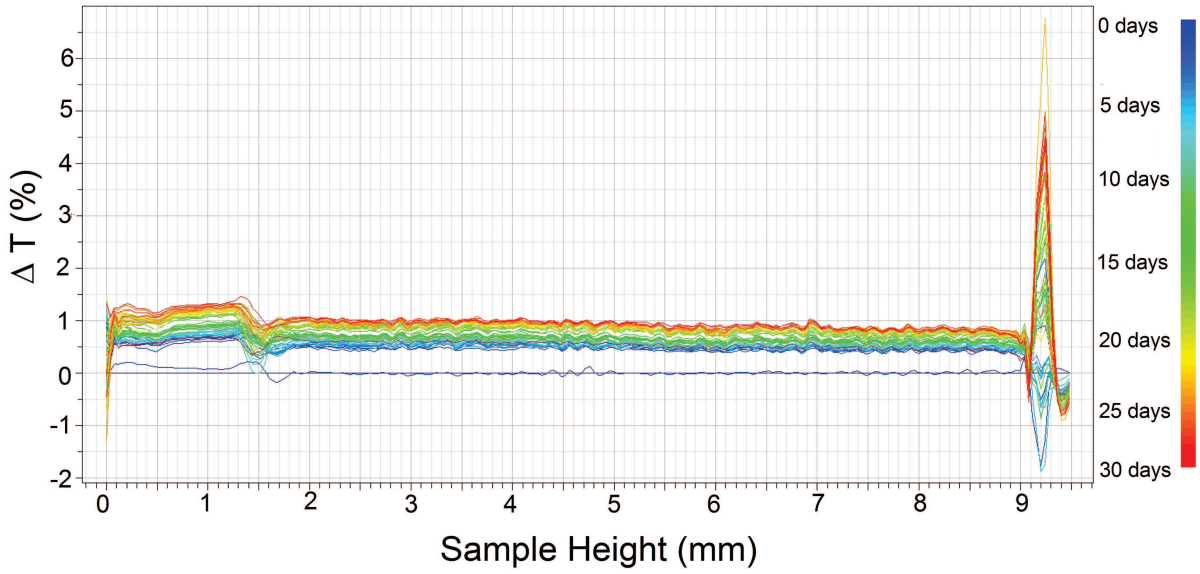

Fig. C.1: Change in transmitance of a PEDOT:PSTFSI sample as a function of time, monitored in a Turbiscan at 30°C for 4 weeks

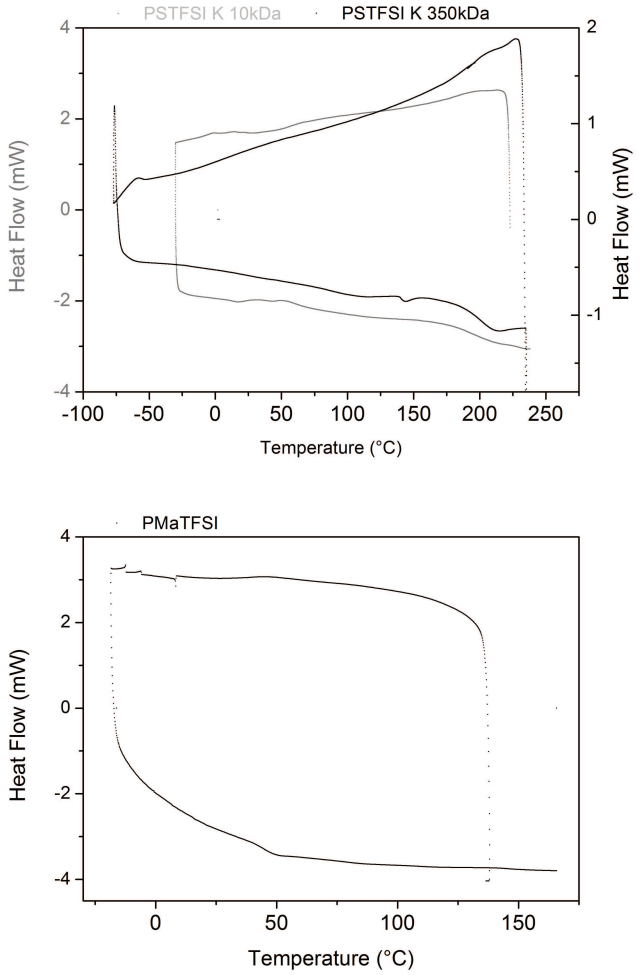

Fig. D.1: DSC curve of PSTFSIK 10kDa and 350kDa and of PMaTFSI

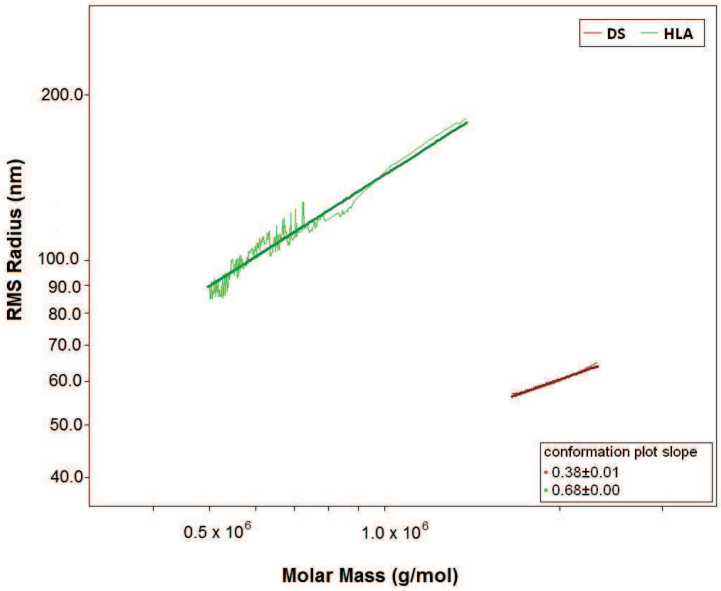

Fig. D.2: Conformation plot of dextran sulfate and hyaluronic acid, determined by size exclusion chromatography

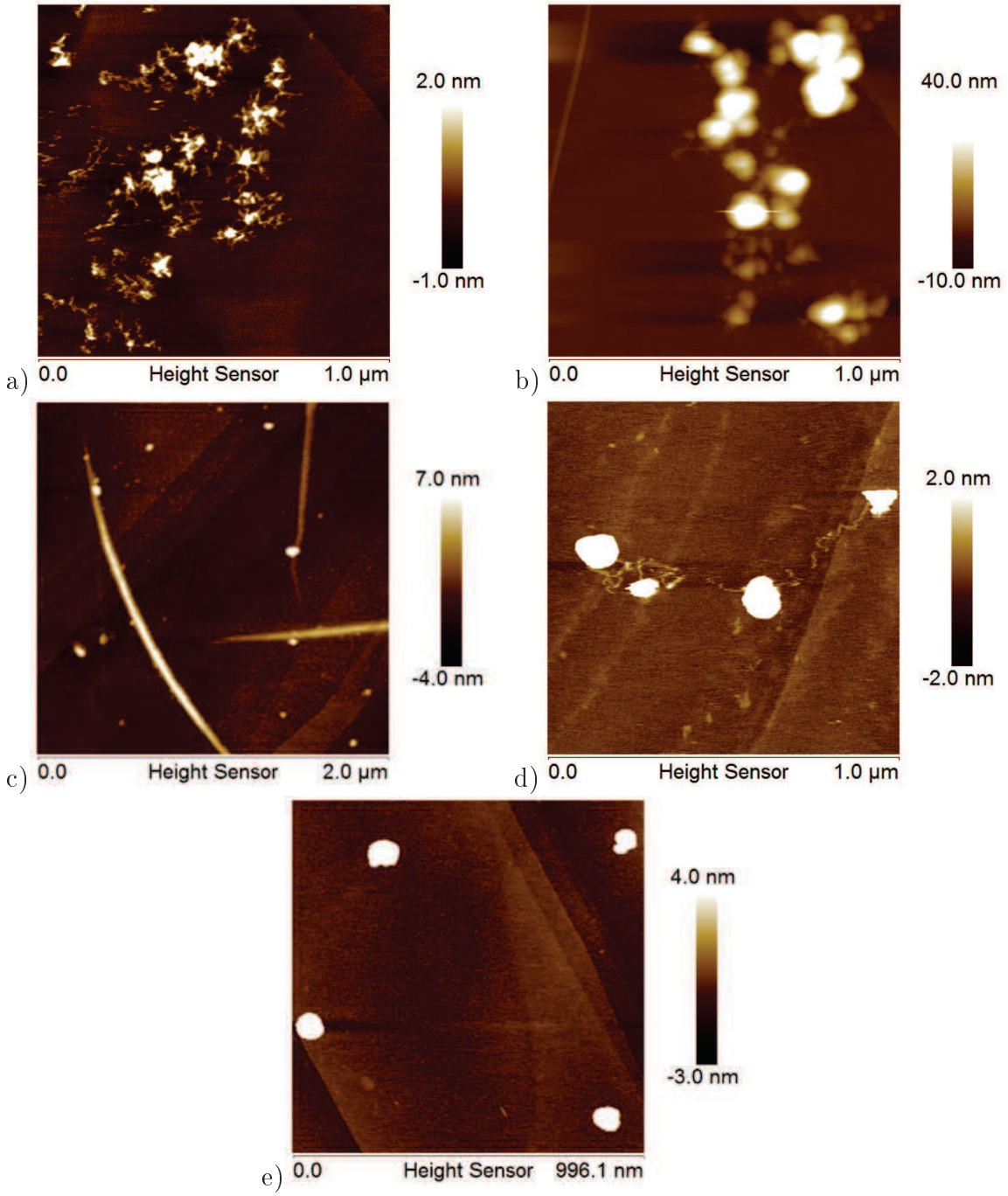

Fig. D.3: Liquid AFM images of a)PEDOT:PSMSI, b) PEDOT:PSTFSI-co-AA, c)PEDOT:PSPSI, d)PEDOT:Pectin and e)PEDOT:HLA

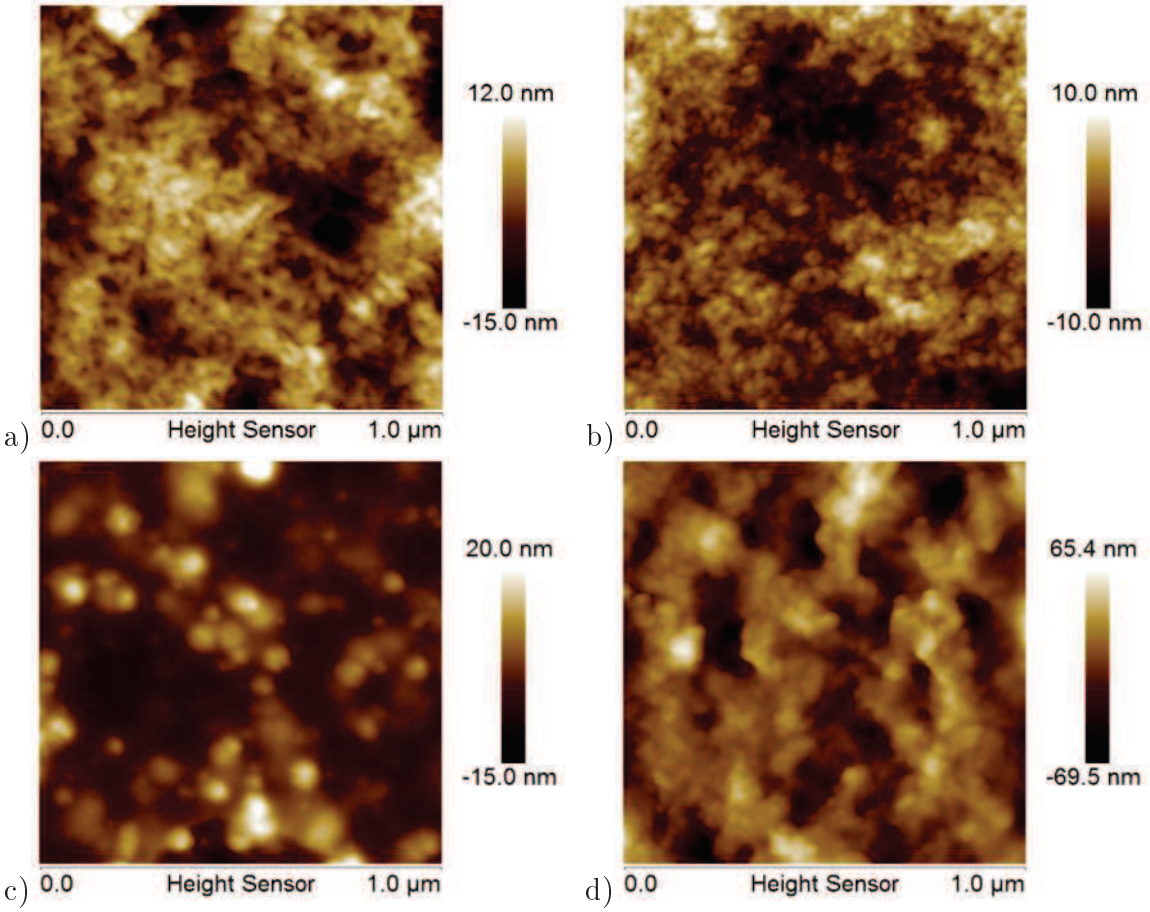

Fig. D.4: AFM height images of a)PEDOT:PSS, b)PEDOT:PSTFSI, c)PEDOT:DS and d)PEDOT:PMaTFSI

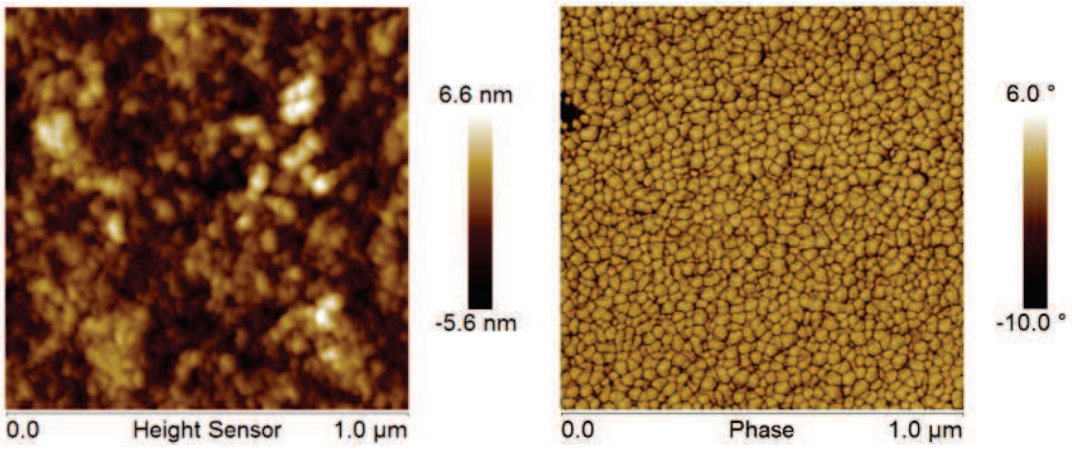

Fig. D.5: AFM height and phase image of PEDOT:PSTFSI upon 1min CF_4 plasma etching

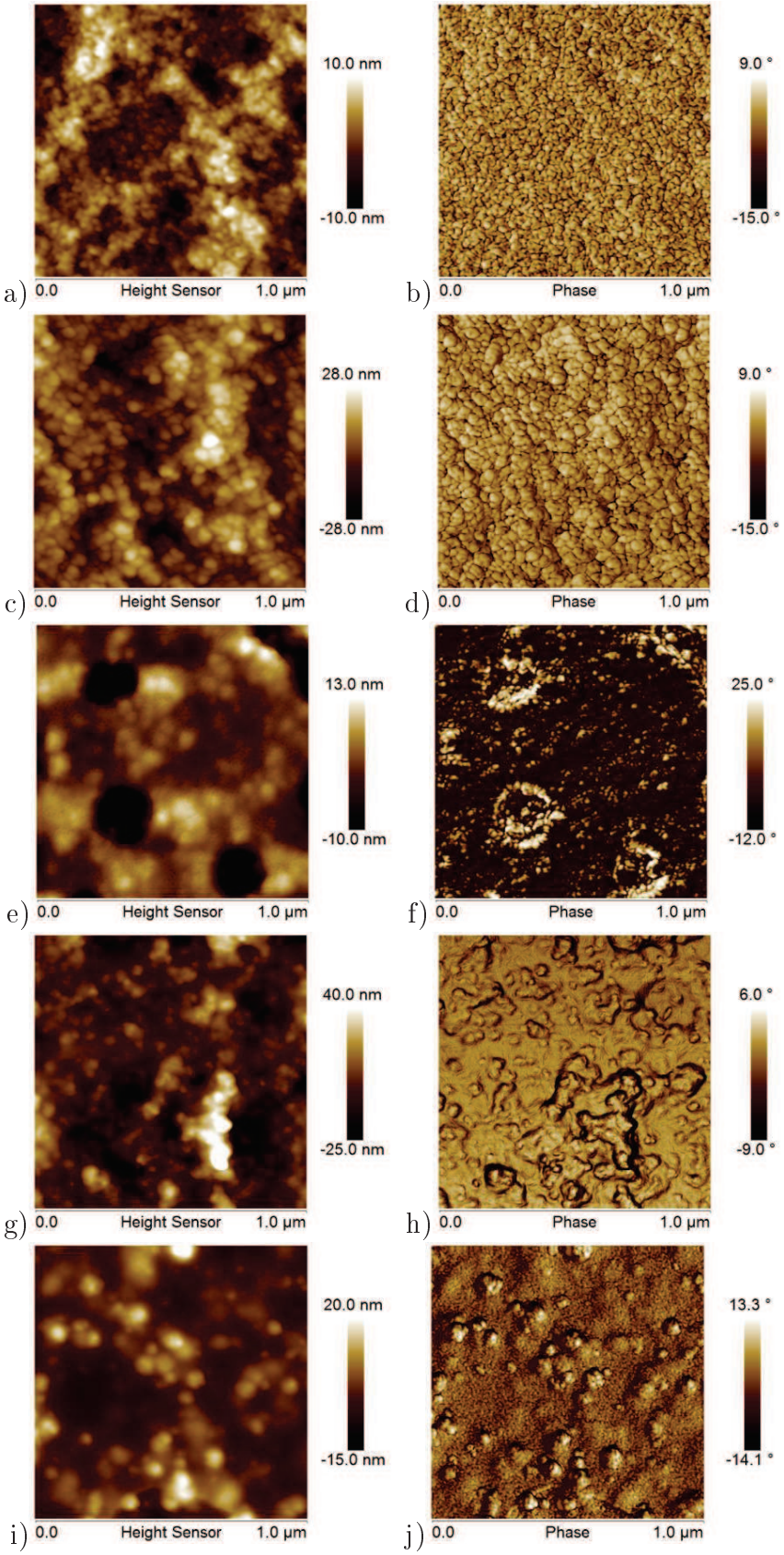

Fig. D.6: AFM height and phase images of a),b)PEDOT:PSMSI, c),d)PEDOT:PSTFSI-co-AA, e),f)PEDOT:PSPSI, g),h)PEDOT:Pec and i),j)of PEDOT:HLA

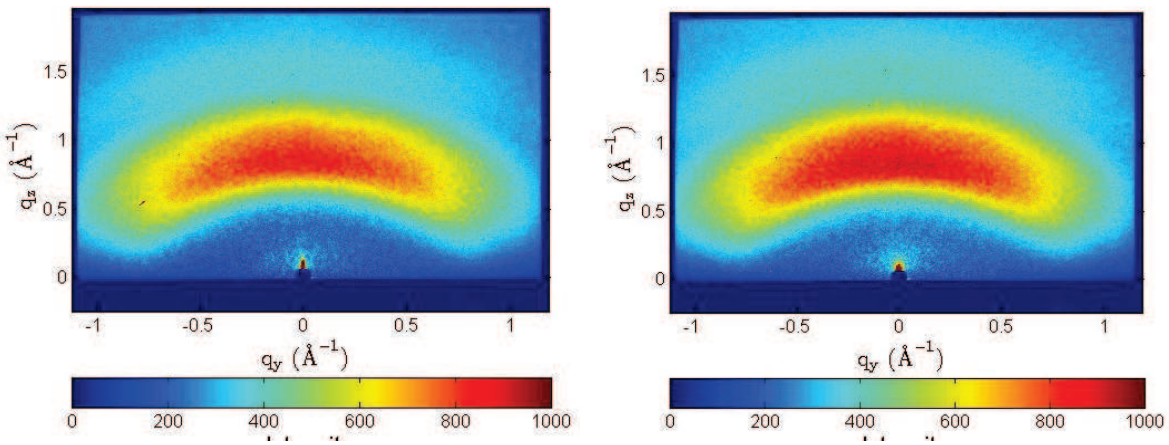

Fig. D.7: GIWAXS analysis of a pristine PEDOT:PSTFSI film (left) and of a PEDOT:PSTFSI film with 5% DMSO co-solvent, showing the absence of crystalline diffraction patterns